MOULD THERMAL RESPONSE, BILLET SURFACE QUALITY AND MOULD-FLUX BEHAVIOUR IN THE CONTINUOUS CASTING OF STEEL BILLETS WITH POWDER LUBRICATION

by

CARLOS A. M. PINHEIRO

Eng. (Metallurgical Engineering) Universidade Federal de Minas Gerais, Brazil, 1981

M. Sc. (Metallurgical Engineering) Universidade Federal de Minas Gerais, Brazil, 1988

A THESIS SUBMITTED IN PARTIAL FULFILLMENT OF

THE REQUIREMENT FOR THE DEGREE OF

DOCTOR OF PHILOSOPHY

in

THE FACULTY OF GRADUATE STUDIES

(Department of Metals and Materials Engineering)

THE UNIVERSITY OF BRITISH COLUMBIA

December 1997

Abstract

The main objectives of this study were to examine mould thermal response and billet surface quality during continuous casting of steel billets with powder lubrication, and to compare with oil lubrication. Measurements were carried out on an operating billet caster to determine mould-wall temperature profiles for different mould-flux types, mould cooling-water velocity, oscillation frequency and steel grade. The trial involved data acquisition on mould displacement, casting speed, metal level and mould powder temperature field. In addition, mould powder consumption and liquid flux pool depth were also measured.

An inverse heat conduction model was developed to determine mould heat flux from measured mould wall temperatures. Existing mathematical models were utilized to investigate mould/billet binding and mould taper. Results from plant measurement, mathematical models and billet sample evaluation were used to compare mould-powder and oil casting in terms of mould thermal response, transverse depression, rhomboidity, oscillation mark and mould level variation. Finally, a mathematical model was developed to analyze the influence of mould-flux properties and feeding strategies on melting behaviour.

This work has led to a very comprehensive understanding of mould thermal response and mould-related quality problem in billet casting with powder lubrication. Transverse depressions were found to be formed in steel grades with high coherency temperature due to metal level fluctuation. For Boron(Ti)-alloyed medium-carbon steel cast with powder transverse depressions were eliminated due to a substantial decrease in meniscus heat flux, thus producing a thinner, hotter, more flexible shell, and also due to lower metal level fluctuations on account of pouring with SEN.

An understanding of the role of titanium and nitrogen on transverse depressions resulted in the establishment of maximum values for these elements. In order to minimize transverse depression in billet casting with oil lubrication the nitrogen content of the steel must be kept below 60 ppm and the titanium content below 0.019%.

Mathematical modelling of billet shrinkage, corroborated by billet inspection, showed that excessive mould taper caused the mould to squeeze the solidifying shell which led to the formation of longitudinal depressions. To eliminate this problem a double mould taper with 1.8% m^{-1} up to 450 mm from the mould top and 0.9% m^{-1} for the rest of the mould is recommended. Mathematical modelling of mould powder melting has led to further understanding of the response of the molten-flux pool to changes in powder properties, feeding strategies and casting speed.

Table of Contents

List of Tables

List of Figures

List of Symbols

A, B	internal dimensions of the mould (mm)
C_p	specific heat (J kg^{-1} $°C^{-1}$)
C_{pw}	specific heat of water (J kg^{-1} $°C^{-1}$)
d_w	width of cooling-water channel gap (m)
D_H	hydraulic diameter (m)
$\mathbf{e}_i^j$	first-order interaction coefficients in liquid iron
f_B, f_N, f_{Ti}	activity coefficient for boron, nitrogen and titanium, respectively
f_s	fraction of solid
G	rate of energy generation or consumption (W/m^{-3})
h_c	heat transfer coefficient at the mould-powder/air interface (W m^{-2} $°C^{-1}$)
h_r	effective heat transfer coefficient due to radiation (W m^{-2} $°C^{-1}$)
h_w	heat transfer coefficient at the mould/cooling-water interface (W m^{-2} $°C^{-1}$)
H	enthalpy (J/kg)
H^{new}	nodal enthalpy at time t+Δt (J/kg)
H^{old}	nodal enthalpy at time t (J/kg)
ΔH	latent heat (J/kg)
I	identity matrix
k	thermal conductivity (W m^{-1} $°C^{-1}$)
k_c	thermal conductivity of continuous phase (W m^{-1} $°C^{-1}$)
k_{cu}	thermal conductivity of mould copper walls (W m^{-1} $°C^{-1}$)

k_d	thermal conductivity of discontinuous phase (W m^{-1} $°C^{-1}$)
k_{eff}	effective thermal conductivity (W m^{-1} $°C^{-1}$)
k_w	thermal conductivity of cooling-water (W m^{-1} $°C^{-1}$)
L	mould internal side-length (m)
L_w	length of the cooling-water channel (m)
L^o	initial nodal length (m)
ΔL	billet shrinkage (m)
M	number of heat fluxes components for inverse analysis
M_p	total mass of mould-powder consumed (kg)
Pr	Prandtl number
q	mould heat flux estimated from inverse analysis(W m^{-2})
q	vector of estimated mould heat fluxes
q^o	initial mould heat flux for inverse analysis (W m^{-2})
$\mathbf{q}^o$	vector of initial mould heat fluxes
q_c	convective heat flux losses at top of mould-powder (W m^{-2})
q(z)	mould heat flux profile (W m^{-2})
Q	mould powder consumption (kg/tone of steel)
Re	Reynolds number
S	sum of squares
t	time (s)
t_N	negative-strip time (s)
T	temperature (°C)

T_a	ambient temperature (°C)
T^c	calculated mould temperature for the inverse analysis (°C)
T_L	mould-flux liquidus temperature(°C)
T^m	measured mould wall temperatures (°C)
T^o	temperatures calculated using the initial mould heat flux q^o (°C)
T_o	temperature at the cold face of the mould (°C)
T_s	temperature of rapid sintering or softening of mould-flux (°C)
T_{steel}	liquid steel temperature at the mould-flux/steel interface (°C)
T_{top}	mould-powder temperature at the top (free) surface (°C)
T_w	temperature of cooling-water (°C)
T_w^{inlet}	cooling-water inlet temperature (°C)
V	casting speed (m/min)
V_d	volume fraction of discontinuous phase
V_w	cooling-water velocity (m/s)
x, y, z	spatial coordinates
X_{ij}	sensitivity coefficients
$\mathbf{X}$	matrix of sensitivity coefficients
$\mathbf{X}^T$	transpose of $\mathbf{X}$
α^*	regularization parameter
$\delta(z)$	nodal distance (m)
δij	Kronecker delta

Δ	delta for temperature and heat-flux perturbation
ε	mould-flux emissivity
η_w	viscosity of water (Pa s)
μ	mass attenuation coefficient for gamma rays (cm^{-1})
ρ	density (kg m^{-3})
ρ_{flux}	density of molten mould-flux (kg m^{-3})
ρ_{powder}	bulk density of loosely packed mould-powder (kg m^{-3})
ρ_{steel}	density of liquid steel (kg m^{-3})
ρ_w	density of cooling-water (kg m^{-3})
σ	Stefan-Boltzmann constant (5.6703×10^{-8} W m^{-2} K^{-4})

Subscripts

i, j, k	dummy summation indices
l	liquid phase
γ	γ-iron phase

Acknowledgements

I would like to express my sincere gratitude to my supervisors Dr. Keith Brimacombe and Dr. Indira Samarasekera for giving me the opportunity to work with them and for their invaluable guidance and support throughout the course of this research. I also wish to thank the Brazilian National Research Council (CNPq) for granting me a scholarship that allowed me to pursue a Ph.D. degree in Canada. Financial support from MRM-Gerdau, The University of British Columbia and the Natural Sciences and Engineering Research Council of Canada is gratefully acknowledge.

The assistance of staff and students of the "Intelligent Mould" research group: Mr. Neil Walker, Sunil Kumar, Vladimir Rakocevic and Randy Gurton during the industrial plant trial and other parts of the work is deeply appreciated. Sincere thanks are due to Henry Wong, who helped me with the inverse heat conduction analysis, and to Ola Gussias for his assistance with the measurements of billet surface profiles and with the Fortran code for calculating mould wall temperatures. Besides the aforementioned individuals I am also grateful to Joan Kitchen, Mary Jansepar, Pat Wenman, Peter Musil and Binh Chau.

I would also like to thank Yan, Bernardo, Eduard, Victor, Cornelius, Edmund, Bill, Himanshu and specially Mark Ritchie, and Junpei Konishi for their friendship which helped to make my student years at UBC a thoroughly rewarding experience.

Finally, I would like to thank my wife Rose for her encouragement and loving patience and our families for their unwavering support.

1. INTRODUCTION

Over the past three decades continuous casting of steel has been widely adopted, almost eliminating ingot casting as a mass production process. In the 1960s, virtually all steel produced in the world was cast into ingots while in 1995, 75% of the world's steel production was continuously cast. In countries such as Japan and Canada continuous casting represents more than 95% of the steel production[1]. Compared to conventional ingot casting the continuous casting process presents lower cost, higher yield, and the ability to achieve more uniform and higher quality cast products.

Worldwide the bulk of molten steel is produced via two main routes, pig iron/**B**asic **O**xygen **F**urnace (BOF) or scrap/electric furnace. After molten steel is produced using one of the above two routes, the liquid metal is transferred to a ladle where it can be further refined. Subsequently, the ladle is moved to a continuous casting station where the liquid steel is continuously poured from the ladle into an intermediate vessel, or buffer, called the tundish. From the tundish, the molten steel is poured at a controlled rate into a water-cooled, oscillating copper mould as shown in Figure 1.1. The mould extracts heat and a solid steel shell is formed. The partially solidified strand is continuously withdrawn and solidification of steel is completed below the mould where water sprays and radiant cooling take place.

The withdrawal of the steel strand is aided by the oscillation of the mould and a constant supply of lubricant that flows between the mould wall and the strand surface. Traditionally, oil has been used as lubricant for casting billets while for the continuous casting of steel slabs and

---

[1] Iron and Steel Institute. Statistical Information, Iron and Steelmaker, vol. 23, n. 13, 1996

blooms mould powder is the primary lubricant. When mould powder is used, the pouring of liquid steel from the tundish into the mould is accomplished through a refractory tube called Submerged Entry Nozzle (SEN), while with oil lubrication the common practice is to use open stream pouring.

The reasons behind the use of oil in billet casting are two fold: lower cost when compared to powder, and no billet-size restriction. Powder prices are higher than oil, moreover the use of mould powder requires the liquid metal to be delivered from the tundish into the mould through a submerged entry nozzle, which represents an additional cost. This is necessary, because without the SEN some of the mould powder would be carried by the steel stream into the metal pool thus contaminating the steel. For small billets (< 150 mm sq), the use of SEN is not feasible since there would be a risk of steel freezing between the nozzle and the mould walls, or the SEN would have to be very small. The solution for the above limitation seems to be the use of smaller SENs. However, this is still an unsolved technical challenge since a small SEN is prone to internal clogging and cannot last long due to external wear.

Although oil casting is less costly, the practice of open stream pouring is particularly problematic. A fluctuating meniscus, caused by rough streams, interacts with the lubricating oil and creates variations in heat transfer and mould lubrication which negatively affects billet quality. Also, the common practice of operating without tundish flow control results in an inherently transient process. Changes in the steel flow rate from the tundish alter the metal level causing the speed control system to modify the casting speed to return to the preset metal level. Metal level variation, heat transfer and lubrication all have a significant effect on the generation of surface defects such as transverse depressions, laps and bleeds.

The use of a SEN when casting with mould powder can potentially improve metal level stability, since steel splash and surface turbulence are eliminated. However, stability of the metal level is also dependent on the nature of the metal flow control, casting speed control system, and the metal level sensor. Mould powders are better lubricants than oil, they usually provide liquid lubrication which results in lower mould friction while with oil there is more intimate contact between the billet and the mould. Generally mould powders tend to result in lower and more uniform mould heat flux. Powders also provide chemical and thermal insulation to the liquid steel pool which allows casting with lower superheats. All the above factors positively affect billet quality, rendering powder casting a superior process when compared to oil casting. Therefore, as global competition has driven North-American mini-mills to improve billet quality, the adoption of powder lubrication for larger billets seems to be the answer to achieve a higher quality level.

In the past two decades, extensive research has been conducted on heat transfer, solidification and defect formation during billet casting with oil lubrication. Also there have been numerous investigations linking mould flux to slab quality, which has resulted in excellent progress with respect to mould flux development for slab casting. Unfortunately, studies of a similar nature have not been conducted for billet casting with powder lubrication and is therefore the objective of this research.

This study was undertaken to examine mould thermal response during billet casting with powder lubrication, and also to compare powder lubrication with oil lubrication in the context of the mould thermal response and billet surface quality. Measurements were made on an operating billet cast machine to determine mould wall temperature profiles for different mould-flux type, mould cooling-water velocity, oscillation frequency and steel grade. An

inverse heat conduction model was developed to determine mould heat flux from measured mould wall temperatures. Existing mathematical models were utilized to investigate mould-billet binding and mould taper. Results from plant measurements, mathematical models and billet sample evaluation were used to compare mould powder and oil casting in terms of mould thermal response, transverse depression, rhomboidity, oscillation mark and mould level variation. Finally, a mathematical model was developed to analyze the influence of mould powder properties and feeding strategies on the melting behaviour of mould powders.

This work has led to a very comprehensive understanding of mould thermal response and mould-related quality problems in billet casting with powder lubrication. The mould inverse heat conduction model proved to be a very fast and reliable tool for determining mould heat flux from measured temperatures. Mathematical modelling of billet shrinkage and powder melting has led to recommendations for improvement in mould taper and powder type.

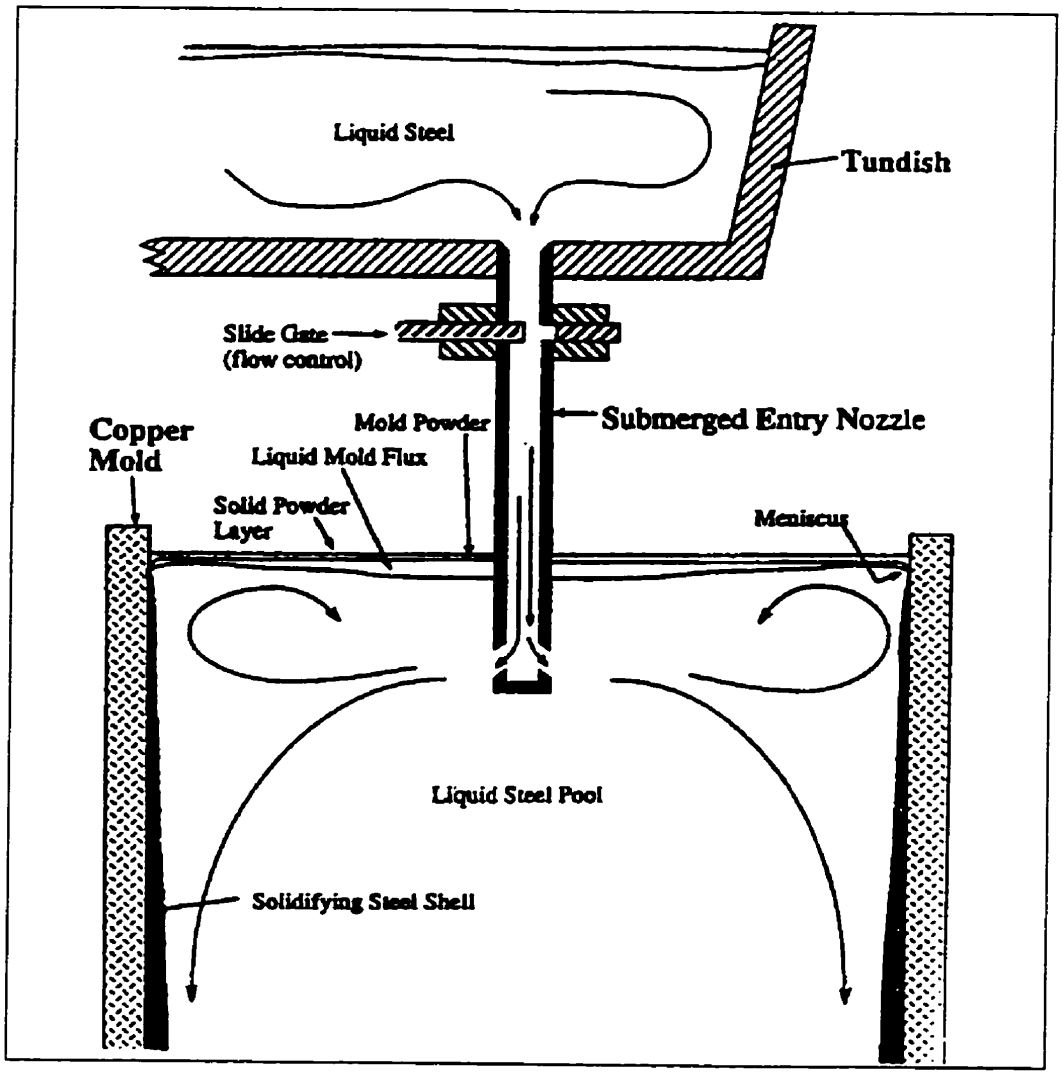

Figure 1.1 Schematic diagram of tundish and mould of continuous casting of steel with powder lubrication [147]

2. LITERATURE REVIEW

This chapter reviews the state-of-the art on mould flux for continuous casting of steel. The extensive literature on mould powders deals almost exclusively with their behaviour and performance during slab casting. Very few papers consider or even make reference to any aspect of mould flux in billet casting. Apparently, most billet casters who do use mould flux rely on knowledge from their slab counterparts.

2.1 Mould Flux

Mould fluxes are synthetic slags used during the continuous casting of steel. The fluxes, which are continually fed onto the liquid pool surface during casting, melt and the liquid slag flows down between the mould walls and the strand shell. Figure 2.1 shows the general disposition of a flux in the continuous casting mould. The flux above the surface of the molten steel generally consists of three different layers viz., (i) An unmelted, dark, unreacted powder layer on top, (ii) A heterogeneous, sintered layer in the middle, (iii) A molten flux layer directly over the steel.[1-2]

Also, a rim is formed by flux in contact with the water-cooled copper mould walls at the meniscus level. This rim features all the different phases from solid to liquid (glassy, crystalline and liquid). This multi-phase, wedge-like crust which oscillates with the mould, depending on its size, can exert considerable influence on the heat transfer process at the meniscus. The thickness of the rim ranges from 1 to 3mm at the meniscus level[3] and depends partly on the flux thermal conductivity, meniscus level fluctuation and mould wall temperature.

The flux layer on the strand surface below the meniscus consists of a solid film directly in contact with the mould walls and a liquid film in contact with the strand surface. It is not

certain whether this layer takes the form of a thin film covering the entire surface or whether it is more intermittent in nature, only partially covering the surface[1,3].

Mould fluxes are used to: (1) provide thermal insulation, (2) protect the liquid steel against reoxidation, (3) absorb inclusions which rise to the metal surface, (4) lubricate the strand, reduce strand friction, and (5) control the heat transfer between the strand and the mould.

Mould fluxes have a decisive effect on both the efficiency of the continuous casting process and the surface quality of the steel product. There are several key phenomena for the successful performance of a casting flux viz., (1) the melting of the powder, (2) the formation of a molten flux pool, (3) the infiltration of the molten flux into the mould/strand gap, and (4) the formation of solid and liquid flux films to provide liquid lubrication throughout the mould and a uniform and correct level of heat transfer between the strand and the mould, mainly at the meniscus[1]. The most critical is the infiltration of the flux into the mould/strand gap but all of the phenomena are important since failure of the powder to perform satisfactorily in the other areas can lead to inferior quality of the product or even to sticker breakouts.

2.2 Chemical Composition of the Fluxes

Mould fluxes are designed for specific steel grades and casting conditions; their chemical composition varies greatly depending on the properties required. Typically mould fluxes contain the following major constituents - CaO-SiO_2-Al_2O_3-Na_2O-CaF_2 - and lie in the pseudo-wollastonite area within the ternary diagram CaO-SiO_2-Al_2O_3. The building block of most mould fluxes is the SiO_4^{2-} tetrahedron, which forms a silicate chain whose properties such as viscosity, melting range, glass transition temperature and crystallization temperature

can be modified by proper choice of glass formers, modifiers and fluidizers. Glass formers, Al_2O_3 and B_2O_3, increase the chain length; modifiers, CaO, MgO, BaO, SrO, Na_2O, Li_2O, K_2O, break the silicate network; and fluidizers like fluorine(F^-) ion can easily replace the divalent oxygen ion resulting in break-down of the Si-O network, consequently decreasing the viscosity of the slag. Carbon is also added to the powder to control its melting rate but it is not a constituent of the liquid flux. Table 2.1 shows the typical ranges of chemical composition for commercial mould powders.

Besides the chemical composition, the mineralogical constitution of the powder is of particular importance since it influences the melting rate of the powder. Riboud et al.[21] showed that although two powders may have identical overall chemical composition, their melting behavior depends upon the mineralogical constitution of their components[1].

The chemical composition of the molten flux can undergo changes during the casting process. The main concern is the absorption of alumina while casting Al-killed steels, which can profoundly alter the viscosity of the flux. Depending on steelmaking and casting practices, the alumina in the mould flux can rise from 3% to 15%[5].

2.3 Mould Flux Properties

2.3.1 Viscosity and Glass Transition Temperature

As Newtonian fluids, the viscosity of mould fluxes is the proportionality factor (η) between the shear stress (τ) and the velocity gradient,(dv/dx) when these fluids are subjected to an external force, as defined in Equation 2.1.

$$\tau = \eta\left(\frac{dv}{dx}\right) \tag{2.1}$$

2.3.1.1 Viscosity measurements

The viscosity of liquids at high temperatures is usually measured with a rotating viscometer[6-10] in which the torque, developed when a spindle is rotated at a fixed speed in a crucible filled with the liquid, is measured. There are also other types of viscometers: sphere pulling-up and oscillating-plate[11]. These techniques are not free of problems, and viscosity values recorded in different laboratories are prone to large differences[1,12]. This is shown in Figure 2.2, which is the result of an inter-laboratory comparison carried out on a reference material, using the rotating cylinder method. It can be seen that the values obtained for η at 1300°C varied between 10 and 25 poise.

The errors associated with viscosity measurements arise mainly due to a lack of standardization of the calibration procedure with a reference material of known viscosity. Although the available measuring techniques can provide values reproducible to within 10%[8,11], Mills[8] believes that the overall experimental uncertainties with viscosity measurements are much larger(±25%).

2.3.1.2 Factors determining flux viscosity

The viscosity of a molten flux is primarily determined by its temperature and chemical composition. The temperature dependence of viscosity over a given temperature range follows the Arrhenius equation:

$$\eta = A \exp\left(\frac{E}{RT}\right) \tag{2.2}$$

where A is the Arrhenius constant, E is the activation energy for viscous flow, R is the gas constant and T is the absolute temperature (K). The usual way to present viscosity as a function of temperature is by plotting $\ln\eta$ versus 1/T[7,13,14]. Figure 2.3 shows typical flux

viscosity-versus-temperature curves. The curves consist of: (1) a linear portion with slope E/R in the higher temperature range, (2) a narrow non-linear transition region and (3) a vertical portion in the lower temperature range.

Because the transition region of the viscosity-temperature curve is usually quite narrow, for practical purposes it is often considered that a "breakpoint"[9] exists, which is determined by the intersection of the linear and vertical portions of the curve. This breakpoint has been called the "freezing point"[15], solidification temperature[13,14] and crystallization temperature[7]. This temperature is associated with a change in the rheological behavior of the flux, below which the flux behaves as a non-Newtonian fluid or similar to a solid; and hence the terms freezing point or solidification temperature are clearly not a correct description of this phenomenon. Neither is the term crystallization temperature to describe the transition temperature correct. Crystallization temperature is the temperature at which the solid transformation -glassy to crystalline- occurs; and measurement of it must be conducted by differential thermal analysis(DTA). Hereafter the transition temperature will be referred as the breakpoint or simply transition temperature.

In terms of chemical composition, it has been found that silica is the major factor determining mould flux viscosity[7,10,16,17]. This was demonstrated by work conducted at IRSID, where 16 slags without alumina were compared[10]. As shown in Figure 2.4, an increasing SiO_2 content leads to higher viscosities due to a heavier interlacing within the silicate chain.

Mould flux viscosity also increases with increasing Al_2O_3, content since alumina in concentrations up to 20% for a V-ratio(wt%CaO/wt%SiO_2) ranging from 0.67 to 1.20, which is a typical range for mould fluxes, has the same molar effect on viscosity as silica[7]. Figure

2.5 shows the effect of alumina on viscosity. It can be seen that although the addition of alumina always increases the viscosity, the level of influence depends on the flux, i.e., it depends on the other constituents of the flux[18]. The result of numerous studies on the effect of alumina on viscosity indicates that it is possible to formulate powders that render fluxes whose physical properties are only slightly altered by alumina content variations[13,18,19]. In order to achieve this result the flux established under production conditions must have less than 10% Al_2O_3.

In addition to silica and alumina, other constituents of mould fluxes, so called network modifiers, such as fluorides (NaF,CaF_2), alkali (Na_2O,K_2O,Na_2O) and basic oxides (CaO,MgO, BaO,SrO) lower the viscosity and the glass transition temperature. Boric oxide (B_2O_3), although a network former, also reduces the viscosity as a result of lowering the melting temperature range remarkably [13,18,19]. Figure 2.6 shows the effect of some of these constituents on the viscosity of mould fluxes.

2.3.1.3 Models for calculating viscosity

Several investigators have developed empirical models for calculating the viscosities of casting fluxes from their chemical composition. Table 2.2 shows the mould flux composition range studied in each of these investigations and Table 2.3 shows the equations established by these studies.

The first model is due to McCauley and Apelian[20]. They found that the viscosity at a given temperature can be expressed as a function of the ratio of network forming ions to anions or as a function of the mole fraction of silicon.

Riboud et al.[10] at IRSID carried out viscosity measurements on a set of 23 synthetic and 22 industrial fluxes. IRSID's model utilizes the Frenkel equation (η=A.T.exp(B/T), where A

and B are constants, and T is the temperature in K), to correlate the viscosity with temperature and composition. The model divides the components into 5 constituents: CaO*, Na_2O*, SiO_2, Al_2O_3 and CaF_2, where the molar fraction of CaO is defined as: $XCaO^*=XCaO+XMgO+XFeO+XMnO+XB_2O_3$ and that for Na_2O is $XNa_2O^*=XNa_2O+XK_2O$. Riboud and Larrecq[21] compared IRSID's equation with that of McCauley and Apelian[20]. They concluded that: (1) IRSID's model gave an accurate estimation for viscosity, (2) the McCauley and Apelian equation, expressed as a function of the ratio of network forming ions to anions, renders an acceptable estimation, even though it is less accurate than IRSID's, since CaF_2 and NaF contents are not over 15.

Koyama et al.[16] at Nippon Steel carried out extensive viscosity measurements on mould fluxes. They found that the IRSID equation also gives good agreement for fluxes with Li_2O and without MgO but predicts viscosity values that disagree with measurements for fluxes that contains MgO. They concluded that considering MgO as CaO is a source of error. Their equation yielded a correlation coefficient of 0.96 which was superior to the IRSID equation for a powder system containing MgO.

Lee et al.[13] at RIST(Korea) measured the viscosity of 35 experimental mould powders. Although Lee et al. did not compare the RIST equation with the previous equations, they reported that it can be applied to powder systems containing MgO, Li_2O and B_2O_3. They also determined an equation for the transition temperature which they named solidification temperature (T_S).

$$T_S=1241.6-2.15(X\mathrm{MgO})-1.41(X\mathrm{Al_2O_3})-4.49(X\mathrm{NaO})-8.55(X\mathrm{CaF_2})-6.41(X\mathrm{Li_2O})-15.28\,(X\mathrm{B_2O_3}) \qquad (2.3)$$

where T_S is given in °C and X in mole %.

The equations presented in Table 2.3, respecting their limitations and range of validity, are a powerful tool in helping to design a powder composition that provides a desired viscosity and glass transition temperature.

2.3.2 Crystallization Temperature

When a slag is cooled below its liquidus temperature, it may or may not crystallize depending upon its chemical composition and the thermal cycle. Silica-rich slags can easily be cooled to form glasses in the temperature range where they should crystallize under equilibrium conditions. On the other hand, basic slags rich in CaO, are extremely difficult to quench as glasses: crystals appear in the liquid at temperatures slightly below the liquidus[22].

Most continuous casting mould fluxes lie between these two extremes. The existence of glassy and crystalline layers has been confirmed by the examination of flux samples taken from the mould[13,23,24] and also from simulation experiments[1].

Kyoden at al.[23] observed: (1) a slag film 800μm thick, consisting of a crystalline layer of approximately 150μm on the mould side and a 650μm glassy layer on the strand side; (2) that there was no difference in the chemical composition between both layers; and (3) small pores in the crystalline layer. They believed that these pores were the major reason why mould fluxes with high crystallization temperature present a greater resistance to heat transfer, as shown in Figure 2.7. Another reason for this behavior is that the contribution to heat transfer by radiation is reduced in the presence of highly crystalline flux films[12].

The observations of Yoshida et al.[24] were similar to those of Kyoden et al.[23]. They found a glassy layer on the strand side which was considered to be molten during casting and a crystalline layer on the mould side, believed to be solid during casting. They observed the

presence of many crystallized nuclei in the glassy layer and that the crystallized layer consisted of several layers with different structures.

Kawasaki Steel[15,25] introduced an index to evaluate the degree of crystallization based on the relative area of white color (which was proved to be crystalline by X-ray diffraction) at a cross section of solidified flux samples after being poured into a stainless steel receptacle. The index assumes a value of 0 for a completely glassy flux and 3 for a wholly crystallized flux. Chang et al.[26], following a similar procedure, defined a crystallization ratio as the thickness of crystallized flux to the total thickness of the solidified flux.

A lower heat-transfer rate is believed to be responsible for reduction in the occurrence of longitudinal cracks but also for a higher frequency of breakouts by sticking, as shown in Figures 2.8 and 2.9, respectively[14,15,26].

2.3.2.1 Crystallization temperature measurements

The crystallization temperature is measured by differential thermal analysis (DTA), which records the temperature lag (or advance) when a specimen undergoes an endothermic (or exothermic) transformation on being heated (or cooled) at a fixed rate. A typical DTA (cooling) trace for a mould powder is shown in Figure 2.10. It can be seen that Flux A does not exhibit a distinct exothermic peak, indicating a lack of crystallinity. Conversely, Fluxes D, E and F do exhibit characteristic crystallization during cooling as manifested by the exothermic peaks[14]. An alternative method to estimate the crystallization temperature of mould powder was developed by Kawasaki Steel[15,25]. The technique is based on loss of transparency when a molten flux is cooled at 20°C/min. in a high temperature microscope.

Sorimachi et al.[27], using X-ray diffraction, showed that a powder which exhibited glass forming properties in the laboratory, underwent crystallization during continuous casting,

despite the rapid cooling. They believed that the transition from glassy to crystalline was induced by the large kinetic energy associated with mould oscillation. Their results demonstrated that laboratory results are not necessarily applicable to the actual casting operation.

2.3.2.2 Factors affecting crystallization temperature.

Like viscosity, the crystallization temperature is also strongly dependent on chemical composition of the mould flux. Figure 2.11 from Kyoden et al.[23] shows the influence of V-ratio on the crystallization temperature. Thus a mould powder with higher CaO/SiO_2 ratio has a higher crystallization temperature. The same results were obtained by Nakato et al.[15]. Table 2.4 confirms the major influence of V-ratio on crystallization temperature and crystallization index (as defined by Kawasaki Steel[15] and previously explained). They also found that the addition of BaO can prevent a mould flux from crystallizing.

Alumina also influences the crystallization temperature. Sardemann and Schrewe[5] showed that, beginning with an initially crystalline structure, the mould flux can change into a fully vitreous structure upon addition of a certain amount of alumina (+5% to +10%).

The influence of the V-ratio and alumina on crystallization behavior of mould fluxes was confirmed by the results of Chang et al.[26]. They also showed that fluoride increased the crystallization ratio while the addition of boric oxide and MgO decreased it. Their results are shown in Figure 2.12. It also was observed that an increase in the Na_2O content results in a greater tendency for the flux to crystallize[1,2].

2.3.3 Melting Range

The following methods have been adopted to determine the melting range of mould powders:

High temperature microscope. In this technique the specimen is heated and monitored for signs of melting. The test consists of heating an agglomerated sample pressed into the form of a cube or cylinder at a controlled rate, and then monitoring the changes in sample dimensions[16,19,28-31]. The Leitz high-temperature microscope test is the most widely used of these methods[16,19,31].

Quench Test. Riboud[21] determined the melting (liquidus) temperature by sealing decarburized samples (100-150mg) of mould powders in platinum tubes and heating them to the test temperatures (10°C apart). The samples were kept at the test temperature until equilibrium was attained and then were rapidly quenched. The quenched samples were examined metallographically for signs of melting.

Differential Thermal Analysis (DTA). In DTA the powder and alumina (reference) are placed into identical crucibles in a furnace. The temperature difference between the sample and reference is monitored continuously as the furnace is heated at a fixed rate. Any thermal event, such as a transformation, is revealed as a departure from the base line.

Mills et al.[8] determined liquidus(T_{liq}) and solidus temperatures(T_{sol}) of mould powders using the DTA method. Initially, they carried out the measurements on as-received and decarburized samples and obtained identical results in each case; all subsequent tests were carried out on decarburized powders because the DTA output was better defined. The results for T_{liq} were found to be in excellent agreement with those determined by Riboud and Larrecq.[21] using the quench method, although the values sometimes differed from those

quoted by the manufacturers. The latter values were obtained using high temperature microscopy, as shown in Table 2.5

Mills et al.[8] observed that the values for T_{sol} shown in Table 2.5 should be treated with some caution because they were determined during the cooling cycle; the onset of melting was frequently masked by heat release related to the oxidation of carbon and to the sintering of the specimen. The phases that form during cooling can differ appreciably from those present in the as-received powder, which may be a source of error.

2.3.3.1 Effect of chemical composition on melting range

There is very little data available on the effect of chemical composition on the melting range of mould fluxes. The most comprehensive study was conducted by Scheel and Korte[19] who investigated the influence of the fluxing agents Na_2O and CaF_2, basicity ($wt\%CaO/wt\%SiO_2$), and alumina on the melting temperatures. In their study they altered the basic flux composition by gradual addition and reduction of one flux constituent at a time. Figures 2.13 and 2.14 show that the melting temperatures vary almost proportionally with the Na_2O content while with increasing fluorspar content the hemisphere and flow temperatures, as specified in the high temperature microscope method, are not perceptibly altered, although the initial sintering temperature is reduced. These results were confirmed by Mills[32] who found that mould fluxes which contained an excess of Na_2O had a lower T_{liq} than fluxes of similar composition but with an excess of CaF_2.

With respect to the effect of basicity, the initial mould fluxes (V-ratio=0.97) gave the lowest melting temperatures, as shown in Figure 2.15. Scheel and Korte[19] explained this behavior by the fact that the content of the fluxing agents was correspondingly diluted. Sardemann and Schrewe[5] obtained a different result as shown in Figure 2.16. For a basicity

between 0.92 to 1.27, the melting temperature increased steadily as the basicity increased, probably because in their case, the content of the other constituents of the flux was kept constant.

In order to check the effect of alumina on the melting parameters, Scheel and Korte[19] gradually added 5 to 20% Al_2O_3 to the initial flux powder. Their results revealed an increase of the melting temperature at higher Al_2O_3 additions, especially for concentrations over 5% Al_2O_3. Similar was observed by Sardemann and Schrewe, too[5].

It is also reported in the published literature that Li_2O and B_2O_3 produce a dramatic reduction in the melting range[4,13,16,23,32], lowering both the softening [15,23] and the melting[13,16] temperatures determined by the hot stage microscope, and also the liquidus temperature[32] determined by DTA.

2.3.4 Inclusion Absorption

Continuous casting fluxes must be able to absorb and dissolve nonmetallic inclusions, especially alumina, which rise up to the liquid steel/molten flux interface. At the same time, the physical properties of the flux should not be altered substantially by the pick-up of alumina, in order to ensure stable lubrication between the strand and the mould.

In order to optimize solid inclusion removal at a slag-metal interface a high contact angle between the inclusion and the liquid steel is needed as well as a flux covering which is designed to dissolve or wet the inclusion. Work carried out by Riboud et al.[10,22] and Jimbo et al.[33] showed that the emersion of solid particles arriving at the liquid steel-molten slag interface was always favored, whatever the liquid flux composition, since the contact angles were greater than 90° (~130° for alumina) which means that mould fluxes always wet alumina particles.

Differences between fluxes in terms of their capacity to absorb alumina appear in the process of dissolution of solid inclusions into the liquid flux. Failure to dissolve these solid particles, as soon they arrive, leads to a heterogeneous flux saturated with solids which are carried over the periphery of the meniscus. These solids can become entrapped in the solidified steel shell, and impair lubrication because their presence increases flux viscosity; they also may cause non-uniform heat transfer and, in the worst situation, can lead to breakouts[4].

Several investigations[11,18,19,34,35] were carried out on the kinetics of alumina dissolution by continuous casting mould fluxes. It was concluded that the Al_2O_3 dissolution was assisted by (1) a homogeneous liquid slag of low viscosity, (2) an increase in fluoride content (with NaF>LiF>CaF_2), (3) the replacement of Na_2O by Li_2O, (4) an increase in basicity (%CaO/%SiO_2) and (5) a decrease in the initial content of Al_2O_3. However, the inevitable concomitant is a fast erosion of the submerged entry nozzle (SEN)[2,4].

Nakano et al.[16,18], investigated the effect of powder composition on the Al_2O_3 absorption capacity and established an empirical relationship between the alumina absorption rate and a basicity index B_i, given by:

$$Bi = \frac{1.53(\%CaO) + 1.51(\%MgO) + 1.94(\%Na_2O) + 3.55(\%Li_2O) + 1.53(\%CaF_2)}{1.48(\%SiO_2) + 0.10(\%Al_2O_3)} \quad (2.4)$$

They found that the larger the basicity index B_i, the higher the Al_2O_3 absorption rate, as shown in Figure 2.17.

Scheel and Korte[19] investigated the amount and rate of alumina pick-up by casting fluxes and the extent to which the properties of the flux were modified by Al_2O_3 enrichment. As shown in Figure 2.18, the enrichment rate is approximately similar for all fluxes studied.

Extended tests of 2 hours resulted in a final content of about 40% Al_2O_3. This high value is confirmed by results obtained by Do and Lange[35] who found values over 20%, and Emi et al.[6] whose calculated mass-transfer coefficients could lead to alumina enrichment up to about 30%. These numbers show that most commercial casting powders are well suited in terms of their alumina absorption capacity.

Since the alumina enrichment raises the melting temperature and the viscosity of the mould flux, as shown in Figure 2.19, the thickness of the liquid film tends to decrease, impairing lubrication. To avoid this problem it is necessary to minimize alumina input and dilute its content in the molten flux by increasing the powder consumption[6].

The viscosity of the mould flux needs to be designed (via the flux formulation) taking into consideration the extent of alumina that would be absorbed during casting. Depending on the ladle metallurgy and the effectiveness of the system applied to minimize reoxidation, the alumina content in the mould flux can rise from 3 to 15%[2,5,6,14,18,23].

Bommaraju[14] reported that ladle-to-tundish shrouding reduced alumina pick-up in the mould flux from 12 to 5%. Further improvements at Inland Steel No.1 slab caster led to a typical alumina pick-up for low carbon Al-killed steels (LCAK) of 2 to 3%. In Table 2.6 are listed the changes in alumina pick-up and the modifications to the initial viscosity of the mould flux in order to maintain the operating viscosity of the in-mould flux, i.e. the viscosity of the flux after absorbing alumina from the liquid steel, between 2.0 and 2.5 poise, which Bommaraju[14] reported to be a good value for casting LCAK slabs of high quality and low sliver rejections.

Scheel and Korte[19] reported an average pick-up of about 3% for casting with shrouds from ladle-to-tundish-to-mould, which is common practice. Their values, although low, were

highly variable. Higher pick-up of alumina was reported to take place in the vicinity of the submerged nozzle and decreased slightly towards the narrow sides. According to Scheel and Korte[19], casting fluxes generally feature an adequate alumina pick-up capacity and pick-up rate. The danger of undissolved particles being drawn into the casting gap (heterogeneous slag film) exists only in the case of larger alumina agglomerates. Because long retention times of the flux on the melt surface enhance the dissolution of alumina, they state the necessity of operating with a sufficiently thick liquid flux pool which is in agreement with Emi et al.[6].

2.3.5 Insulation

The flux must provide thermal insulation to prevent bridging and/or formation of isolated portions of solidified steel ("steel floaters"), and also to maintain the temperature in the region of the meniscus. Improved thermal insulation reduces the severity of oscillation marks, maintains the channel for flux infiltration at all times and reduces sub-surface defects such as pinholes. The reduction of pinholes with better insulation occurs because the solidification of the meniscus is suppressed due to a higher working temperature of the liquid steel. These conditions prevent the entrapment of bubbles and other possible inclusions.

The rate of heat loss from the steel surface through the mould flux layers is controlled by convection in the top unreacted layer which behaves as a packed bed with hot gases passing through it, i.e., CO and CO_2 from the oxidation of free carbon and carbonate decomposition, and argon, sometimes injected into the liquid steel. In a gas-solid packed bed system the overall heat transfer is comprised of conductive and convective components[36,37]. The conductive component is characterized by a heat-transfer coefficient, h_c, which is related to the effective conductivity, k_e, by:

$$h_c(\Delta T) = -k_e\left(\frac{dT}{dx}\right) \tag{2.5}$$

Balakrishnan and Pei[37] analyzed the conduction heat transfer in packed beds subjected to flowing gases. They concluded that (i) the convective heat-transfer coefficient, h_{fp}, see Equation (2.6), had a significant effect on the conduction mode - k_e or (h_c) was found to increase with the Biot modulus: $Bi=(h_{fp}\times a)/k_s$; (ii) the effective thermal conductivity depended on the contact area between particles, which is related to the density of the bed material and the bed height - the smaller the contact area, i.e., lower density and lower height, the lower is the effective conductance; (iii) the effective conductivity depended on the packing geometry of the particles.

The convective heat transfer between the bed particles and the flowing gases is represented by the convective heat-transfer coefficient, h_{fp}, for which Balakrishnan and Pei[38] established an empirical correlation as follows:

$$h_{fp} = 0.016\left(\frac{k_f}{2a}\right)(Ar_m)^{0.35}(\mathrm{Re}_p)^{0.5} \tag{2.6}$$

where k_f is the thermal conductivity of the fluid; Ar_m is a modified Archimedes number $\left(Ar_m = 8a^3 g\rho_f\left[\rho_p - \rho_f\right]/\mu_f^2\right)$; ρ is density; μ is viscosity; a is the radius of particles; g is the acceleration due to gravity; and Re_p is the Reynolds number. The subscripts f and p represent fluid and particles, respectively.

Equation (2.6) shows that the convective heat-transfer coefficient increases with both the size and density of the particles. Since both the conduction and convection heat-transfer modes increase with increasing density, reducing the bulk density of mould fluxes is an effective way of enhancing their insulation capacity. Furthermore, because the total heat-

transfer rate also depends on the particle size and packing geometry, it can be concluded that insulation is also dependent on particle size range and particle geometry since these two determine the packing arrangement.

Bommaraju[14] reported that physically blended powders for LCAK steels present an average particle size around 20μm and that it is important to keep the particle size distribution to within a window of 10 to 80μm to restrict stratification of the fines and coarse particles. Depending on the specific raw material, these physical blends can have a loose-packed density ranging from 0.9 to 1.2g/cm^3, and provide excellent thermal insulation during low-throughput situations such as a tundish switch or shroud change.

Taylor and Mills[39] measured the thermal diffusivity of three different powders in vacuum and in a nitrogen atmosphere. The results, presented in Figures 2.20 and 2.21, show that the values recorded with a nitrogen atmosphere were twice those obtained in vacuum, which confirms the major role of convection in heat transfer through the unreacted powder layer.

Taylor and Mills[39] also found that the thermal conductivity increased with decreasing density, which they considered a surprising result since it contradicted the well known influence of bulk density on insulation characteristics of mould powders[2-4,14,15,22,40-42]. Their results also contradict the available knowledge on heat transfer in gas-solid packed bed systems[36-38,43]. The main problem with their conclusion is not the measured values themselves but rather their inability to provide any general correlation. Since the effective thermal conductivity is not only a function of density and average particle size, but also depends on the particle size range, particle geometry, conductivity of the particles and

convection parameters, the data is meaningless in the absence of a complete characterization of the powders.

Nakato et al.[15,41] reported that since the heat loss through the mould powder was controlled by convection, it could be minimized by adjustment of the thickness of the unreacted powder layer and its permeability; the latter could be controlled in the proper range by adjusting the shape of the flux particles and the sintering characteristics of the powder.

They also determined the sintering characteristics of mould powders by measuring the pressure drop of argon flowing through a steel pipe filled with powder. The pressure drop increased as sintering occurred and, therefore, could be used as an index for permeability as well as for sintering. Since convection controls the rate of heat loss, the permeability of the mould flux bed can be used as a measure of insulating characteristics.

Nakato et al.[15,41] found that the pressure drop through the unmelted layer of mould powder at room temperature varied inversely with the square of average diameter of the particles (Figure 2.22). Figure 2.23 shows the change in pressure drop with heating. The abrupt decrease at about 800-900°C marks the initiation of rapid sintering of particles. The pressure drop for mechanically mixed powders was the highest, followed by spherical and cylindrical granules, respectively. This is explained by the fact that naturally packed cylindrical granules, when compared to spherical granules, had larger and continuous air gaps between particles, which favors gas flow, thus resulting in greater convective heat transfer. They concluded that in order to enhance heat insulation, the air gaps between mould powder particles should be discontinuous and small, while keeping a low value of bulk density.

The general opinion in the literature is that satisfactory insulation is usually obtained by (i) low bulk density[2-4,14,15,22,40,41], and (ii) maintaining a dark cover throughout the cast by

adding a sufficient quantity of fresh powder to areas which begin to glow and produce flames, before any melted flux is exposed[3,5,14].The carbon content of the flux, its type and grain size distribution, also influence the insulation capability of the flux by retarding its sintering and melting[2,4,10,22,44].

A total powder thickness of 25 to 30mm is recommended to provide a dark-cover practice. Bommaraju[14] suggested that around the SEN a thicker layer of unreacted powder, should be maintained because heat transfer from the SEN accelerates the melting of the surrounding powder causing excessive liquid generation. Lack of insulation could lead to bridging between the SEN and the mould wall.

Mould fluxes for ultra-low carbon steel must have a low-carbon content to prevent carbon pick-up. In order to compensate the loss in insulation capacity due to the low carbon level, the powder density should be reduced. One effective way of achieving this is to use hollow granules. The bulk density of such mould fluxes can be as low as $0.5g/cm^3$[14,41]. The usage of spherical semi-hollow mould powder was also reported[42] as an effective means of improving insulation at the meniscus.

The utilization of exothermic mould fluxes seems to be an increasing trend[26,40,45]. These powders were found to be effective in reducing pinholes for low carbon, aluminum-killed steels cast at high speeds[26,40]. For high-carbon steels, the temperature at the meniscus increased by 3 to 4°C when exothermic powders were used. The higher temperature at the meniscus helped to stabilize the melting and consumption rate of these fluxes and also resulted in a more homogeneous subsurface structure with smaller hooks at the bottom of oscillation marks.

2.3.6 Molten Structure and Melting Rate

The melting of a mould powder, particularly its melting rate, has a significant effect on powder performance since it determines the ability of the flux to maintain a stable liquid pool depth; which is required to maintain an adequate and continuous supply of molten flux to the mould/strand gap.

When the melting rate is too high, it is not possible to maintain a stable layer of dark, unreacted powder on the surface of the mould. This instability can result in intermittent exposure of the molten pool ("red-practice"), which increases the heat losses, eventually leading to formation of "floaters", growth of a large flux rim and freezing of the steel meniscus. On the other hand, if the melting rate is too low, the lack of molten flux will lead to an uneven infiltration of the flux into the strand/mould gap, resulting in strand defects such as longitudinal cracks and possibly breakouts[14,40,46-48].

Ogibayashi et al.[46] investigated the melting behavior of 15 prefused-type, granulated powders with viscosity varying from 0.5 to 3.8 poise and vitrification ratio between 25 and 90%. The vitrification ratio was defined as the percentage of molten flux formed when 25g of powder were unidirectionally heated at 1400°C for 7 min. in an alumina crucible. When the vitrification rate exceeded 80%, the flux tended to form a thick flux rim and caused partial solidification of the liquid steel surface in the mould. When it was too low the index of longitudinal cracks increased. In order to prevent such defects, they established an optimum flux pool depth of approximately 10mm, which corresponded to an optimum vitrification rate of about 60%.

2.3.6.1 Molten structure

A number of studies involving laboratory melting tests[1,6,47,48] and plant sampling[19,29,47,49] have shown that the flux covering the liquid steel surface in the mould consists of different layers, as mentioned earlier. In the study by Emi et al.[6] the melting mode of different powdered and granulated mould fluxes were examined in laboratory. The granulated fluxes were found to melt in a layer-by-layer fashion, forming a granule/sintered/half-molten/melted structure. Powdered or partially pulverized granules did not undergo a layer-by-layer melting process, but exhibited many islands of molten flux inside the sintered layer.

Sakuraya et al.[29] studied the influence of the carbon-particle size on the melting behavior of premelted fluxes by examining samples taken from the mould. They found that fine carbon particles delayed the coalescence of individual droplets of molten flux and favored the formation of a thin layer of semi-molten material, whereas coarse particles led to the formation of large agglomerates of liquid flux. The first kind of powder, containing mainly finer carbon particles, was termed α-type and the second β-type. Compared to β-type, α-type powder exhibits a thinner semi-molten layer and a steeper temperature gradient; consequently it provides better thermal insulation and more stable melting behavior.

Xie et al.[48] studied the dependence of the molten structure of mould fluxes on the type and amount of carbon used. Depending on these variables, they reported three different kinds of molten structure, as shown in Figure 2.24. When the content of carbon black , the finest type of carbon, was more than 2%, they obtained a double layer structure consisting of raw material and liquid flux. For carbon black less than 1.5%, or for coarse graphite, the fluxes exhibited a three-layer structure: raw material/sintered layer/molten flux. When carbon black

and graphite were simultaneously used, but carbon black did not exceed 2%, a multi-layer structure formed consisting of the raw material or unreacted layer, the sintered layer, a semi-molten layer and the molten flux.

2.3.6.2 Melting rate

Various tests have been developed to determine the melting rate of mould powders: Serge cone or button, crucible test and molten slag drip tests.

Seger cone or button[6,7,29]: The time required to melt either a cone or flux button (cylinder) placed inside a furnace is utilized as an index of the melting rate. These tests, however, are inadequate to represent the melting conditions in the mould, i.e., the unidirectional heat flow.

Crucible test[1,6,16,47]: An alumina crucible filled with mould powder is unidirectionally heated at 1400°C for a set time. The crucible is cooled then cut through the center and the height or % of liquid flux is taken as an index of the melting rate - the % of liquid flux formed was termed the vitrification rate by Nippon Steel[16,47]. Mills[1] reported that this test was found to perform reliably.

'Molten slag drip' tests[1,7,21,30,44,48,50]: Each of these tests uses an apparatus similar to the one shown in Figure 2.25 which was originally developed by Lidefelt and Hasselström[44]. The samples are heated to 1400°C~ 1500°C and the conical base of the crucible allows the liquid flux to drip out of the furnace into a vessel which is continuously weighed. These tests provide a more realistic measurement of the actual melting rate than the previously mentioned methods, but the results can be affected by the fluidity of the flux formed[1,50].

Mills[1] observed that although these tests cannot completely simulate the conditions in the mould, they are used to identify the influence of key parameters, such as: (i) the chemical and mineralogical components of the flux and (ii) particularly the size, type and amount of carbon in the powder, on the melting rate of mould fluxes.

Free carbon controls the flux melting by providing an inert barrier between the solid particles and /or liquid flux pools. Because carbon is not soluble in the liquid flux, its particles form a skeleton which prevents, or hinders, the agglomeration of liquid flux droplets[1,3,6,7, 14,29,47, 48]. Not only is the level of the carbon content important, but so is its type, as shown in Figure 2.26. As far as type of carbon is concerned two parameters are important: the grain-size distribution and the ignition temperature. Lampblack or carbon black, due to its fine size is the most effective in delaying the melting of mould[3]. This is because it is able to coat each particle in a mould flux. Graphite also is effective in delaying mould powder melting. It is available in smaller particle sizes than coke dust and has a higher ignition temperature than both, carbon black and coke dust[14]. Higher ignition temperature leads to longer burn-off times that favor the skeleton effect (i.e., delays in the melting of the flux). But, the use of graphite has been limited because its higher cost.

Riboud and Larrecq[21] determined the melting rate of several casting powders in an apparatus similar to the one shown in Figure 2.25. The results confirmed that the free carbon content of the powder had a profound influence on the rate of fusion and that powders with similar overall chemical composition could have different rates of fusion. The latter led to the conclusion that the mineralogical nature of the powder constituents influences the melting rate. Also a relationship between either viscosity or T_{liq} and the rate of melting could not be established. However, in plant trials they observed that the flux pool depth was very sensitive

to T_{liq}, which is a strong indication that the melting rate of a flux depends on its liquidus temperature.

Kawamoto et al[51] investigated the effect of carbon content, bulk density and the carbonate content of mould powders on its melting rate. The results confirmed the influence of carbon content and particle size and also showed the effect of bulk density and carbonate content, as can be seen in Figures 2.27 and 2.28. They concluded that the increase of melting rate with carbonate content was due to the elevation of the specific thermal conductivity caused by the gas generated during the decomposition of the carbonates.

Based on their experimental results, Kawamoto et al. [51] established an empirical equation for the melting rate of mould powders, given by:

$$R_m = 16.8\ \Sigma K^* (\%\text{carbonate}) - 0.00336 C_v + 0.0477 \qquad (2.7)$$

where R_m is the melting rate (mm/s), K^* is the decomposition reaction rate of carbonate at 1623 K and C_v is the carbon content per unit volume, i.e., C_v=(weight percent C × mould flux bulk density).

2.4 Behaviour of the Flux in the Mould

Once the flux has been added to the mould, two major phenomena occur: (i) the powder is heated in contact with the liquid metal, melts and feeds the surface with a liquid phase, and (ii) the liquid phase spreads over the steel surface and infiltrates into the strand/mould gap during the oscillation cycle. The infiltrated flux solidifies in contact with the water-cooled copper mould wall and forms a solid layer; against the strand shell, a molten flux layer remains, which ensures the lubrication of the strand-mould interface.

2.4.1 Melting

According to Nakano et al.[47] the melting process experienced by a flux in a continuous casting mould can be divided into the following stages:

(1) After being added into the mould the powder is heated but still retains its original structure and morphology. *(2)* As the heating proceeds, the carbon in the powder begins to burn. Some parts of the base material contact each other, which starts a sintering process. This sintering process advances with the further heating of the powder and combustion of the carbon. *(3)* The base material begins to melt, forming droplets of molten flux surrounded by carbon particles. As the carbon particles are consumed, the melted base material coalesces. *(4)* A molten flux pool is formed.

2.4.2 Molten Flux Pool Thickness

The molten flux pool formed above the meniscus of the steel acts as a reservoir which ideally provides a continuous supply of liquid flux to the mould/strand gap. It is important that this flux pool has sufficient depth to feed the gap adequately at all times. It has been reported that the depth of the flux pool increases with increasing casting speed and melting rate, and decreasing "melting" temperature of the powder[49]. It is also affected by the powder consumption rate and the mould dimensions.

While mould powder is melting to form the flux pool, the liquid lubricant flows into the strand/mould gap; therefore, the flux pool depth is a balance between consumption rate and melting rate. Since the consumption rate decreases with increasing casting speed while the melting rate tends to increase due to a higher thermal input in the mould, it is expected that the flux pool is deeper at higher casting rates. However the opposite has also been reported

for some specific flux compositions and steel stirring intensities[29,49]. Figure 2.29 shows the relationship among consumption rate, casting speed and flux pool depth.

Riboud and Larrecq[21] observed in plant trials that the flux pool deepened with increasing cast speed. They concluded that it was caused by the greater supply of heat to the mould when the casting speed increased, i.e., the vertical heat flux through the flux layers increases which accelerated the melting rate of the flux.

Figure 2.30 shows the response of the liquid pool depth during a steep increase in casting speed. It can be seen that initially the increased demand for molten flux, not immediately compensated by a higher melting rate, resulted in a decrease in the flux pool depth. However, a higher melting rate ensued due to increased heat transfer associated with the higher casting speed. The result was a gradual increase in the pool thickness, until a new steady-state condition was established[1,7,21,29]. During such transient casting conditions the flux infiltration is greatly reduced, which can lead to breakouts. Sakuraya et al.[29] found that the uniformity of melting could be ensured over a larger range of casting speed by using fine grained carbon (α-type powder).

The depth of the molten pool has been measured by "slag dip" tests in which a probe constructed from Fe and Cu wires is inserted into the mould for two to three seconds. Since the melting points of Fe and Cu correspond approximately to the temperatures of the liquid steel and the molten flux, the difference in the lengths of the two wires yields an estimate of the depth of the flux pool[1,14,47,49]. Figure 2.31 shows one of these devices, in which an aluminum wire was employed as well to determine the thickness of the sintered layer. An eddy current sensor for measuring the thickness of molten flux was reportedly developed and applied at Nippon Steel [52], but sustained performance of the device was not yet proved.

Riboud and co-workers[21,49], using the "slag dip" test, observed very significant depth variations as a function of time and position in the mould. As shown in Figure 2.32, the flux pool is thinner in the vicinity of the mould narrow faces and is thicker close to the SEN. They also observed that the flux pool deepened as the flux melting temperature decreased and the melting rate increased[21]. The latter was thought to be caused by a decrease in the amount of micron-size carbon particles. This was confirmed by Nakano et al.[47] who showed that the flux pool thickness was dependent on the amount of carbon black. They also showed that agitation on the liquid steel surface accelerated the melting of mould fluxes and increased the thickness of the flux pool.

A flux pool thickness in the 10 to 15mm range has been recommended as an optimum value[5,15,30,46,53]. For higher casting speeds Mills[1] recommended a minimum of 20mm; however, this value was not supported by other workers. Bommaraju[14] recommended a minimum thickness of 6 to 12mm, which is in the same range reported by Tsai and Mastervich[54].

It is generally accepted that the flux pool depth should be larger than the oscillation stroke length. Tsai and Mastervich[54] suggested a value between 1.3 to 1.5 times the stroke length in order to avoid the entrapment of unmelted mould powder into the cast strand; however, Sardemann and Schrewe[5] argued that the current tendency to work with small stroke lengths (about 6mm), in order to reduce the depth of oscillation marks leads to very low values of flux pool depths. Depending on the steel flow rate from the SEN, waves with a height between 5 and 10mm can be formed on the liquid steel surface; thus the values recommended by Tsai and Mastervich would not be adequate to prevent entrapment.

Nakano et al.[47] suggested a minimum flux pool depth(Y_P) given by:

$$Y_p = S\sin\left(\frac{\pi N}{2}\right) - \frac{500NV_c}{f} + \delta \tag{2.8}$$

where S is the stroke of mould oscillation (mm), f is the frequency of oscillation (cycles/min.), Vc is the casting speed (m/min.), δ is the molten steel surface oscillation (mm) and N is the negative-strip ratio, which is given by:

$$\mathrm{N} = 1 - \left(\frac{2}{\pi}\right)\sin^{-1}\left(\frac{1000\,\mathrm{V_c}}{\pi\,\mathrm{Sf}}\right) \tag{2.9}$$

2.4.3 Modeling of Melting Behavior

Niggel and Felder[50] derived a system of equations for calculating the depth of the liquid flux layer which Mills[8] presented as follows:

$$d = \left(\frac{a}{V_f}\right)\ln\left[\frac{(1-f)C_{p,\ell}(T_m - T_{liq})}{\Delta H^{fus} + C_{p,s}(T_{liq} - T_{amb})}\right] \tag{2.10}$$

Where a is the thermal diffusivity of the liquid flux; C_p and ΔH^{fus} are the heat capacity and enthalpy of fusion of the flux, respectively; f is the fraction of volatiles in the powder; V_f is the rate of flux descent and T_m, T_{liq} and T_{amb} are the temperatures of the metal, flux melting point and the surroundings respectively. The subscripts s and ℓ represent the solid and liquid phases of the flux, respectively. Although Equation (2.10) seems very attractive in its simplicity it was incorrectly represented by Mills since its logarithmic part always renders a negative number.

Delhalle et al.[49] developed a steady-state mathematical model to describe the behavior of the casting powder on the free steel surface. They solved the general heat-conduction equation using an implicit finite-difference method for a system consisting of steel, liquid flux

and solid powder. They found that the liquid flux depth increased with decreasing powder melting temperature and increasing effective thermal conductivity of the flux. For a given melting temperature, the flux depth decreased with increasing consumption and as long as the surface temperature remained below 800°C ("dark-practice"), the flux pool depth did not change significantly with the powder layer thickness.

Nakano et al.[47] investigated the melting and flux pool formation behavior with the aid of a mathematical model. Figure 2.33 shows the basic configuration of the model. They integrated the transient one-dimensional heat-transfer equation using a finite-difference scheme. Figure 2.34 shows a comparison between measured and calculated values of the flux pool depth. They found that the effective thermal conductivity of the molten flux pool was 4 to 6 times the thermal conductivity reported in the literature. This difference was attributed to convection in the pool.

Goldschmit et al.[55] investigated the sensitivity of the liquid pool depth to variations in the mould powder properties and operational parameters by means of a finite-element model. From their sensitivity analysis, they concluded that the most influential controlling factors were (1) the melting temperature of the powder and (2) the consumption rate.

2.4.4 Formation of Flux Films

At the beginning of the casting sequence some of the molten flux infiltrating into the mould/strand gap freezes against the mould wall. The resultant flux film consists of solid and liquid layers which typically have thickness of 1-2 and 0.1-0.2mm, respectively[1,3]. Frictional forces ensure that the solid layer is held against and travels with the mould, whereas the liquid layer travels with the strand. In the lower half of the mould the thermal contraction of the shell results in the formation of an air gap located between the mould and the solid flux layer.

The flux film solidified against the mould, which usually consists of a glassy layer produced by the quenching of the molten flux against the mould, remains unaltered; closer to the liquid flux layer, the solid flux tends to be crystalline during the casting sequence. The examination of flux films formed in trials where (i) a starter powder was used and (ii) a tracer was added to the mould 20 minutes after the beginning of casting, revealed that the flux layer which adhered to the mould had no tracer for distances of up to 0.6mm from the mould wall[46].

The crystalline zone, between the glassy region and liquid film can form gradually from the glassy layer, when the local temperature is above the temperature of crystallization of the flux[1,22], or possibly, directly against the mould when the flux basicity or Na_2O content is high[1]. As outlined earlier, the presence and relative thickness of the crystalline layer depends on basicity, Na_2O and Al_2O_3 contents, and carbon particles[15,26]. High basicity and high Na_2O content enhance crystallization while high Al_2O_3 content favors a vitreous structure. Carbon particles promote crystallization by providing nucleation sites for the transformation[1]. The relative proportion of these two phases is important since they have different thermal properties.

The solid flux film thickens with increasing flux viscosity and decreasing heat flux from strand to the mould. The heat flux is dependent upon the thermal resistance of the mould/solid flux interface which is largely due to the structure of the solid film -glassy or crystalline- and to the air gap formed by the thermal contraction of the flux which may be dependent upon its mineralogical constitution.

2.4.5 Infiltration of Molten Flux

The infiltration of liquid flux into the mould/strand gap is the key process in continuous casting since it is necessary to ensure both good lubrication and uniform heat transfer between the strand and the mould. Failure to provide these conditions can result in the formation of surface defects and sticker breakouts.

The molten flux is pumped into the strand/mould gap by the action of the descending mould wall and the solid flux rim attached to it during the downward movement of the mould[6,56,57]. In principle, the mould flux can be drawn back upward during the upstroke of the mould but this is resisted by the movement of the meniscus toward the mould during positive strip which, at least partially, seals the gap. Anzai et al.[58] confirmed this behavior by a mathematical model. They found that a positive pressure exists during the downward movement of the mould and a slight negative pressure occurs during most of the upward movement.

Obviously it is difficult to observe the infiltration of the flux into the mould strand gap. However some insight into the infiltration process can be derived from examination of flux films collected at either the bottom of the mould or from the frozen shell formed in the mould when casting is interrupted. Mills[1] reported that Lainez et al. found that coherent flux films are probably formed by most low-viscosity fluxes, while flux with a high viscosity of 13 poise at 1300°C produced an intermittent film.

2.4.6 Mould Flux Consumption

Information on powder consumption gives basic data concerning the infiltration and lubricating characteristics of mould flux. Assuming homogeneous flux infiltration, it is possible to define an average thickness of consumed lubricant. This value gives a reasonable

approximation for the thickness of the liquid lubricating film, since there is evidence to suggest that about 90% of the consumption arises from the provision of the liquid flux film[1].

However, as pointed out by Riboud and Larrecq[22] the thickness calculated from consumption values should not be confused with the actual overall thickness of the flux film present between the strand shell and mould wall. The latter is several times greater than the former, due to the presence of the solid layer attached to the mould wall and to velocity gradients in the infiltrated layer. Furthermore, a substantial amount of flux can be entrapped in oscillation marks. The overall thickness has been found to be 1-2mm and the liquid layer calculated from consumption values is generally below 0.1mm[3,22].

The average quantity of infiltrated flux is evaluated by weighing the mould powder added during a period of time at constant casting conditions. The loss on ignition of volatiles and carbon must be subtracted and the start-up of the casting sequence must be excluded. Bommaraju[14] suggested that the first 10 minutes should be excluded because of the demand for fresh powder to provide a cover for the surface of the steel.

Mould powder consumption has been expressed in different forms, such as kg/ton of steel, kg/m^2, and kg/min. However, because the consumption depends upon the size of the cast slab and is proportional to the surface of the strand, the amount of powder consumed per unit of strand surface area (kg/m^2) is most suitable for evaluating the lubrication capability of mould fluxes.

Measured average consumption lies in the range 0.30 to 0.60 kg/m^2[5,13,23,30,59-62], or 0.3 to 0.7 kg/ton of steel[2,6,15,22,45,54]. Values over 1.0 up to 1.2 kg/ton of steel have been reported for low viscosity powders (~ 1.0 poise @ 1400°C) and low casting speed (0.5

to 0.7 m/min.)[63]. High consumption can be an indication of surface defects such as flux entrapment and deep oscillation marks; on the other hand, consumption below 0.25 kg/m^2 may lead to breakouts due to insufficient lubrication.

Nuri et al.[63] investigated the consumption pattern in the direction of the mould width. The researchers found that consumption was highest close to the narrow faces, lower by the region around the SEN and lowest in between these two regions and also that consumption increased with lowering flux viscosity. They showed that the consumption pattern varied greatly for high viscosity fluxes and was relatively uniform for low viscosity fluxes, as shown in Figure 2.35.

The consumption has been found to increase with decreasing flux viscosity, casting speed and mould oscillation frequency[1,5,13,23,30,60-66], and decrease when both liquid steel temperature and powder melting rate decrease[60,62,63]. Figure 2.36 shows the relationship between powder consumption and casting speed for two different mould oscillation frequencies.

Several modeling efforts have been undertaken but reasonably accurate prediction of consumption has not been achieved[21,50,63,67]. Takeuchi et al.[67] found that the flux consumption, was highest when the downward mould velocity was maximum and confirmed that mould powder consumption decreased with increasing casting speed. Although their model is the most comprehensive lubrication model in the literature surveyed its results do not agree well with measured values of powder consumption.

Another approach to predict flux consumption is to establish empirical equations by regression analysis of plant trial data. Wolf[60] fitted the effect of primary casting parameters to obtain the following equation:

$$Q = 0.55\left(\frac{60}{f}\right)\left(\frac{1}{\eta V_c^2}\right)^{0.5} + 0.1 \qquad (2.11)$$

where: Q is the consumption (kg/m^2), f is the frequency (cpm), η is the viscosity@1300°C (poise), and V_c is the casting speed (m/min.). Wolf suggested that Equation (2.11) was subjected to bias since it was obtained under common operating practice in which casting speed and oscillation frequency were not varied independently. By using a set of data obtained for two independent oscillation frequencies he established the following equation:

$$Q = 1.8 \times 10^{-4}\left(\frac{1}{\eta V_r^2 t_c}\right) \qquad (2.12)$$

Where: V_r is the relative strand/mould velocity (m/min.) [$V_r \equiv V_{r,max.}$ during positive strip time], and t_c is the cycle time (seconds). Figure 2.37 shows a comparison of measured flux consumption with predicted values using Equation (2.12).

Kwon et al.[62,13] established the following regression equations, for flux consumption corresponding to two groups of carbon content and the range of casting variables shown in Table 2.7,

(1) %C<0.08:

$$Q = \left(\frac{0.40}{A^{0.5}}\right)\left(\frac{60}{f}\right)\left(\frac{1}{\eta V^2}\right)^{0.5} + 0.22 \qquad (2.13)$$

(2) 0.08≤%C≤0.16:

$$Q = \left(\frac{0.74}{A^{0.5}}\right)\left(\frac{60}{f}\right)\left(\frac{1}{\eta V^2}\right)^{0.5} + 0.17 \qquad (2.14)$$

Where: Q is given in kg/m^2, η is viscosity in poise@1300°C, f is frequency (cpm), and A is the half stroke (mm).

The empirical equations previously presented can be quite useful for estimating the effect of changes in one or several of the casting parameters on mould powder consumption. One inherent drawback with these equations is that they can only be used with confidence for the same range of casting variables under which the original data were obtained.

2.5 Lubrication

In the upper part of the mould, due to high temperature and fairly uniform pressure, the liquid frictional forces are operative whereas in the lower mould region, solid-solid friction may arise from contact between the solidified flux, or the strand, and the mould[22,61,68]. The total friction force is given by the sum of the liquid and solid frictional forces.

Assuming that the velocity gradient between the mould wall and the strand surface is linear, which is an approximation since the static pressure gradient and the transverse temperature gradient affect the velocity gradient, the liquid frictional force F_ℓ is given by the following [46,59,61-62,68-69].

$$F_f = \frac{\eta(V_m - V_c)A}{d_f} \tag{2.15}$$

Where V_m and V_c are the mould velocity and casting speed; η is the viscosity; d_f is the thickness of the liquid flux layer; and A the area of the mould/strand contact.

Thus liquid friction is expected to decrease when: (1) the viscosity of the flux decreases; (2) the liquid flux film thickness, d_f, increases (which occurs when the viscosity of the flux and the casting speed decreases, and the frequency of mould oscillation increases); (3) the casting speed decreases; and (4) the surface area of the mould decreases.

Assuming that the coefficient of sliding friction is independent of the velocity, the solid friction is given by,[46,59-62,68-69]

$$F_s = \eta_s \times H \tag{2.16}$$

where η_s is the coefficient of sliding friction and H is the force resulting from the ferrostatic pressure $(= \rho g h)$.

The analysis conducted above implies that in the case of liquid friction controlling the mould wall forces, the force curve sensed by load cells is cyclical with a sinusoidal shape since F_ℓ follows the pattern of V_m; On the other hand, the force curve would be a square wave, i.e., F_s has a constant modulus and changes sign depending on mould velocity direction, if controlled by solid friction[69]. This behavior is shown in Figure 2.38.

The effect of mould flux properties on mould friction was investigated in a very comprehensive study on high speed slab casting by Gilles et al.[69]. Based on data from an instrumented mould, five mould powders were characterized through analysis of friction force profiles, as shown in Figure 2.39. Powders with low transition temperature, B and E, resulted in low friction and the shape of the friction curves was rounded, indicating a strong liquid friction component. Powder A with a high transition temperature, 1100°C, and low viscosity, resulted in high friction with an apparent strong component of solid friction. The shapes of the curves of powders C and F, with high transition temperature and high viscosity, also appeared to have a strong solid friction component. Gilles et al.[69] concluded that the shape of the friction curve was more a function of the transition temperature than of the viscosity for the range of variables in their study. A lower transition temperature means that liquid flux in the form of a lubricating film is present over a greater fraction of the mould length and thus provides a greater potential for hydrodynamic lubrication.

Data from different plant trials[22,69-70] revealed that frictional forces, as a function of casting speed, pass through a minimum value, as shown in Figure 2.40. Wolf[60] attributed

this behavior to a transition from liquid to mixed friction. High friction at low casting speed was thought to be caused by a lower average temperature in the flux film due to a lower slab surface temperature[22,60,69]. Wolf[60] believes that this could also be connected with an excessive mould flux consumption in the regime of low casting speed, which would lead to a liquid flux pool depth below the minimum required for stable flux infiltration. The increase in the friction force at high casting speed is caused by a decrease in the liquid flux film thickness and an increase in the relative speed between the mould and strand (V_m-V_c) [62,70]. The influence of casting speed on friction force must be examined carefully, since the friction force also depends on oscillation frequency[71]. The common practice of varying frequency with casting speed hinders assessment of the influence of each variable separately.

Mills[1] reported that plant trials carried out to measure frictional forces have shown that a decrease in steel temperature increased the frictional force and in some cases caused fluctuations in friction, presumably due to the concomitant increase of flux viscosity (i.e., F_f) and amount of solid friction, F_s. There are also contradictory findings concerning the influence of negative-strip time on the value of the frictional force.

2.5.1 Lubrication Modeling

The flow of flux in the mould has been of interest to several investigators, particularly the flow at the meniscus and through the shell/mould gap. Emi et al.[6] proposed that the pressure generated in the flux channel at the meniscus deforms the partially solidified shell and produces the oscillation marks. Also, Nakato et al.[15], Takeuchi and Brimacombe[56] and Anzai et al.[58] showed that the positive flux pressure during the negative-strip period, "indents" the shell to produce the oscillation marks. These models have concentrated mainly on the interaction between mould wall movement and strand shell deformation at the

meniscus. The lubrication aspect of the mould flux and the temperature dependence of flux properties were not considered. With regard to the flow of flux down the length of the mould, several models were developed[22,59,72,73]. These models obtained a solution of the Navier-Stokes equation making various simplifying assumptions. Some of the major drawbacks with these models are: (i) some do not provide information on the thickness of the flux film and a constant value must be provided[59,72], (ii) some do not take into account the oscillation of the mould[22,73], (iii) none of them take into account the variation of the temperature along the mould wall and the difference between the broad and narrow faces.

It can be concluded that a more comprehensive lubrication analysis is needed in order to characterize the influence of flux properties and casting parameters on the behavior of the infiltrated flux, and to predict their impact on the efficiency of lubrication and on the intensity of heat transfer through the mould. Further developments, like accounting for the flux melting and the presence of a flux rim, should also be undertaken.

2.6 Heat Transfer

Heat transfer in the mould is one of the most important phenomena taking place during the continuous casting of steel. Proper heat extraction by the mould results in slabs with good surface quality and prevents breakouts. If the rate of heat removal is excessive and/or uneven, thermally induced stresses, which may cause longitudinal cracks, are generated in the shell. On the other hand, insufficient heat removal can lead to a thin strand shell which is more prone to bulging and breakouts[74-76].

Heat from the liquid/solid steel interface is transferred to the mould by a sequence of steps, which consist of: (1) convection in the liquid steel pool, (2) conduction through the

strand shell, (3) heat transfer across the flux layer infiltrating the strand/mould gap, (4) heat transfer across any air gap separating the strand and the mould, (5) conduction through the mould walls, and (6) convection at the mould/cooling-water interface.

The largest resistance to heat extraction resides between the solid shell and the mould wall; therefore, the mould heat transfer is regulated by those factors determining the thickness of the gap separating the strand shell from the copper wall and the properties of the flux infiltrating the gap[74,77,78].

Several studies have been performed to analyze the influence of casting parameters on the heat transfer between the strand and the mould wall. Traditionally casting speed, steel composition and casting powder properties have been recognized as the major controlling parameters[74-79]. Mould geometry, oscillation frequency, SEN design, submergence depth and, recently hydrogen content in the liquid steel[75], also have been related to the heat flux in the mould. The effect of variables other than the properties of mould flux has been explained primarily in terms of gap dimensions; however, Mahapatra et al.[77] suggested that the effect of casting speed was more likely due to the higher heat transfer from steel to mould flux, which resulted in a hotter less viscous flux and reduced slag rim thickness.

Although this review acknowledges the influence of the above-mentioned parameters on mould heat transfer, the objective of this section is to highlight the influence of mould flux properties. Figure 2.41 shows a typical profile of mould heat flux determined from mould temperature data obtained in plant trials. The shape of the profile shown, with a maximum heat flux at the meniscus or just below it, decreasing values toward the bottom of the mould and a slight increase before the mould exit, has been reported as typical by the majority of investigators[4,22,23,59,74,77-80]. The decline of the heat flux with distance below the

meniscus is due to: (i) an increase in the gap separating the steel from the mould wall; (ii) an increase in the fraction of solid flux between the strand and the mould; (iii) an increase in the thickness of the solid shell; and (iv) reduced convection in the liquid core, thus decreasing heat transfer from the liquid steel to the solid shell. The increase in heat flux in the lower part of the mould is due to a reduction in the steel/mould gap as a result of locally excessive mould taper or binding[77,80].

The heat flux measured in plant trials has overall values between 0.8 and 1.9 MW/m^2, with peak values of 2.0 to 3.0 at the meniscus[1,74,77,79,80]. As shown in Figure 2.41, the mould heat flux is higher on the narrow face than on the broad face because the liquid steel streams from the bifurcated SEN are directed towards the narrow walls of the mould[77,80].

It has been found that the mould heat flux increases with decreasing viscosity, transition temperature, melting range and crystallization temperature[23,40,54,74,76,77,79]. Low viscosity favors infiltration of the molten flux in the upper part of the mould. A more fluid flux gives a higher flux consumption, and a thicker lubricating film; lower in the mould this film reduces the air gap between the mould and the shell. The influence of the flux viscosity on the mould heat transfer can be seen in Figure 2.42.

Emi et al.[40] found that the overall heat-transfer coefficient had a stronger correlation with the transition temperature than did viscosity. They concluded that a higher transition temperature allows a thicker solid flux layer to form between the mould and the steel and this acts as a heat flow barrier. Also there is less molten flux to effectively fill all the resultant air gaps toward the bottom of the mould due to contraction of the shell. However, a higher transition temperature gives rise to increased friction and a higher propensity for sticker breakouts because the extent of hydrodynamic lubrication is reduced. On the other hand,

when the transition temperature is low, the heat transfer in the mould increases which can exacerbate the formation of longitudinal cracks[40].

In addition to controlling the solidified mould flux thickness between the mould and strand shell by controlling the transition temperature of the flux, it is also essential to monitor the crystallization tendency of the mould flux. Fluxes with low crystallization temperature produce thicker glassy layers which enhances the heat flux, while high crystallization temperature fluxes produce a thicker crystalline layer which contain pores. The presence of pores in the solid flux layer reduce the heat flow across the faces of the mould and evens out transverse temperature gradients by decreasing the thermal conductivity of the flux[1,14,23,26,81]. Figure 2.43 shows the influence of the presence of pores in the crystalline layer on the heat flux in the mould.

2.7 Mould Flux-Related Defects

2.7.1 Surface Defects

2.7.1.1 Longitudinal face cracks

Steel grades with a carbon content in the range of 0.08 to 0.14% are particularly vulnerable to longitudinal cracking. The carbon effect has been attributed to the relatively large thermal contraction as δ-ferrite transforms to austenite near the meniscus giving rise to wrinkles in the solidifying shell. Due to the resulting non-uniformity of the mould/shell gap, local hot spots are created which concentrate tensile strains leading to longitudinal cracks.[82-84]

It is known that mould powder has a decisive influence on longitudinal cracking through: the overall heat flux between the strand and mould; high friction forces; and variations of heat

flux along the mould width direction[85-89]. Nakato et al.[87] showed that casting speed and mould flux characteristics are the most important factors influencing the mean heat flux in the mould; therefore, correct selection of mould flux is critical to controlling longitudinal cracking; reducing cast speeds is an undesirable option for productivity reasons.

Ogibayashi et al.[46] pointed out that to prevent longitudinal cracks, the thickness of the molten flux pool must exceed 10mm. Because the flux pool depth is controlled by the melting rate of the powder, the latter is an important factor in optimizing surface quality. They also proposed that the most stable conditions for infiltration of liquid flux into the mould/strand gap are established when the parameter ηV_c lies between 1 and 3.5. Within this range the variations of both the heat flux and liquid film thickness are at a minimum. Wolf[64] chose a different parameter, $\eta V_c^{\frac{1}{2}}$, to define optimum casting conditions and proposed that the overall heat flux and frictional forces are at a minimum when $\eta V_c^{\frac{1}{2}}$ is about 5. In both cases η is given in poise and V_c in m/min, and both parameters are in agreement with previous work carried out by Gray and Marston[85] who observed that in order to minimize cracking, the flux viscosity must increase as casting speed decreases. Mills[1] reported that calculated values of ηV_c and $\eta V_c^{\frac{1}{2}}$ from five different sources, for the condition corresponding to minimum longitudinal cracking, showed that optimum casting conditions occurred around ηV_c = 3-5 and $\eta V_c^{\frac{1}{2}}$ = 3-7 with the latter parameter showing the least variation.

Ogibayashi et al.[46] reported that longitudinal cracks can be reduced using powders with a high basicity (CaO/SiO_2) ratio. Fluxes formed by more basic powders are expected to contain a higher proportion of crystalline phases which should result in a decrease of mould heat flux, as indicated earlier. Therefore, fluxes having a high crystallization temperature are

well suited for crack-sensitive steel grades. Sardemann and Schrewe[5] showed that the occurrence of longitudinal cracks was clearly reduced when applying fluxes with basicity ratio above 1.1.

Work carried out at British Steel[86,89] confirmed that the frequency of longitudinal cracks can be correlated with the variability of the heat flux in the upper half of the mould, particularly in the meniscus region, and the lubrication index (LI), which represents the fraction of the mould enjoying liquid lubrication. Using moulds fitted with thermocouples to obtain thermal profiles, the *LI* was determined as follow:

$$LI = \frac{\text{distance from meniscus to position where } T = T_{transition}}{\text{distance from meniscus to mold bottom}} \qquad (2.17)$$

The lubrication index varies with the casting powder used and the casting speed. It was found that optimum surface quality was obtained using a powder with a lubrication index close to unity; powders with higher index values were found to produce a thin and unstable flux film which caused cracking.

Thornton et al.[89] found that the use of an exothermic starter powder, which was a fast melting flux, in conjunction with the normal casting powder, reduced substantially the severity of longitudinal cracks. They observed a significant reduction in the temperature variability in the mould plates when the starter powder was used. This improved performance was attributed to the formation of a stable film when the starter flux first infiltrated the mould/strand gap, in contrast to the unstable film formed by the normal powder. Since the solid flux film against the mould wall remains essentially unchanged during casting, the subsequent switch to the normal powder only affected the flux film on the strand side. While the latter film strongly influences lubrication, the former affects the mould heat flux because

the mould/strand gap is in fact formed between the mould and the solid flux layer against the mould.

It has been suggested that the best way to minimize longitudinal cracking is to produce a thin, uniform solid shell at the meniscus by reducing both the magnitude and the variation of heat flux.[86,90]. This has been achieved by reducing the heat removal at the meniscus level through decreasing the mould water flow rate or by machining grooves in the mould which provided air gaps between the mould and the solid flux film[90]. Subsequently, the shell thickness and mould temperature were found to be more uniform which resulted in improved surface quality for crack-sensitive steel grades[91].

Although the heat transfer can be controlled by selecting the optimum properties and composition of the powder, casting under uniform conditions is just as indispensable. Therefore, other sources of heat flux variation such as mould level variations, variation in casting speed and variation in shroud immersion must be kept under certain limits. Birat et al.[92] reported that 70% of longitudinal cracks were caused when the mould level variation was $\geq$ 10 mm, or casting speed variation was $\geq$ 0.2m/min., or the variation in shroud immersion was $\geq$ 40mm, or by a combination of all three.

2.7.1.2 Star cracks

Star cracks have been associated with the presence of copper in the surface of the strand and are usually generated in the lower half of the mould where the copper is scraped from the mould plates by the descending solid shell[82,86]. The cause lies in the phenomenon called hot shortness in which the low-melting copper from the mould plates is abraded and penetrates the strand shell through the grain boundaries. Because of the high strand shell

temperature, the copper remains liquid and prevents the formation of a solid inter-granular bond, resulting in cracks that run along the grain boundaries.

Although star cracking is usually overcome by plating Ni, Cr,or a multi-layer coating on the copper plates, the mould powder does exert an influence as well. Billany et al.[86] found that: (1) the severity of cracking correlated well with the magnitude of the heat flux variations, (2) the cracking decreased as the relative length of mould undergoing liquid lubrication approached 1.0 and (3) the use of a low-viscosity starter powder helped to reduce cracking by establishing a stable flux film in the mould/strand gap. They concluded that star cracks, like longitudinal cracks, are associated with variations of the heat flux and that this is possibly caused by spalling and cracking of the flux film in the lower half of the mould which would lead to mould-strand contact, thus solid-solid friction Consequently, in order to minimize star cracking, it is necessary to use a powder that provides liquid lubrication throughout the mould.

2.7.1.3 Oscillation marks and transverse corner cracks

The formation of oscillation marks is largely the result of the interaction between the casting flux and the mould movement. Howe and Stewart[93] observed that with oil lubrication, the depth of oscillation marks was virtually independent of mould oscillation frequency whereas with mould flux, the depth was inversely proportional to frequency.

Various mechanisms have been proposed to explain the formation of oscillation marks; the majority of them are based on the assumption that the first solid formed is bent inward during the mould downstroke, although there are different theories to explain the driving force for this movement[1,3,6,22,56,92-96].

The distance between oscillation marks, also called the pitch, can be evaluated by the following

$$\ell = \frac{V_c}{f} \tag{2.18}$$

where ℓ is the pitch, V_c is the casting speed and f is the frequency of mould oscillation. Equation (2.18) shows that the pitch decreases by raising the frequency. The depth of these marks is said to be dependent on the negative-strip time; the depth decreases by lowering negative-strip time which is obtained by raising the frequency or decreasing the stroke[1,3,6,60,65,97]. The depth and pitch of the oscillation marks are primarily determined by the mould oscillation characteristics, however the casting powder can also have an effect; both, the depth and pitch, were found to decrease as mould flux viscosity increased and powder consumption decreased[60,64,98].

Transverse cracks are found along the bottom of oscillation marks and may be initiated as hot tears in the mould region. They propagate along the grain boundaries during plastic deformation at bending or unbending.[88,97]. The factors influencing the occurrence of these cracks are considered to be the hot ductility of the steel and the depth of oscillation marks. This kind of defect is particularly prevalent in steels containing > 1% Mn and Nb or V, the last two as low as 0.05%, which exhibit very low ductility between 700 and 900°C. Deep oscillation marks create a large local thermal resistance between the mould wall and the shell surface and also cause non-uniformity of the shell profile and of the subsurface structure, and consequently are preferential sites for cracking. It has also been suggested that the bottom of oscillation marks can act as a notch to enhance the propagation of cracks. Because cracking

increases with greater oscillation mark depth, higher viscosity fluxes have been used to prevent the problem since these kind of fluxes can lead to shallower oscillation marks[59,98].

2.7.1.4 Surface inclusions

Inclusions trapped in the surface of the strand originate from casting powders and from reoxidation products, mainly Al_2O_3.The ability of the molten flux pool to absorb and dissolve inclusions plays a significant role in the reduction of the number of inclusions. As mentioned earlier, Riboud et al.[10,22] showed that the absorption of alumina through the metal/flux interface was always favored, so the ability to dissolve alumina is the controlling step. The ability to dissolve alumina is assisted by: (i) an increase in fluoride content; (ii) the replacement of Na_2O by Li_2O; (iii) an increase in basicity; and (iv) a decrease in the initial Al_2O_3 content.

2.7.1.5 Carburization of the strand surface

Carburization is a particular problem when casting ultra low-carbon steels. It mainly occurs in strand sections cast with turbulent, heavily fluctuating mould levels and can be especially high at the beginning of casting when the volume of liquid steel in the mould is low; turbulence tends to be high and the molten flux pool is not fully developed[1,3,41,44,99,100]..

Although, carburization of the strand surface can originate from the mould flux or refractories used in the tundish and SEN, it has been found that the recarburization is principally due to the powder[1,41,44,100,101].

Takeuchi et al.[101] found that surface carburization does not occur under stable casting operations but only takes place when a carbon-rich flux layer, formed between the sintered layer and the molten flux pool, contacts the steel solid shell. The importance of the presence

of the carbon-rich layer was confirmed by Terada et al.[100] who found that carbon pick-up takes place when liquid steel contacts unmelted mould flux, due to turbulence or mould level fluctuations. However, even if stable casting conditions are maintained, some carbon pick-up still occurs due to the enriched carbon layer, which was found to be 0.3 to 3 mm thick and has a carbon concentration 1.5 to 5 times higher than that of the original powder. Consequently, in order to prevent carbon pick-up, it is very important to decrease the enriched carbon layer, which was successfully achieved by adding MnO_2 to the mould powder. Additions of MnO_2, which is a strong oxidizing agent, increase the molten flux pool depth and decrease carbon content in the enriched layer; therefore, being very effective in minimizing carbon pick-up.

In general carbon pickup can be minimized by maintaining sufficient liquid flux pool depth combined with stable casting conditions, i.e. minimum turbulence in the mould, and reducing the fixed carbon content of the mould flux[2,100]. Bommaraju[14] suggested a carbonate content of the raw material base lower than 2% to reduce turbulence in the mould powder layers and to use hollow granules with least amount of carbon added. Nakato et al.[41] reported that high speed casting of ultra low-carbon steel slabs below 28 ppm in carbon have been successfully achieved by the use of mould fluxes with less than 1% free carbon; the amount of carbon pick-up was reduced to below 10 ppm at the beginning of casting and to below 2 ppm during steady-state casting. In order to reduce the carbon content of the mould flux without degrading melting and insulation characteristics they suggested spherical granules manufactured by a spray method.

2.7.2 Sticker Breakouts

Breakouts, in which liquid steel flows out below the mould, are the most troublesome aspects of continuous casting, resulting in significant costs and disturbance of production.

Emling and Dawson[76] estimated that a "typical" breakout for a slab caster can result in a cost approaching US$200,000. As the continuous casting process matured, the incidence of breakouts has changed from heat-transfer related to the present day predominance of mould sticking[76,104]. Tsuneoka et al.[104] reported that at Nippon Steel 79% of the breakouts were due to shell sticking while cracks represented 17% and scum entrapment 4%.

Sticking-type breakouts are induced by shell-sticking which starts at the meniscus with resulting shell rupture moving successively down the mould. Various mechanisms have been proposed to explain the occurrence of sticker breakouts. Emling and Dawson[76], Mills et al.[102] and Lu et al.[103] recently published very comprehensive studies on sticker breakouts in which these mechanisms were reviewed.

Studies of initial sticking based on analysis of friction force between the shell and the mould indicated that a large friction force brings about a shell rupture near the meniscus and the ruptured shell is stuck to the mould. Therefore it has been concluded that for prevention of sticking the friction force should be reduced by using low-viscosity mould flux or by increasing the flux film thickness, i.e., increasing flux consumption. It has been also reported that fluxes containing Li and Mg, fluxes with low melting point, and non-sinusoidal mould oscillation improve the flux consumption and reduce the friction force[105]. Some of these results were confirmed by Mimura[105] with the aid of mathematical models, who showed that high- viscosity flux, high casting speed, and high cycle mould oscillation, are likely to cause sticking while low-melting point fluxes and large flux pool depth reduces its occurrence.

Mould lubrication and the ability to maintain an open channel for molten flux infiltration is critical to reduce the occurrence of sticking type breakouts[23,40,59]. By decreasing the flux viscosity and its transition temperature, the mould flux consumption rate increases, which

enhances the liquid lubrication; therefore, reducing the friction between the mould walls and the strand shell and consequently reducing the occurrence of breakouts. However, low viscosity and low transition temperature favor a high mould heat transfer rate which can be a problem for steels with carbon content between 0.10%-0.14%, due to longitudinal cracking. The ability to maintain a constant inflow of molten flux between the mould walls and strand shell is related to the flux pool depth and slag rim thickness. An excessive slag rim growth can lead to conditions that obstruct the flux flow. Also, an inadequate mould powder melting rate can lead to a lack of molten flux for infiltration[40].

Table 2.1: Typical composition ranges for mould fluxes[2].

CaO: 25-45%	Na_2O: 1-20%	BaO: 0-10%
SiO_2: 20-50%	K_2O: 0-5%	Li_2O: 0-4%
Al_2O_3: 0-10%	FeO: 0-5%	B_2O_3: 0-10%
TiO_2: 0-5%	MgO: 0-10%	F: 4-10%
C: 1-25%	MnO: 0-10%	

Table 2.2: Composition range(wt%) of mould powders used in viscosity prediction models.

Model	SiO_2	Al_2O_3	CaO	CaF_2	Na_2O	MgO	Li_2O	B_2O_3
McCauley and Apelian [20]	27-48	10	23-42	0-12	4-15	-	-	-
IRSID [10]	34-56	0-12	8-46	0-18	0-22	-	-	-
NIPPON STEEL [16]	25-50	0-23	16-41	5-20	5-20	0-15	0-7	-
RIST [13]	V-ratio 0.7-0.9	0-15	V-ratio 0.7-0.9	(F) 0-12	0-15	0-13	0-10	0-15

Table 2.3: Equations for evaluating viscosity of mould fluxes.

MODEL	EQUATION	*A*	*B*
IRSID [10]	$\eta = A T \exp(B/T)$ η(Pa.s) T=temperature(K)	A=exp[-19.81+1.73(X_{CaO^*}) +5.82(X_{CaF_2})+7.02(X_{Na_2O}) -35.76($X_{Al_2O_3}$)]. X=molar fraction.	B=31140-23896(X_{CaO^*})- 46356(X_{CaF_2}) -39159(X_{Na_2O}) +68833($X_{Al_2O_3}$).
NIPPON STEEL [16]	$\ln\eta = \ln A + B/T$ η(poise) T=temperature(K)	$\ln A$=-0.242 Al_2O_3-0.061 CaO -0.121 MgO+0.063 CaF_2-0.19 Na_2O -4.8160. composition=mole %	B=-92.54 SiO_2+283.186 Al_2O_3 -165.635 CaO-413.646 CaF_2 -455.103 Li_2O+29012.564
RIST [13]	$\log\eta = \log A + B/T$ η(Pa.s) T=temperature(K) X=mole %	$\log A$=-2.307-0.046(X_{SiO_2})- 0.07(X_{CaO}) -0.041(X_{MgO})-0.185($X_{Al_2O_3}$) -0.035(X_{CaF_2})-0.095($X_{B_2O_3}$)	B=6807.2+70.68(X_{SiO_2}) +32.58(X_{CaO})+312.65($X_{Al_2O_3}$) -34.77(X_{Na_2O})-176.1(X_{CaF_2}) -167.4(X_{Li_2O})+59.7($X_{B_2O_3}$)

Table 2.4: Influence of V-ratio on crystallization temperature and crystallization index[15].

Powder	CaO/SiO_2	Crystallization Temperature (°C)	Crystallization Index.
L	0.97	1100	3
M	0.94	1100	2
N	0.89	850	0
P	0.82	room temp.	0

Table 2.5: Liquidus and solidus temperatures of different mould powders, ℃ [8].

Powder	B	C	D	I	J	K	M	P	Q	U
T_{liq} (Mills')	1212	1276	1192	1212	1215	1133	1212	1187	1125	1223
T_{liq} (Riboud')	1215	1260	--	--	--	1125	--	--	--	1230
T_{liq} (manufacturer)	1160	1260	1165	1182	--	--	1165	1165	--	--
T_{sol}	905	--	--	--	1000	--	--	--	1000	--

Table 2.6: Alumina pick-up and viscosity of LCAK mould fluxes at Inland Steel No.1 slab caster, after Bommaraju[14].

	1975-80	1980-85	1985-91
Alumina pick-up in mould slag (%)	10-12%	5-6%	2-3%
Initial viscosity of mould flux (poise @ 1300°C)	0.4	0.8	1.1
Operating viscosity of in-mould flux (poise @ 1300°C)	2.0-2.5	2.0-2.5	2.0-2.5

Table 2.7: Range of casting variables employed by Kwon et al.[62] to obtain Equations (2.13) and (2.14).

VARIABLE	LOW CARBON	MEDIUM CARBON
Flux viscosity@1300°C (poise)	0.33-0.86	0.70-2.37
Casting speed (m/min.)	1.20-1.65	1.00-1.50
Stroke (mm)	8-10	8-10
Oscillation frequency (cycles/min.)	99-134	81-130
Steel casting temperature (°C)	1557-1562	1539-1555

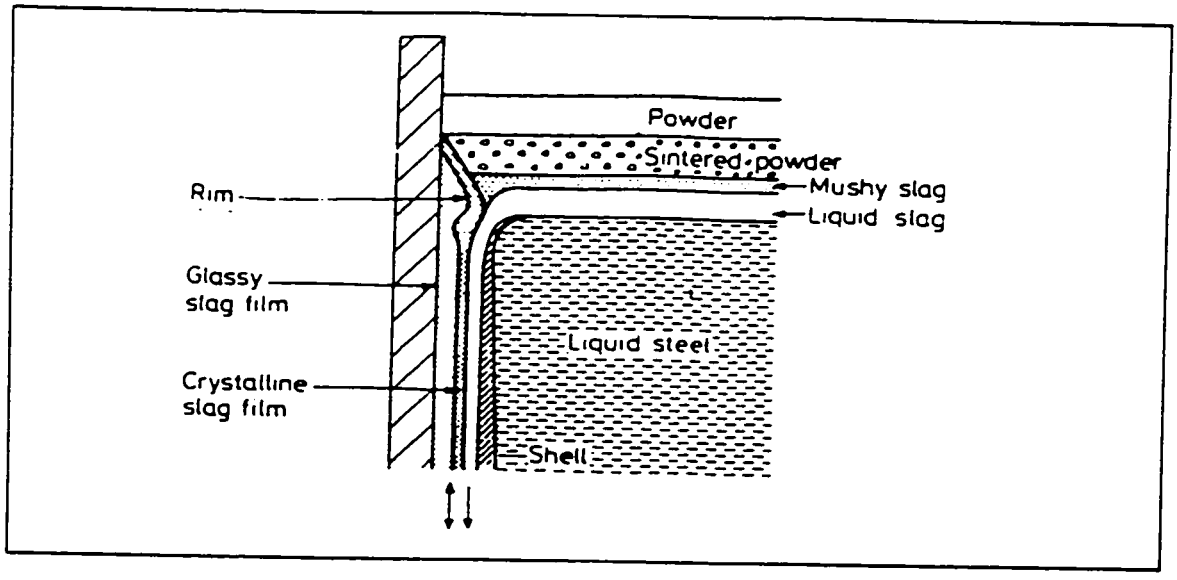

Figure 2.1 Schematic representation of a flux in the continuous casting mould.[1]

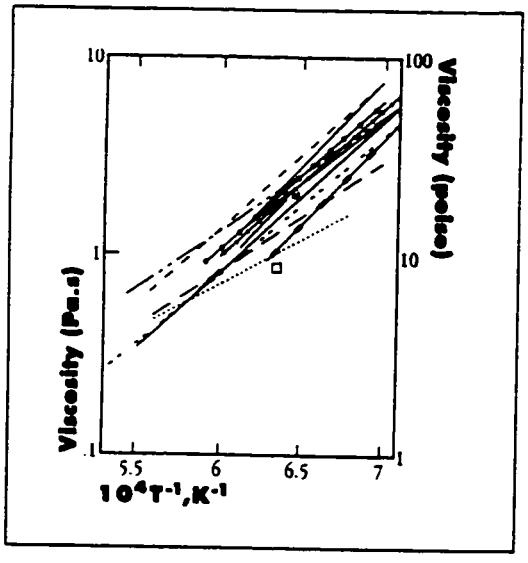

Figure 2.2 Viscosities measured in different laboratories as a function of the reciprocal temperature (K^{-1}) [1]

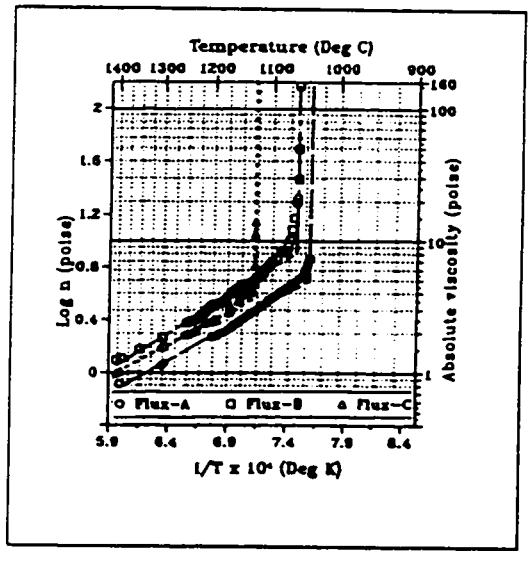

Figure 2.3 Viscosity vs. temperature relationship for different mould fluxes[14]

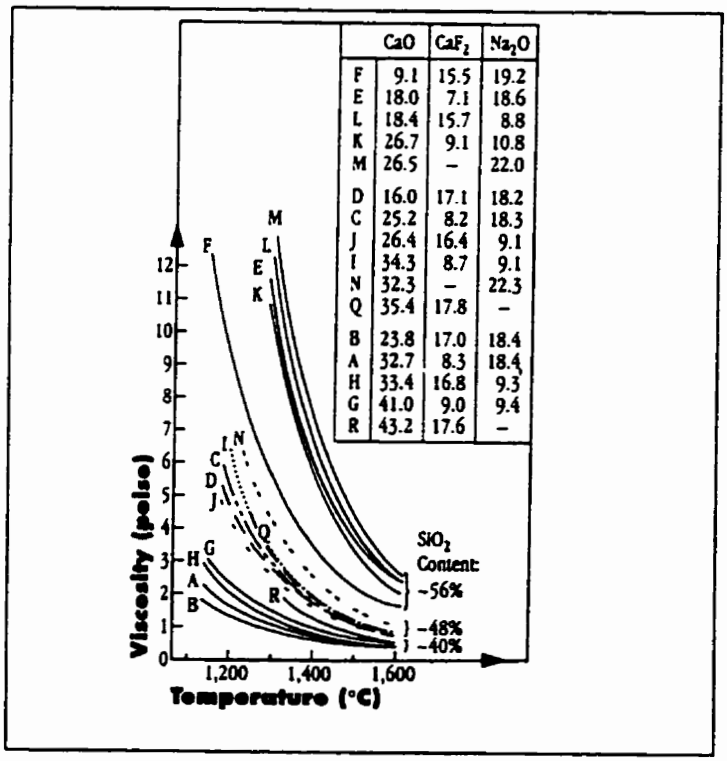

Figure 2.4 The viscosity of flux melts in the system SiO_2-CaO-CaF_2-Na_2O as a function of the temperature and silica content[4,10].

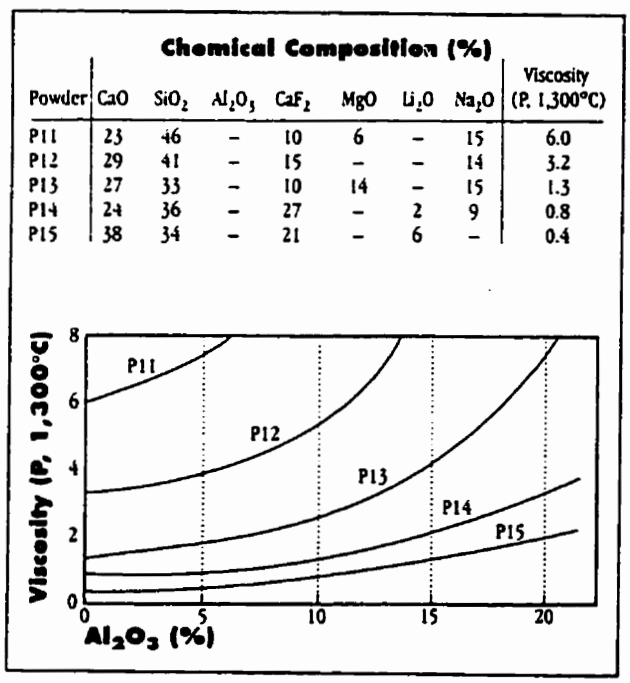

Figure 2.5 Change in the viscosity of the molten powder as a function of Al_2O_3 content[18].

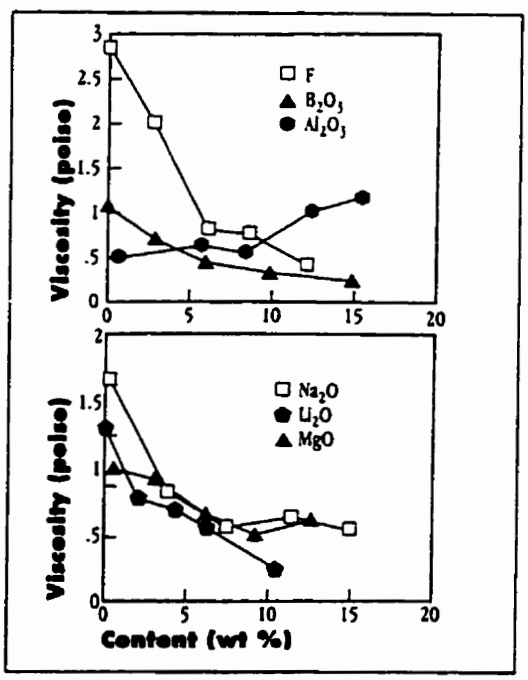

Figure 2.6 Effect of F, Al_2O_3, B_2O_3, Li_2O, Na_2O, and MgO content on the viscosity at 1300℃[13].

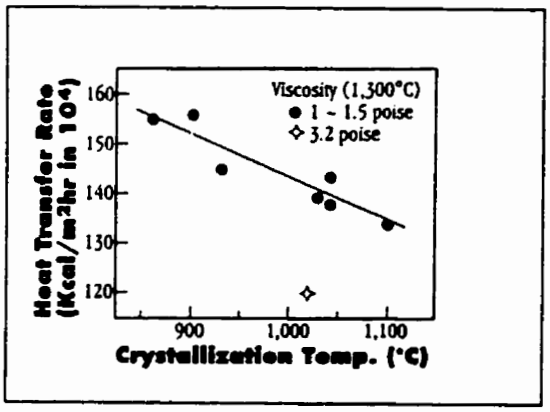

Figure 2.7 The relationship between crystallization temperature and mean heat transfer rate at 1.2 m/min.[23].

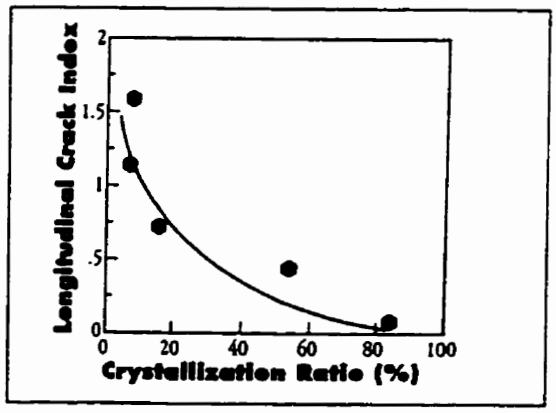

Figure 2.8 Effect crystallization ratio of mould fluxon on the occurrence of longitudinal crack in slabs[26].

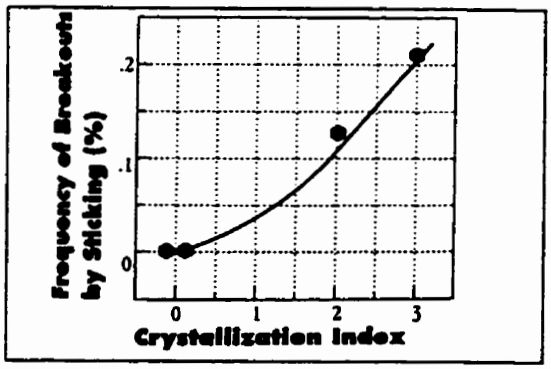

Figure 2.9 Effect of crystallization on the frequency of sticker breakouts[14].

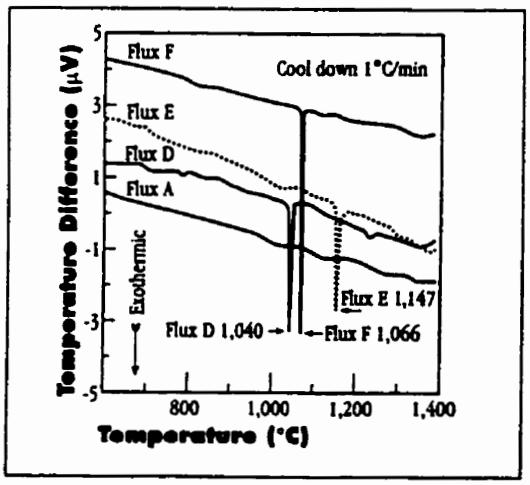

Figure 2.10 Thermal analysis curves for different mold fluxes[14].

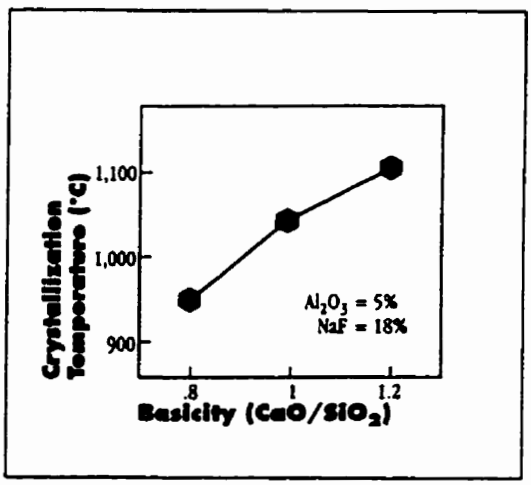

Figure 2.11 Influence of CaO/SiO_2 on crystallization temperature[23].

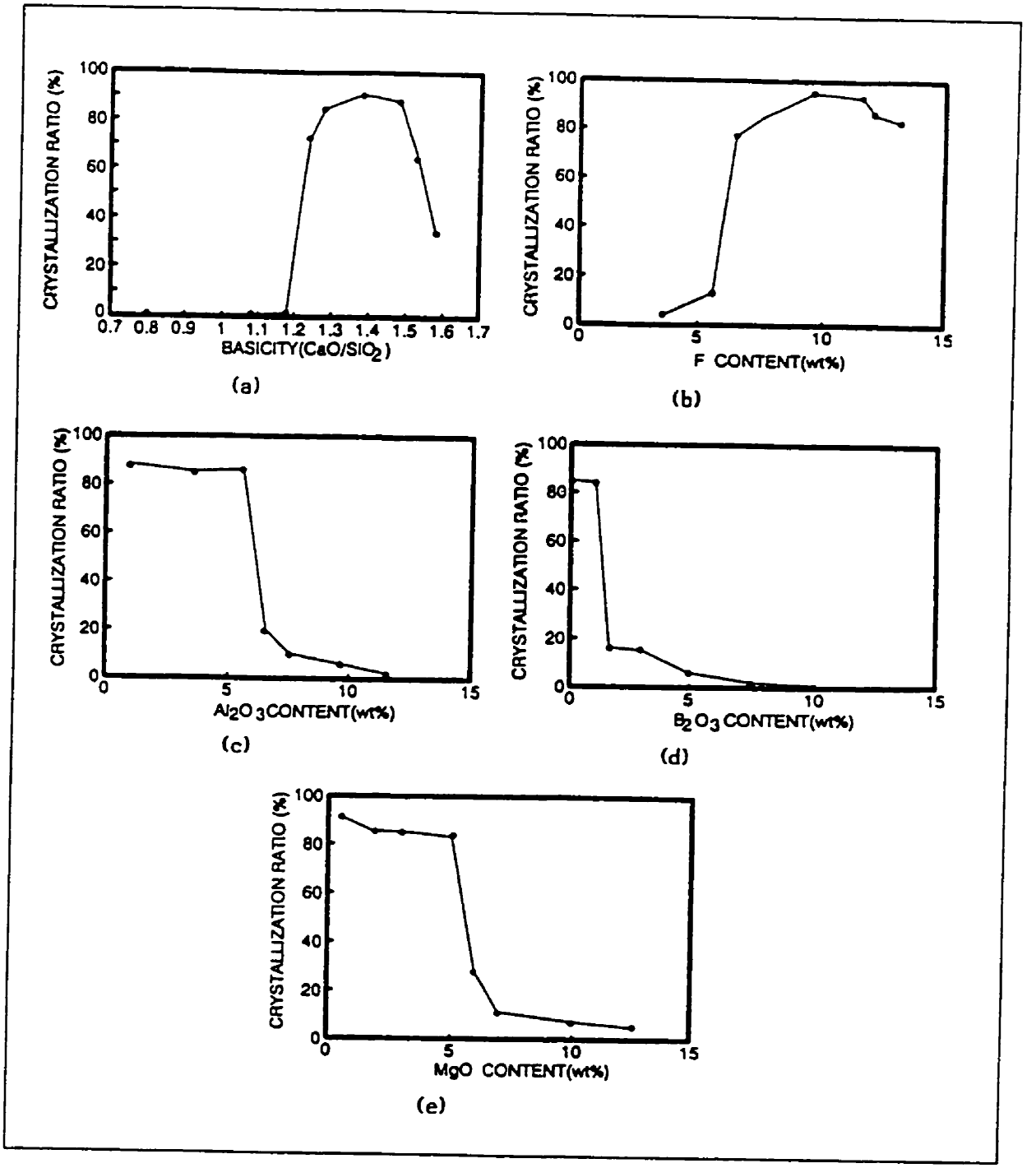

Figure 2.12 The effect of (a) basicity and (b-e) the constituents of mold flux on the crystallization ratio of mold flux film[26]

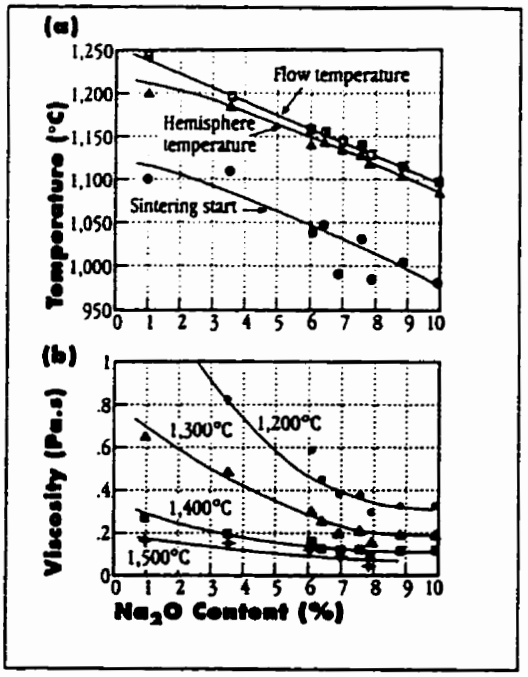

Figure 2.13 (a) Melting temperature and (b) viscosity as a function of the Na_2O content (F=5%)[19]

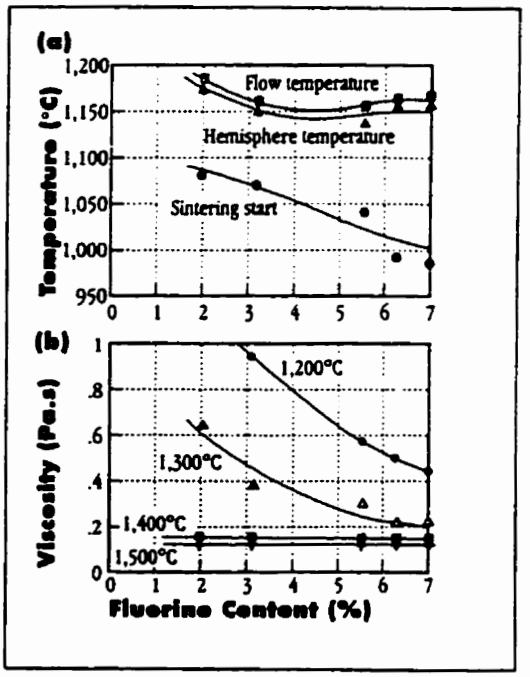

Figure 2.14 (a) Melting temperature and (b) viscosity as a function of the Fluorine content (Na_2O =6%) [19]

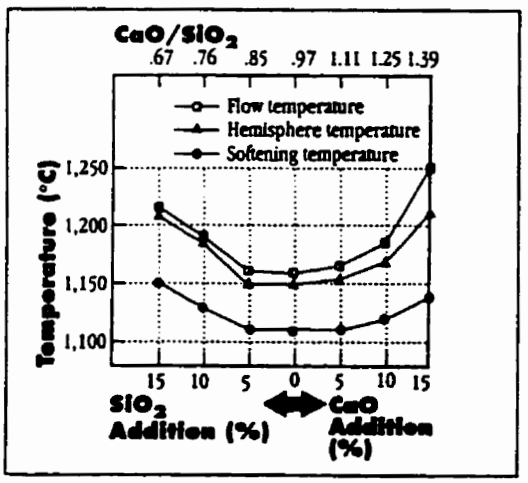

Figure 2.15 Melting temperatures as a function of the basicity CaO/SiO_2 [19]

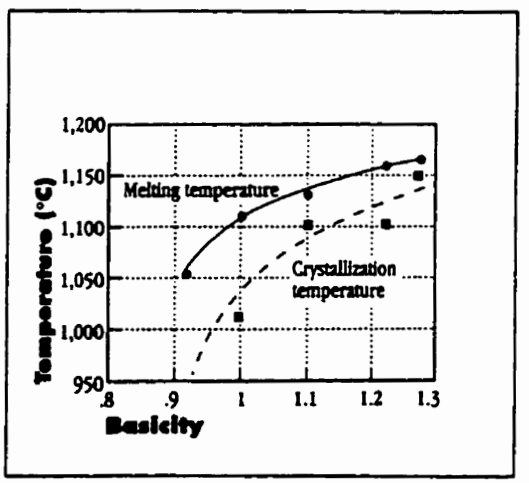

Figure 2.16 Influence of basicity on melting and crystallization temperature[5].

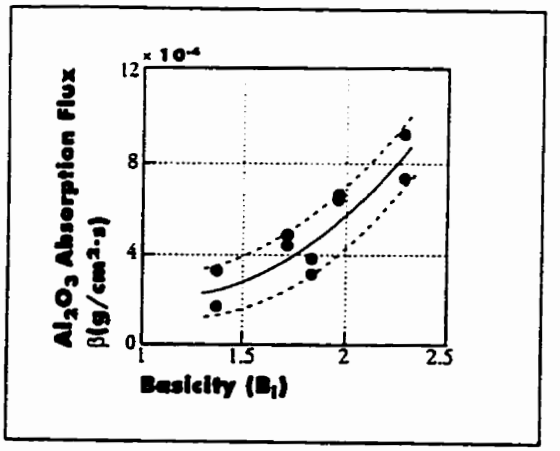

Figure 2.17 Relationship between basicity (B_i) and the Al_2O_3 absorption rate of the molten flux[18].

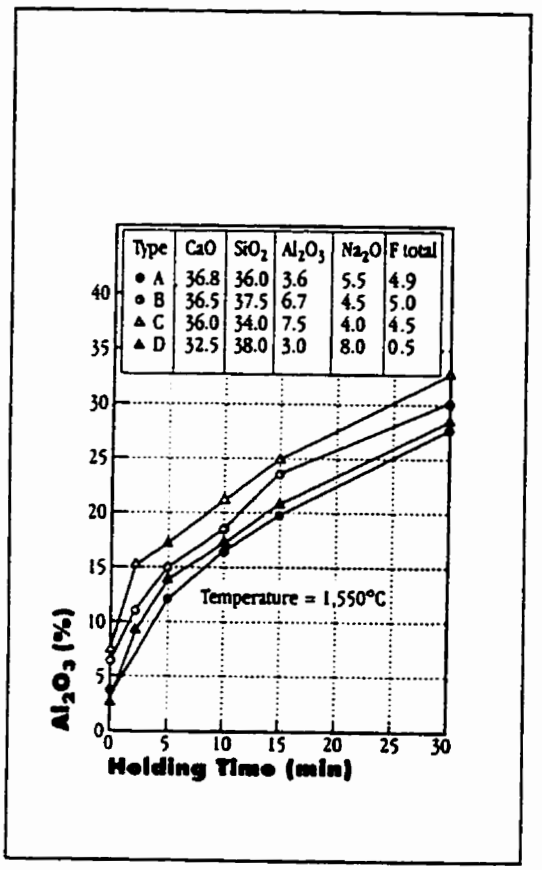

Fig. 2.18 Alumina pick-up by liquid mould flux[19]

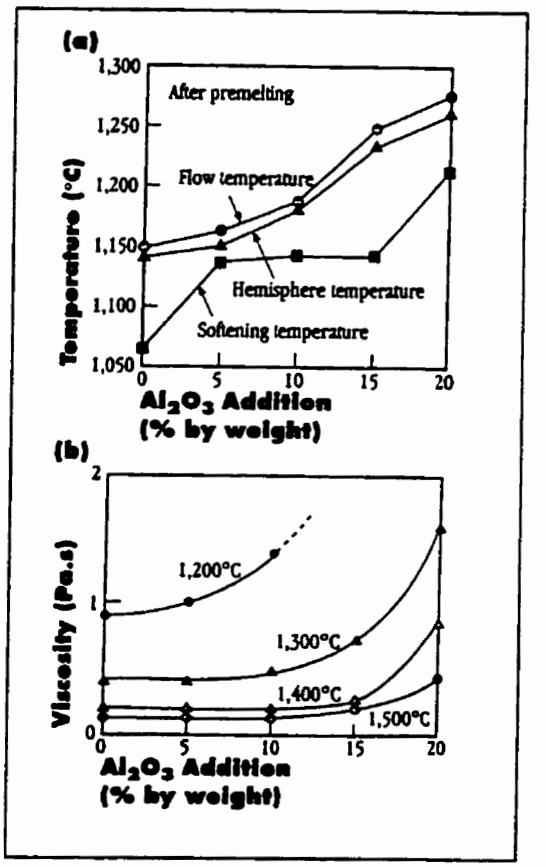

Fig. 2.19 (a) Melting temperature and (b) viscosity of mould flux as a function of alumina addition[19]

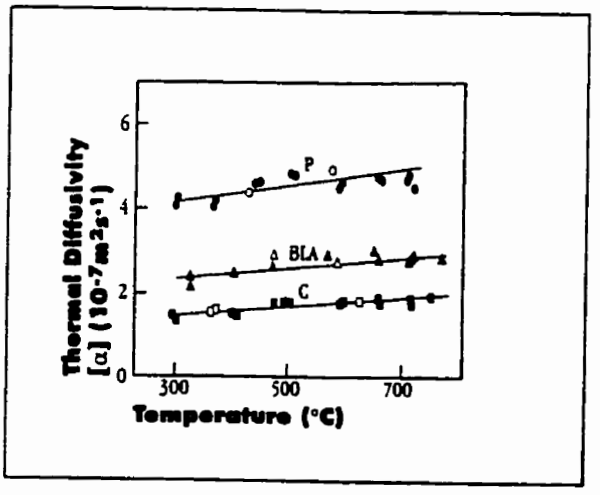

Figure 2.20 Thermal diffusivities of casting powders in vacuo; closed symbols heating cycle, open symbols cooling cycle[39].

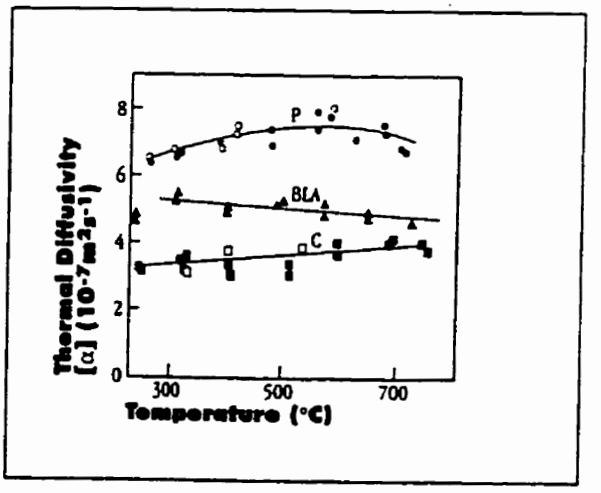

Figure 2.21 Thermal diffusivities of casting powders in nitrogen atmosfere; closed symbols heating cycle, open symbols cooling cycle[39].

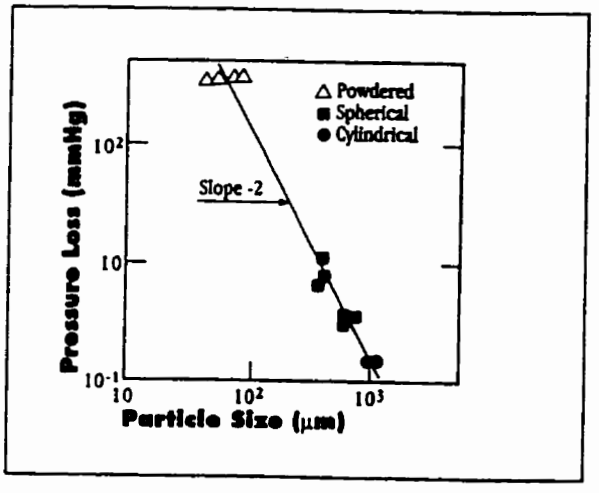

Figure 2.22 Influence of particle size on pressure drop of gas flow in unmelted flux layer[41].

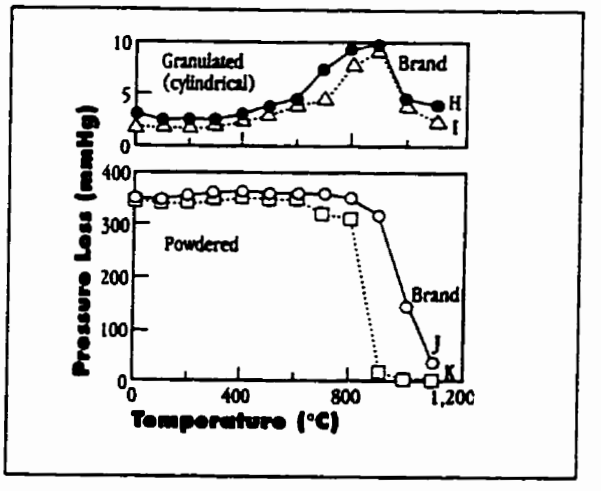

Figure 2.23 Change of pressure drop of gas flow with heating[41].

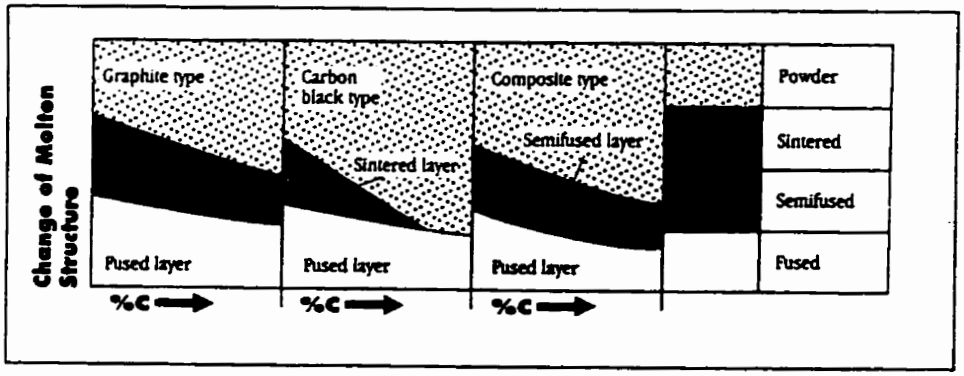

Figure 2.24 Effect of carbon on the molten structure of mold fluxes[48].

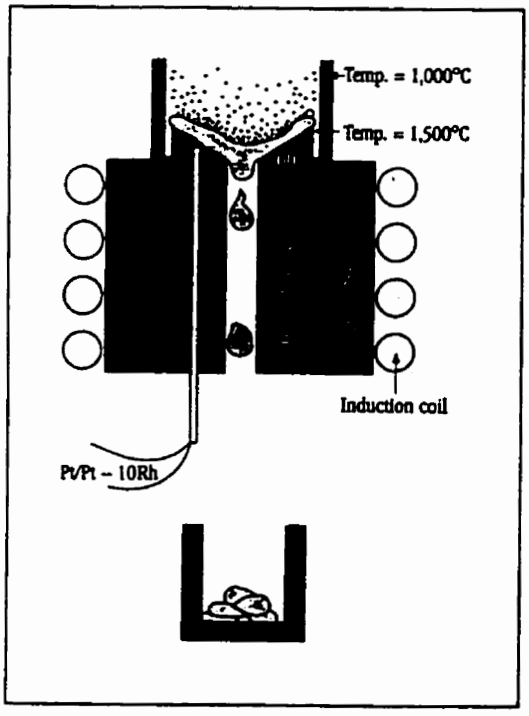

Figure 2.25 Schematic diagram of the apparatus used to measure the melting rate of mold fluxes[7].

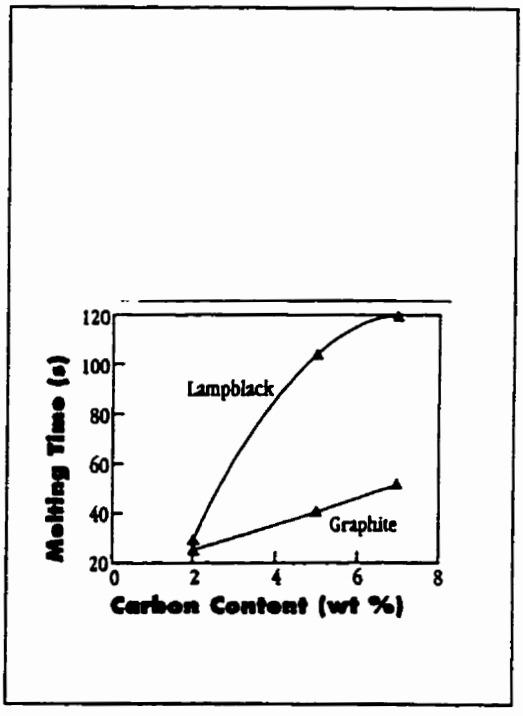

Figure 2.26 Effect of carbon type and amount on the melting rate of mold flux[7].

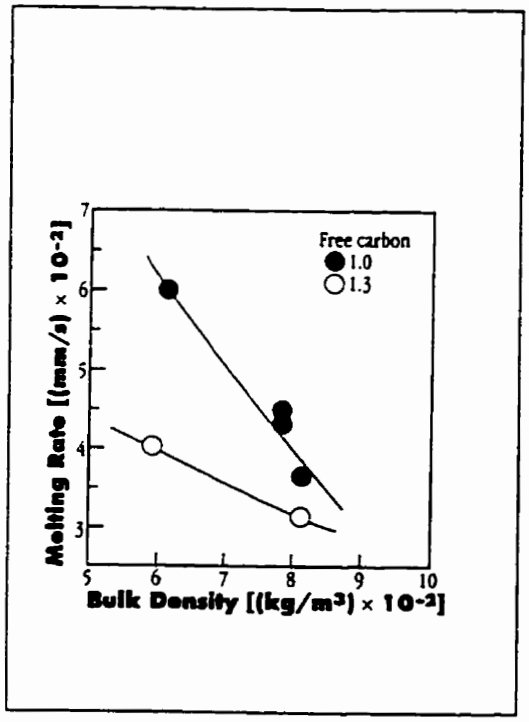

Figure2.27 Effect of bulk density on mould flux melting rate[51].

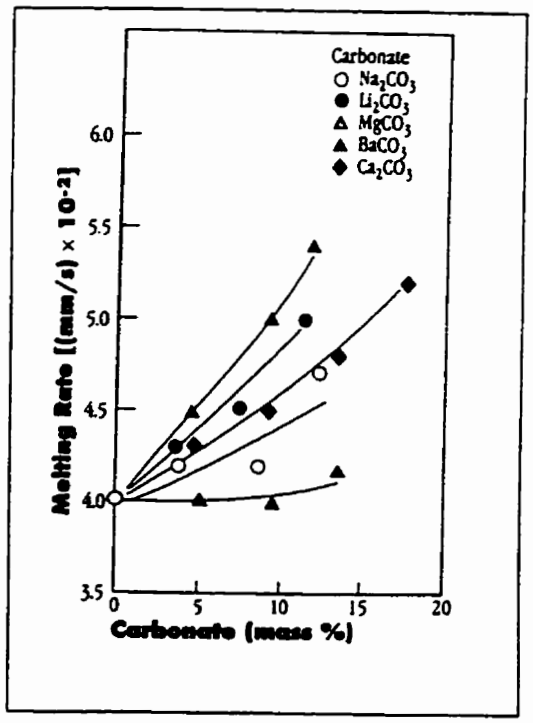

Figure 2.28 Effect of carbonate content on mould flux melting rate[51].

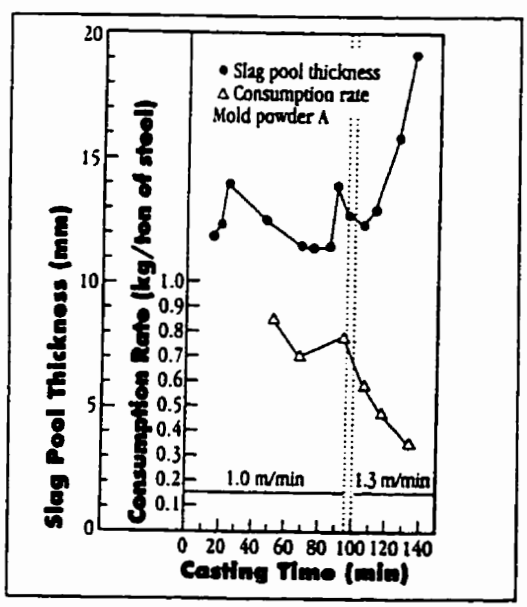

Figure 2.29 Variation of flux consumption and molten flux pool depth during casting[30].

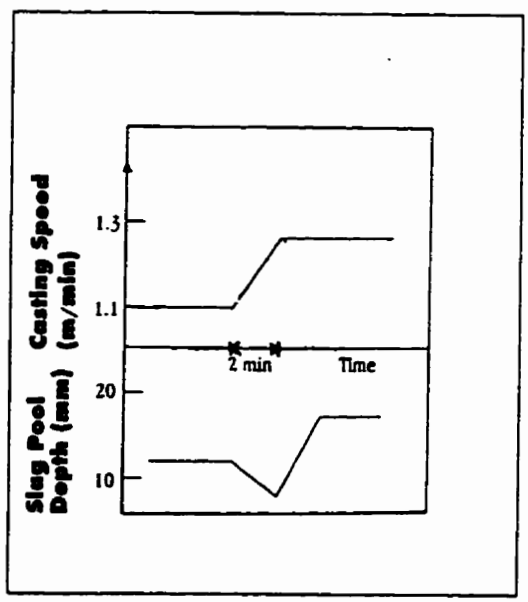

Figure 2.30 The depth of molten flux pool after an increase in casting speed[1].

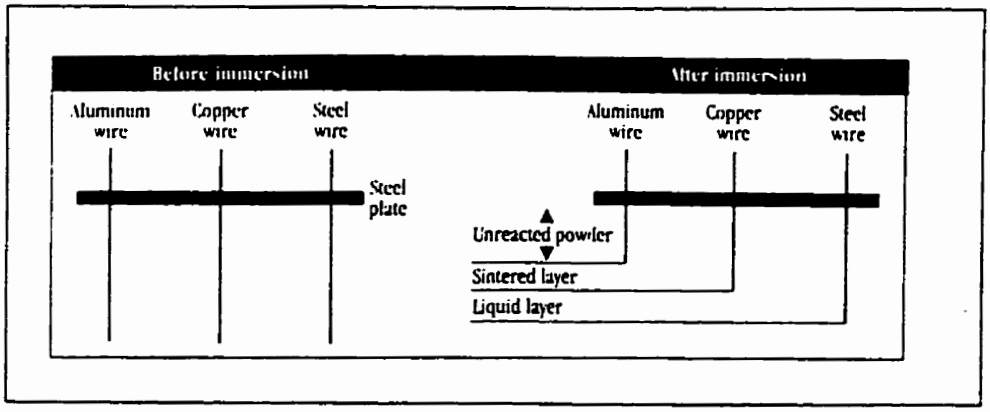

Figure 2.31 Three-wire method to characterize melting layers of mold flux[14].

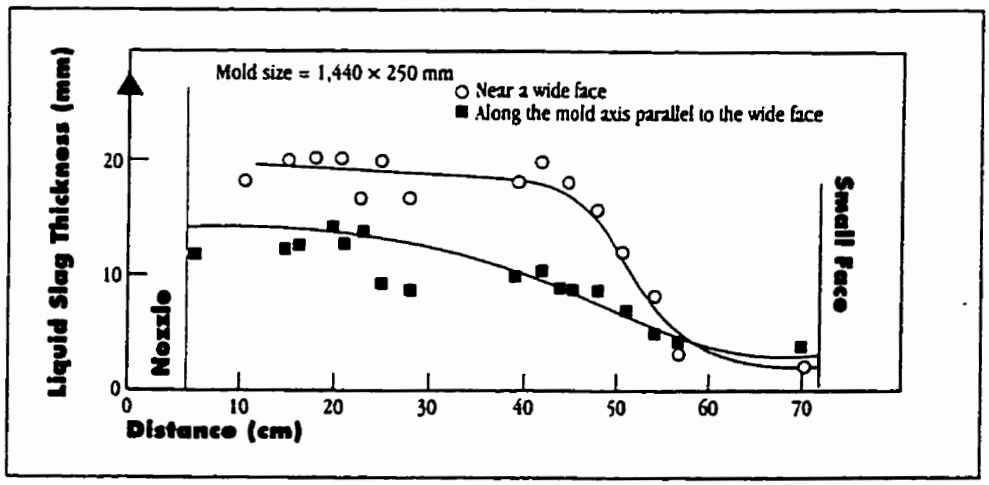

Figure 2.32 Molten pool depth as a function of the position in the mold measured with the two wire method[49].

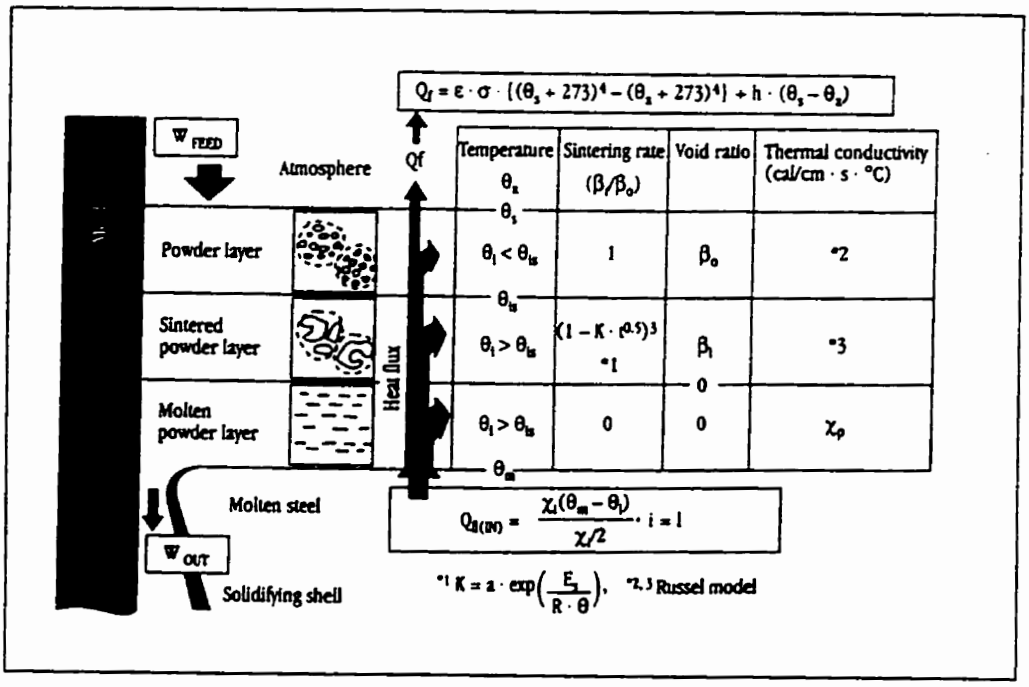

Figure 2.33 Model for melting process of mold powder in continuous casting[47].

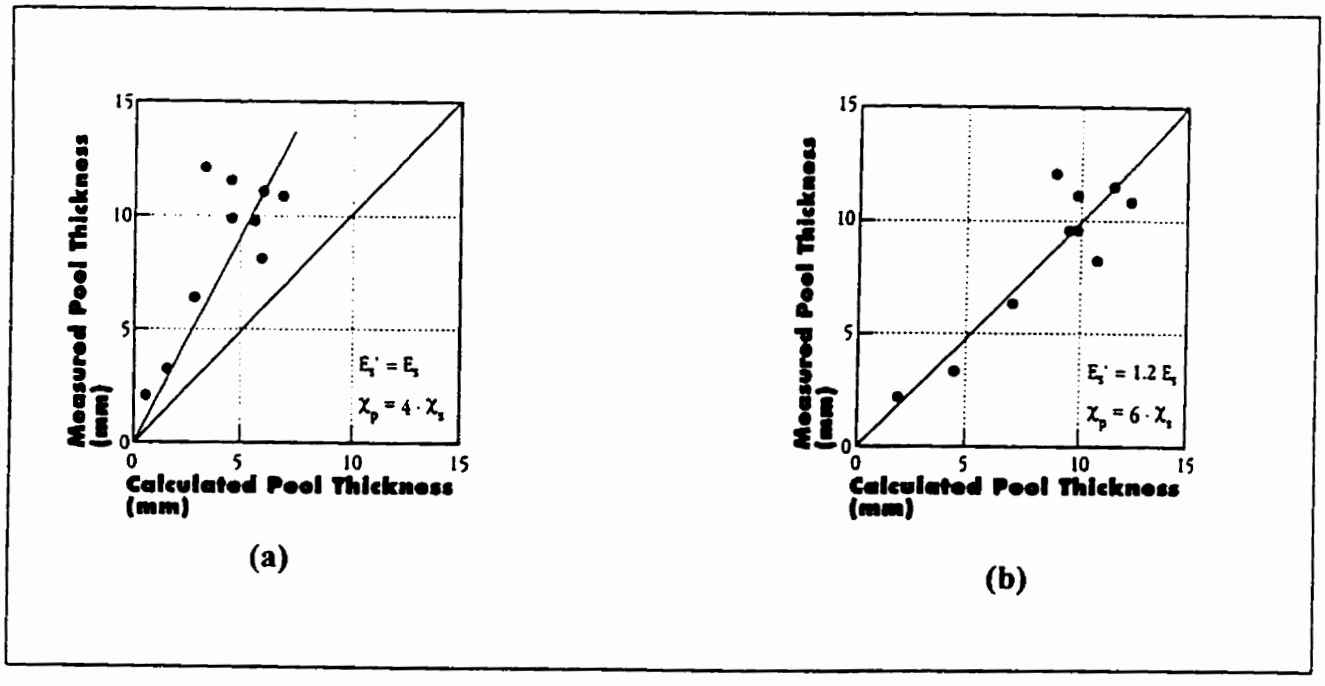

Figure 2.34 Comparison between values of pool depth measured in a continuous casting mould and calculated values; (a) thermal conductivity enhanced 4 times, (b) thermal conductivity enhanced 6 times and activation energy for sintering enhanced 1.2 times[47].

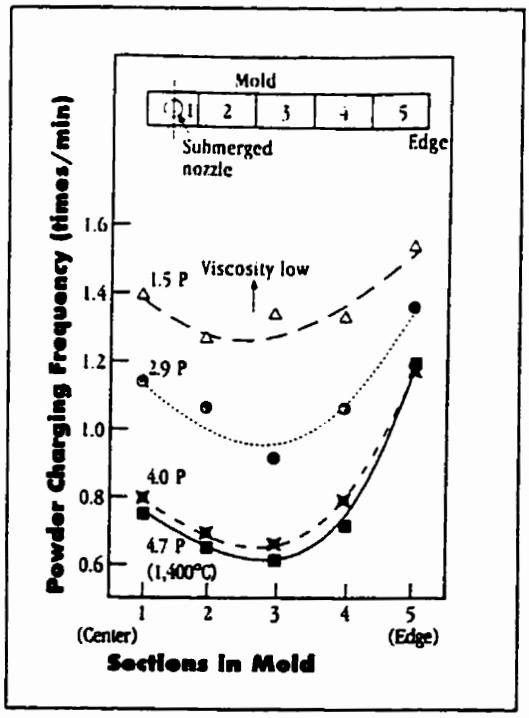

Figure 2.35 Influence of position in the mould and flux viscosity on powder consumption[63].

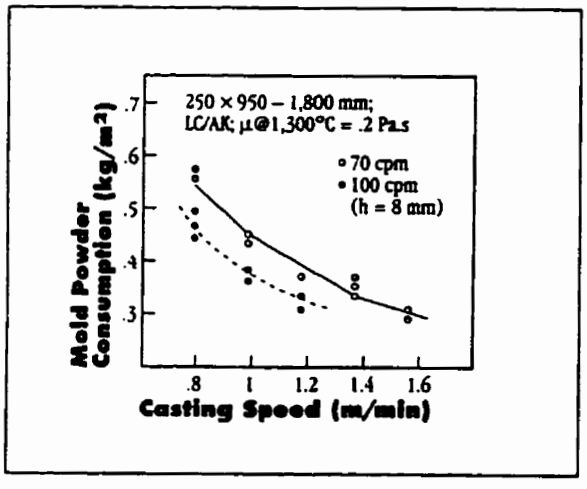

Figuer 2.36 Powder consumption vs. casting speed for two oscillation frequencies in slab casting[60].

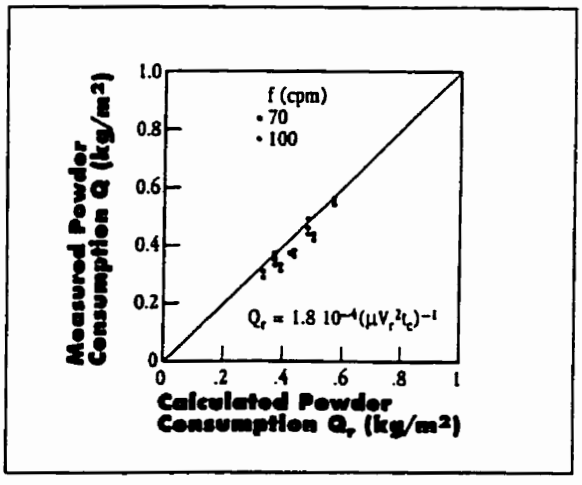

Figure 2.37 Comparison of measured powder consumption with predicted values, according to Equation (2.12) [60]

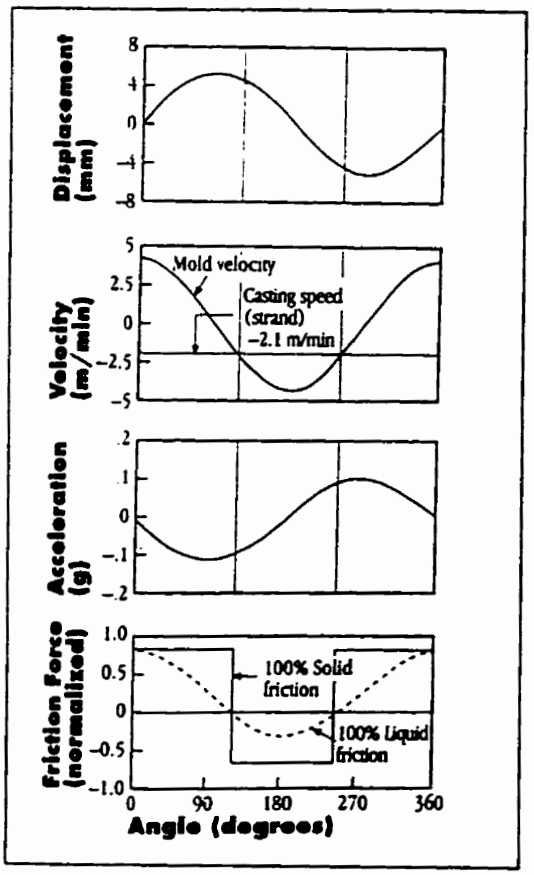

Figure 2.38 Displacement, velocity, acceleration and force curves in a continuous casting mold[69].

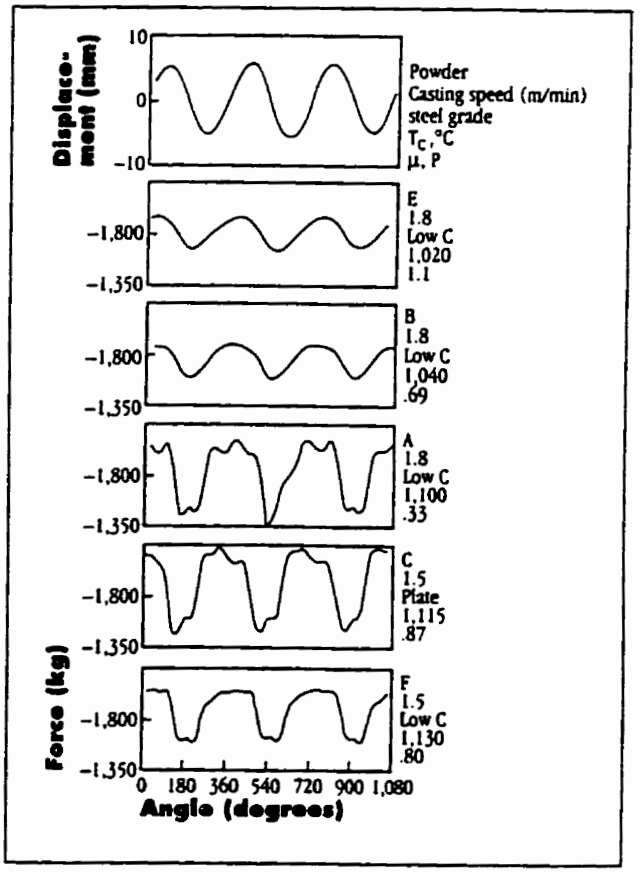

Figure 2.39 Instantaneous displacement and force curves in a continuous casting mold[69].

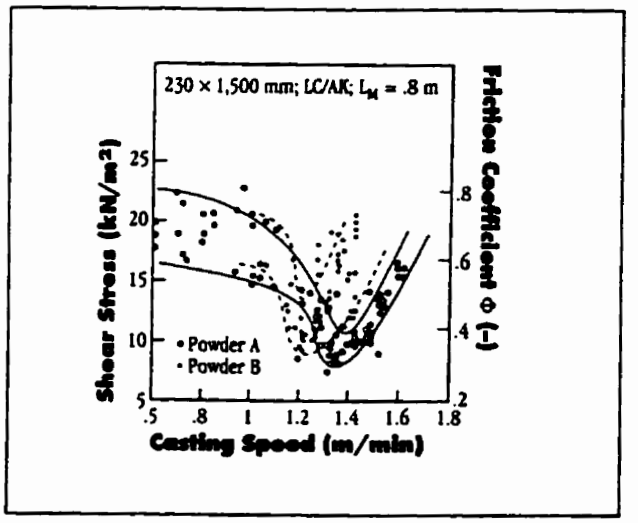

Figure 2.40 Friction shear strees versus. casting speed for two mould powders in slab casting (Lm is active mould length; mould stroke = 7.8 mm and NST = 1.3)[60].

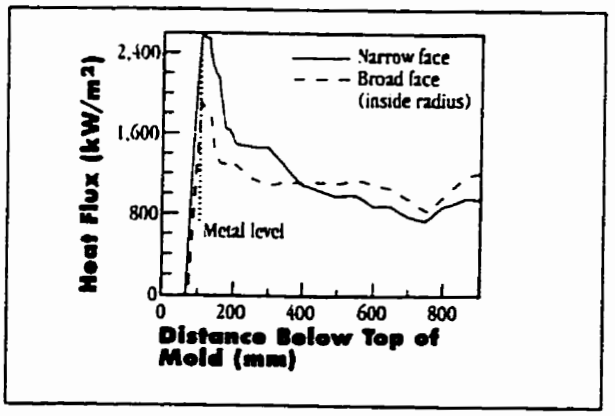

Figure 2.41 Axial heat-flux profile at the narrow and broad faces (0.17%C; casting speed=1.0m/min; with Stg-type mold flux[77].

Chemical Composition (wt %)	Pemco 389	Stg 179
SiO_2	29.0	27.5
CaO/MgO	44.4	33.0
Na_2O/K_2O	13.6	8.0
Al_2O_3	–	5.5
B_2O_3	4.9	–
F	8.1	6.5
MnO	–	6.0
Properties		
Softening temperature (°C)	1,050	1,040
Melting temperature (°C)	1,125	1,165
Viscosity (poise)		
1,400 °C	0.4	2.3
1,300 °C	0.6	2.9
1,200 °C	1.0	4.9

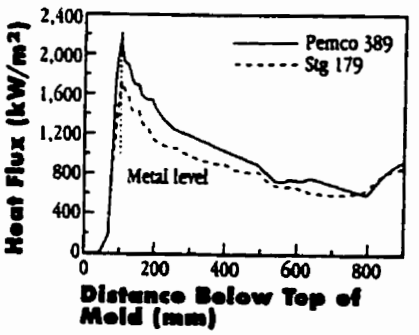

Figure 2.42 Influence of mould-flux type on axial heat-flux profiles at the narrow face. (0.07%C, casting speed:0.63-0.68 m/min, tundish temperature: 1550-1558°C) [77].

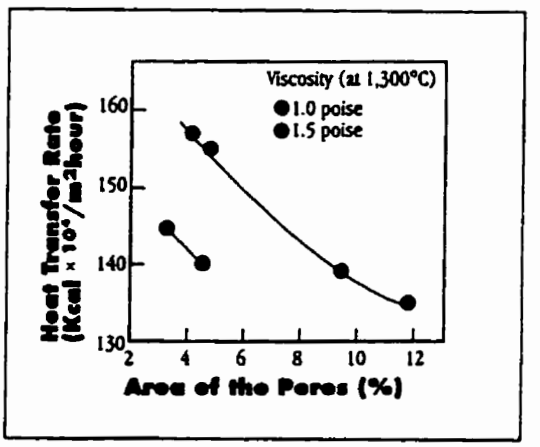

Figure 2.43 Relation between the percentage of area of pores and the mean heat transfer rate at 1.2 m/min [23].

3. SCOPE AND OBJECTIVES

Although oil lubrication is cheaper than mould-flux, quality problems and cleanliness issues have led some billet producers to switch from oil to powder lubrication for casting bigger-section (> 200 x 200 mm^2) billets. However, as stated before, there is very little information available to answer the following crucial questions: what are the optimum properties of the mould powder for billet casting for a range of conditions, what should the mould taper be for mould flux lubrication? This lack of information regarding the use of mould powder in billet casting was the driving force behind this research investigation. The ultimate goal was to gather information and generate knowledge in order to help billet producers make the best choices in terms of mould powder, casting variables and mould taper.

The objective of this research was to investigate billet casting with powder lubrication and compare it to oil lubrication in the context of mould thermal response and billet surface quality. The following tasks were performed to meet these objectives:

1. An instrumented-mould trial was conducted to measure mould temperature, mould displacement, metal level, casting speed, mould powder consumption, mould powder temperature profile and to acquire billet samples.
2. Development of an inverse heat conduction model of the billet mould to determine mould heat transfer from measured mould wall temperatures.
3. Investigation of mould thermal response during billets casting with powder lubrication in terms of mould wall time-averaged temperature, mould heat flux, mould cold- and hot-face temperatures.

4. Calculation of strand shell thickness and billet shrinkage to specify optimum mould taper.
5. Evaluation of billet surface quality and relate the surface defects found (transverse depression, rhomboidity and longitudinal depression) to measured mould thermal response.
6. Evaluation of the overall performance of the two powders used in the plant trial and investigate the influence of mould water velocity on mould powder performance.
7. Comparison of powder lubrication with oil lubrication in terms of mould heat flux, transverse depression, rhomboidity, oscillation marks and mould level variation.
8. Development of a mathematical model of mould powder melting.

4. MATHEMATICAL MODELLING

This chapter presents the application of the inverse heat conduction method for determining mould heat transfer in billet casting from thermocouple measurements. It also presents the mathematical modelling of powder melting using the enthalpy method. Results of the melting model in conjunction with molten flux pool measurements and powder properties were used to interpret mould powder behaviour during billet casting. Also, in this chapter a previously developed mathematical model of billet shrinkage, that is used to investigate mould/strand binding and mould taper in Chapter 7, is briefly introduced.

4.1 Inverse Heat Conduction Model

Mould heat flux can be determined from measured mould wall temperatures. Traditionally a trial-and-error technique has been used to estimate the mould heat flux. In this approach an assumed heat flux profile is used as a first estimate of the boundary condition along the hot-face of the mould wall in the mathematical model that simulates the thermal field in the mould. The initial input is judiciously altered so as to match the predicted mould temperatures with those recorded by thermocouples[106-110].

A mathematically more rigorous approach consists of solving the **I**nverse **H**eat **C**onduction **P**roblem (**IHCP**) by analytical or numerical methods[111-114]. The IHCP is the estimation of the time- or spatial-profile of a surface heat flux given one or more measured temperatures inside a body. As Beck et al.[114] pointed out the word *estimation* is significant because errors are always present in measured temperatures and they affect the accuracy of the heat flux calculation.

Among the variety of proposed methods for solving the IHCP, the regularization method is a procedure that minimizes a modified least squares function of the differences between the temperatures measured by thermocouples and temperatures predicted by a direct model of the problem. The regularization procedure modifies the least squares function by adding factors to reduce fluctuations in the unknown function to be estimated[111-114]. These fluctuations or instabilities are not of physical origin but are inherent in the solution of ill-posed problems unless they are specially treated[115]

This chapter presents details of the mathematical model developed to estimate the axial profile of mould heat flux from measured mould wall temperatures. The model consists of the regularization procedure coupled with a solution of the two-dimensional, steady-state heat transfer equation of the mould walls, also called the forward or direct problem.

4.1.1 Direct problem

A two-dimensional model of the mould wall, that predicts the thermal field in a longitudinal section through the mid-face of the copper tube, was developed to provide a forward problem solution for the inverse program. This model is based on a previous model developed by Samarasekera and Brimacombe[106]. A schematic diagram of the mid-face longitudinal section of the mould wall is shown in Figure 4.1.

The following assumptions have been made in the heat flow model:

(i) Steady-state - the mould is at steady state, which is valid if no nucleate boiling occurs in the water cooling gap[108].

(ii) Two-dimensional - transverse heat flow perpendicular to the plane of interest is negligible.

(iii) Thermal conductivity of copper is constant. Mahapatra[108] calculated mould temperature, utilizing both a constant (127°C) and a temperature dependent thermal conductivity, and found the differences in mould temperature between the two cases to be negligible, less than 1°C at the mould hot face. Between 25°C and 300°C the thermal conductivity of copper only varies ~3%[108]

(iv) The top and bottom surfaces of the mould walls are considered to be adiabatic.

(v) The cooling water channel extends from the bottom to the top of the mould walls. The cooling water is in plug flow and the heat transfer coefficient at the mould/water interface is constant throughout the length of the mould. Heat transfer between the cooling water and water jacket is negligible.

The differential equation governing heat conduction in a billet mould wall in two-dimensions, rectangular co-ordinates, under steady-state conditions, is given by,

$$\frac{\partial}{\partial x}\left(k_{cu}\frac{\partial T}{\partial x}\right)+\frac{\partial}{\partial z}\left(k_{cu}\frac{\partial T}{\partial z}\right)=0 \qquad (4.1)$$

Where T is temperature, x is the direction along the thickness of the mould wall, z is the direction along the height of the mould and k_{cu} is the thermal conductivity of copper.

The governing equation describing the heat transfer in the cooling water channel is given by,

$$\rho_w V_w d_w C_{pw}\frac{\partial T_w}{\partial z}=h_w\left[T_0(z)-T_w(z)\right] \qquad (4.2)$$

Where ρ is density, V is velocity, d_w is the width of the water channel gap, C_p is specific heat, T is temperature, z is the direction along the mould height and h is heat transfer coefficient. The subscripts w and 0 refer to water and mould wall cold face, respectively.

The appropriate boundary conditions to solve Equation 4.1 and 4.2 are as follow:

(i) cold face of the mould wall ($x = 0$, $0 \le z \le Z_m$)

$$-k_{cu}\frac{\partial T}{\partial x} = h_w\left[T_0(z) - T_w(z)\right] \tag{4.3}$$

(ii) top and bottom of mold wall ($0 \le x \le X_m$, $z = 0$ and $z = Z_m$)

$$-k_{cu}\frac{\partial T}{\partial z} = 0 \tag{4.4}$$

(iii) hot face of the mould wall ($x = X_m$, $0 \le z \le Z_m$)

$$-k_{cu}\frac{\partial T}{\partial x} = q(z) \tag{4.5}$$

where $q(z)$ is a given heat flux profile.

(iv) inlet temperature of mould cooling water ($z = Z_m$)

$$T_w(Z_m) = T_w^{inlet} \tag{4.6}$$

Equations 4.1 was discretized using a fully implicit finite-difference scheme[112]. The resulting system of linear equations was solved using the Gauss-Seidel iterative method with Successive Over-Relaxation (SOR)[116]. The grid consisted of 5 nodes in the x(transverse) direction and 141 in the z(longitudinal) direction. The initial-value problem posed by Equation 4.2 was discretized using a control volume approach[112] and solved simultaneously with Equation 4.1. The convergence criterion was 10^{-6} °C for both the mould and water temperatures. The model was coded in FORTRAN and the code was verified against an analytical solution for a 1-D heat conduction problem and a numerical solution for a 2-D conduction problem presented by Chapra and Canale[117].

The heat transfer coefficient (h_w) between the cold face of the mould wall and the cooling-water (i.e., boundary condition i) was determined from the following dimensionless correlation[118, 144-145],

$$\frac{h_w D_H}{k_w} = 0.023\left(\frac{\rho_w V_w D_H}{\eta_w}\right)^{0.8}\left(\frac{C_{pw}\eta_w}{k_w}\right)^{0.4} \qquad (4.7)$$

where the left side term is the Nusselt (Nu) number, the first term on the right side is the Reynolds (Re) number and the second is the Prandtl (Pr) number. h is the heat transfer coefficient, D_H is the hydraulic diameter, ρ is density, V is velocity, η is viscosity, C_p is specific heat and k is the thermal conductivity. The subscript w refers to the cooling fluid, water.

The above correlation is applicable to fully developed turbulent flow in circular pipes in the absence of nucleate boiling. Its validity is constrained by the following conditions:

(i) $0.6 < \mathrm{Pr} < 160$,

(ii) $\mathrm{Re} \geq 10000$ (turbulent flow),

(iii) $\frac{L_w}{D_H} > 10$, where L_w is the length of the cooling-water channel,

(iv) and with the properties of the fluid evaluated at its bulk temperature, typically 30°C.

Calculation of the water saturation temperature under the pressures observed in the plant trial showed that as long as the mould cold-face is less than 166°C no boiling occurs. This criterion was easily met since in all cases studied the mould cold-face temperature did not exceed 130°C. Also, calculations performed to examine the sensitivity of the model prediction of heat fluxes to the heat transfer coefficient, Equation 4.7, showed that the mould heat flux varies less than 3.0% when the temperature of the water increases from 30 to 40°C.

4.1.2 The Inverse problem

A variety of techniques have been proposed for the solution of IHCP[112-114]. For this investigation in which the spacewise distribution of surface heat flux, *q(z)*, (with no prior knowledge of the functional form of this quantity) is sought, requires the use of a function estimation technique. Function estimation requires the determination of a large number of surface heat flux components, thus it is referred to as an infinite dimensional minimization problem. If prior knowledge of the functional form of *q(z)* is available, it can be parameterized and another approach called parameter estimation can be used to solve the inverse problem. Such problems are referred as finite dimensional minimization problem because only a limited number of parameters are to be estimated.

4.1.2.1 Formulation

The mathematical formulation of the inverse problem of estimating the heat flux at the hot-face of a billet mould is given by Equation (4.1) and the boundary conditions expressed by Equations (4.3) to (4.5). However, *q(z)* in Equation (4.5) now is an unknown quantity, thus equation (4.5) is rewritten as:

$$-k_{cu}\frac{\partial T}{\partial x} = q(z) = ? \tag{4.8}$$

Since the surface heat flux *q(z)* is unknown, temperature measurements taken with multiple thermocouples placed inside the mould wall are given. The inverse problem can be stated as follows: Given M measured temperatures T_j (j = 1,2,...,M) estimate the heat flux profile given by its components q_i, (i = 1,2,...,M). Figure 4.2 shows a schematic of the stated problem.

The inverse problem as stated above is ill-posed; that is, the existence, uniqueness, and/or stability of its solution is not ensured under small changes to the input data. The existence of

the solution is guaranteed by transforming the inverse problem into a minimization problem. The inverse solution minimizes the least squares norm rather than make it necessarily zero.

To solve the above problem the estimated temperature T_i^c, i = 1,2,... M, computed from the solution of the direct problem by using the estimated values of the heat flux components q_i, i = 1,2,...,M, should match the measured temperature T_i^m, i = 1,2,...,M as closely as possible. This matching can be done by minimizing the standard least squares norm with respect to each of the unknown heat flux components.

The problem of uniqueness and stability can be solved by the introduction of a regularizer to the standard least squares technique. A regularizer is a mathematical tool that restricts the functional form which the surface heat flux is allowed to follow. A zeroth-order regularization term was used. A zeroth order regularization term describes the qualitative desire to choose the solution of minimum length - it reduces the maximum magnitudes of estimated values of q_i.

The least square norm modified by the addition of a zeroth-order regularizer can be defined as:

$$S(q) = \sum_{J=1}^{M}\left(T_J^m - T_J^c(q)\right)^2 + \alpha * \sum_{J=1}^{M}\left(q_J - q^o\right)^2 \qquad (4.9)$$

Where S is the sum of squares, M is the number of heat flux components and also, in this study, the number of thermocouple data; T_J^m is the measured temperature; T_J^c is the temperature calculated using the direct model; α^* is the regularization parameter, q_J is the estimated surface heat flux at the boundary, q^o is a given heat flux and j = 1,2,...,M.

As the regularization parameter $\alpha^* \rightarrow 0$, the solution exhibits oscillatory behaviour and can become unstable. For large values of α^* , the solution is over-damped and deviates from the exact results. By proper selection of α^*, fluctuations can be alleviated[112].

The least-squares equation (4.9) is minimized by differentiating it with respect to each of the unknown heat flux component and then setting the resulting expression equal to zero.

$$\frac{\partial S}{\partial q_i} = -2\sum_{j=1}^{M}\left(T_j^m - T_j^c\right)\frac{\partial T_j^c}{\partial q_i} + 2\alpha^*\sum_{i=1}^{M}\left(q_j - q^o\right)\frac{\partial q_j}{\partial q_i} = 0 \qquad (4.10)$$

Equation (4.10) can be reduced to

$$\sum_{j=1}^{M}\left(T_j^m - T_j^c\right)\frac{\partial T_j^c}{\partial q_i} = \alpha^*\sum_{i=1}^{M}\left(q_j - q^o\right)\frac{\partial q_j}{\partial q_i} \qquad (4.11)$$

In Equation (4.11) the first derivative of the dependent variable T_j^c with respect to the unknown parameter q_j is called the Sensitivity Coefficient X_{ji}, i.e.,

$$X_{ji} = \frac{\partial T_j^c}{\partial q_i} \qquad (4.12)$$

and

$$\frac{\partial q_j}{\partial q_i} = \delta_{ji} = \begin{cases} 0 \ for \ i \neq j \\ 1 \ for \ i = j \end{cases} \qquad (4.13)$$

Therefore, substituting Equations (4.12) and (4.13) into Equation (4.11), Equation (4.11) can be simplified to

$$\sum_{j=1}^{M}\left(T_j^m - T_j^c\right)X_{ji} = \alpha^*\sum_{i=1}^{M}\left(q_j - q^o\right)\delta_{ji} \qquad (4.14)$$

The sensitivity coefficient X_{ji} represents the changes in T_j^c with respect to the changes in q_i. Small value of X_{ji} indicates insensitivity of T_j^c to changes in q_j; for such cases the inverse analysis become very sensitive to measurement errors and the estimation process become

difficult. Also it is desirable to have them large and uncorrelated. If they are linearly dependent, the minimization procedure defined by Equation (4.10) will not have unique solution with $\alpha^* = 0$[112,113].

To solve the system of least-squares equations represented by Equation (4.14) several pieces of information are needed: (i) an expression for T_J^c as a function of q_i and (ii) the sensitivity coefficients. The technique employed in this work uses the direct model to compute both of these. Given a heat flux distribution q_i^o the direct model is used to calculate the corresponding temperatures T_J^o.

Expanding the temperature field T_J^c in a Taylor series in terms of the given heat flux q_i^o,

$$T_J^c = T_J^o + \sum_{k=1}^{M} \frac{\partial T_J}{\partial q_k}\left(q_k - q^o\right) \tag{4.15}$$

and substituting it into Equation (4.14) we obtain,

$$\sum_{J=1}^{M}\left[T_J^m - T_J^o - \sum_{k=1}^{M}\frac{\partial T_J}{\partial q_k}(q_k - q^o)\right]X_{Ji} = \alpha^* \sum_{i=1}^{M}\left(q_J - q^o\right)\delta_{Ji} \tag{4.16}$$

which can be rearranged to

$$\left(\sum_{J=1}^{M}\sum_{k=1}^{M} X_{Jk}\, X_{Ji}\, \Delta q\right) + \alpha^* \sum_{i=1}^{M}\left(q_J - q^o\right)\delta_{Ji} = \sum_{J=1}^{M}\left(T_J^m - T_J^o\right)X_{Ji} \tag{4.17}$$

The matrix form of Equation (4.17) can be expressed as

$$(\mathbf{X}^T\mathbf{X}+\alpha^*\mathbf{I})\,(\mathbf{q}-\mathbf{q}^o) = \mathbf{X}^T(\mathbf{T}-\mathbf{T}^o). \tag{4.17}$$

The solution of Equation (4.17) can be written in matrix form as

$$\mathbf{q} = \mathbf{q}^o + (\mathbf{X}^T\mathbf{X}+\alpha^*\mathbf{I})^{-1}\mathbf{X}^T(\mathbf{T}-\mathbf{T}^o) \tag{4.18}$$

Where the vectors $\mathbf{T}$, $\mathbf{T}^o$, $\mathbf{q}$ and $\mathbf{q}^o$ are defined as

$$\mathbf{T} = \begin{bmatrix} T_1^m \\ T_2^m \\ \vdots \\ T_M^m \end{bmatrix} \quad \mathbf{T}^o = \begin{bmatrix} T_1^o \\ T_2^o \\ \vdots \\ T_M^o \end{bmatrix} \quad \mathbf{q} = \begin{bmatrix} q_1 \\ q_2 \\ \vdots \\ q_m \end{bmatrix} \quad \mathbf{q}^o = \begin{bmatrix} q_1^o \\ q_2^o \\ \vdots \\ q_M^o \end{bmatrix}$$

the regularization matrix $\alpha^*\mathbf{I}$ is expressed by

$$\alpha * \mathbf{I} = \begin{bmatrix} \alpha & 0 & \dots & 0 \\ 0 & \alpha & \dots & 0 \\ \vdots & & & \\ 0 & 0 & \dots & \alpha \end{bmatrix}$$

and the sensitivity matrix $\mathbf{X}$ as

$$\mathbf{X} \equiv \frac{\partial \mathbf{T}}{\partial \mathbf{q}^T} = \begin{bmatrix} \frac{\partial T_1}{\partial q_1} & \frac{\partial T_1}{\partial q_2} & \dots & \frac{\partial T_1}{\partial q_M} \\ \frac{\partial T_2}{\partial q_1} & \frac{\partial T_2}{\partial q_2} & \dots & \frac{\partial T_2}{\partial q_M} \\ \vdots & & & \\ \frac{\partial T_M}{\partial q_1} & \frac{\partial T_M}{\partial q_2} & \dots & \frac{\partial T_M}{\partial q_M} \end{bmatrix}$$

Equation (4.18), which gives the estimated values of the heat flux components q_i, is the formal solution of the inverse heat conduction problem considered here. Once the sensitivity coefficients $\mathbf{X}$, the regularization parameter α^*, the measured temperatures $\mathbf{T}$ are known and $\mathbf{T}^o$ is computed from the given heat flux $\mathbf{q}^o$ using the direct model, the surface heat flux $\boldsymbol{q}$ is computed from Equation (4.18). The sensitivity coefficients however must still be determined, which can be accomplished from a numerical solution of the direct problem or analytically, if the associated direct problem is linear, by the application of Duhamel's theorem[112].

In this work a perturbation technique was used to arrive to an explicit expression for the X_{ij}'s. Firstly, the given heat flux components q_j^o's were used a boundary condition in the direct

problem to predicted temperatures at the thermocouples locations T^o_i's. Then each one of the q^o_j's was sequentially perturbed by some small amount (e.g., 10%) to q^j_j in order to obtain a series of new predicted temperatures T^j_i. Each perturbation is done one at a time since the change in temperature at each measurement location need to be known for each change in q_j.

Following the above procedure the sensitivity coefficients were computed

$$\frac{\partial T_i}{\partial q_j} \approx \frac{T_i^1 - T_i^o}{q_j^1 - q_j^o} \equiv \frac{\Delta T_i}{\Delta q_j} \tag{4.19}$$

Thus, the sensitivity matrix can be explicitly expressed as

$$\mathbf{X} \equiv X_{ij} = \begin{bmatrix} \frac{\Delta T_1}{\Delta q_1} & \frac{\Delta T_1}{\Delta q_2} & \cdots & \frac{\Delta T_1}{\Delta q_M} \\ \frac{\Delta T_2}{\Delta q_1} & \frac{\Delta T_2}{\Delta q_2} & \cdots & \frac{\Delta T_2}{\Delta q_M} \\ \vdots & & & \\ \frac{\Delta T_M}{\Delta q_1} & \frac{\Delta T_M}{\Delta q_2} & \cdots & \frac{\Delta T_M}{\Delta q_M} \end{bmatrix}$$

A conceptual flow-chart of the FORTRAN program developed to compute Equation (4.18) is shown in Figure 4.3.

4.1.2.2 Model validation

To validate the inverse heat conduction program arbitrary heat flux distributions were used as boundary conditions for the direct model. Discrete values of temperatures calculated using the arbitrary heat fluxes were input into the inverse model to back calculate the heat fluxes. The values of heat fluxes obtained by the inverse was compared to the exact values used to calculated the temperatures.

Figure 4.4 shows that for both types of heat flux profile tested, constant heat flux and triangular profile, the match between the exact profile and the profile estimated by the inverse

analysis was perfect. These results confirm that in the absence of noise the inverse code developed works perfectly.

The definitive test for the inverse model was performed by comparing mould heat flux profiles estimated by the inverse code developed with heat fluxes adjusted by trial-and-error using a direct program called SMOULD[109]. Figure 4.5 shows the results of these comparisons for two different cast heats. In both cases, heat 262 (Figure 4.5A) and heat 265 (Figure 4.5B), the agreement between both procedures is excellent. These results confirmed the reliability of the inverse heat transfer code developed, thus all heat flux calculations in this work were performed using the inverse code. For a grid of 700 nodes it takes ~10 seconds to run the program, while the trial-and-error approach can consume hours to get the same level of fitting.

To test the sensitivity of the inverse model to the size of the discrete segments of heat flux, $q_1, q_2, \ldots, q_M$, chosen to estimate the mould heat flux, the number of segments at the meniscus region was doubled. In Figure 4.6A profiles obtained by the inverse code (standard and finer segments) with the profile obtained by trial-and-error are compared. As in Figure 4.5, the agreement obtained is excellent. The presence of a local minimum heat flux just below the meniscus, is confirmed as a real feature of the mould heat flux profile, and not a bias of the inverse code, since in all cases tested, standard-IHC, finer-IHC and trial-and-error, this local minimum appears. Similar local minimum was also found by Kumar[110] and Gurton[124] for the continuous casting of peritectic-carbon steels (0.10~0.12%C) billets cast with oil and powder lubrication. A detailed explanation for the entire shape of a typical mould heat flux profile will be presented in chapter 7. Figure 4.6B compare the temperature difference (calculated minus measured) for both, the inverse calculation and the trial-and-error

procedure. In both cases, the agreement is very good, which confirms that the inverse code developed renders results equivalent to trial-and-error.

From numerical simulations it was found that for values of $\alpha^* > 10^{-7}$, the estimated heat fluxes were over-damped towards the values of the initial guess (q_i^o). On the other hand, if $\alpha^* < 10\text{-}12$ there was no damping and the estimated heat fluxes presented oscillatory behaviour. Values of α^* between 10^{-11} and 10^{-9} were found to give the best results.

Besides being reliable, as confirmed by the tests carried out, the inverse procedure is much easier and faster to perform when compared to the trial-and-error procedure.

4.2 Mathematical Modelling of Mould Powder Melting

To analyze the influence of mould powder properties and feeding strategies on the melting behaviour of mould powders in a continuous casting mould a mathematical model was developed. The model describes the thermal field across the mould flux, from the time fresh powder is initially added to the top of the mould until it reaches a stationary state, including the effect of consumption and addition of new powder. The model is capable of computing the instantaneous thickness of powder, the thickness of the liquid layer, and variations of temperature and position of the free surface of powder as a function of powder properties, powder consumption and frequency of addition of fresh material. This chapter describes the formulation of the model and its validation.

4.2.1 Model Assumptions

A schematic diagram of a longitudinal mid-plane through the mould powder-steel system is shown in Figure 4.7. The simplifying assumptions of the unsteady-state, one-dimensional, mathematical model are as follows:

(i) Heat flow is considered one-dimensional, i.e., along the casting direction (Z-axis), and taking place by conduction only. Convection due to movement of liquid flux and flow of gases through the powder layers are accounted by increasing the thermal conductivity of the layer.

(ii) The thermal contact between the liquid flux and the steel is perfect (i.e., the contact temperatures are the same in both phases).

(iii) Consumption of the liquid flux follows plug flow, thus all layers remain horizontal and unmixed (the low viscosity of the flux in contact with the liquid steel ensures that the lateral flow of molten flux being consumed at the periphery is much faster than the downward speed of all the other layers).

(iv) Heat is lost at the top layer by radiation and natural convection.

(v) The thermal conductivity of the powder layer is calculated using Bruggman model[8]. An enhancing factor is use to account for convection.

(vi) Above its sintering temperature the density of the loosely packed powder increases exponentially with temperature until it reaches the density of the liquid flux.

(vii) The enthalpy method, as shown in Appendix D, is used to formulate the melting of the mould powder.

4.2.2 Mathematical Formulation

Equation (B.6) from Appendix D, simplified to one-dimension, can be expressed as:

$$\rho \frac{\partial H}{\partial t} = \frac{\partial}{\partial z}\left(\kappa \frac{\partial T}{\partial z}\right) \tag{4.20}$$

where z is the axial direction along the layers of mould flux.

In order to solve Equation (4.20) two boundaries conditions and an initial condition need to be specified. The first boundary is defined by the steel/flux interface, taken as z = 0 (bottom surface). The second is the powder free surface, top surface, taken as z = Z. According to assumption (ii), the molten flux temperature at the steel/flux interface is equal to the liquid steel temperature (T_{steel}), which mathematically is expressed as:

$$t > 0,\ z = 0,\ T(z=0) = T_{steel} \tag{4.21}$$

According to assumption (iv), the boundary condition at the top surface is expressed in terms of heat losses by radiation and natural convection.

$$t > 0,\ z = Z,\ -k\frac{\partial T}{\partial z} = \sigma\varepsilon\left[(T_{top}+273)^4 - (T_a+273)^4\right] + q_c \tag{4.22}$$

where Z is the total length of mould flux, σ is the Stephen-Boltzman constant, ε is the emissivity of the powder, T_{top} is the temperature of the upper most layer of powder, T_a is the temperature of the surroundings above the powder and q_c is the heat flux due to natural convection.

The convective term of Equation (4.22), q_c, is expressed by:

$$q_c = h_c(T_{top} - T_a) \tag{4.23}$$

where h_c, the heat transfer coefficients due to natural convection, is given by[141]:

$$h_c = 0.59\left(\frac{T_{top} - T_a}{L}\right)^{0.25} \tag{4.24}$$

Equation (4.24) is a simplified equation valid for horizontal square plates with a surface warmer than the fluid and facing upward. L is the length of the side of the square in meters and h_c is given in $W/m^2\,°C$.

In order to express Equation (4.22) in terms of heat transfer coefficient, the radiation part of it can be written as:

$$\sigma \varepsilon \left[(T_{top}+273)^4-(T_a+273)^4\right]=h_r(T_{top}-T_a) \tag{4.25}$$

Thus h_r is expressed as:

$$h_r=\sigma \varepsilon (T_{top}+T_a+546)\left[(T_{top}+273)^2+(T_a+273)^2\right] \tag{4.26}$$

Substituting (4.23) and (4.25) into (4.22) the boundary condition at the top surface is simplified to

$$t>0,\ z=Z,\ -k\frac{\partial T}{\partial z}=(h_r+h_c)(T_{top}-T_a) \tag{4.27}$$

with h_r and h_c given by Equations (4.24) and (4.26), respectively.

The initial condition for Equation (4.20) assumes that at the start of the process the temperature of the powder is uniform and equal to the ambient temperature (T_a), except for the boundary at the steel/flux interface where it is equal to the steel temperature. mathematically this condition is expressed as follow

$$t=0,\begin{cases} z=0, T=T_{steel} \\ z>0,\ T=T_a \end{cases} \tag{4.28}$$

4.2.3 Powder Consumption and Shrinkage

According to assumption (iii) when liquid flux is consumed only a thin layer of low-viscosity fluid moves sideways from the liquid pool into the mould/strand-gap while all other layers just move downwards. Therefore, for a constant consumption (Q) the downward velocity of molten flux is defined by the thickness Δz (m) removed during a time Δt (s).

The mass of powder consumed, M_p (Kg), can be expressed as

$$M_p = (A \times B)\,\Delta z\,\rho_{flux} \tag{4.29}$$

and

$$M_p = (A \times B)\left(\frac{V}{60}\right)\Delta t\,\rho_{steel}\,(Q \times 10^{-3}) \tag{4.30}$$

where A and B are the internal dimensions of the mould in m, ρ_{flux} and ρ_{steel} are respectively the densities of the liquid flux and steel in Kg/m^3, V is the casting speed in m/min and Q is the powder consumption in Kg of powder/ton of steel.

Eliminating M_p between Equations (4.29) and (4.30) we obtain the following expression for the downward displacement of mould powder

$$\Delta z = \frac{\Delta t\,(Q \times 10^{-3})V}{60}\left(\frac{\rho_{steel}}{\rho_{flux}}\right) \tag{4.31}$$

The density of the of mould-flux changes from that of a loosely-packed powder (~1000 Kg/m^3) at the top, to that of a molten flux (~ 3000 Kg/m^3) at the bottom. Therefore, the whole column of powder is shrinking due to this density variation. This shrinkage (ΔL) can be expressed as

$$\Delta L = L^0\left(1 - \frac{\rho^0}{\rho(T)}\right) \tag{4.32}$$

where L^0 is the initial thickness of powder, ρ^0 is its initial density and $\rho(T)$ is the density at any specific temperature. Since there is no available experimental data on the variation of the density of mould fluxes during heating a model has to be specified. Permeability measurements made by Nakato et al.[41] during heating of loosely packed fluxes showed that for powdered fluxes sintering begins slowly and then at about 800 to 900°C an abrupt decrease in pressure loss marked the initiation of rapid sintering; also according Jander's.[41] equation for sintering

the rate of reaction is an exponential function of (temperature)$^{-1}$ and a cubic function of time. Based on this behaviour the variation of density with temperature was specified as

$$\rho = \begin{cases} \rho_{powder} & for\ T \le T_S \\ \rho_{flux} - (\rho_{flux} - \rho_{powder}) \times \exp\left[-0.02\,(T - T_S)\right] & for\ T_S < T < T_L \\ \rho_{flux} & for\ T \ge T_L \end{cases} \tag{4.33}$$

where ρ_{powder} is the density of the loosely-packed powder, T_S is the temperature of rapid sintering or softening, and T_L is the liquidus temperature.

4.2.4 Numerical Method

Equation (4.20) subject to the conditions expressed by Equations (4.21), (4.27) and (4.28) was solved using an explicit finite-difference method.

Since during melting the density through the flux layer changes significantly, the numerical method must account for this variation, which requires the use of a non-uniform grid[112]. For a non-uniform grid spacing the finite-difference approximation for the second derivative is given by:

$$\left(\frac{\partial^2 T}{\partial z^2}\right)_i = \frac{2}{(\delta z)_{i+1} + (\delta z)_{i-1}} \left[\frac{T_{i+1} - T_i}{(\delta z)_{i+1}} - \frac{T_i - T_{i-1}}{(\delta z)_{i-1}} \right] \tag{4.34}$$

Substituting Equation (4.31) in (4.20) the general equation for an the interior node is obtained as follow

$$H_i^{new} = H_i^{old} + \frac{2\,k\,\Delta T}{\rho\left[(\delta z)_{i+1} + (\delta z)_{i-1}\right]} \left[\frac{T_{i+1} - T_i}{(\delta z)_{i+1}} - \frac{T_i - T_{i-1}}{(\delta z)_{i-1}} \right] \tag{4.35}$$

where $(\delta z)_{i-1}$ is the nodal distance between nodes (i) and (i+1) and $(\delta z)_{i-1}$ is the distance between (i) and (i-1).

To handle the density variation the number of nodes was kept constant and the distance between nodes was shrunk proportionally to the density variation. Considering that the mass of material contained in each unit cell of length L is constant and the nodes are located in the center of the cells, the nodal distance between any two adjacent nodes (i) and (i+1) can be expressed as

$$(\delta z)_{i+1}^{new} = \left(\frac{\rho_{powder}}{\rho_i(T_i)}\right)\frac{L_i^0}{2} + \left(\frac{\rho_{powder}}{\rho_{i+1}(T_{i+1})}\right)\frac{L_{i+1}^0}{2} \tag{4.36}$$

where $(\delta z)_{i+1}^{new}$ is the nodal distance after shrinkage, ρ_{powder} is the initial density of the loosely packed powder, ρ_i is the density of the node (i) at the temperature T_i and L_i^0 is the initial length of the cell pertaining to node (i).

For discretizing the convective boundary condition at the free surface of powder (z=Z) with a second-order accuracy, i.e. $O[(\Delta x)^2]$, the fictitious node concept was applied to Equation (4.27). To implement this approach in the computational procedure the temperature of the fictitious node was calculated and substituted into the interior node equation, as if the fictitious node was part of the physical system. The fictitious node temperature is given by

$$T_{m+1} = T_{m-1} - \frac{2\delta z(h_r + h_c)}{k}(T_m - T_a) \tag{4.37}$$

where T_{m+1} is the temperature at the fictitious node, $T_m \equiv T_{top}$ and δz is the distance between nodes (m) and (m-1).

4.2.5 Model Parameters

4.2.5.1 Thermal Conductivity

The lack of data on the thermophysical properties of mould fluxes make the task of modelling their behaviour very difficult. However, the few data available on the thermal conductivity of mould fluxes unequivocally show that their thermal conductivity increases with increasing the temperature. Measured values vary from 0.4 to 0.9 $Wm^{-1}K^{-1}$ for powder (measurement done in nitrogen atmosphere)[8], from 1.0 to 2.0 $Wm^{-1}K^{-1}$ for sintered flux[8] and from 1.0 to 4.0 $Wm^{-1}K^{-1}$ for liquid flux[119].

The Bruggeman model was used to calculate the effective thermal conductivity of two-phase mixtures between 25°C and the sintering temperature (~ 900°C). Bruggeman equation for spherical particles states that

$$1 - V_d = \left(\frac{k_{eff} - k_d}{k_c - k_d}\right)\left(\frac{k_c}{k_{eff}}\right)^{\frac{1}{3}} \tag{4.38}$$

where V_d is the volume fraction of discontinuous phase (air, CO, CO_2), k_{eff} is the effective thermal conductivity of the mixture, k_d is the thermal conductivity of the discontinuous phase and k_c is the thermal conductivity of the continuous phase (flux).

Between sintering and liquidus temperature the thermal conductivity was specified in the same way as the density. Above the liquidus temperature the effective thermal conductivity was specified as a function of the superheat in order to account for the convective effects reported by Nakano et al.[47] and Microvas et al.[119].

4.2.5.2 Thermophysical Data

The thermophysical properties of the mould powders used in the mathematical simulations are presented in Table 4.1. Bulk density was measured by weighing known volumes of both powders used in the trial. The liquidus and solidus temperature were assumed to be equal to their transition temperature and temperature of start of softening, respectively; both supplied in their product data sheet. The other properties were estimated from values available in the literature for powders with the closest chemical composition to the ones used in the trial.

4.2.6 Model Validation

To validate the mathematical model, temperatures within the powder layer were measured using an arrangement of three Type S (Pt-10%Rh) thermocouples enclosed in high purity alumina protection tube. The wires inside the protection tube were insulated by double-bore high purity hard-fired alumina tubes. The thermocouples were mounted in a steel bar through screw nuts that allowed adjustment of their length. A laptop computer with data acquisition board and Labtech Notebook software was used as the data acquisition system. Figure 4.8 shows a schematic diagram of the set-up for measuring the mould powder temperatures.

Due to experimental problems it was not possible to get good data for powder A. Two incomplete (one thermocouple failed in set #1 and two in set #2) sets of data was collected using powder B. The data collected was used to adjust some of the unknown properties of powder B to fit the model predictions.

Primarily the adjustment of the model consisted in using the two temperatures (thermocouples placed at 25 and 50 mm from the metal level) from the first set of experiments to establish effective thermal conductivities for the solid and liquid phases, thus accounting for convection. Also, the fraction of volatiles and the total heat of decomposition of carbonates

were adjusted within ranges presented in the literature[8,49,51]. Using the adjusted parameters the calculations were confirmed using the only good temperature collected from the third set of experiments (thermocouple placed at 4.8 mm). Figure 4.9 shows good agreement between the measured and calculated temperatures for both cases discussed above. (In Figure 4.9 the X-axis: *Time from start of "steady-state"*, means that the original time scale, as shown in Figure 6.17, was cropped of ~20-30s. Thus, Time = 0 corresponds to an arbitrarily time selected after the thermocouple signal had stabilized).

4.2.7 Sensitivity analysis

To investigate the influence of model parameters on liquid flux pool height, a sensitivity analysis was performed. Table 4.2 lists all the variables tested, with their respective basic values, range of variation and units.

In Table 4.2, total powder height refers to the total amount of powder covering the liquid steel, which includes all existent layers (powder, sintered and liquid). Steel temperature is the temperature of the liquid steel in the mould in contact with the liquid flux. The thermal conductivity is a value chosen from the literature and it refers to measurements done on samples of solidified flux. Powder density is the bulk density of the loosely packed fresh powder. Lastly, both convection factors refer to multiplication factors used to enhance the thermal conductivity in order to account for convection in the powder layer due to flow of gases, and in the liquid layer due to a velocity field in the liquid pool.

Figures 4.10 to 4.12 show the results of the sensitivity analysis. Figure 4.10A shows that the molten flux depth increases with increasing total amount of powder until it reaches a plateau (40mm for the case studied). Further simulations, not shown here, showed that the plateau value depends on the density of the powder, and can vary between 35 to 45 mm. The

important point here is to recognize that above a certain limit it is ineffectual to add more powder. This finding agrees with simulation results from Goldschmit et al.[55] and also McDavid and Thomas[148], and supports the industrial practice, observed in slab casting, of not keeping a powder layer thicker than 35 mm.

Figure 4.10B shows that the depth of the liquid pool varies very little with the steel temperature. It varies no more than 1mm between 1500°C and 1560°C, which is the temperature range normally found in practice for casting of low- and medium-carbon steels. On the other hand, the depth of the flux pool strongly depends on the flux liquidus temperature, as shown in Figure 4.10C. Powders used in steel plants present a wide range of liquidus temperature, which can vary from 900 to 1200°C. Within this temperature range Figure 4.10C shows that the depth of the liquid pool can vary from 12 to 6mm. This is a very significant variation considering that the liquid pool depth should be at least equal to the amplitude of the mould oscillation stroke and that in modern steel casting the stroke tend to be set at between 5 and 8mm.

Figure 4.11A shows that the enthalpy of fusion (latent heat) of the powder does not significantly affect the depth of the flux pool. Data published by Mills et al.[8] show latent heat values of around 400 to 500 kJ/kg for powders with mainly crystalline constituents, and ~250 kJ/kg for a glassy slag. Since the sensitivity analysis showed that the liquid pool depth is quite insensitive to latent heat any value between 250 and 500 kJ/kg would be acceptable. The flux thermal conductivity and bulk density are much more important variables. Published data give values for mould powder conductivity between 0.5 and 2.5 kW/mK, which is a very significant variation considering, according to Figure 4.11B, that the molten flux depth more than double when the thermal conductivity increases from 0.5 to 2.5 kW/mK For these low

values, a variation of only 1.0 W/mK can represent an increase of 100% or more. Unfortunately, the lack of reliable data makes it difficult to establish what would be a realistic range for testing the sensitivity of the flux pool to variations on mould powder thermal conductivity.

Another important mould powder property is the bulk density. Commercial powders can present a wide range of bulk densities, varying from 450 to 1000 kg/m^3[8,51] depending on their chemical composition and particle size. On the other hand, the density of the liquid phase only dependents on the liquid composition after all volatiles and carbon are removed, and varies between 2500 and 2700 kg/m^3[8,134]. It is important to note that the same liquid flux can result from different powders, depending on the raw materials and the fabrication process used. However, the melting behaviour and thus performance of each powder can be completely different, even though they result in identical liquid fluxes.

Figure 4.11C shows that the liquid pool decreases with decreasing powder bulk density. This happens because the thermal conductivity, as defined by Bruggeman's model[8,141], decreases as the fraction of continuous phase (powder particles) decreases. As a limiting situation, Figure 4.11C shows that if the bulk density of the powder was the same as the liquid flux, i.e. 2700 kg/m^3, the flux pool would be at its deepest (~14mm). However, under these circumstances the powder layer would cease to behave as a porous bed, thus convection due to hot gases flowing through the powder would be replaced by pure conduction as the main heat transfer mechanism. Consequently, the melting process would be retarded, since one of the model's assumption is that convection enhances six fold the original conductivity of the flux. Since powder bulk density not only influences the heat transfer in the powder layer, but also the kinetics of fusion, which the model does not address, the result presented in Figure

4.11C should be understood as the model's response to thermal conductivity changes only due to density variation, without considering further implications.

Experimental results reported by Kawamoto et al.[51] showed that mould powder melting rate decreases with increasing bulk density and also that two powders with same bulk density but a small difference in their free carbon content can have completely different melting rates. With the exception of pre-fused fluxes the majority of commercial powders are heterogeneous material. They melt without a definite melting front, instead forming small islands of liquid material that are enveloped by carbon particles. Until the carbon is burnt the liquid droplets cannot agglomerate and join the liquid pool. Therefore, the amount, size and nature of the carbon particles and the size of the powder particles are crucial in controlling the powder melting rate. Since the model does not address the kinetics of melting, the overall influence of bulk density on melting is overlooked and Kawamoto's results can not be verified.

Figure 4.12 shows the influence that convection, powder consumption and casting speed have on mould flux pool depth. The model accounts for convection in the liquid pool and in the powder layers in terms of an effective thermal conductivity. The effective conductivity is calculated by multiplying the thermal conductivity of the phase by an enhancing factor. This approach has been extensively used to account for convection in the liquid metal pool during solidification of continuously cast steel. Nakano et al.[47] used the same technique to account for convection in the molten flux pool, but convection was not considered in their treatment of the powder and sintered layers. Figure 4.12A shows that convection strongly influences the depth of the liquid pool. For the liquid phase, an enhancing factor of 6 increases the liquid pool depth about 60%, while a factor of 15 increases it ~80%. These results match those of McDavid and Thomas[148] who applied a three-dimensional coupled heat-transfer and fluid-

flow finite element model to analyze the behaviour of the top-surface flux layers in the continuous casting of steel slabs. The former researchers clearly showed the importance of convection in the liquid flux pool and also that steel flow in the mould controls the liquid flux layer thickness profile.

For the solid phase, the same thermal conductivity enhancing factors used for the liquid layer, lead to an increase of the flux pool of about 4 and 10 times respectively. Figure 4.12A also shows that if no convection occurs in the solid phase, i.e. convection factor equal to 1, the liquid pool would be practically nonexistent for the consumption rate used in the simulations (Q=1.1 kg/ton). This is the first time that the importance of convective heat transfer in the solid powder, i.e. the effect of hot gases flowing upwards through the powder, has been demonstrated by means of a mathematical model. Experimentally, this has been demonstrated by Kawamoto et al.[51], as shown in Figure 2.43, which shows that the melting rate increases with increasing carbonate content in the powder. Since carbonate decomposition is endothermic, and robs heat from the system, it should instead retard the melting process. Therefore, Kawamoto et al.[51] concluded that the increase in mould powder melting rate with carbonate content was due to the elevation of the thermal conductivity caused by the gas generated during the decomposition reactions.

Figures 4.12B and 4.12C show that the liquid flux pool decreases with the increase of powder consumption and casting speed. In both cases the decrease in the depth of the liquid pool is caused by an increase in the rate at which powder is removed from the system. However, as previously shown in Chapter 2,the consumption of a given powder strongly depends on casting speed; therefore, unless different powders are used, it is not possible independently to increase casting speed without decreasing consumption. When these two

variables are changed together, the net result, as will be shown in Chapter 7, is that an increase in casting speed is usually more than compensated by a decrease in powder consumption, leading to a deeper flux pool.

4.3 Mathematical Model of Billet Shrinkage

A mathematical model developed by Chandra[109] was employed to analyze mould-billet binding. The model describes heat flow in a continuously cast strand and computes the shrinkage of the billet as a function of its axial position in the mould. Details of this model were presented elsewhere[109]. The billet shrinkage model requires the dimensions of the hot mould (distorted mould) as input data. For this study no mould distortion calculations were performed, instead values previously calculated for the same mould and similar casting conditions of the plant trial were used[121].

Table 4.1: Thermophysical properties of mould flux

Property	Powder A	Powder B	Reference
Density [Kg/m^3]:			
Powder(ρ_{powder})	700	820	Measured
Liquid flux(ρ_{flux})	2700	2700	Estimated[120]
Temperature [°C]			
Liquidus (T_L)	1000	1135	Product data sheet
Solidus (T_{sol})	900	1000	Estimated
Heat capacity (C_p) [kJ/kgK]	1.1	1.1	Estimated [8]
Latent heat [kJ/kg]:			
Crystalline (L_{crys})	500	500	Ref. [8]
Glassy (L_{glass})	250	250	Ref. [8]
Thermal conductivity [kW/mK]			
Powder (k_{powder})	Bruggeman	Bruggeman	Ref. [8]
Sintered (k_S)	0.002	0.002	
Liquid (k_{flux})	$6\times k_S$	$6\times k_S$	Ref. [47,119]

Table 4.2: List of model parameters tested in the sensitivity analysis

Model Parameter	Unit	Basic Value	Range of Variation
Total powder height	[mm]	50	15-90
Steel temperature	[°C]	1540	1500-1560
Flux liquidus temperature	[°C]	1135	950-1200
Latent heat	[kJ/kg]	500	0-1000
Thermal conductivity	[W/mK]	2.0	0.5-2.5
Powder density	[kg/m^3]	1000	700-2700
Convection factor(Powder)	[-]	6	1-15
Convection factor(Liquid)	[-]	13	1-15
Powder consumption	[kg/ton]	1.1	0.5-1.3
Casting speed	[m/min]	1.0	0.9-1.5

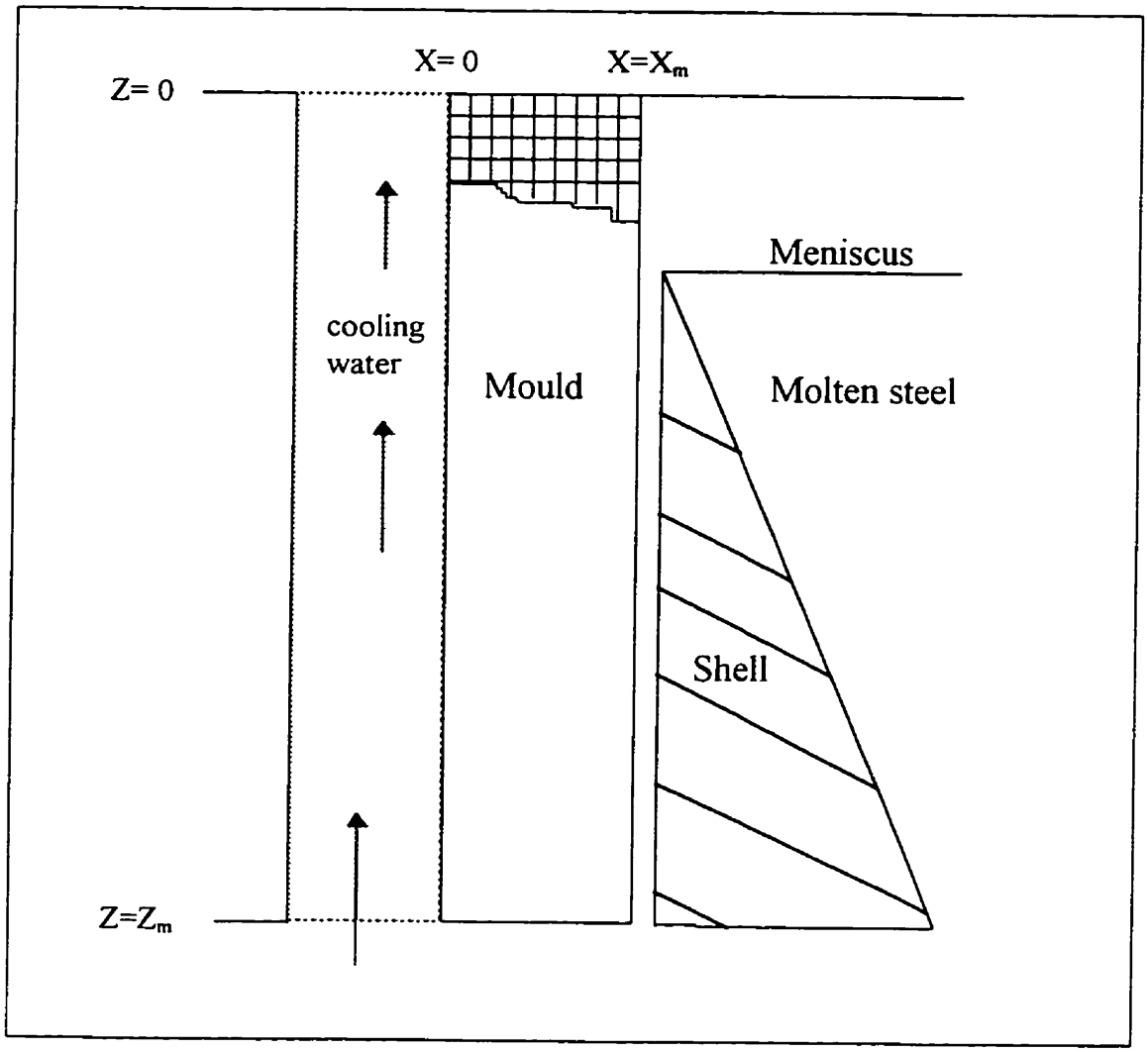

Figure 4.1 Schematic diagram of a longitudinal slice through the mid-face of a billet mould

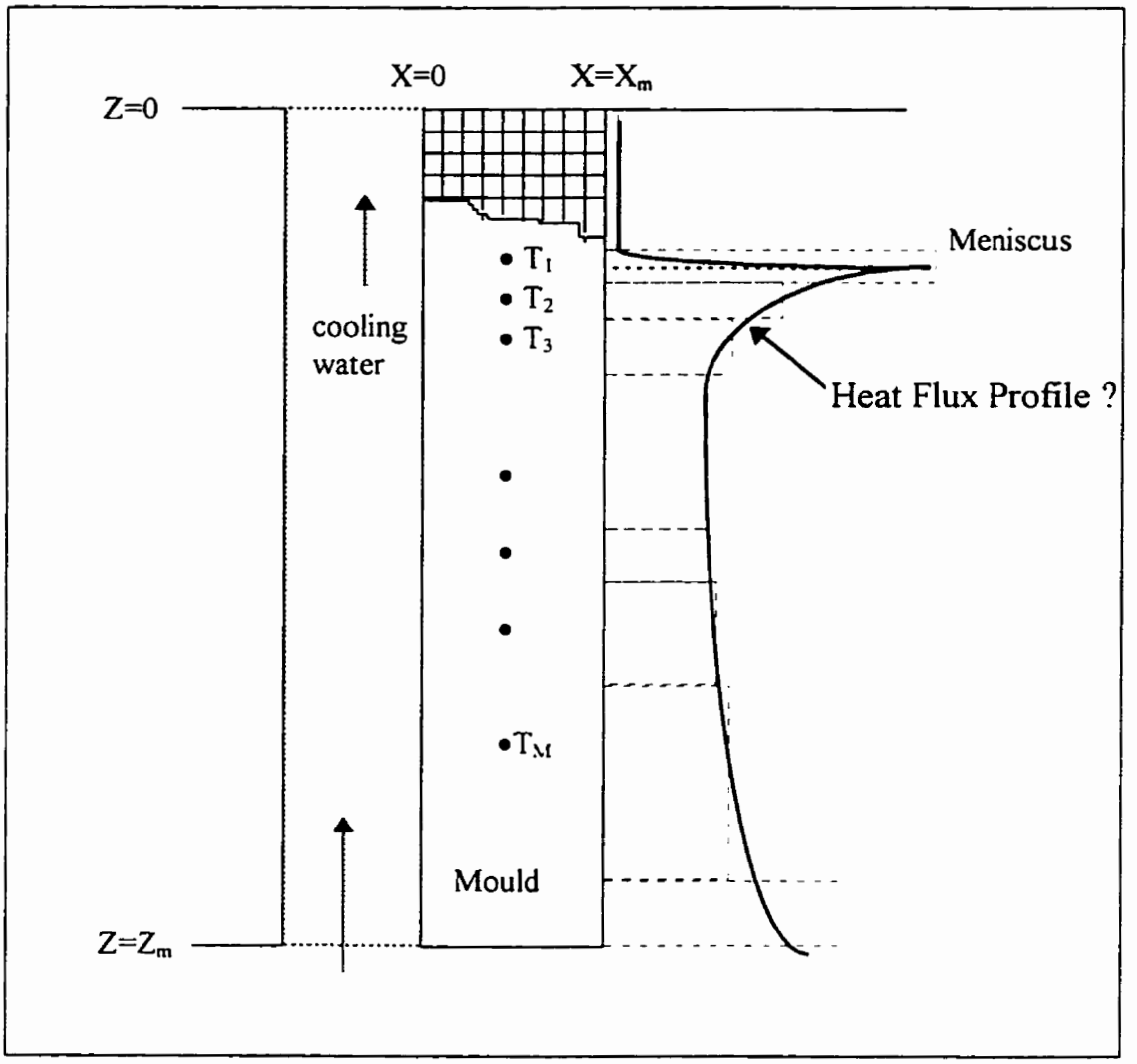

Figure 4.2 Schematic diagram showing the domain for the Inverse Heat Conduction analysis

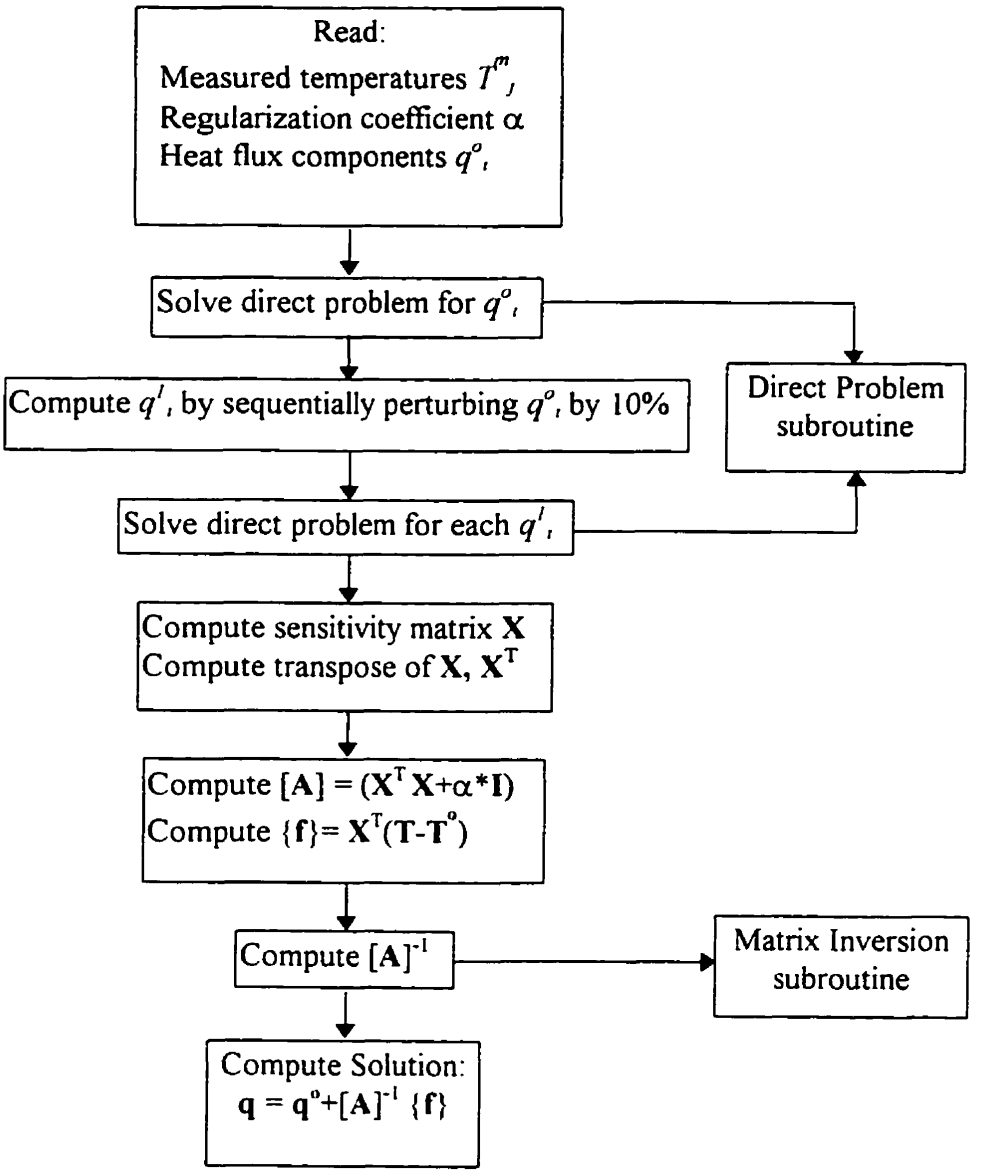

Figure 4.3 Conceptual flow-chart of the FORTRAN program developed to compute the solution for the IHCP associated to estimation of mould heat flux profile.

(A)

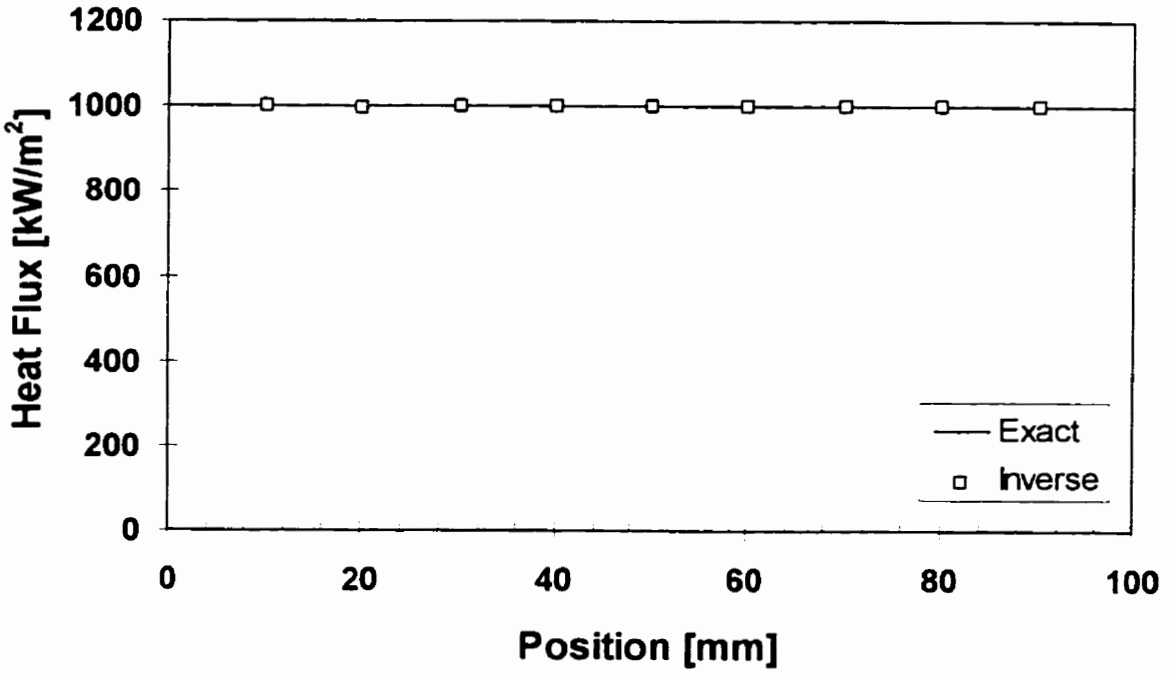

(B)

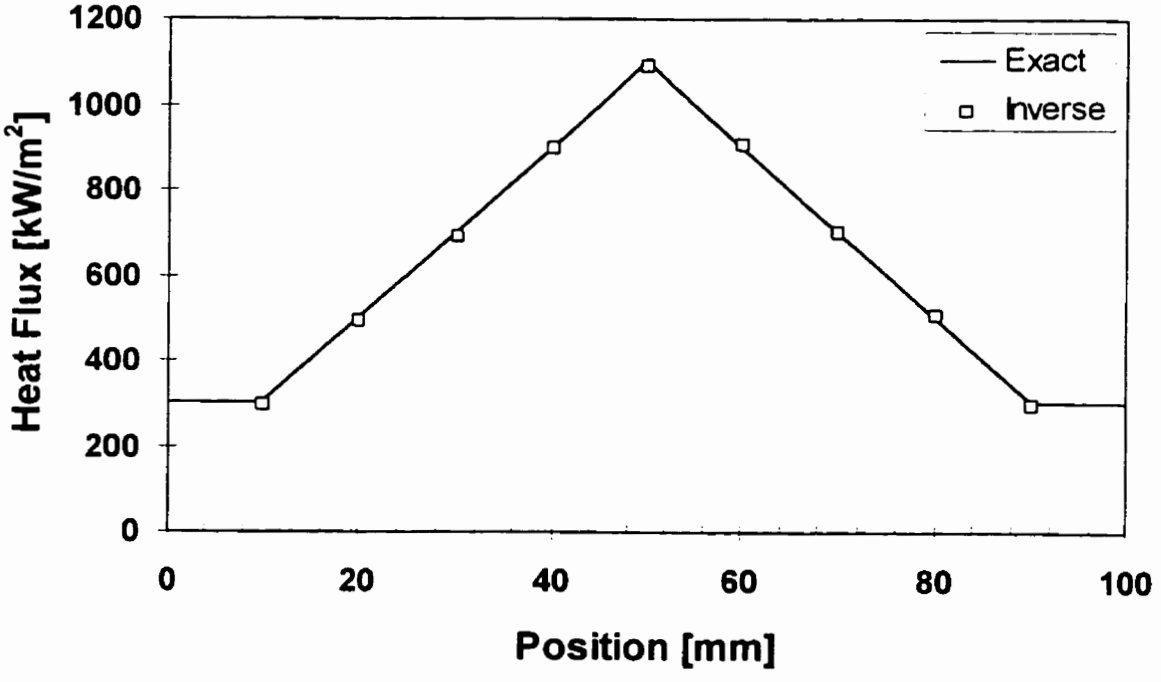

Figure 4.4 Validation tests for the IHC code- comparison between inverse estimation and exact solution for (A) constant heat flux input and (B) triangular heat flux profile.

(A)

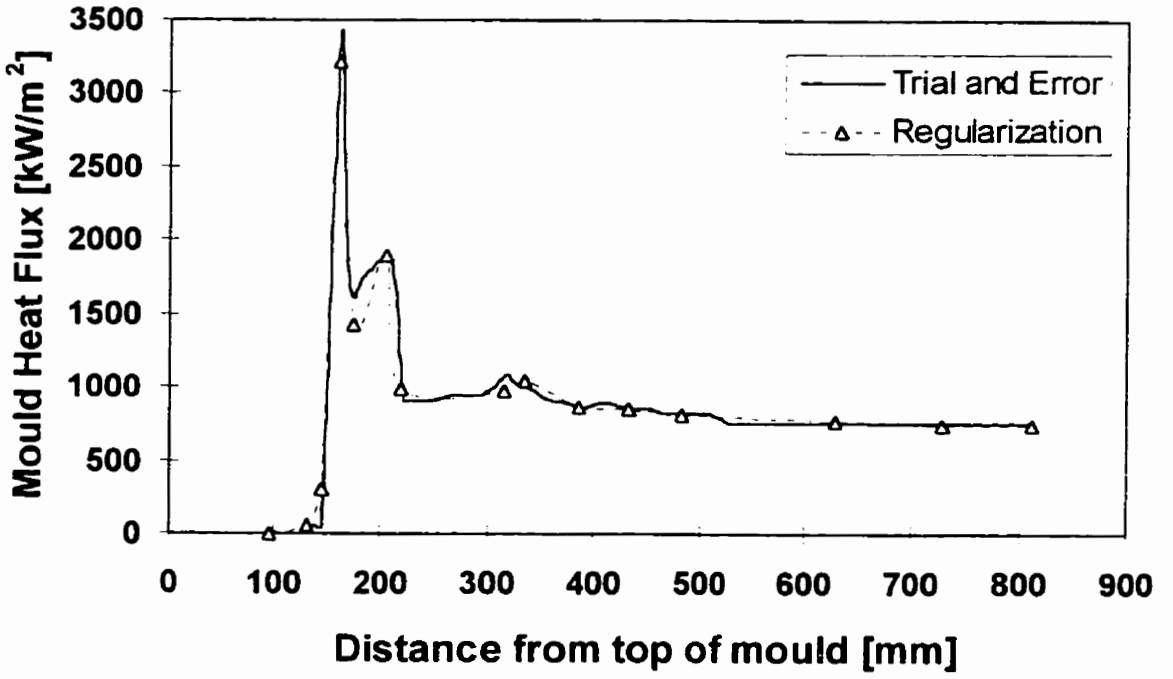

(B)

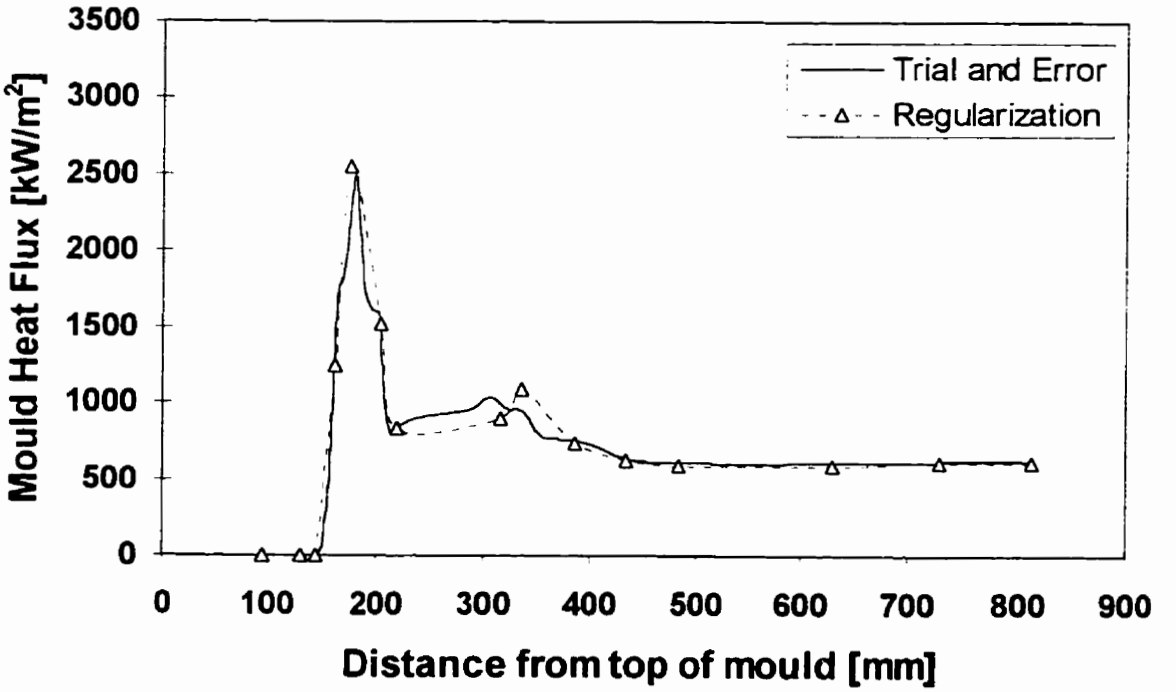

Figure 4.5 Comparison of heat flux profile between inverse estimation with regularization and trial-and-error adjustment; (A) heat 262 and (B) heat 265.

(A)

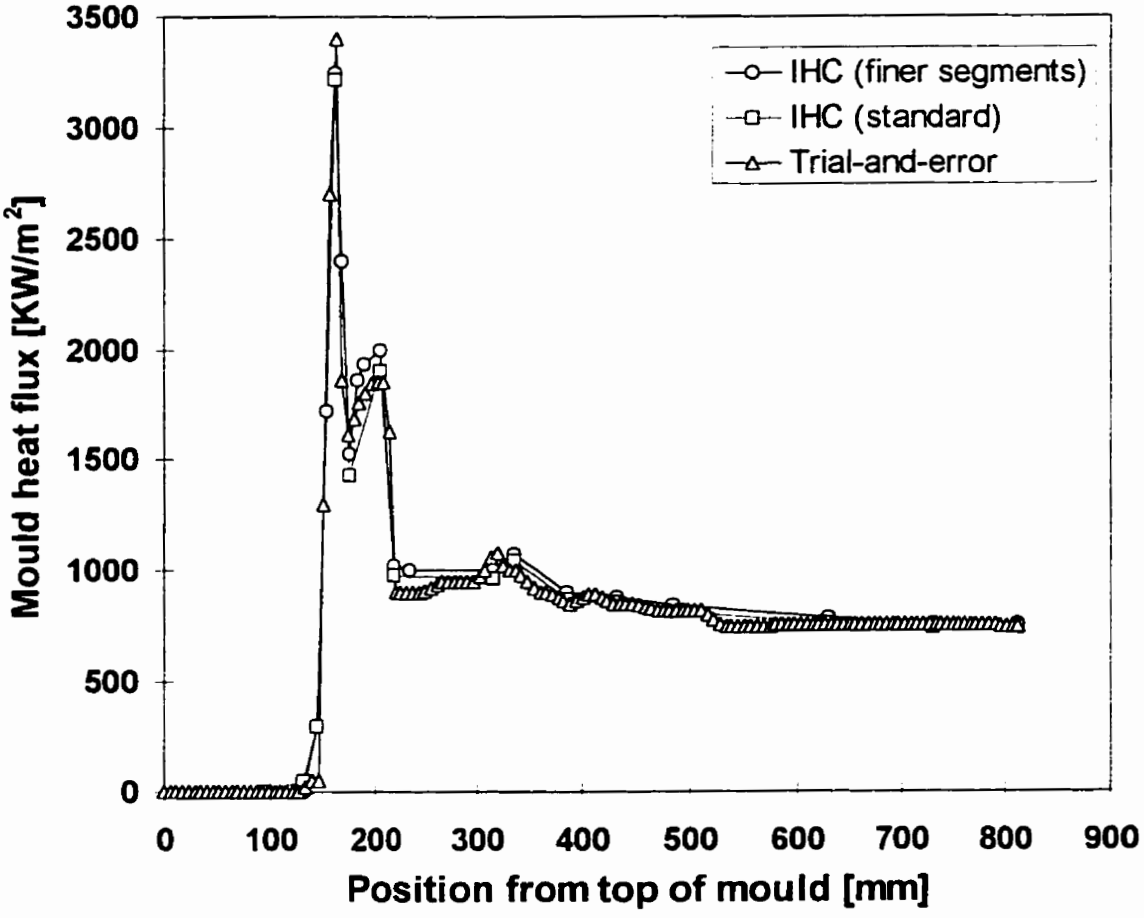

(B)

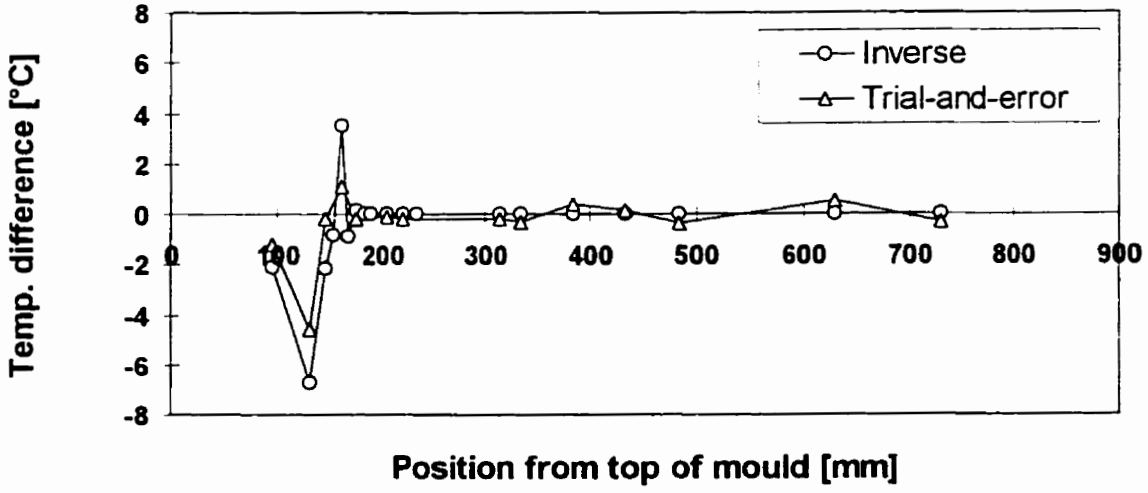

Figure 4.6 Comparison between inverse estimation with regularization and trial-and-error adjustment; (A) heat flux profile ; (B) temperature difference.

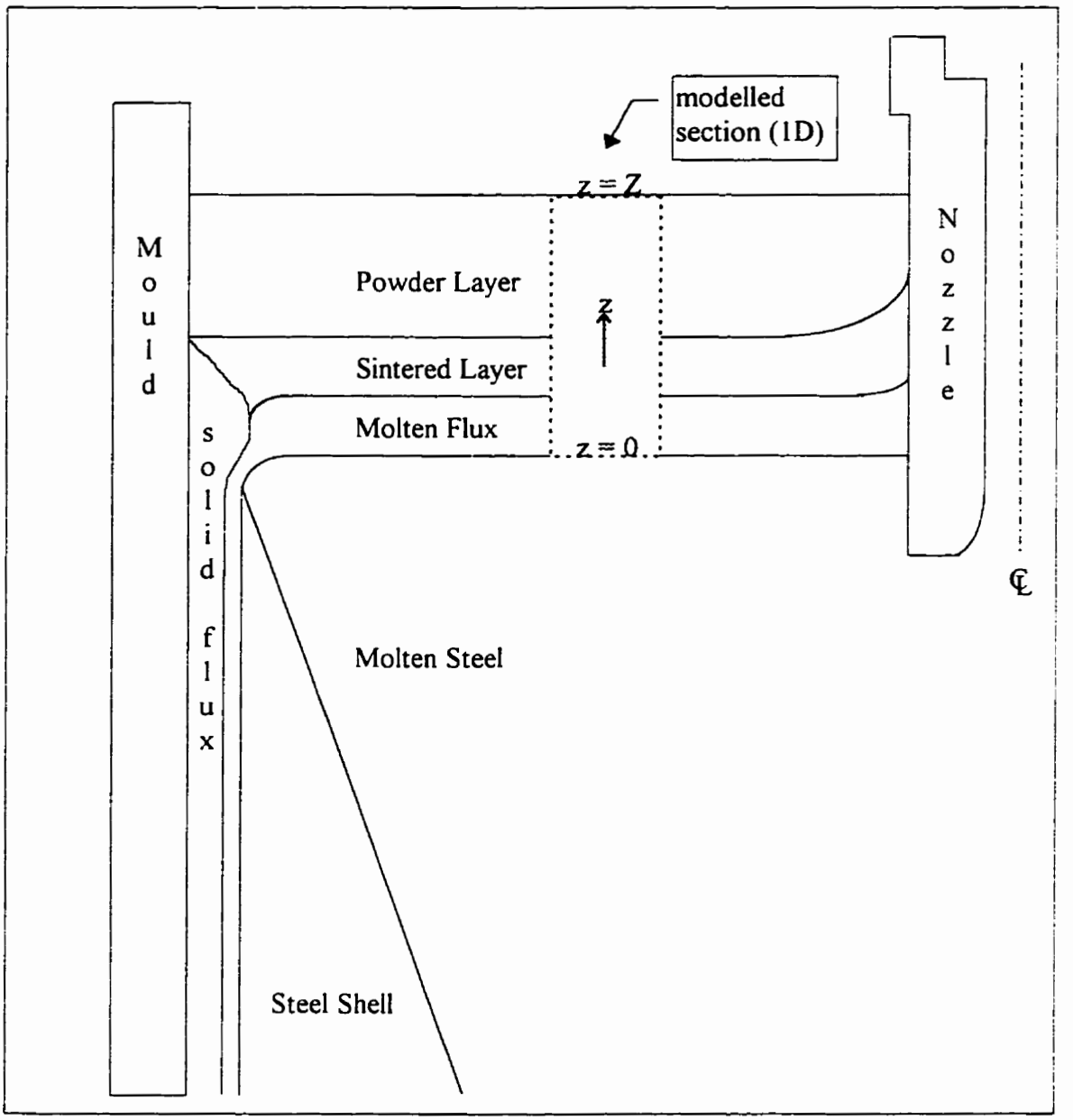

Figure 4.7 Schematic of a longitudinal mid-plane of a continuous casting mould system showing the section modelled.

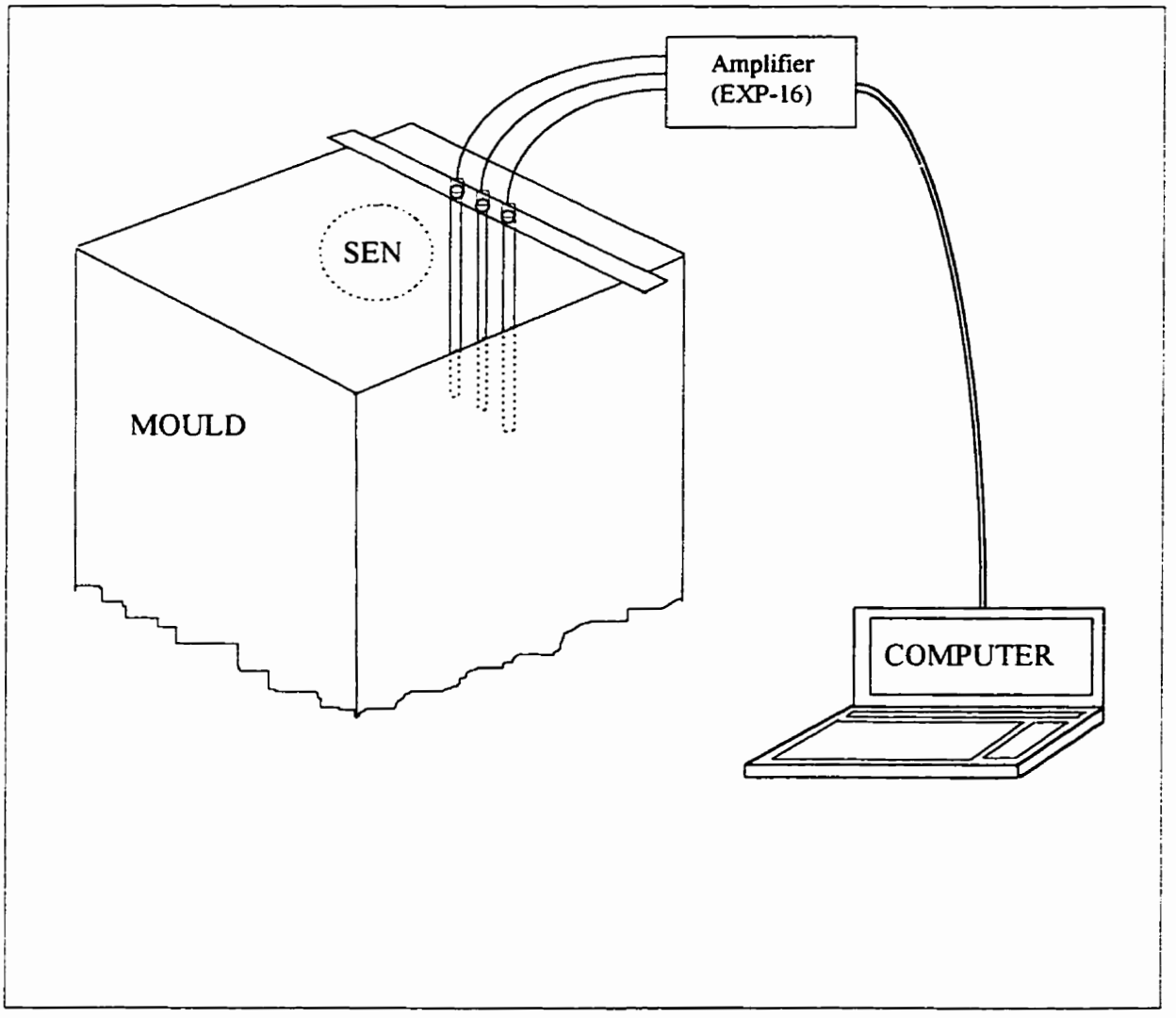

Figure 4.8 Schematic showing thermocouples and data aquisition system used to measure mould powder temperature profile

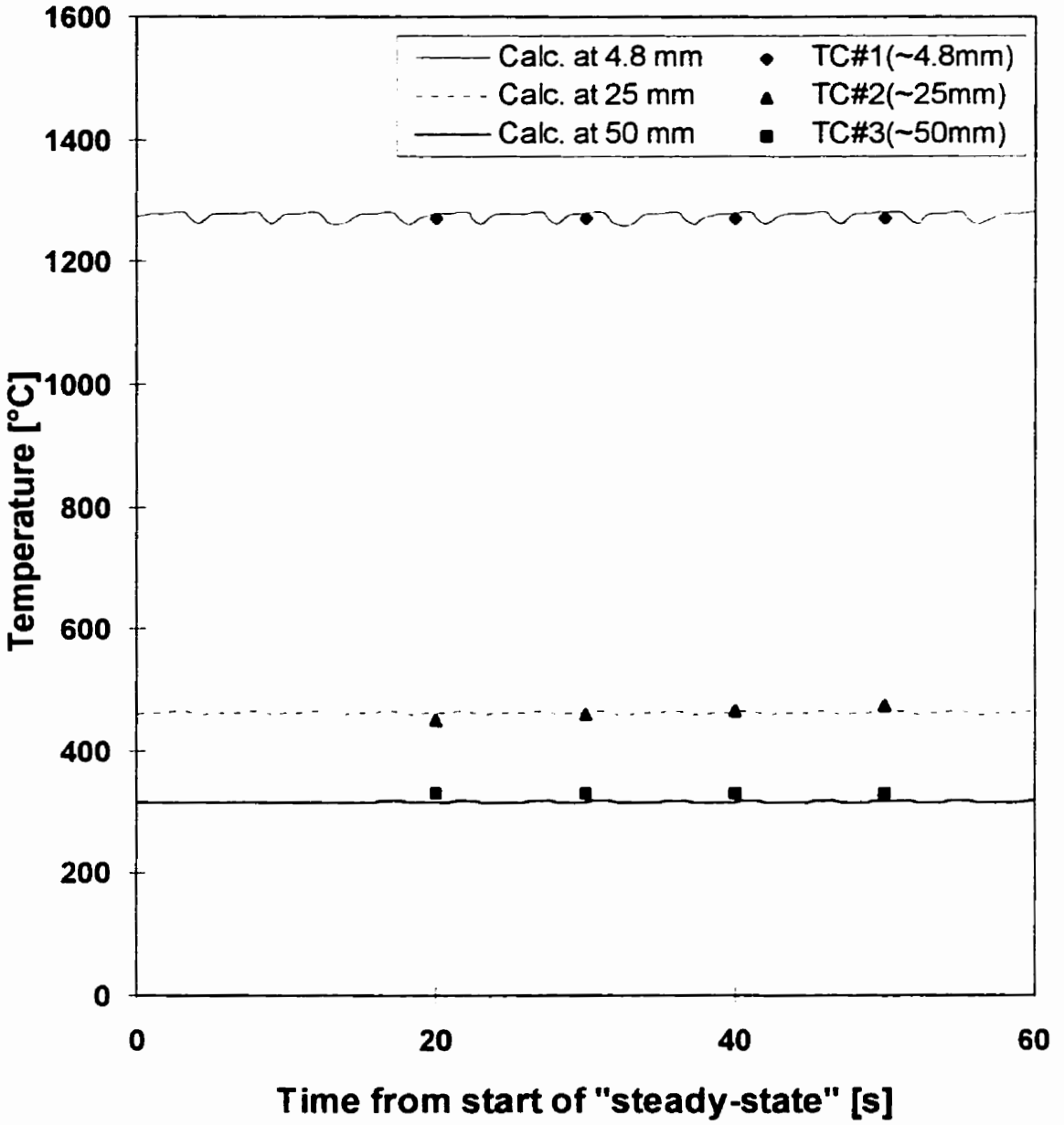

Figure 4.9 Model validation: measured vs. calculated temperature at three different positions within the mould power layers.

(A)

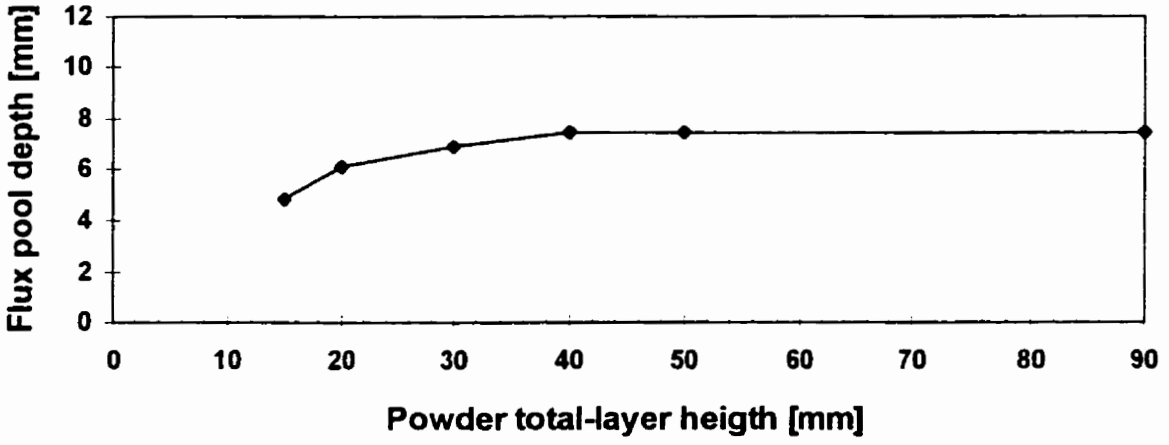

(B)

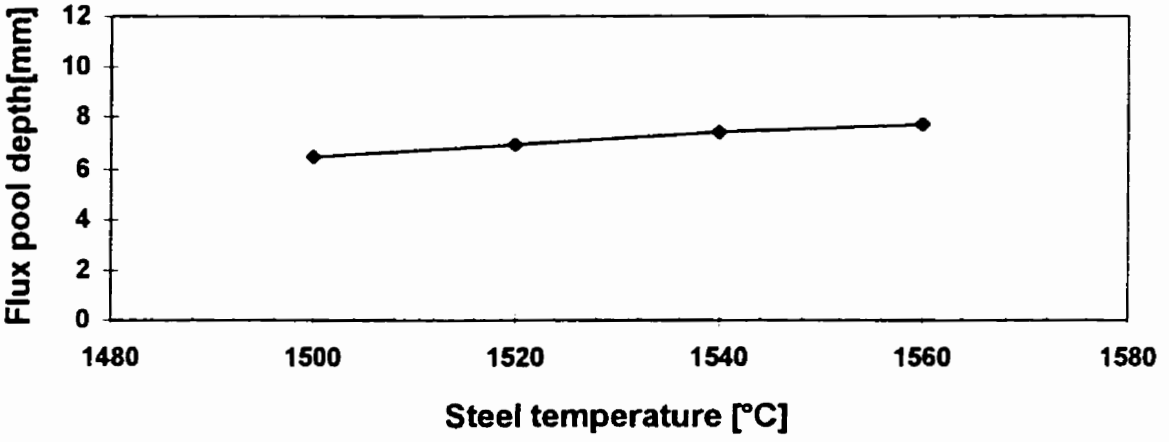

(C)

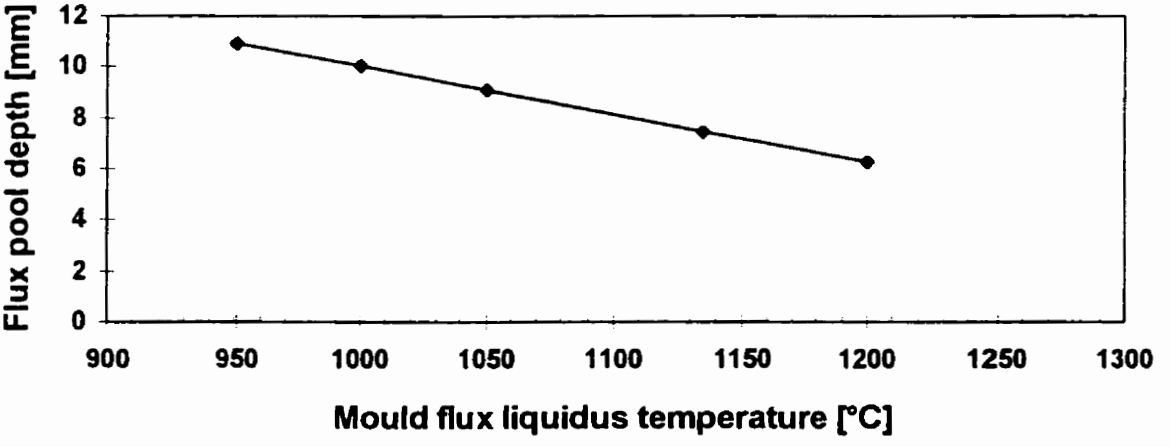

Figure 4.10 Influence of model parameters on calculated depth of the liquid flux pool: (A)-total height of powder on top of the liquid steel, (B)- temperature of the liquid steel in the interface steel/flux, (C)- liquidus temperature of the mould powder.

(A)

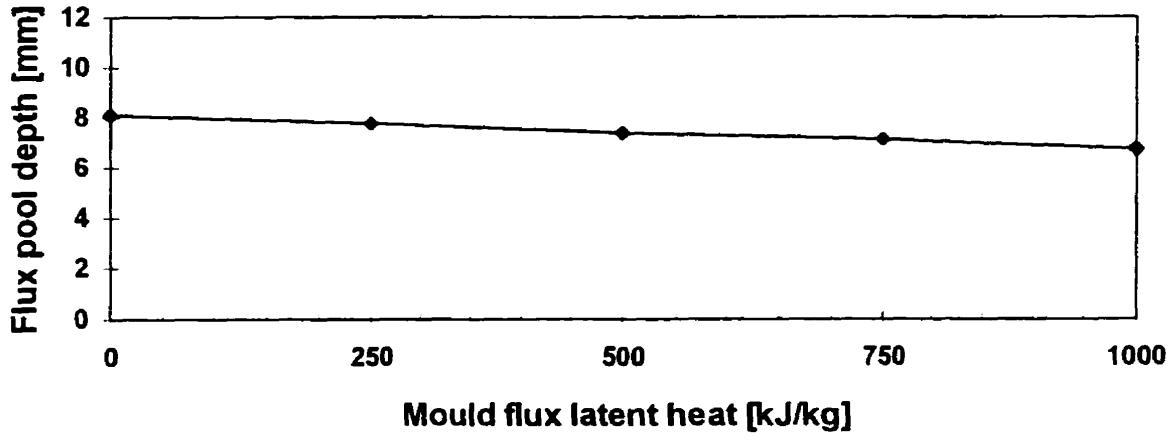

(B)

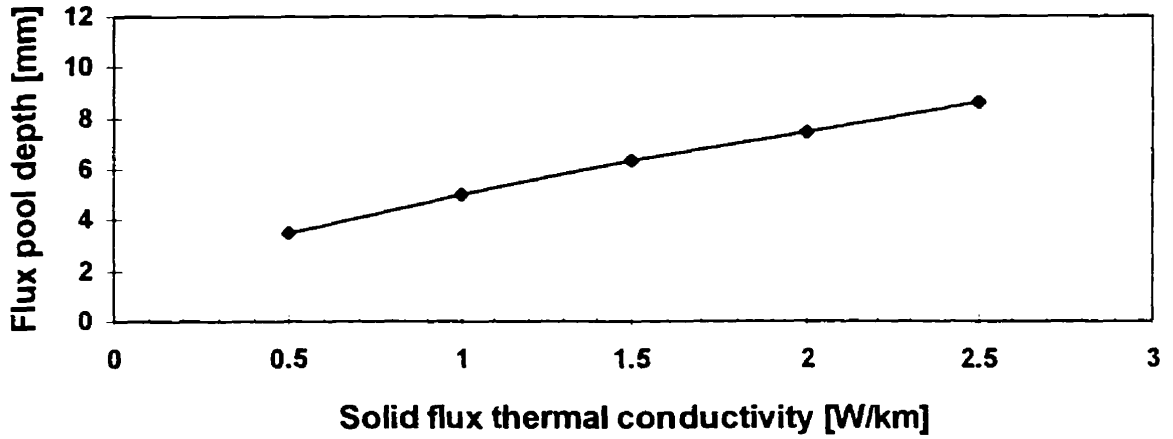

(C)

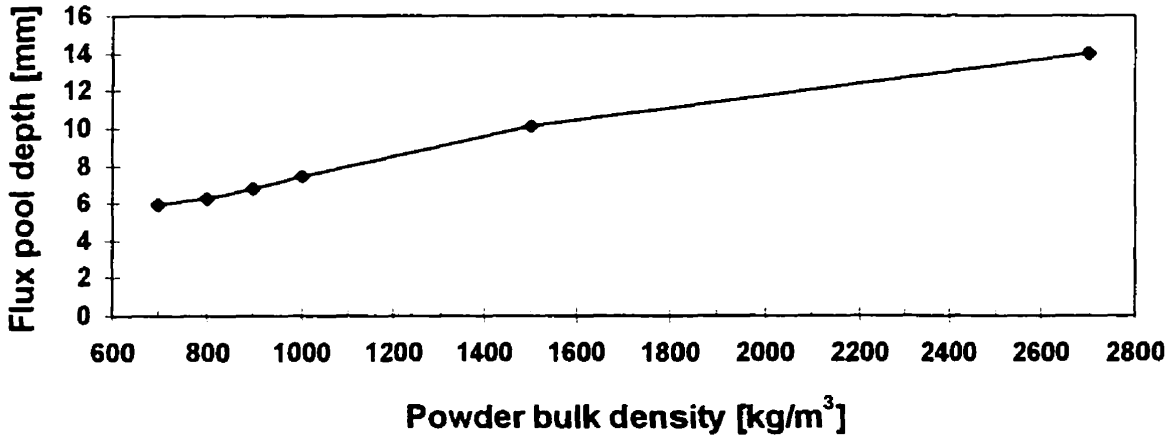

Figure 4.11 Influence of model parameters on the depth of the liquid flux pool: (A)- mould powder latent heat (B)- thermal conductivity of solidified flux, (C)- powder bulk density.

(A)

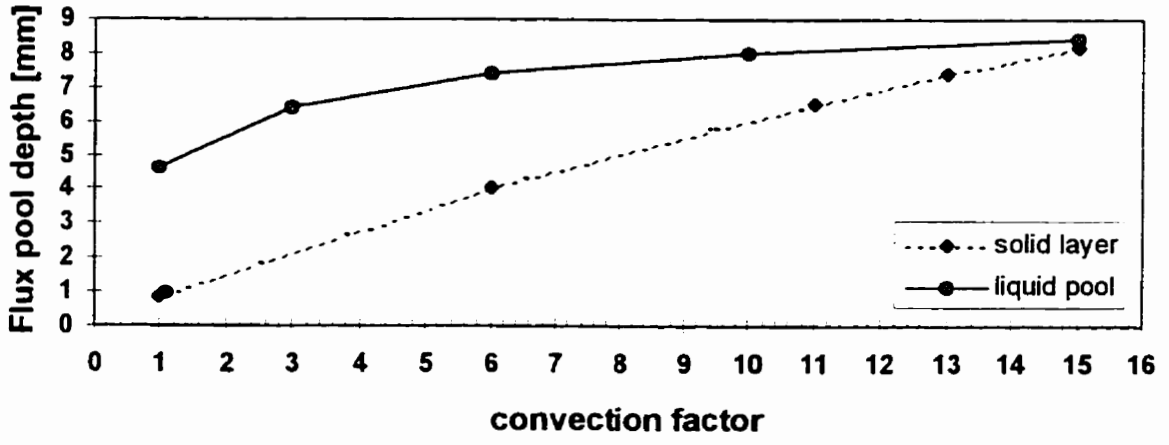

(B)

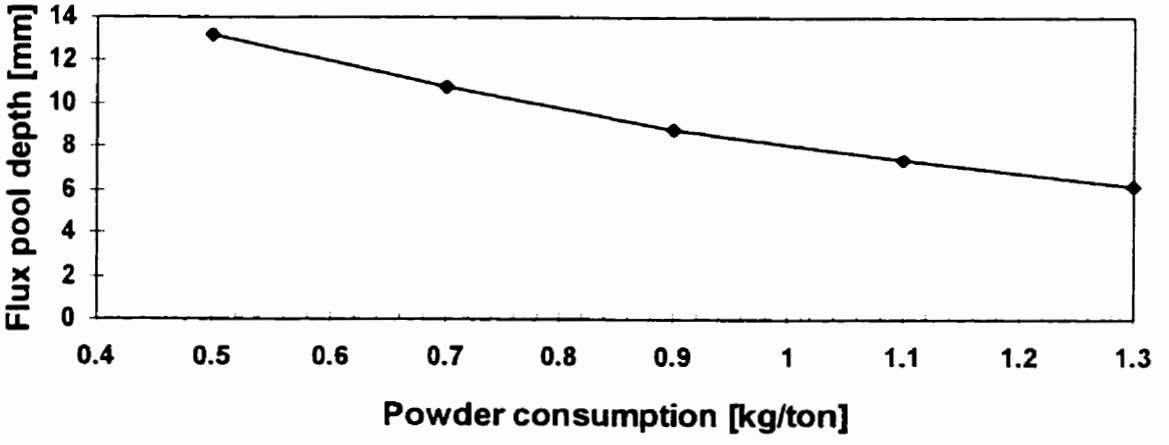

(C)

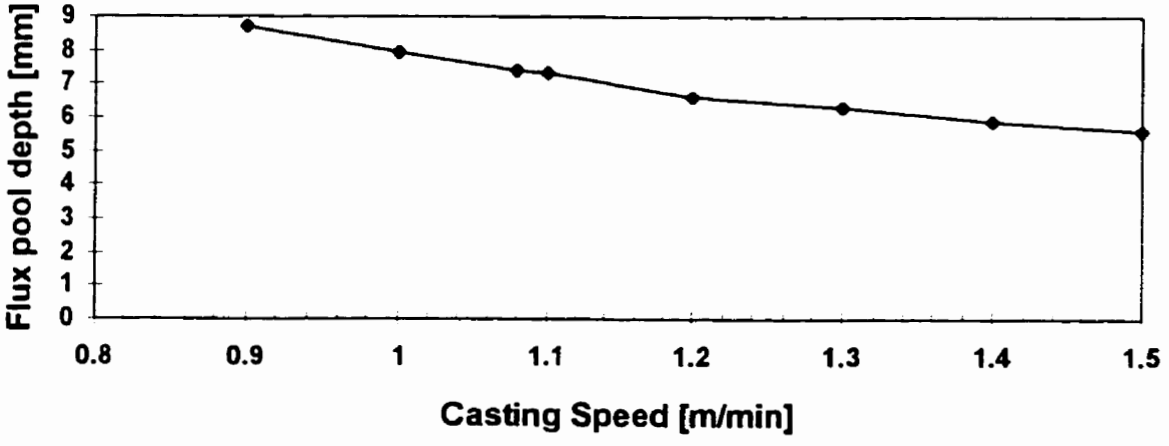

Figure 4.12 Influence of model parameters on the depth of the liquid flux pool: (A)- thermal conductivity enhancing factor due to convection in the powder layer, (B)- mould powder consumption, (C)- casting speed.

5. PLANT TRIAL

In this study an instrumented-mould trial was conducted at a Canadian billet casting mini-mill. The trial involved data acquisition on mould thermal response, mould displacement, casting speed, metal level and mould flux temperature field. In addition, mould powder consumption and liquid flux pool depth were also measured. Samples of the billets cast at the trial were collected and analyzed at the University of British Columbia (UBC). This chapter discusses the instrumentation of the mould and casting conditions of the plant trial.

5.1 Instrumentation

5.1.1 Mould temperature measurement

The UBC continuous casting group has for the last two decades successfully instrumented billet moulds with thermocouples to measure mould wall temperatures. The technique implemented has been developed by Brimacombe, Samarasekera and co-workers[109-110,122].

Type T, single-wire, intrinsic copper-constantan thermocouples, recommended for a maximum temperature range of -200°C to 350°C[123], were employed to measure the mould wall temperature. The thermocouples were prepared by forming a bead on the constantan wire (diameter = 0.8 mm) with a TIG welder. The bead was filed flat to produce an end of approximately 0.3-0.4 mm thick, then heat-shrink tubing (1.6 mm in diameter) was applied to the wire to insulate it. Figure 5.1 shows the design of the thermocouples.

To install the thermocouples into the mould, threaded holes were prepared through the water baffle and half-way into the copper mould wall. The bead-side of the wires were inserted through the water baffle into the holes drilled in the mould wall and held in place by

copper plugs screwed into the threaded holes. Silicone sealant was employed to prevent any water leak through the baffle. The constantan wires were then attached to insulated copper wires in the cooling water plenum. Groups of wires were bunched together and connected to a data acquisition system through a pipe fitting in the side of the mould jacket. Rubber plugs and silicone sealant were placed in the fitting for a water-tight seal, which was retained by a pipe thread collar. The thermocouple configuration was then tested for electrical continuity and the assembly was pressure tested with water. After the trial, the thermocouples were again tested to identify those that failed during the trial.

To measure inlet and outlet water temperatures Type T two-wire thermocouples were installed in the water channel. Temperature of the cold junction which was located at the data acquisition system, was measured with a mercury thermometer. The thermocouple layout adopted in the plant trial is presented in Figure 5.2. Appendix A details the depth and axial position of the arrangement. Thermocouples were installed at both the mid-face and off-corner locations on the four faces of the mould. A higher concentration of thermocouples was installed in the meniscus region so the mould peak heat flux and metal level fluctuations could be monitored more accurately, since both are associated with surface and shape defects.

5.1.2 Process control signals

Casting speed

The casting speed signal was acquired directly from the plant control system as a voltage which originated from a withdrawal roller tachometer. Casting speed calibration was supplied by the plant maintenance team.

Metal level

The metal level signal was also acquired directly from the plant control system. It was calibrated by inserting a billet into the mould at various levels from the top of the mould and measuring the output voltage at each level.

5.1.3 Other measurements

Mould displacement

The mould displacement was measured using a Linear Variable Differential Transformer (LVDT). The LVDT was attached to a magnetic clamp and anchored to the mould housing near the centre of the oscillator table. The LVDT was calibrated on-site with a block of known dimension.

Internal dimensions of the mould

The internal dimensions of the mould were measured using a LVDT-based profilometer. This measurement was performed before the trial to evaluate the mould taper, and also after the trial to check for any permanent distortion of the mould tube

Mould-strand friction forces

Although not part of this research mould-strand friction forces were measured using both load cells and a strain gage. These measurements were part of a separate study conducted by Gurton[124]. The experimental details as well as the analysis of mechanical sensor signals was examined elsewhere[124] and will not be discussed here.

5.2 Data Acquisition System

The data acquisition system consisted of a personal computer, an analog-to-digital converter, a multiplexer and data acquisition software.

Personal Computer

An IBM PC clone featuring an Intel 80486DX2-66 microprocessor, 16 Mbytes of RAM, two hard drives with total capacity of 1.7 Gbytes and a 1.2 Bytes Colorado tape drive, was used for data acquisition.

Analog-to-Digital Converter

A metrabyte DAS-8 data acquisition card was installed into the PC-ISA bus slot. All connections were made through a standard 37 pin D male connector that projects through the back of the computer. Metrabyte's DAS-8 is an 8 channel, 12 bit high speed, Analog-to-Digital (A/D) converter and time/counter board designed for the IBM-PC. It features a 12-bit successive approximation analog-to-digital converter with sample/hold. The full scale of each channel is ±5.0 V with a resolution of 2.44 mV and the inputs are single ended with a common ground. Conversion time is typically 25 microseconds, 35 microseconds maximum. Input frequencies of up to 2.5 MHz can be handled by the programmable timer/counter.

Multiplexer

The multiplexer consisted of 8 cascaded EXP-16 boards called an EXP-ENC device. A power supply powered the multiplexer through a splitter in the ribbon cable between the DAS-8 and EXP-ENC. The multiplexer is capable of handling 128 input channels of standard voltage and 112 ($16 \times 7 = 112$) of thermocouple measurement.

Metrabyte's Universal Expansion Interface, model EXP-16 is an expansion multiplexer/amplifier system that can be used with any data acquisition system. Each EXP-16 concentrates 16 differential analog input channels into 1 analog output channel. The input channels are selected by a solid state 4 bit TTL-CMOS compatible address. The EXP-16 boards also provide signal amplification, filtering and conditioning. The amplifier provides

gains of 0.5, 1.0, 2.0, 10.0, 50.0 and 100.0 as well as programmable gain capability. Provision is made on the board for filtering, attenuation and measuring current instead of voltage. When used with DAS-8, channel selection is via the OP1-4 digital outputs of SAS-8.

Software

Keithley Labtech Notebook for windows was used as the data acquisition software. This software allows the customization of the input channels to be read, the data sampling rate, the output data format and real time graphical display of selected inputs. The data was stored in binary files instead of ASCII because the former format is memory-wise much more efficient.

CONVERT[125], a computer program coded in FORTRAN 77 developed by the Billet Casting Group at UBC, was used to convert the binary data to ASCII data. This program has a number of useful features that allow easy manipulation of data, such as data thinning; user-defined calibration polynomials for different data channels; and user-defined output files.

5.3 Plant Trial

Casting Machine

The plant trial was carried out on a two-strand billet casting machine, whose major design details are given in Table 5.1. An important feature of the variable tapered mould is its very steep initial taper (4.9% m^{-1}). The real taper at the meniscus can vary between 3 and 5% m^{-1}, depending on the meniscus level.

Casting Conditions

A total of 17 heats consisting of two sequences of peritectic steels and one of Boron(Ti)-alloyed medium-carbon steel were monitored. Appendix B details the chemical composition of the heats monitored in the plant trial. For some of the heats, approximately half way through

the heat, the mould water or the mould powder was changed. In all three sequences the oscillation stroke was kept constant, 6 mm, but the frequency was varied. Details of the trial casting conditions for each of the sequences are shown in Tables 5.2, 5.3 and 5.4. The peritectic-carbon heats were cast using mould water flow rates of 650 and 500 US gallons per minute, i.e., mould water velocities of 9.9 m/s and 7.6 m/s respectively. The Boron(Ti)-alloyed steels heats were cast with flow rates of 650 and 400 US gallons per minute, the latter corresponding to a water velocity of 6.0 m/s.

Mould Powders

Two different mould powders, hereby identified as powder A and B, were tested in the trial. Table 5.5 shows the main characteristics of these powders.

5.4 Billet Samples

Two billet samples, 400 mm long and corresponding to each half of a heat, were acquired for each heat monitored in the plant trial. The first sample was cut at 30 min. from the start of the heat, which corresponded to the steel in the mould at approximately 14~18 min. from the start of the heat. The second sample was cut at 60 min. The billet samples were marked with heat number, casting direction and face orientation, then shipped to UBC for quality evaluation.

At UBC each billet sample had its torch-cut ends cut off and were shot blast to clean their surface. A 10~15 mm thick transverse section was cut from each sample for sulfur-printing and macro-etching analysis. The samples had their east and west faces photographed, were inspected and their surface profile was measured. More detailed description of the procedures

adopted for preparation and inspection of billets samples have been documented elsewhere[109,122].

For this study the samples were inspected for:

1. Surface quality:
    - Oscillation marks
    - Depressions: transverse and longitudinal
    - Bleeds, laps and sticking marks
    - Mould flux entrapment
2. Dimensional quality:
    - Rhomboidity or off-squareness (difference between two diagonals)
3. Internal quality:
    - Cast structure

Oscillation mark were of particular interest to this study because the depth of these marks has been linked to mould-flux viscosity and mould Negative-Strip Time (NST). The depth of oscillation marks were measured using a profilometer table featuring three LVDT's. The LVDT signals were logged using a Toshiba 286 laptop featuring a Metrabyte DAS-8 data acquisition board and Keithley Labtech Notebook for DOS data acquisition software, and a Metrabyte EXP-16 analog multiplexer and amplifier.

5.5 Analysis of Mould Temperature Data

5.5.1 Converting measured voltage into temperature

Thermocouple voltage was converted to temperature using the capability of CONVERT[125] to calibrate data with polynomial equations. For Type T thermocouples, a seventh order polynomial of the form

$$T = a_0 + a_1X + a_2X^2 + \ldots + a_7X^7 \qquad (5.1)$$

yields an accuracy of ±0.5°C over the range -160 to 400°C[123]. In Equation (5.1) T is temperature (°C) and X is the measured voltage (Volts). The polynomial coefficients are listed in Table 5.6.

Figure 5.3 shows the thermocouple connections employed in the plant trial. It should be noted that the voltage measured for each mould thermocouple wire was the sum of the voltage of two copper-constantan junctions; one in the mould (V1), the other in the water channel (V2). Since the potential at these junctions opposes each other, the measured voltage is actually V1 minus V2. Thus, the voltage recorded by the two-wire thermocouples in the cooling water were used to compensate for the copper-constantan junction in water channel. As shown in Figure 5.3 a flange separates the inlet and outlet water flows. The upper chamber contains the outlet water and therefore, the value of V2 was set equal to the voltage recorded for the outlet water for all junctions located in the upper chamber, and equal to the voltage recorded for the inlet water temperature for all junctions located in the lower chamber. Thus to calculate mould temperature, the mould thermocouple voltages were added to the water channel thermocouple voltage plus reference temperature voltage (voltage corresponding to the ambient temperature measured by a mercury thermometer at the data acquisition computer room), then converted to temperature using the calibration equation.

Table 5.1: Casting machine major design details

Machine type	curved
Mould material	DHP copper
Mould Section (mm×mm)	209×209
Mould Length (mm)	812.8
Mould wall thickness (mm)	15.6
Corner radius (mm)	3.175
Mould Taper	parabolic
Initial taper (100 mm below top of mould, $pct.m^{-1}$)	4.9
Mould constraint	4-sided
Water channel gap (mm)	4.99
Metallurgical length (mm)	19787

Table 5.2: Operating casting conditions for 1st sequence of the plant trial -

Steel Grade: Peritectic steel (0.10≤%C≤0.15) Mould Oscillation Frequency: 150 cpm Average casting speed: ~21 mm/s Negative-strip time: ~0.14 s			
Heat No.	**C Content**	**Mould Powder**	**Water Flow rate**
260	0.11% C	A	650 US gpm
261	0.12% C	A	650→500 US gpm
262	0.11% C	A	500→650 US gpm
263	0.11% C	A→B	650 US gpm
264	0.12% C	B	650→500 US gpm
265	0.12% C	B	500→650 US gpm

Table 5.3: Operating casting conditions for 2nd Sequence of the plant trial

Steel Grade: Peritectic steel (0.10≤%C≤0.15) Mould oscillation frequency: 170 cpm Average casting speed: ~22 mm/s Negative-strip time: ~0.12 s			
Heat No.	**C Content**	**Mould Powder**	**Water Flow rate**
277	0.14% C	A	650→500 US gpm
278	0.13% C	A	500→650 US gpm
279	0.14% C	A→B	650 US gpm
280	0.13% C	B	650→500 US gpm
281	0.13% C	B	500→650 US gpm
282	0.13% C	B→A	650 US gpm

Table 5.4: Operating casting conditions for 3rd Sequence of the plant trial

Steel grade: B(Ti)-alloyed medium carbon steel (0.30 ≤%C≤0.35) Mould oscillation frequency: 137 cpm Average casting speed: 21 mm/s Negative-strip time: ~0.14 s			
Heat No.	**Wt.% C**	**Mould Powder**	**Water Flowrate**
311	0.33% C	A	400→650 US gpm
312	0.30% C	A	650→400 US gpm
313	0.33% C	A→B	400 US gpm
314	0.31% C	B	400→650 US gpm
315	0.32% C	B	650→400 US gpm

Table 5.5: Mould powders used in the trials

POWDER	**A**	**B**
Type	Fine powder	Semiprefused fine powder
Chemical Composition SiO_2 CaO Al_2O_3 Na_2O MgO F Free carbon CaO/SiO_2	(wt%) 32.0 30.1 6.7 14.6 1.4 8.2 3.5 0.94	(wt%) 31.0 38.7 4.7 8.8 2.4 9.8 2.9 1.25
Softening temperature	N/A	Start at 1000°C End at 1020°C
Transition temperature[2]	1000 °C	1135 °C
Viscosity@1400°C (poise) @1300°C @1250°C	0.7 1.3 1.9	0.4 N/A 0.9
Grain Size (mesh)	97% -149	97% -149
Bulk density (kg/m^3)	690	820
Typical Use	All purpose	(0.10≤%C≤0.15)

[2] temperature at which viscosity (η) increases abruptly

Table 5.6: Polynomial coefficients for Type T thermocouple voltage-to-temperature conversion

Coefficient	Value
a_0	+ 0.100860910
a_1	+ 25727.94369
a_2	- 767345.8295
a_3	+ 78025595.81
a_4	- 9247486589
a_5	+ 6.97688×10^{11}
a_6	- 2.66192×10^{13}
a_7	+ 3.94078×10^{14}

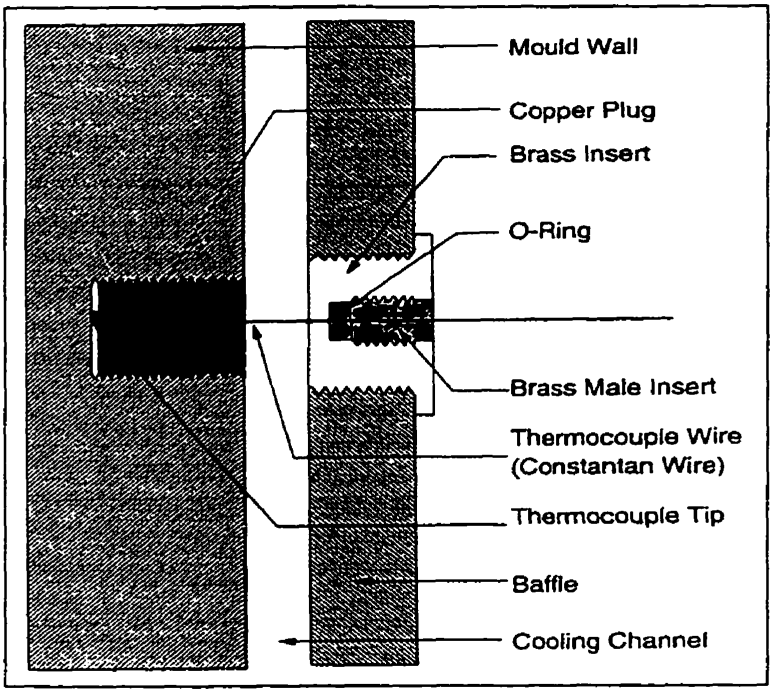

Figure 5.1 Schematic diagram of the thermocouples used at the plant trial

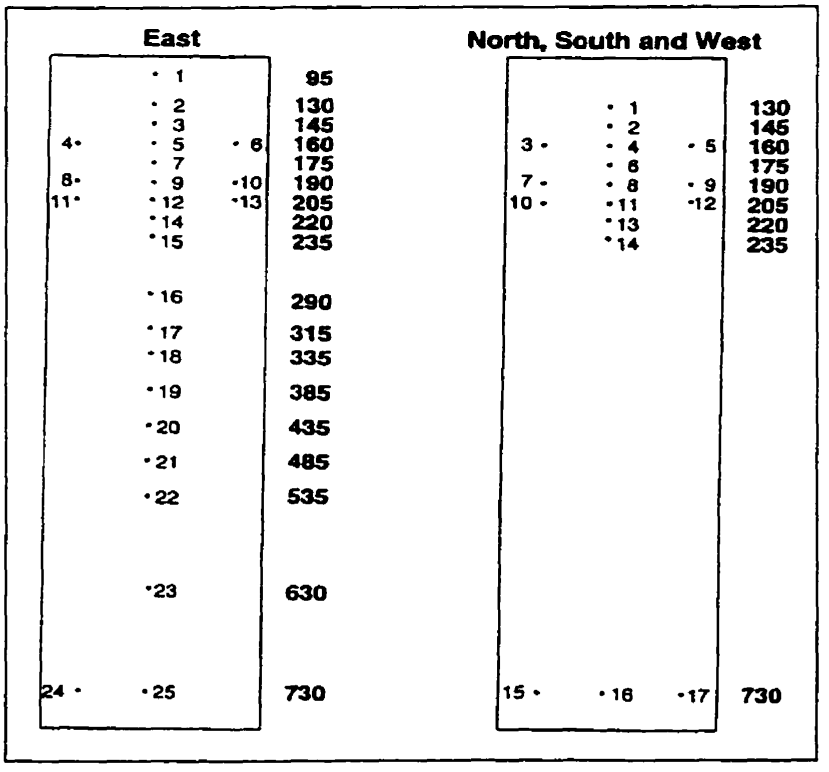

Figure 5.2 Thermocouple layout employed at the plant trial

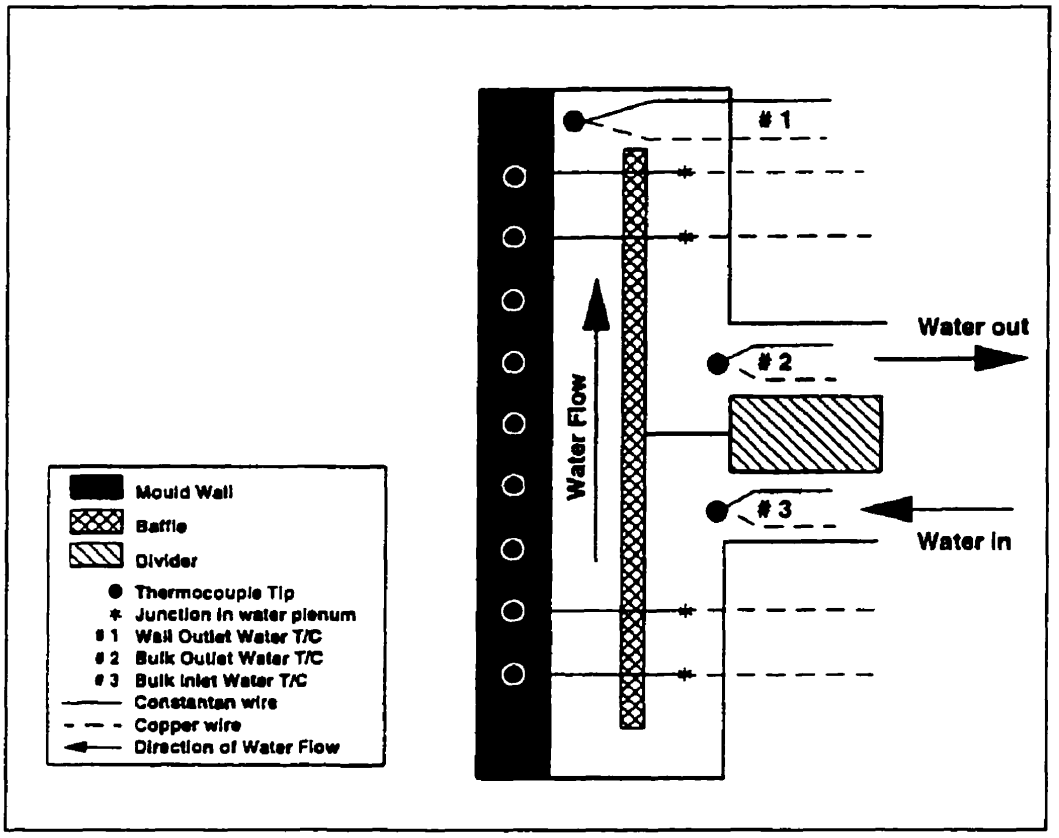

Figure 5.3 Thermocouple arrangement for measuring mould wall and cooling water temperature

6. MOULD THERMAL RESPONSE, BILLET QUALITY, METAL LEVEL CONTROL, POWDER CONSUMPTION AND FLUX POOL

Overall results of the plant trial are presented in this chapter. These include mould temperature measurements, billet sample quality evaluation and molten flux pool depth. Mould wall temperatures can give a good qualitative estimation of the heat transfer from the strand to the mould, however it must be kept in mind that mould temperatures are not only a function of the heat coming from the steel but as well as a function of the heat transfer coefficient at the water-mould interface, which is dependent on the mould water velocity. In this Chapter mould temperature measurements are presented and the influence of process variables on mould heat transfer is examined. In addition, results of visual inspection of billet samples and surface profile measurements are presented and links between these results, the lubricant and process variables are established. Finally, measurements of metal level, powder consumption, molten flux pool depth and mould flux temperature profile are also presented.

6.1 Mould Temperature Measurement

A total of 76 thermocouples were installed to measure the temperature of the mould at several positions on its four faces, as previously shown in Figure 5.2. However, thermocouple 16, located on East face at 290 mm from the top of the mould, was not connected to the data acquisition system due to irreparable failure. Figure 6.1 shows typical temperature response of selected thermocouples located at 95, 145, 161, 205, and 729 mm from the top of the mould. As expected mould temperatures do not remain constant during casting. Fluctuations in temperatures along the mould length can occur due to numerous reasons such as uneven flow of mould flux and surface defects traveling down the mould, however casting speed and/or metal level variation are the more important.

The thermocouples placed above the meniscus at 95 and 145 mm displayed temperature variations of amplitude 54% and 39%, respectively. The temperature of the thermocouple located at 95 mm fluctuates between 27°C and 48°C (avg=39°C and sd=3.7°C), while at 145 mm the temperatures varied between 51°C and 77°C (avg=66°C and sd=4.6°C). Since for the uppermost thermocouple (95 mm), metal level variation should not have much influence on the temperature recorded, it seems that some noise was occurring. It can be clearly noticed that between 0 and 20 seconds all thermocouples except the thermocouple located at 729 mm present a similar signal pattern, this is most noticeable in the thermocouple located at 95 mm because it is the least affected by meniscus level fluctuations. Further analysis showed that the oscillatory component of the thermocouple signals were in phase, resulted in temperature fluctuations up to 20°C (±10°C), and only appeared in the signals of thermocouples 1 to 15 (Figure 5.2), which were all bundled together. This behaviour suggests the presence of an electrical noise caused by poor ground connection in the data acquisition system.

The temperature of the thermocouple located at 161 mm fluctuates between 91° and 125°C (avg=107°C and sd=7.0°C). This variation, which represent 31% of the average temperature, certainly is caused not only by the electrical noise and casting speed variation, but mainly by metal level variation. The temperature at this location varies the most because this is the thermocouple closest to the meniscus. It should be noticed that the meniscus was fluctuating between 161 and 171 mm from the top of mould; and at the same time the casting speed varied between 1.24 and 1.42 m/min (avg=1.33 m/min and sd=0.04); a variation of 14% of its average value. The temperature variation of the thermocouple placed at 729 mm, the lowest position down the mould, had a maximum value of 18% which was probably

responding to variations in casting speed, strand surface topology and thickness of the lubricating film.

6.1.1 Axial mould-temperature profiles

To eliminate electrical noise related to fluctuations in the mould temperature as well as effects of metal level fluctuations and casting speed changes, blocks of data pertaining to "approximately" constant metal level and casting speed were selected. For each thermocouple the recorded temperatures were time-averaged which minimizes the electrical noise since this noise was found to be cyclical and to have a constant magnitude. The term "approximately" constant metal level implies problems with metal level data which will be discussed in section 6.3.1 while for constant casting speed the term is used because at the time of the plant trial the mini-mill still did not have a metal level/flow control system. The metal level was controlled via casting speed variation which resulted in constant changes in casting speed. For each selected block the temperature data recorded by the thermocouples installed at the centreline of the East face of the mould wall were time-averaged to represent the "quasi' steady-state found in continuous casting moulds operating under stable conditions. Finally time-averaged temperature profiles were generated and utilized to analyze the influence of mould powder, oscillation frequency, mould water velocity, meniscus level, steel grade.

Before any steady-state analysis could be done the effect of data sampling rate on axial temperature profile had to be analyzed. As previously mentioned in Chapter 5, the data was originally collected at a rate of 60Hz because of a parallel study on mould mechanical response, however for this study the amount of data collected at 60Hz was excessive. Previously investigations conducted by UBC casting group suggested a sampling rate between 5 to 10 Hz for mould transient analysis[110], therefore sampling rates of 0.02, 1, and 10 Hz

were tested. As shown in Figure 6.2 the difference between these sampling rates is insignificant, and for practical purposes 1 and 10 Hz can be considered identical; therefore to save time, a sampling rate of 1 Hz was chosen for the steady-state analysis. For the sake of completeness Figure 6.2 also shows the standard deviation of the temperature for 10 Hz sampling rate. The maximum values, ~10°C, were found for the thermocouples located between 100 and 205 mm below the top of the mould. The thermocouples located above the meniscus are largely affected by the electrical noise mentioned earlier, while the high temperature thermocouples, located in the meniscus region, are mainly affected by meniscus fluctuations.

The axial temperature profiles were compared to assess whether there were any difference in temperature between the four faces of the mould. Figure 6.3 shows a typical result obtained. The East face was the only face instrumented down the length of the mould wall. Figure 6.3 shows from the meniscus (~177 mm) down to a location of 220 mm, the North face, which is the internal curved wall (ICW), displayed the highest temperatures. The East face had the second highest temperatures while the South and West faces were the lowest. Between 235 mm and 730 mm from the top of the mould no thermocouple was installed on South, West and North faces. The lowest thermocouples (730 mm) again showed North face to be the hottest but the other three were very close in temperature and did not show any significant difference. The above investigation is very important because only the East-face thermocouples were used for analyzing mould thermal response since the East was completely instrumented; however, since key thermocouples placed at the meniscus region failed (190 mm and 235 mm) temperature from the other faces at these locations had to be used as substitute data.

In slab casting differences in temperature among the four faces can be related to uneven liquid steel flow due to the geometry of SEN ports, differences in mould water velocities since each face has an independent water control system and uneven molten flux infiltration because the large dimensions of the slab can hinder an even distribution of the powder. For this study of square billets cast with tubular mould and straight-port SEN the first cause of temperature difference in slab casting can be dismissed because straight-port SEN is much less prone to bias flow and also any bias flow should not be always towards the North face. Also, tubular moulds, which have only one water channel, favor equalization of the mould water velocity for all faces, and the mould inspection performed after the trial showed no traces of solid deposits on its back faces, which suggests the elimination of uneven mould water flow or reduced local heat transfer as cause of the temperature difference. Notwithstanding, slight misalignment of the mould in the housing still can lead to water maldistribution, and thus to temperature differences among the mould faces. However, uneven distribution of powder seems to be the most probable cause of high North face temperatures. During the trial the powder was fed into the mould by an automatic feeder placed in front of the mould North face. The feeder featured a long tube with a single port which tended to accumulate powder on the Northeast corner of the billet. The accumulation of powder on the North face improved the thermal insulation at the top of the mould, thus locally reducing heat losses through the mould top and increasing the depth of the liquid pool; both of which can lead to a local increase in the heat flowing across the mould copper wall. The above explanation also elucidates why the East face tended to be have the second highest temperatures.

6.1.1.1 Typical axial temperature profile

A typical axial temperature profile on the centreline of East face of the mould wall is shown in Figure 6.4. The temperature increases abruptly from the top of the mould until it reaches its maximum value ~ 40 mm below the meniscus which is located 177 mm below the top of the mould. Below the location of peak temperature, there is a decrease in mould temperature, followed by a slight increase in temperature towards the bottom of the mould. The peak temperature is associated with the high heat transfer from the solidifying shell to the mould in the vicinity of the meniscus. Samarasekera and Brimacombe[106-107] showed that the mould wall peak temperature occurs below the meniscus because in the upper part of the mould a significant fraction of heat is flowing up the mould wall and not only directly across to the cooling water. Below the peak temperature the subsequent reduction in mould temperature is a consequence of a decrease in heat transfer. As solidification progresses the strand shrinks, which causes a gap to form between the strand and the mould, the dimension of which could increase depending on mould distortion and taper. The rise in temperature towards the end of the mould indicates an increase in heat transfer, thus better contact, which is probably a result of binding. The inadequacy of mould taper used for casting the trial heats will be addressed later.

Figure 6.4 also shows profiles of the maximum and minimum temperatures in the selected block used to calculated the time-averaged temperature displayed in Figure 6.4A. It is evident that largest fluctuations in temperature occur within a region of 60 mm from the meniscus down the mould. A distribution of standard deviation along the length of the mould for the axial temperatures is shown in Figure 6.4B and it can be seen that a peak in the absolute value of standard deviation occurs approximately at the meniscus. Similar results were reported by

Mahapatra[108] who studied slab casting and Chandra[109] who investigated billet casting with oil lubrication. For raw data, without any filtration technique to eliminate the influence of casting speed and metal level variation, Mahapatra[108] reported a maximum standard deviation of 21°C and Chandra[109] of 17°C. Figure 6.4B shows a maximum standard deviation of only 13.5°C. Although, the data used to calculate the standard deviation shown in Figure 6.4B corresponded to only 40 seconds of casting (time interval to produce one of the samples collected during the trial), some selected blocks of 600 seconds showed similar results. Mahapatra et al.[142] reported that the standard deviation of the thermocouples was reduced to 4°C to 5°C after filtering their mold temperature data, while Chandra[109] did not report the standard deviation of the thermocouples after filtering them. For thermocouples located at 90 and 100 mm from the top of the mould, sheltered from most metal level and casting speed variation influence, Mahapatra[108] reported temperature fluctuations of only ±1.5°C, which he attributed to the mould oscillation. For thermocouples above 100 mm Chandra[109] reported a standard deviation of only 1°C. In this study even for the upper thermocouple, 95 mm, the standard deviation varied between 4 and 10°C (Figures 6.2 and 6.4B), as previously mentioned this was attributed to electrical noise. Fortunately, since the noise had a constant amplitude, time-average temperatures is an appropriated technique to estimate mould heat transfer rates, which will be extensively discussed in the next chapter.

6.1.2 Influence of process variables on mould temperature

As previously explained in Chapter 5, two different mould powders, referred to as powder A and powder B, two mould cooling-water velocities (7.6 and 9.9 m/s) and two mould oscillation frequencies (150 and 170 cpm) were used to cast peritectic (0.11~0.14 pct. C)

steels. For medium-carbon (0.30~0.33 pct. C) steels containing boron and titanium the same two powders were used, also two different mould-cooling water velocities were employed (6.0 and 9.9 m/s); however mould oscillation frequency was kept constant (137 cpm). In the following sections the influence of these variables on the time-averaged mould temperature profile is discussed.

6.1.2.1 Mould powder

Three types of mould flux were used in the plant on a regular basis at the time of the trial, however only two types were tested since the third one was used for high carbon steels (C>0.6%), which were not cast during the trial due to production constraints. Prior to examining the effect of mould powder on mould temperature it is important to establish the differences between powder A and B, whose relevant properties are listed in Table 5.3. Powder A is an all purpose powder used to cast all grades of steel except peritectic-carbon (0.10~0.15 pct. C) and high carbon (C $\geq$ 0.60 pct.). Powder B is specifically used for peritectic grades (0.10~0.15 pct. C). The influence of the two types of powder on the time-averaged mould temperature profile is shown in Figures 6.5 and 6.6.

Figures 6.5 and 6.6 show the influence of type of mould flux on the mould temperature profile for peritectic steel (heat 262: 0.11%C; heat 265: 0.12%C) and Boron(Ti)-alloyed medium-carbon steel (heat 311: 0.33%C; heat 314: 0.31%C) respectively. It should be noted that in each case all other casting variables were constant. Clearly, powder A, the one with lower basicity and higher viscosity, resulted in higher mould temperatures for both steel grades, which indicates an enhancement in mould heat flux with powder A.

6.1.2.2 Mould oscillation frequency

Mould oscillation frequency for casting the peritectic steels (0.11~0.14%C) was changed from its normal value of 150 cpm to 170 cpm. Due to production constraints the same was not possible for Boron(Ti)-alloyed medium-carbon steels. The influence of this change on the mould temperature is shown in Figure 6.7. It can be clearly seen that the mould wall temperature increases with an increase in oscillation frequency. Although, for positions around the peak temperature the difference in temperature is within 1σ (σ≡standard deviation), outside this region the differences can be considered significant. As expected an increase in oscillation frequency decreases mould flux consumption (Equations 2.11, 2.13-2.14 from the literature review - Chapter 2), therefore reducing the lubricating film between the strand and mould and also lowers the negative-strip time (t_N), given by $t_N=(1/\pi\ f)\ \text{arc}\cos(V_c/\pi\ f\ S)$, which reduces oscillation mark depth[1,3,6,60,65,97]. Both effects lead to a decrease in the local mould/strand gap with consequent increase in mould heat transfer and mould wall temperature.

Although the above result was expected, it is contrary to what was found by Chandra[109] during billet casting with oil lubrication in a mould similar to the one used in the present investigation (parabolic taper with 4.9%/m at top and 0.8%/m near end). Chandra[109] attributed his unexpected result to the effect of oscillation mark pitch (Equation 2.18), which increases with increasing oscillation, since he found no noticeable difference in oscillation mark depth when the oscillation frequency was increased; this latter result agrees with findings from Howe and Stuart[93], who found that for oil casting, oscillation marks were virtually independent of mould oscillation frequency. Chandra[109], as well as Brendzy et al.[130] found that for a mould with parabolic taper and steep positive taper at the meniscus

(4.9%/m), there was little difference in the depth of oscillation marks when the negative strip time varied from 0.13 s to 0.17 s. On the other hand, for a double tapered mould (upper part 2.75%/m followed by 0.5%/m from 333 mm down) the oscillation mark depths on billets cast with the higher negative strip time (0.17 s) were significantly deeper than on billets cast with negative strip time of 0.13 s; this latter result agrees with earlier findings reported by Samarasekera et al[143]. Brendzy et al.[130] attributed this difference in behaviour to a stronger mould-strand interaction at the meniscus whenever the mould acquires a negative taper in the upper region; which occurred with the double tapered mould but not with the parabolic. They also reported that oil type and flowrate did not significantly affect the depth of oscillation marks which suggests that lubrication does not play a major role in oscillation mark formation in billet casting with oil. The above discussion clearly indicates a major difference between billet casting with oil lubrication and mould powder lubrication in terms of oscillation mark formation since, as will be discussed in the next Chapter and briefly reviewed in Chapter 2, in billet casting with mould powder the lubricating film (liquid flux) filling the strand/mould gap plays an important role.

6.1.2.3 Mould water velocity

To examine the influence of mould water velocity on mould heat transfer, the velocity was altered from 9.9 m/s (650 US gallons/min) to 7.6 m/s (500 US gallons/min) for peritectic steels and from 9.9 m/s to 6.0 m/s (400 US gallons/min) for Boron(Ti)-alloyed steel. Figure 6.8 is a plot of the axial mould temperature profile measured during casting of peritectic steel in which the first half of the heat was cast with a mould water velocity of 9.9 m/s and the second half with 7.6 m/s. As clearly seen the measured temperatures were consistently higher, approximately 10 to 15°C, for the lower mould water velocity. Similar result was also found

for Boron(Ti)-alloyed medium-carbon grade. Assuming that the heat flux coming from the solidifying shell is not affected by changes in the mould water velocity, the above result was expected. A drop in the cooling-water velocity results in lower heat transfer coefficient at the cold face of the mould, thus increasing the mould temperature. It should be noticed however that if the heat flux entering the mould is affected by variations in the water velocity, depending on the direction (increase or decrease) and magnitude of this effect, the response of mould temperature to mould-water velocity variation could be different from the one obtained. The influence of mould water velocity on mould heat flux will be presented later.

6.1.2.4 Meniscus level

Figure 6.9 shows the influence of meniscus position on mould temperature profile. It can be seen that mould peak temperature follows the direction of displacement of the meniscus. Additionally, Figure 6.9 also confirms which had been previously discussed in section 6.1.2.1, i.e., the mould during the heat cast with powder B (heat 281) runs colder since powder B consistently resulted in lower heat transfer.

6.1.2.5 Steel grade

Two types of steels were cast during the plant trial, plain carbon steel with carbon content between 0.11 and 0.14% and Boron(Ti)-alloyed medium-carbon steel with carbon content between 0.30 and 0.33%. Titanium is added to the boron steel to fix nitrogen as TiN and guarantee that the solid steel will have enough free boron to improve its hardenability, otherwise boron would combine with nitrogen to form BN. Figure 6.10 is a plot of the time-averaged mould temperature profile of three steels containing 0.11, 0.14 and 0.33% C, the last also containing boron and titanium. Plain carbon steel with 0.11 %C cast with oscillation

frequency of 150 cpm gives rise to lower temperatures compared to plain carbon steel with 0.14% C and cast with 170 cpm; although the difference in oscillation frequency does not make this an ideal comparison. It is well known that mould heat flux as a function of carbon content has a minimum value around 0.10~0.11% C[126]. A surprising result was to find that the magnitude of mould temperatures for Boron(Ti)-alloyed medium-carbon steel heats were comparable to the ones obtained for the peritectic steels. Generally medium-carbon steels usually transfer higher heat flux to the mould[108-110,126], and this steel grade when cast with oil results in very high heat flux[110], as will be discussed in the following section.

6.1.2.6 Type of Lubricant: powder vs. oil

The influence of lubricant type on mould temperature profile is shown in Figure 6.11. As mentioned in the previous section, the low mould temperatures measured during casting of Boron(Ti)-alloyed medium-carbon steel with powder lubrication is a surprising result. Figure 6.11 clearly shows a striking difference in mould temperature profile between Boron(Ti)-alloyed steel cast with the different lubricants. The heat cast with powder showed significantly lower mould temperatures than the heat cast with oil, indicating that the heat transfer in the mould was reduced by the use of powder. This is consistent with the experimental research of Singh and Blazek[126] who found that for medium-carbon steel (0.40% C) powder lubrication significantly lowered mould heat transfer over the entire mould length. They explained that 0.4 percent carbon steel does not form a rippled shell and has a more uniform contact with the mould wall. When cast with oil, the result is a lower mould/strand gap thermal resistance, and a higher mould heat transfer. Therefore, when mould flux is introduced it acts as an insulator and decreases the mould heat transfer.

Figure 6.11 also shows that for peritectic steels, compared to oil lubrication the use of powder resulted in higher mould wall temperatures in the vicinity of the meniscus but lower down the mould, which is also consistent with results reported by Singh and Blazek[126]. They believed this behaviour to be caused by the joint effect of mould flux and air gaps. Since peritectic steels shrink the most at the meniscus their shell is very rippled, with deep oscillation marks. During oil cast these large gaps are partly filled with air and the mould heat transfer is locally decrease. When mould flux is introduced it fills the air gaps, thus increasing the mould heat transfer rate near the meniscus region. In contrast, in the lower part of the mould, where the shell has a better contact with the mould due to ferrostatic pressure, the flux acts as an insulator, which result in a decrease in the mould heat transfer. In further investigation Blazek et al.[146] found that when casting 0.1% C steel with high viscosity and high crystallization temperature fluxes the mould heat transfer was lower throughout the mould. They explained that low viscosity, low melting temperature fluxes, as the ones used in the previous study[126] can easily melt and flow to fill completely all gaps formed. On the other hand, high viscosity and high crystallization temperature fluxes would form a uniform slag layer at the meniscus. This solid layer would act as an insulator, even worse than the air gaps formed with oil lubrication, and thus decrease mould heat transfer rate.

6.2 Billet Samples Quality Evaluation

Figures 6.12 to 6.14 illustrates some of the surface features found in the samples collected during the plant trial. A typical billet sample surface is shown in Figure 6.12; the picture corresponds to the west face (straight side) of billet sample 265-30, a peritectic-carbon steel cast with powder B, oscillation frequency of 150 cpm and mould water velocity of 7.6 m/s.

The surface shows no defects and, for the majority of the samples collected during the trial, shows very well defined oscillation marks. Figure 6.13 show an example of transverse depression found in peritectic billet sample cast with powder A. Transverse depressions were only found in heat 277. These depressions ran along the oscillation marks which suggest they are formed near the meniscus while the shell is still weak. Another feature found in most of the samples was the presence of a longitudinal depression in at least one of the faces. The severity of the longitudinal depression varied, mostly below 3 mm in depth, but some as deep as 5 mm; Figure 6.14 shows a photograph of a billet surface displaying a typical midface longitudinal depression. Besides midface the north corner of west face was found to be a preferential position for longitudinal depressions.

As a general observation the performance of powder A was slightly inferior to powder B. The latter had a better performance in terms of longitudinal depression and regularity of oscillation marks. Its better performance must be associated with its higher crystallization temperature with consequent lower heat fluxes. Scratches and indentations found on faces north and south of the boron-grade samples is likely to be caused by dirt accumulated in the pinch rolls that are in contact with these faces. Table 6.1 summarizes the results of surface inspection performed in all samples collected in the plant trial.

6.2.1 Surface roughness (oscillation marks)

A profilometer with three LVDT's was used to measure the surface profile of the samples collected during the plant trial. The measurements were carried out at the centre and at 10 mm off both corners of each sample. Figure 6.15 depicts some of the surface profiles measured at the centreline.

For each profile the distance between a peak and its adjacent valley was measured and taken as the depth of an oscillation mark. The distance between two consecutive peaks was taken as the oscillation mark pitch.

The results in Figure 6.16 show that for peritectic steel ($0.11 \leq \%C \leq 0.12$) an oscillation frequency of 170 cpm resulted in shallower oscillation marks when compared to a frequency of 150 cpm, which is likely to be related to the lower negative-strip time associated with the higher frequency. This confirms Howe and Stewart's[93] observation that with oil lubrication, the depth of oscillation marks was virtually independent of mold oscillation frequency whereas with mold flux, the depth was inversely proportional to frequency. Howe and Stewart's[93] results reinforce the belief that for powder lubrication the formation of oscillation marks is largely the result of the interaction between the mould, casting flux and the shell.

Figure 6.16 also shows that higher-viscosity mould powders ($\eta_{\text{powder B}} > \eta_{\text{powder A}}$) tend to produce shallower oscillation marks, which has also been found by other researchers[60,64,98]. Higher viscosity results in lower powder consumption, so less flux is driven down the mould during the downstroke, and thus the pressure build up in the lubricating film is lower. Since oscillation mark depth in powder casting is enhanced by the positive pressure generated in the flux channel during negative-strip time, the lower pressure results in shallower oscillation marks. It should be noticed that the above rationale, i.e. the decrease of positive pressure with increasing mould flux viscosity, is contrary to results from mathematical modelling[56,58,67], which show an increase in pressure with increasing flux viscosity. A major limitation of these models is their assumption that lubricating film thickness and flux consumption are constant and independent of viscosity, which is not realistic.

Finally, Figure 6.16, shows the influence of carbon content on oscillation mark depth. Boron (Ti)-alloyed steels, containing 0.30~0.33%C, although cast at the lowest oscillation frequency (137 cpm) consistently had shallower oscillation marks than the peritectic steels, the latter with carbon content between 0.11 to 0.14 Wt. %.

Detailed results of oscillation mark depth measurements are presented in Appendix E Table E1, additionally Table E2 shows measured values for oscillation mark pitch. Table E1 shows that Boron (Ti)-alloyed medium-carbon (0.32%C) samples had average oscillation marks depth of 0.34 mm while for peritectic (0.11~0.14%C) grade this value was 0.67 mm when the mould oscillation frequency was 150 cpm and 0.53 mm for 170 cpm.

Table 6.2 summarizes the results obtained. It also includes calculated values for the oscillation mark pitch, which agree very well with the measured values.

6.3 Other Results

6.3.1 Metal level

During the plant trial the metal level signal was not recorded due to failure of the data acquisition channel designated to record it. Therefore, metal level displayed in the casting machine control panel was manually collected as backup-data to substitute the missed data. However, as shown in Table 6.3, local measurement of metal level using a dip-stick indicates a very significant discrepancy between real values (measured with dip-stick) and values displayed by the metal level controller. The difference between the values measured with dip-stick and the correspondent values recorded by the metal level controller varied between 42 and 57 mm. No discrepancy was noticed during oil casting in the same trial[121]; therefore, the problem should be due to incompatibilities between the metal level controller system,

which used a radioactive sensor device, and powder casting. This issue will be addressed in detail in Chapter 7 and Appendix F.

The lack of a metal level signal made it difficult to use a more sophisticated data filtration technique, such as the ones suggested by Mahapatra[108] and Chandra[109]; so a simple selection of data blocks with apparent constant metal level and casting speed was adopted. These blocks were selected by visual inspection of the temperature vs. time plots, based on the steadiness of the signals from the thermocouple located close to the meniscus region. Another problem was that, except for the occasional measurements performed using dip-sticks, it was impossible to clearly associate every temperature and respectively calculated mould heat flux profile to a specific metal level.

6.3.2 Powder consumption

During the plant trial the consumption of the powders tested was calculated. The results are shown in Table 6.4.

Powder A, having a higher viscosity (0.7 poise@1400°C) than powder B (0.4 poise@1400°C), resulted in a lower consumption of 1.14 kg/t(~ 0.45 kg/m^2) compared to 1.34 kg/t for powder B (~ 0.53 kg/m^2). The values expressed in kg/t are higher than values normally reported for slab casting (0.3-0.7 kg/t), however this is expected since a billet has a much higher perimeter/area ratio than slabs and flux infiltration is dependent on the strand lateral area. Even in terms of kg/m^2 the measured consumption of the two powder tested was also higher than values reported in the literature for slab casting. Kwon et al.[62] measured values between 0.26 and 0.38 kg/m^2 for the same kind of steel ($0.08 \leq \%C \leq 0.16$) cast at similar casting speeds (1.0-1.5 m/min). The main concern regarding high consumption is to balance it with the powder melting rate in order to maintain a liquid pool height at least larger than the

oscillation stroke. As will be discussed later, measurements of the molten flux pool height showed very low values. It is interesting to note that for peritectic (0.09≤%C≤0.16) steels Kwon et al.[62] used mould fluxes with higher viscosity than the ones used in the plant where the trial was carried out.

The low viscosity of powder A and B suggests that they would be more suitable for casting low-carbon steels (%C<0.08) at higher casting speeds (>1.2 m/min.) than for casting peritectic steel or medium-carbon boron grade. As previously presented in the literature review (Chapter 2.7) several researchers[1,46.64] have proposed optimum values for mould-flux viscosity(η) × casting speed(V_c) relationships, expressed as ηV_c or ηV_c^2, in order to minimize variations in mould temperature, mould heat transfer and lubricant film thickness, to minimize number of pinholes and oscillation mark depth[46]; also to minimize overall heat flux, frictional forces[64] and longitudinal cracking[1]. Ogibayashi et al.[46] found that a value of ηV_c above 2 minimizes pinholes and oscillation mark depth and between 1 and 3.5 minimizes mould heat transfer variations; thus they suggested ηV_c to be between 2 and 3.5 for the achievement of optimum casting conditions. Wolf[64] and Mills[1] suggested ηV_c^2 as a more reliable relationship and found that optimum casting conditions occur when $\eta V_c^2 = 5 \pm 2$.From the above analysis and the values of ηV_c and ηV_c^2 shown in Table 6.4, all of them smaller than 2, it is clear that for the casting speeds used during the plant the viscosities of both powders were too low. Additionally, as also pointed out in Chapter 2.4.6, both low viscosity and low casting speed promotes high powder consumption which, as will be shown in the next section, can lead to an unacceptable thin molten-flux pool.

The measured mould powder consumption partly agrees with other studies that showed that consumption increases with decreasing flux viscosity and transition temperature[40]. Consumption increases with decreasing transition temperature because of an increase in the liquid slag film thickness, while the increase with decreasing viscosity is because of an increase in the flux flow speed. In our study the consumption increased with decreasing viscosity (powder B), and decreased with decreasing transition temperature (powder A). This simply shows that a decrease of ~42% in the viscosity of powder B, more than compensated for the increase of ~13% in the transition temperature

6.3.3 Molten-flux pool depth

Table 6.5 show results of the measurements of the flux sintered and molten layer. The measurements were conducted using a three-wire (aluminum, copper and steel) dip-stick.

The values shown in Table 6.5 are extremely low, the main reason, as pointed before, is likely to be an imbalance between the high consumption, above 1.1 kg/t (Table 6.4), and the melting rate of the powders tested, aggravated by not keeping a dark layer of unreacted powder on the top surface of the mould, which was the case of the heats measured. Lack of a sufficient liquid flux pool can cause engulfment of solid flux at the meniscus leading to surface and subsurface defects, in severe cases even to loss of lubrication and breakouts. These results show the importance of carefully considering the melting rate of the mould powder before choosing it for billet casting. Powders used for slab casting will not necessarily perform as well for billets. Due to its much higher perimeter/area ratio billet casting requires higher specific consumption (kg per tone of steel) than slab casting.

6.3.4 Mould-flux temperature profile

Temperatures within the powder layer were measured using an arrangement of three Type S (Pt-10%Rh) thermocouples enclosed in high purity alumina protection tube. The wires inside the protection tube were insulated by double-bore high purity hard-fired alumina tubes. The thermocouples were mounted in a steel bar through screw nuts that allowed their length to be adjusted. A laptop computer with a data acquisition board and Labtech Notebook software was used as the data acquisition system.

Three sets of temperatures were measured. The first set was a test to check the thermocouple and adjust their position. A catastrophic failure of the submerged entry nozzle during the third measurement washed away all thermocouples not allowing us to continue the experiment. Figures 6.17 shows the results of the second and third measurement. Unfortunately, in both cases one of the three thermocouples used failed (note thermocouple located at 163 mm below top of mould in Figure 6.17B).

Figure 6.17A shows that soon after the thermocouple is introduced in the mould it heats up for about 40 seconds until it reaches a peak value. After this peak temperature was reached the temperature decreased towards a stable value or rebound back to the peak value, as in the case of the thermocouple placed at 165 mm. This rather odd decrease in the thermocouples temperature is thought to be caused by accommodation of the loose powder surrounding the thermocouple tips after they are initially introduced and begin to oscillate with the mould. The same behaviour (over-shooting) was not verified in Figure 6.17B, probably because in this case the thermocouples were placed deeper in the mould flux. The thermocouple placed at 153 mm shows a rather conventional heating curve, while the thermocouple placed inside the liquid layer (173 mm) did not show any. The absence of a heating period for the thermocouple

placed at 173 mm is explained by a faster heating rate resulting from a much smaller thermal resistance (liquid-flux/thermocouple) compared to the other thermocouples thermal resistance (solid-powder/thermocouple). Additionally, a delay in triggering the data acquisition system reduced the heating period recorded (note that the thermocouple placed at 153 mm only takes 20 seconds to stabilize).

Table 6.1: Summary of results of visual inspection of the samples surface:

Steel Grade	Powder	Oscillation Frequency	(No. of Samples) Results of Visual Inspection:
Peritectic 0.11~0.12 Wt.% C	A	150 cpm	(6 from 4 heats) Rough surface. Off-corner longitudinal depression in three samples. Large centre longitudinal depression in one heat (2 samples).
Peritectic 0.11~0.12 Wt. % C	B	150 cpm	(5 from 3 heats) Good surface in terms of depression and regularity of OSM. Signs of sticking in one of the samples.
Peritectic 0.13~0.14 Wt. % C	A	170 cpm	(4 from 3 heats) 2 samples had good surface Sample 277 had one shallow transverse depressions Sample 282-60' had very rough surface: deep and irregular oscillation marks, lots of pinholes, longitudinal depression and small transverse depressions
Peritectic 0.13 ~0.14 Wt. % C	B	170 cpm	(5 from 3 heats) 2 samples had no surface defects Samples 280 had a longitudinal depression Sample 282-30' had very bad surface, deep and irregular oscillation marks + pinholes.
Boron(Ti) 0.33% C	A	137 cpm	(5 from 3 heats) All samples presented longitudinal depression on West face North and South faces had several indentations (scratches)
Boron(Ti) 0.32% C	B	137 cpm	(4 from 3 heats) All samples with longitudinal depression on the West face. Surface of North and South faces full of indentations

Table 6.2: Pitch and Depth of oscillation marks and negative-strip time (t_N) .

Grade(Carbon) Frequency	Av. C. Speed (m/min.)	Calc. Pitch (mm)	Meas.Pitch (mm)	OSM-Depth (mm)	t_N (s)
Peritectic(0.11%C) 150 cpm	~1.24±0.1	8.25	8.71±0.20	0.67±0.18	~0.14
Peritectic(0.13%C) 170 cpm	~1.32±0.1	7.77	7.52±0.26	0.53±0.13	~0.12
Boron(Ti) (0.32%C) 137 cpm	~1.27±0.1	9.27	9.52±0.28	0.34±0.09	~0.14

Table 6.3: Comparison between measured metal level and metal level controller display

Heat	Metal level (dip-stick) [mm]	Metal level (level controller) [mm]
278	191	140
279	197	140
280	184	142
281	194	142
313	191	140
315	191	142

Table 6.4: Mould powder consumption

POWDER	A	B
Consumption	1.14 kg/t (0.45 kg/m^2)	1.34 kg/t (0.53 kg/m^2)
Average casting speed Oscillation frequency Oscillation stroke	1.20 m/min 150 cpm 6 mm	1.17 m/min. 150 cpm 6 mm
Viscosity@1400°C @1300°C @1250°C	0.7 poise 1.3 poise 1.9 poise	0.4 poise ~0.6 (est.) 0.9 poise
ηV @1300°C ηV^2 @1300°C	1.6 1.9	~0.8 ~1.0

Table 6.5: Results of mould powder layers measurement:

Heat No.	Powder	Liquid layer (mm)	Sintered layer (mm)
260	A	3	1
262	A	1	2
264	B	1	1

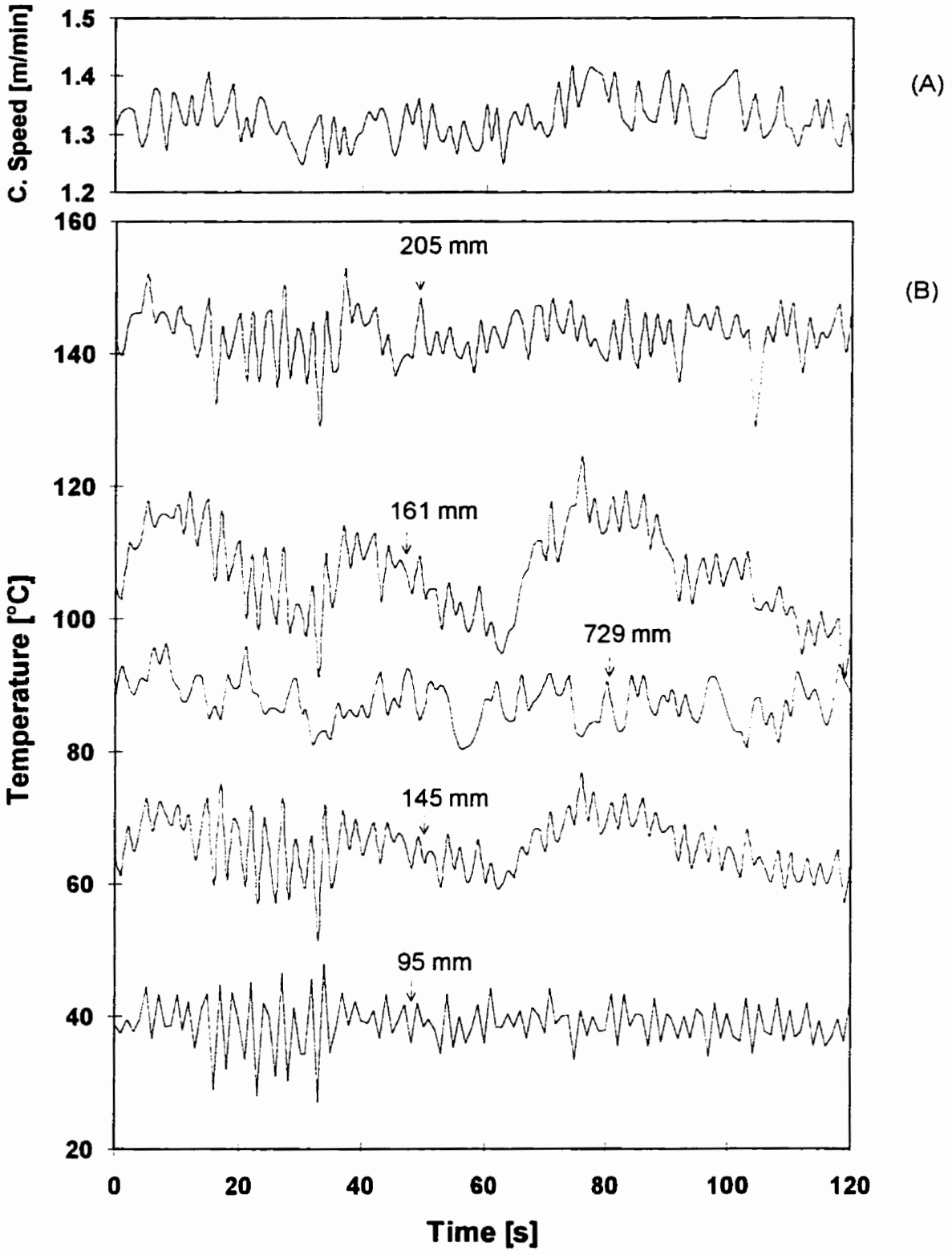

Figure 6.1 Typical (A) Casting speed variation and (B) Temperature response of selected thermocouples on the mould East-face at 95, 145, 161, 205 and 729 from the top of the mould; metal level between 161 ~ 171 mm.

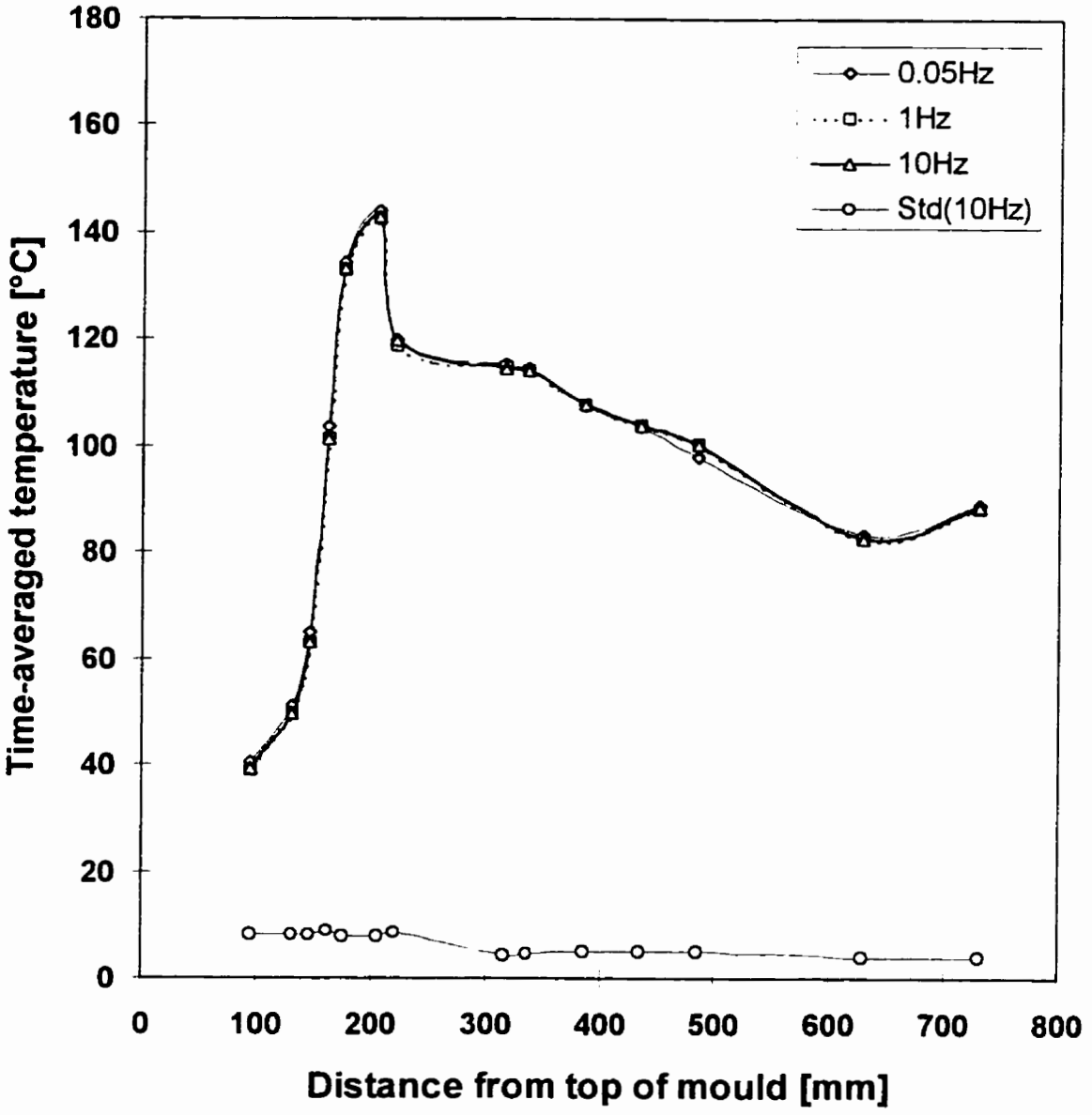

Figure 6.2 Influence of data sampling rate on time-averaged mould axial temperature profile along the centreline of East-face for heat 277 (0.14% C, powder A) and standard deviation of temperature measurements for the sample rate of 10 Hz.

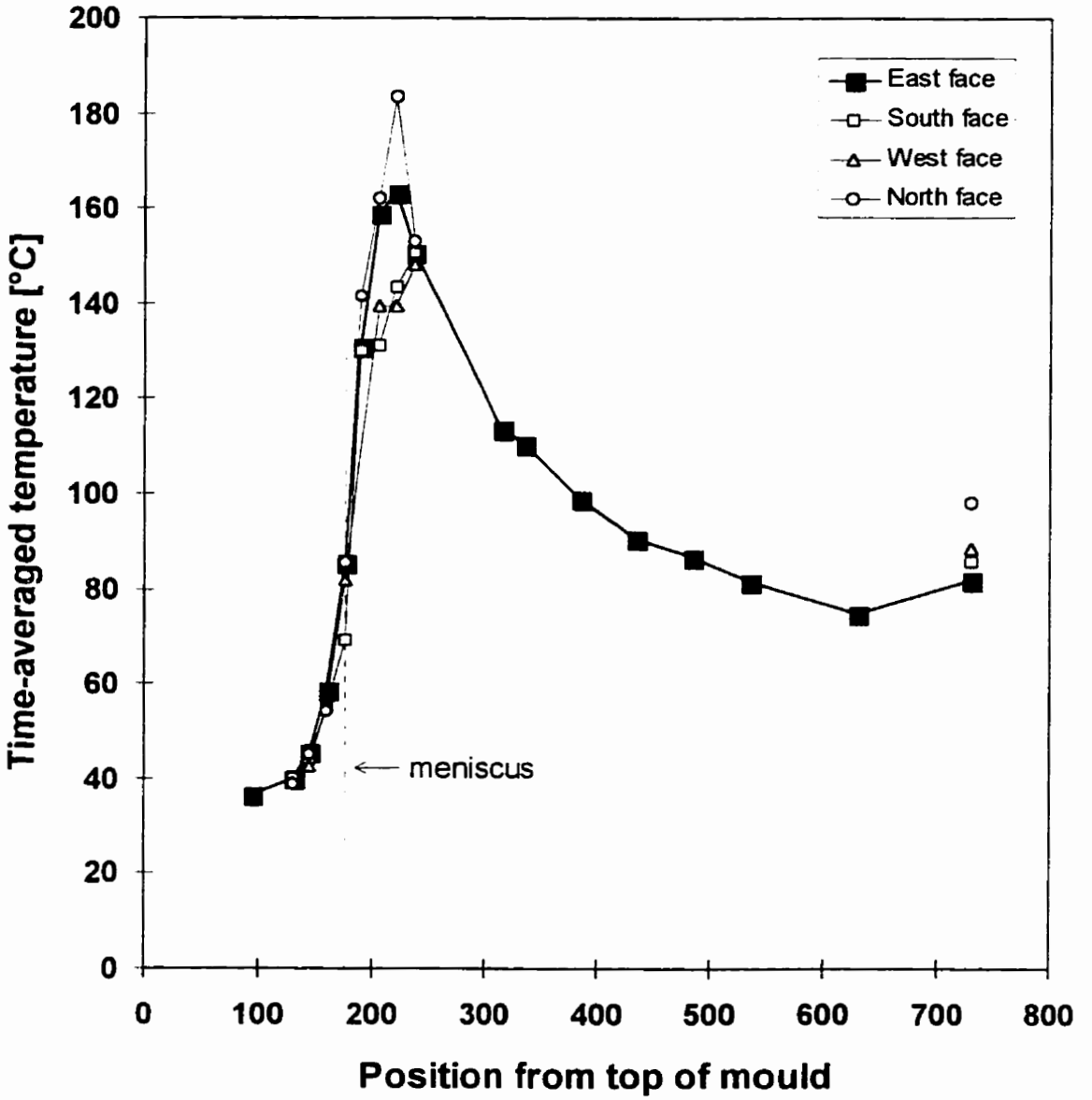

Figure 6.3 Comparison of the axial temperature profiles measured on the four faces of the mould (centreline); Heat 311.

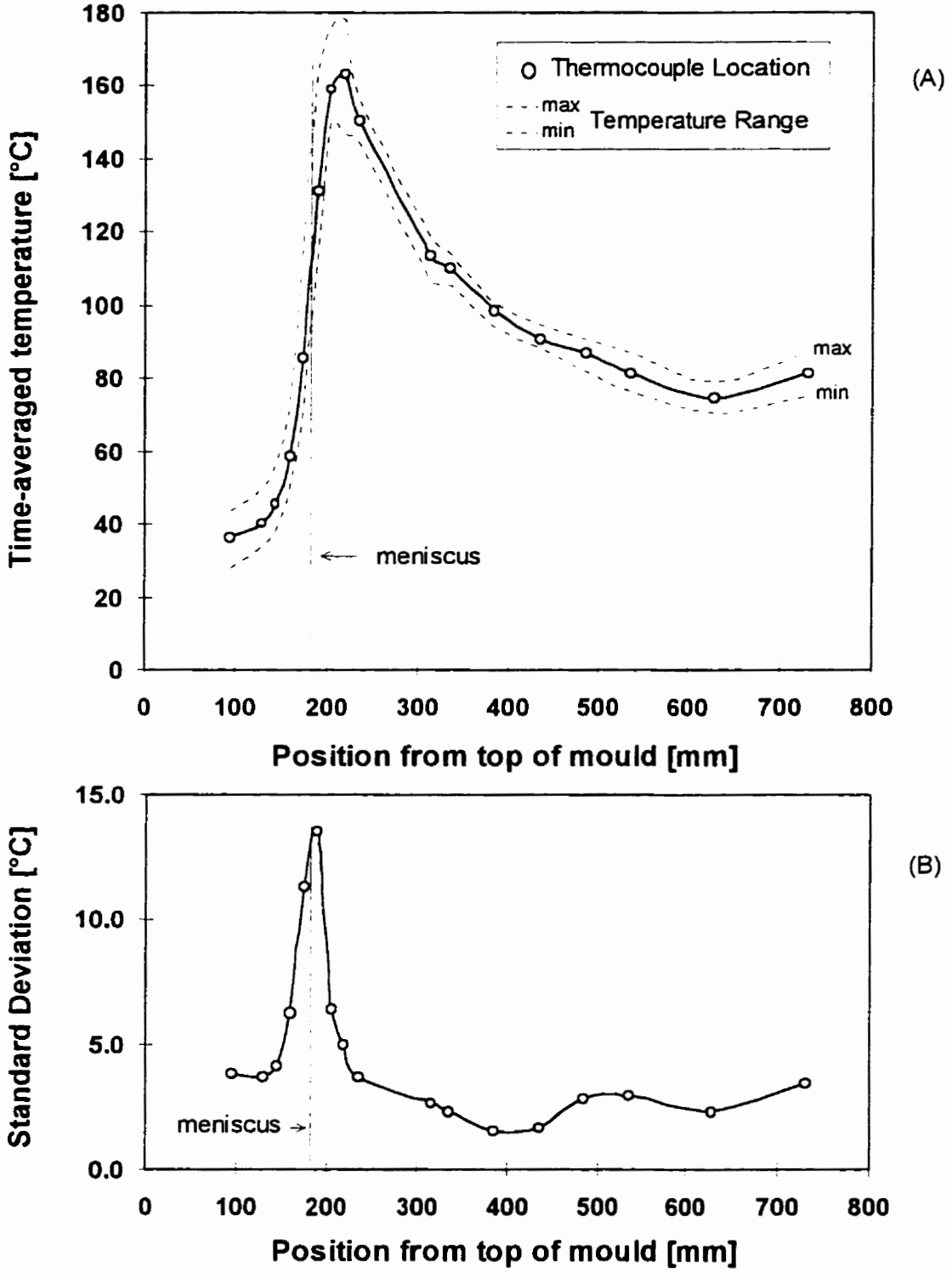

Figure 6.4 Typical axial temperature profile and standard deviation of the temperature measurements made along the centreline of mould East-face for heat 311: 0.33% C , B(Ti)-alloyed cast with powder A; (A) Temperature profile showing time-averaged temperature and total range of temperature variation, (B) standard deviation.

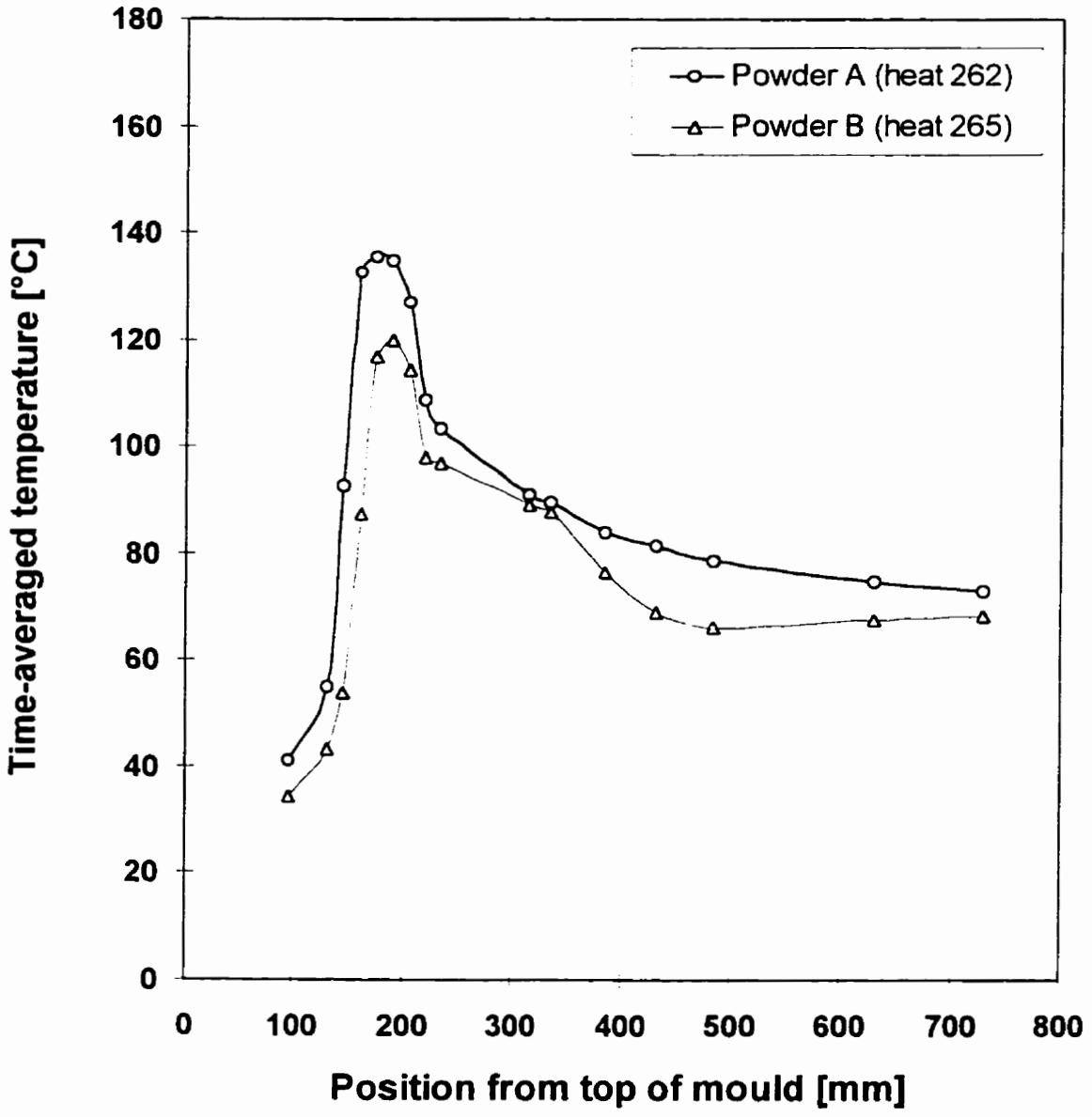

Figure 6.5 Influence of type of mould flux on the time-averaged axial mould-temperature profile for peritectic steel (heat 262: 0.11%C; heat 265: 0.12%C); oscillation frequency 150 cpm, mould water velocity 7.6 m/s.

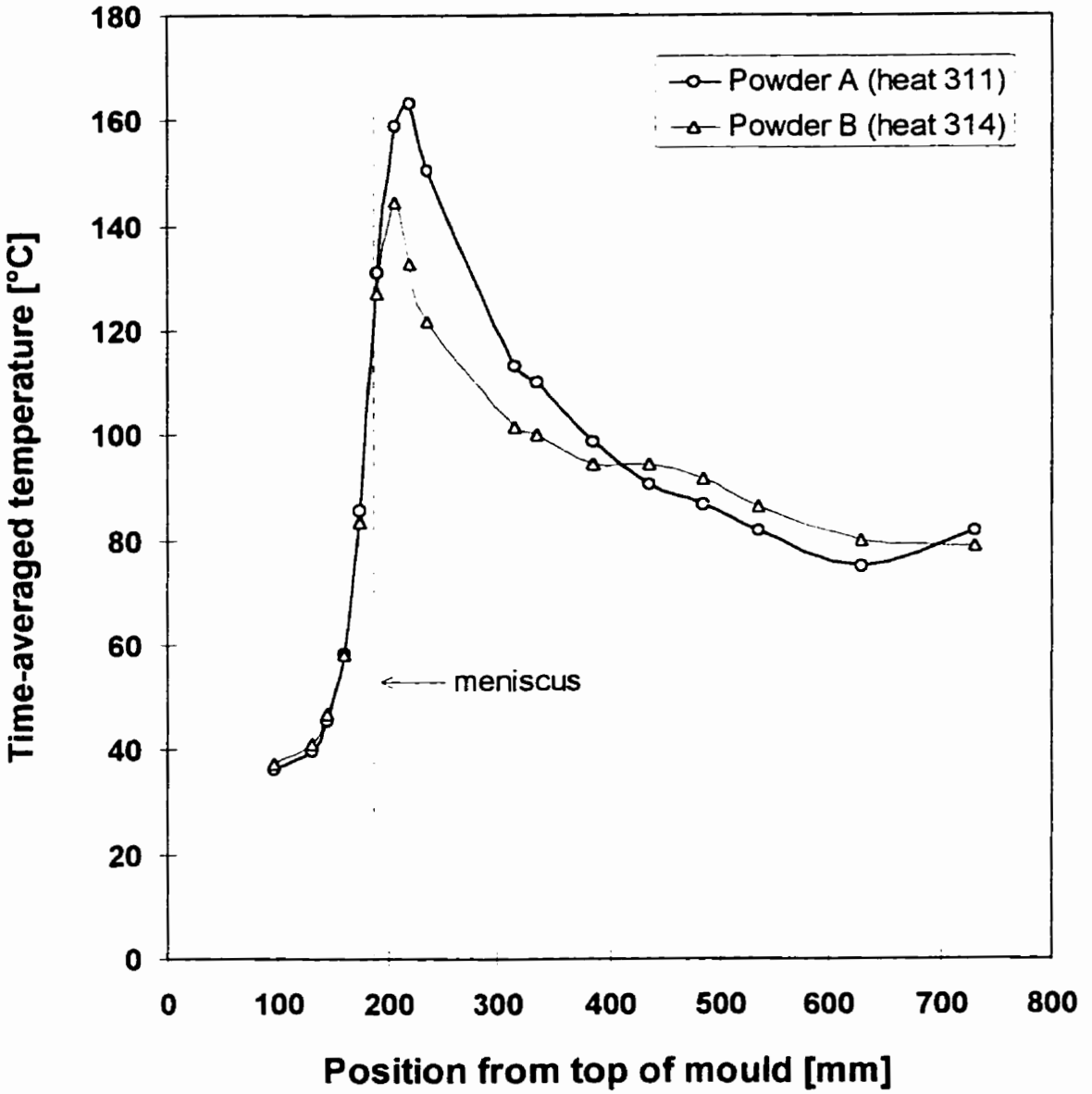

Figure 6.6 Influence of type of mould powder on the time-averaged axial mould-temperature profile for Boron(Ti)-alloyed medium-carbon steel (heat 311: 0.33%C; heat 314: 0.31%C), oscillation frequency 137 cpm, mould water velocity 6.0 m/s.

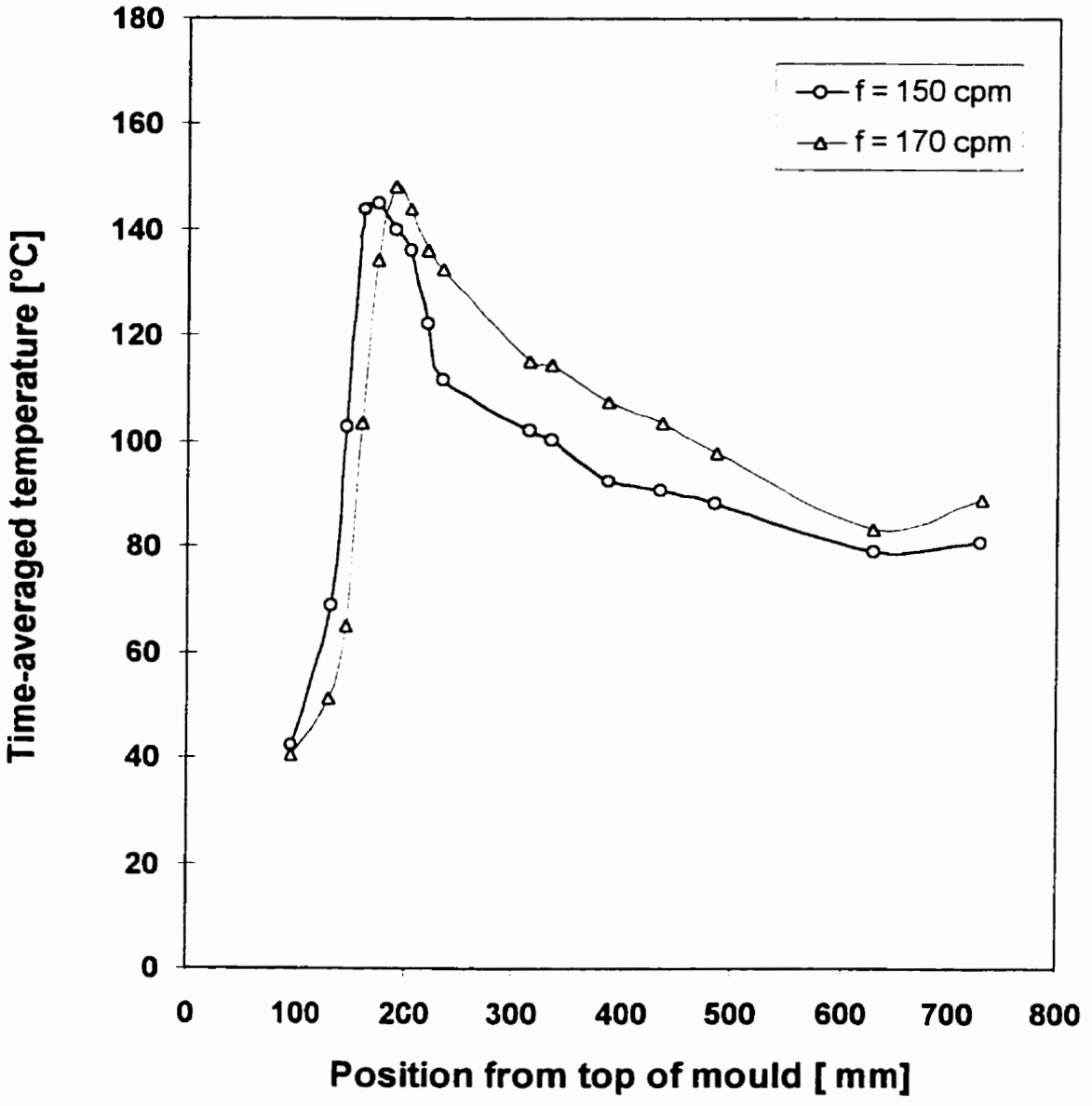

Figure 6.7 Influence of mould oscillation frequency on the time-averaged axial mould-temperature profile; peritectic steel, water velocity 9.9 m/s, powder A.

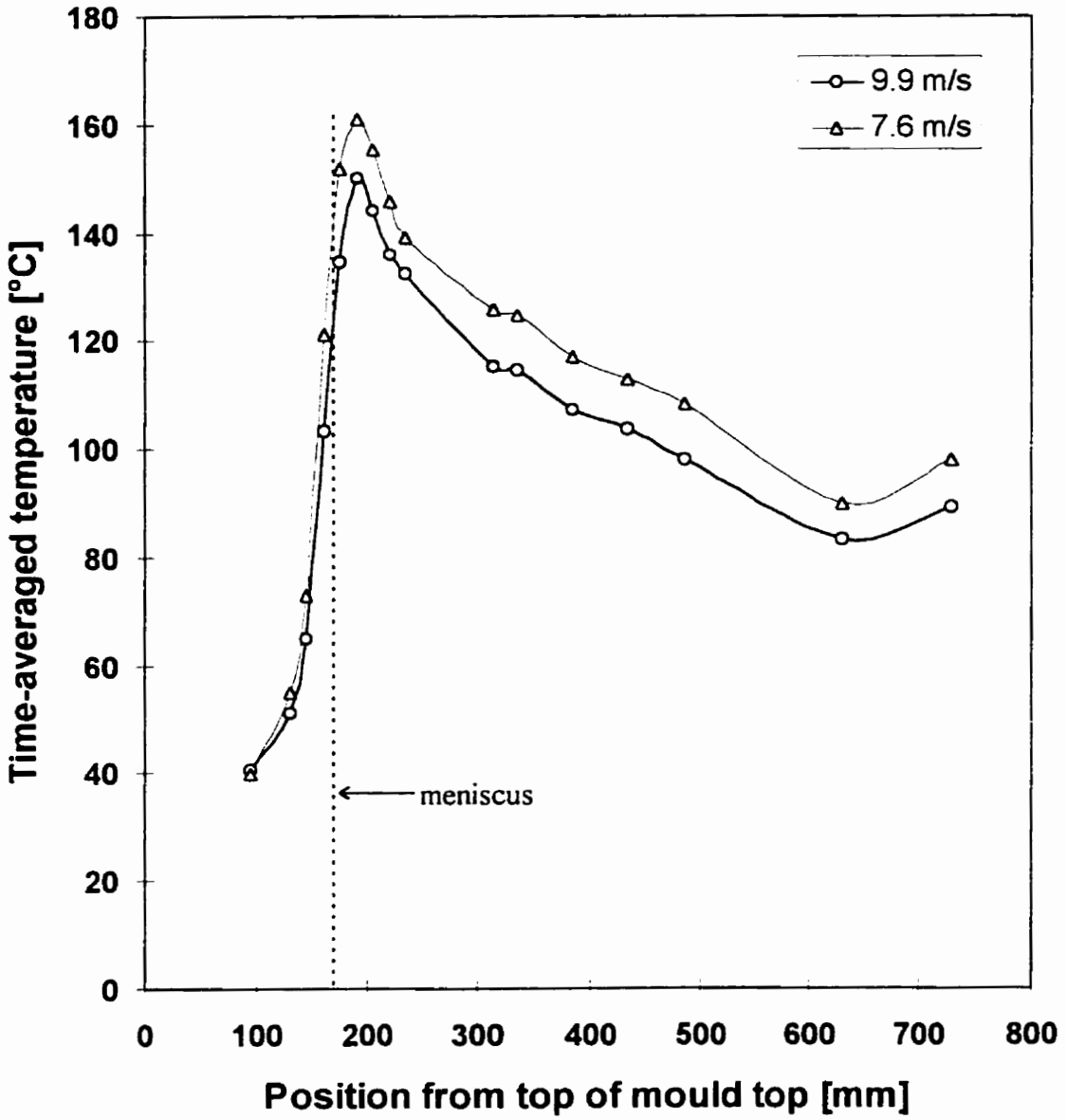

Figure 6.8 Influence of mould water velocity on the time-averaged axial mould-temperature profile; heat 277 (0.14%C), oscillation frequency 170 cpm, powder A

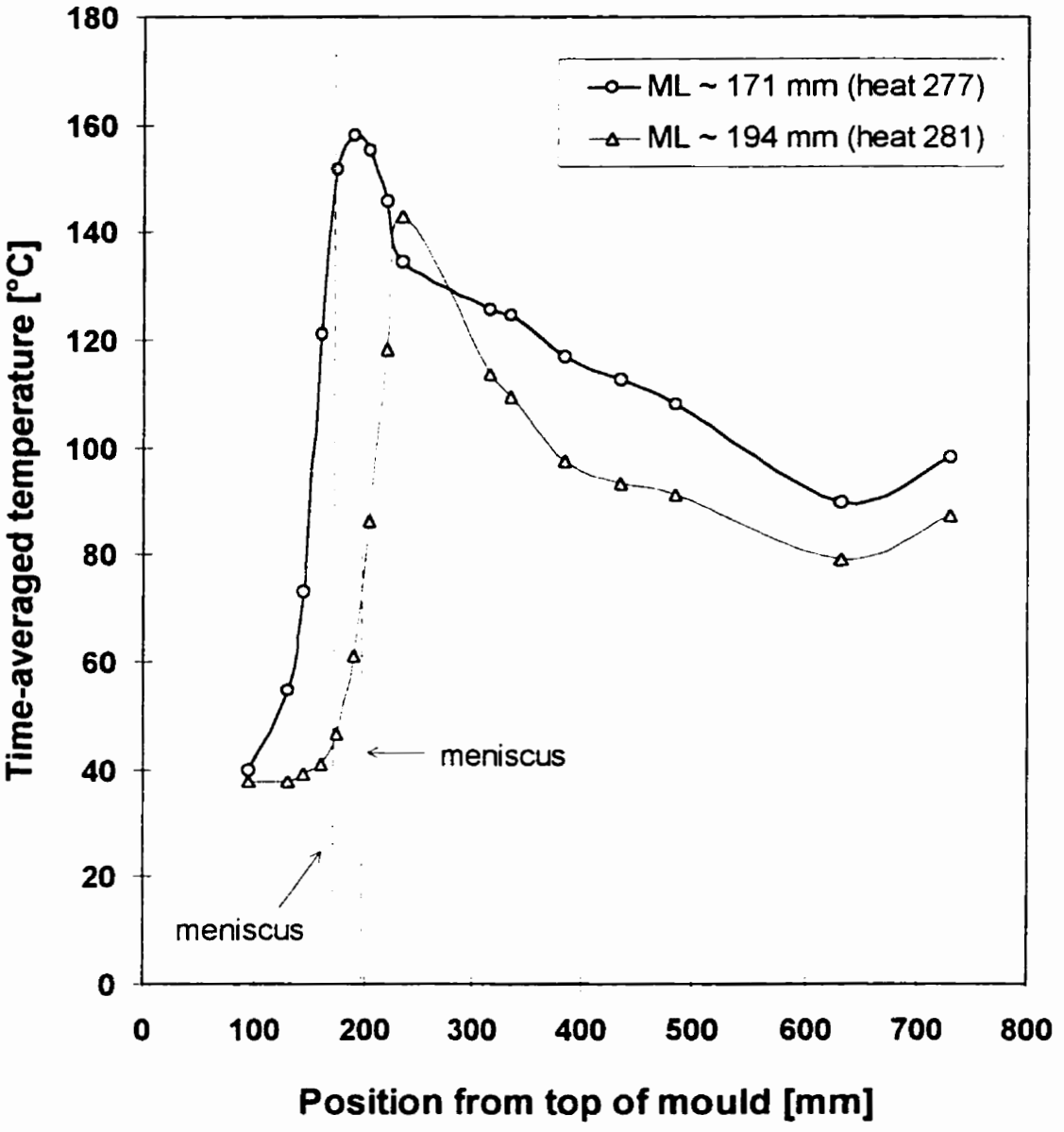

Figure 6.9 Influence of meniscus level on the time-averaged axial mould-temperature profile; peritectic steel, oscillation frequency 170 cpm, mould water velocity 7.6 m/s, heat 277 (0.14%C) powder A, heat 281 (0.13%C) powder B

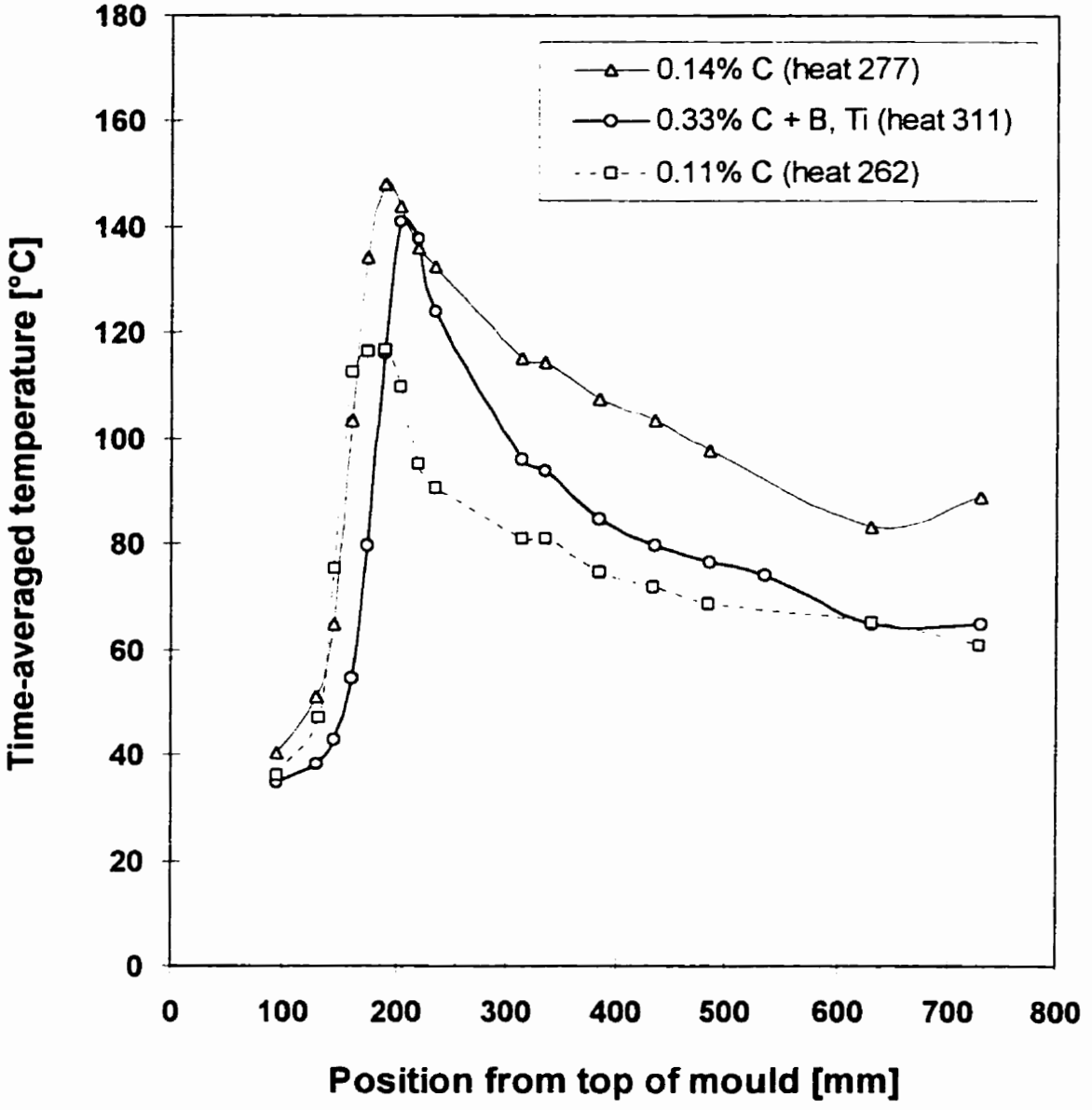

Figure 6.10 Influence of the steel grade on the time-averaged axial mould-temperature profile; mould water velocity 9.9 m/s, mould powder A, oscillation frequency: heat 277 f=170 cpm, heat 311 f=137 and heat 262 f=150 cpm.

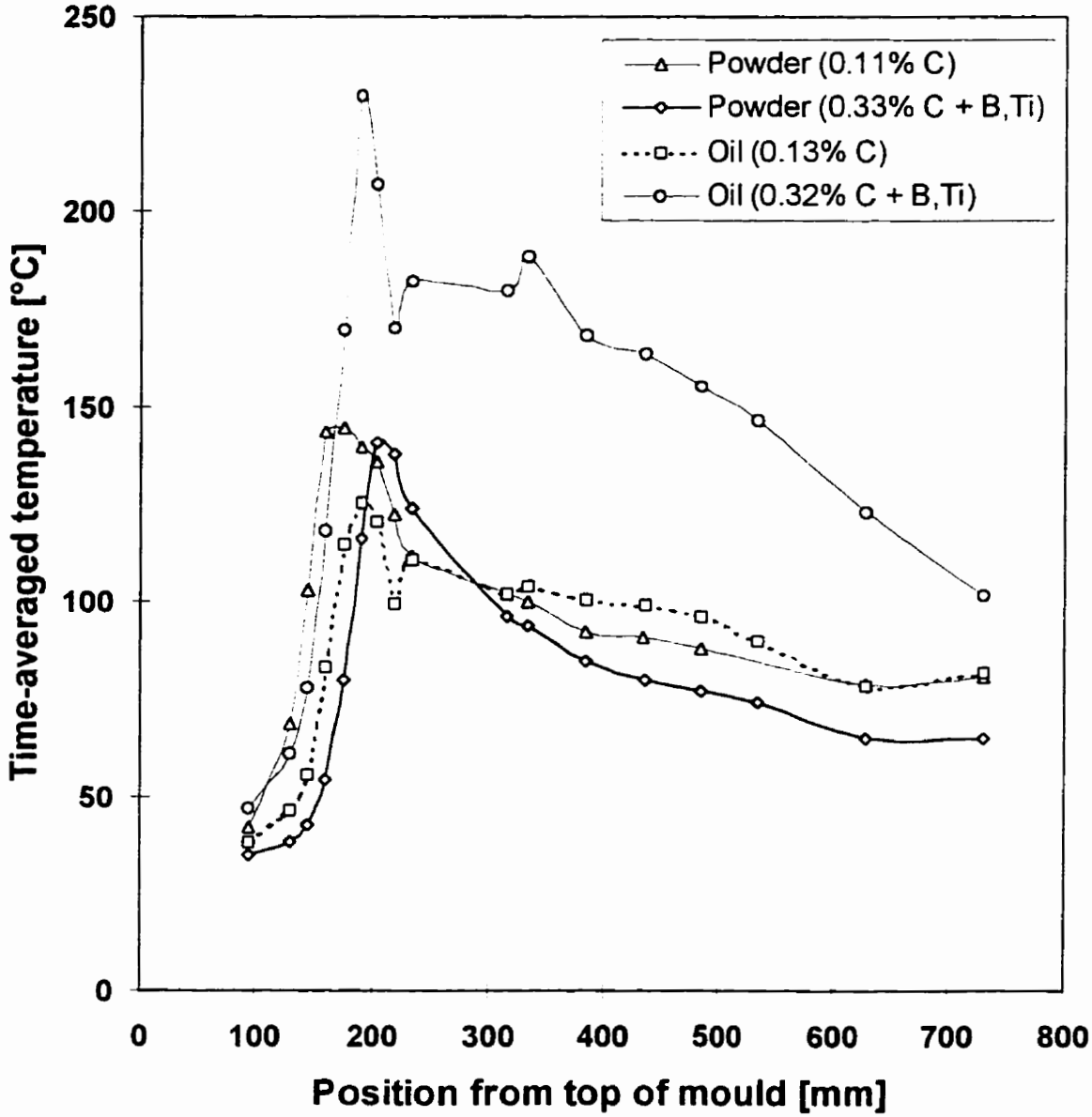

Figure 6.11 Influence of lubrication type on the axial temperature profiles for peritectic and Boron(Ti)-alloyed medium-carbon steel.

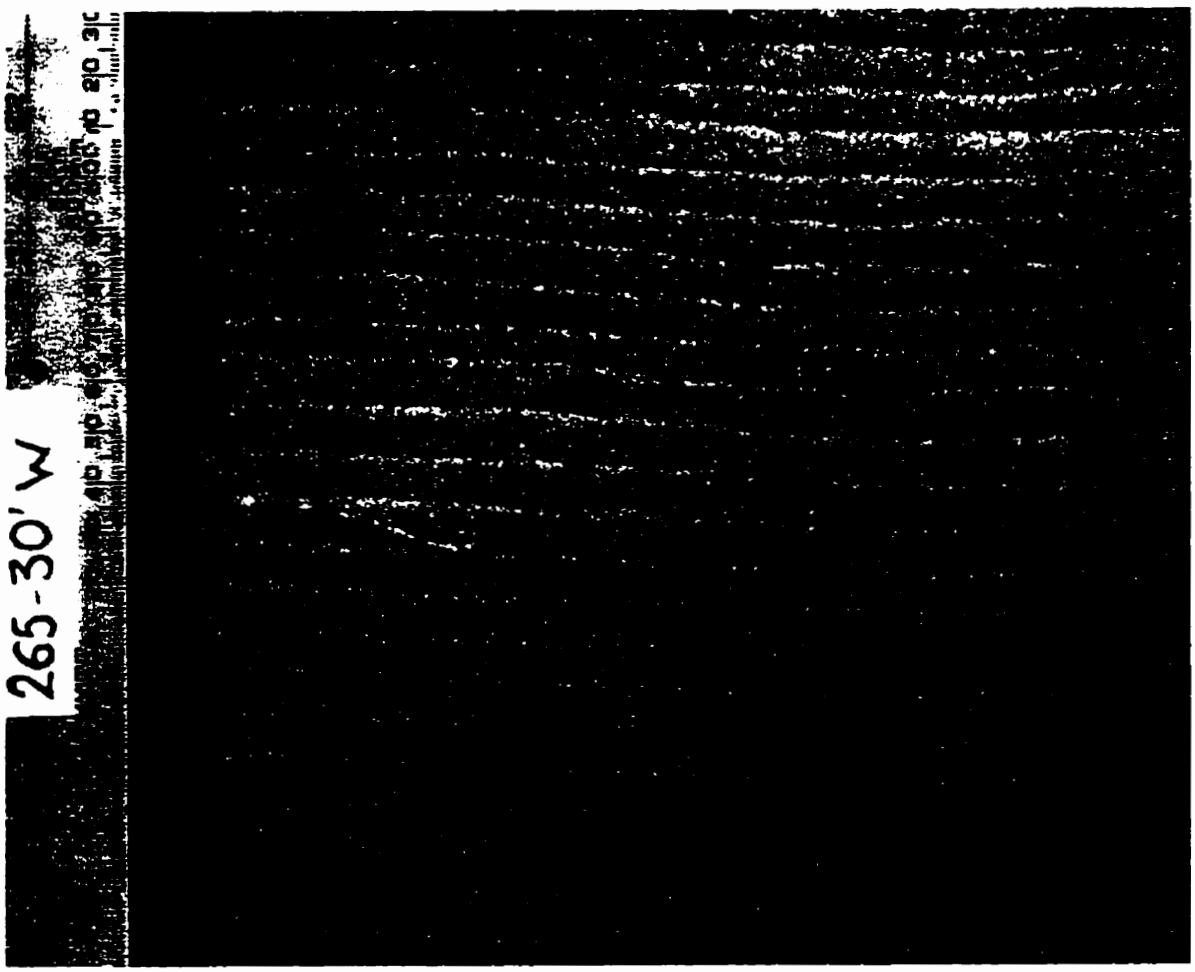

Figure 6.12 Oscillation marks on the surface of a peritectic-carbon steel billet sample (0.12%C); oscillation frequency 150 cpm

(A)

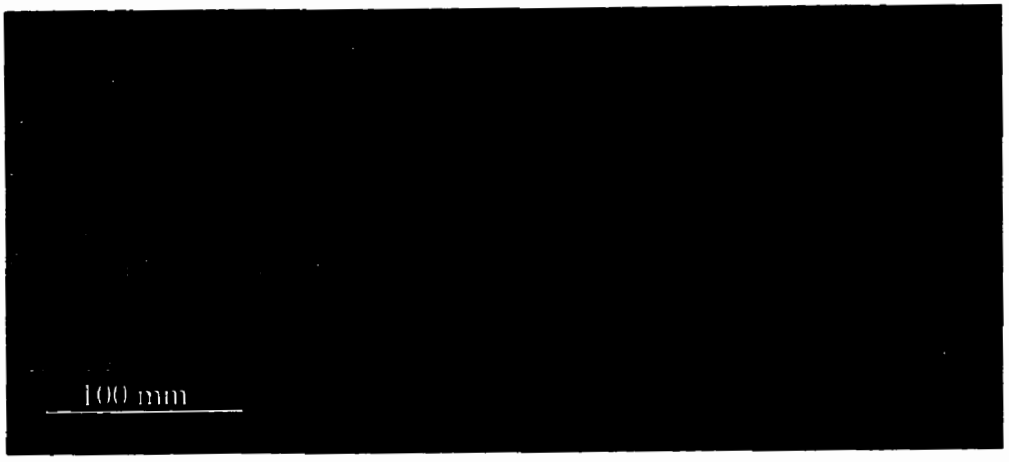

(B)

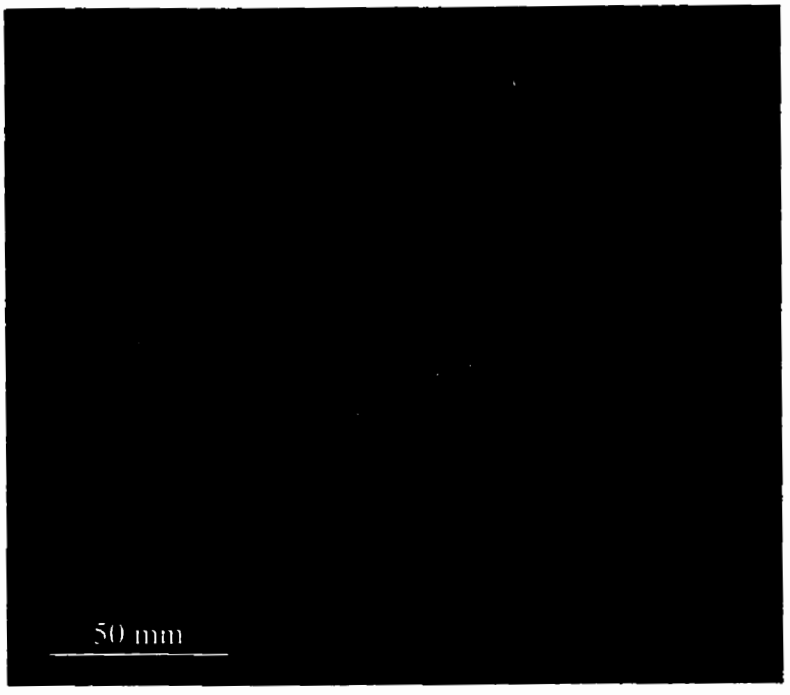

Figure 6.13 transverse depression on the surface of a sample from Heat 277 (0.14%C, oscillation frequency 170 cpm): (A) billet sample; (B) close-up

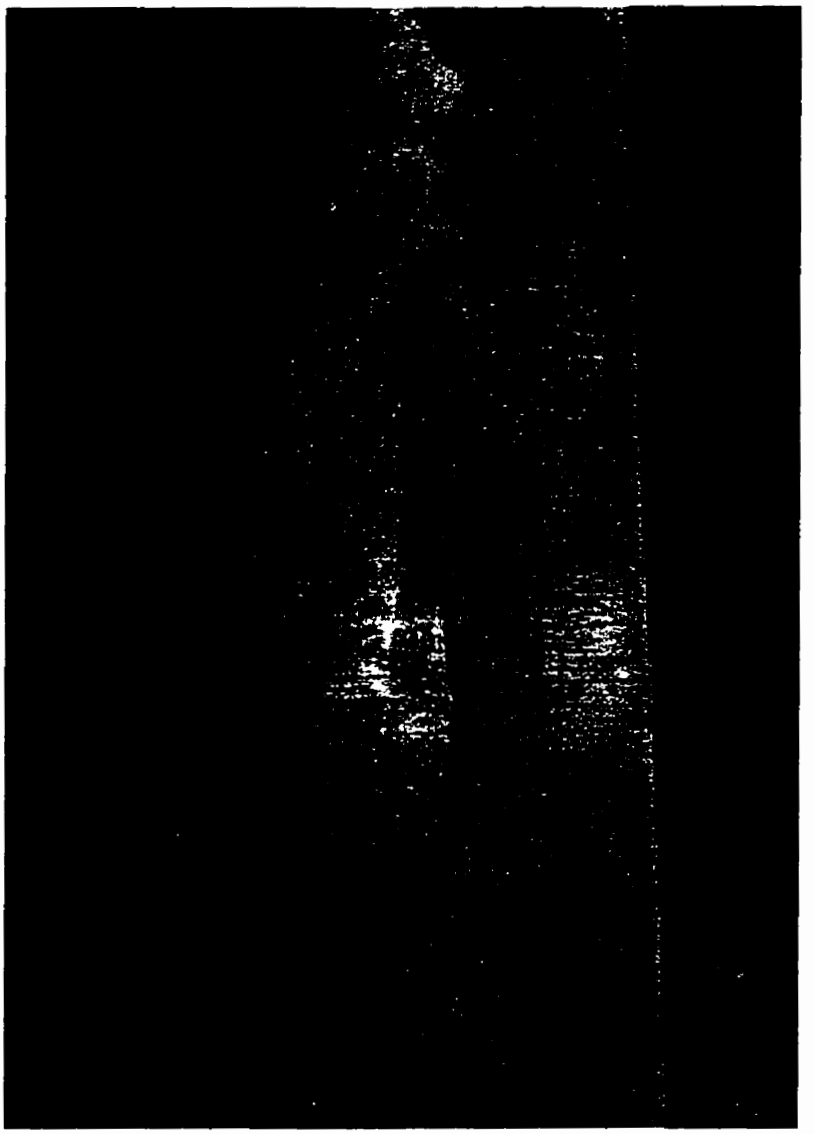

Figure 6.14 *Longitudinal depression on the surface of a peritectic-carbon steel billet sample (0.14%C)*

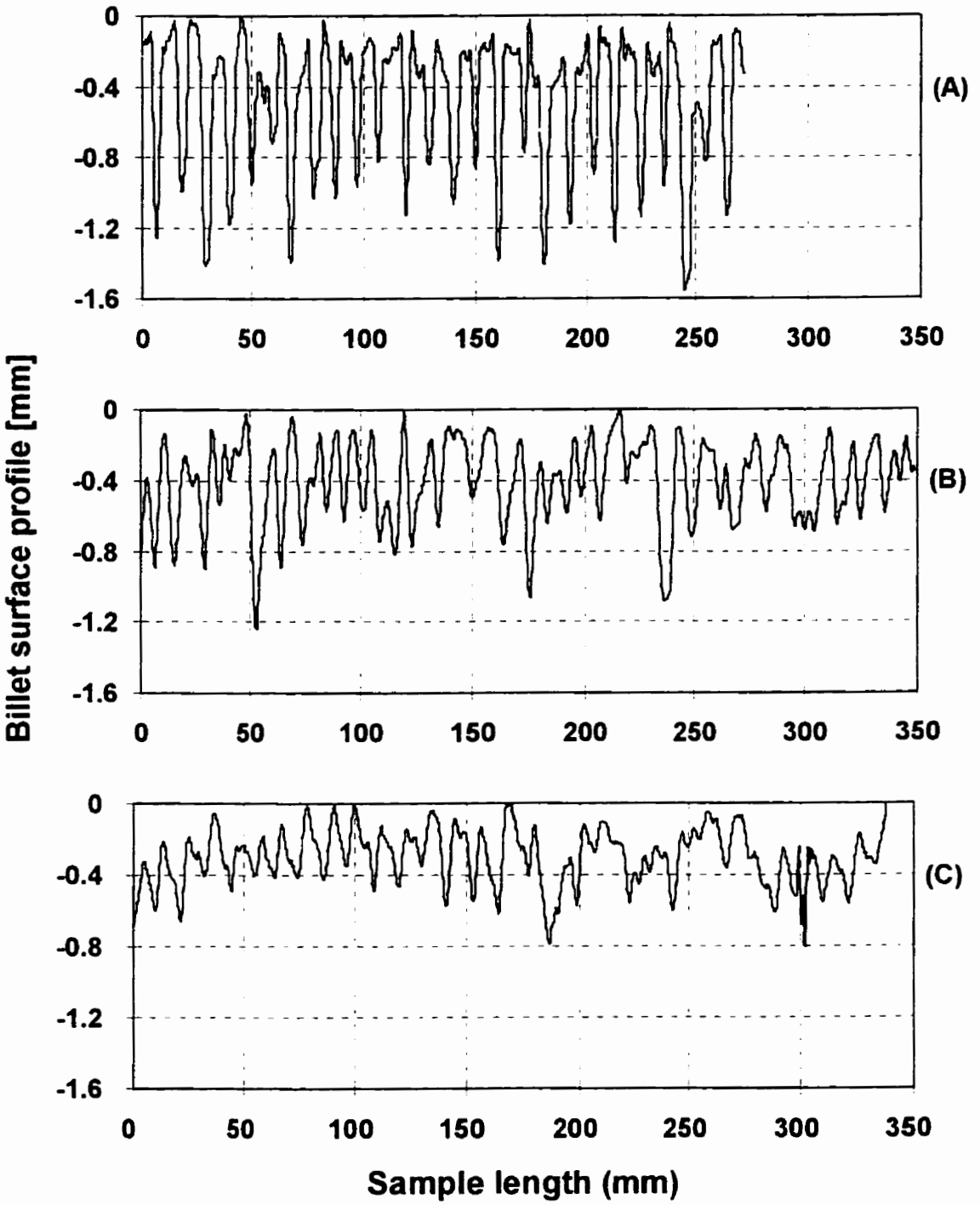

Figure 6.15 Centre-surface profiles of billet sample; (A) Heat 265, peritecti steel, 0.12 pct. C, oscillation frequency 150 cpm, powder B; (B) Heat 280, peritectic steel, 0.14 pct. C, oscillation frequency 170 cpm, powder B; (C) Heat 311, Boron(Ti)-alloyed steel, 0.33 pct. C, oscillation frequency 137 cpm, powder A

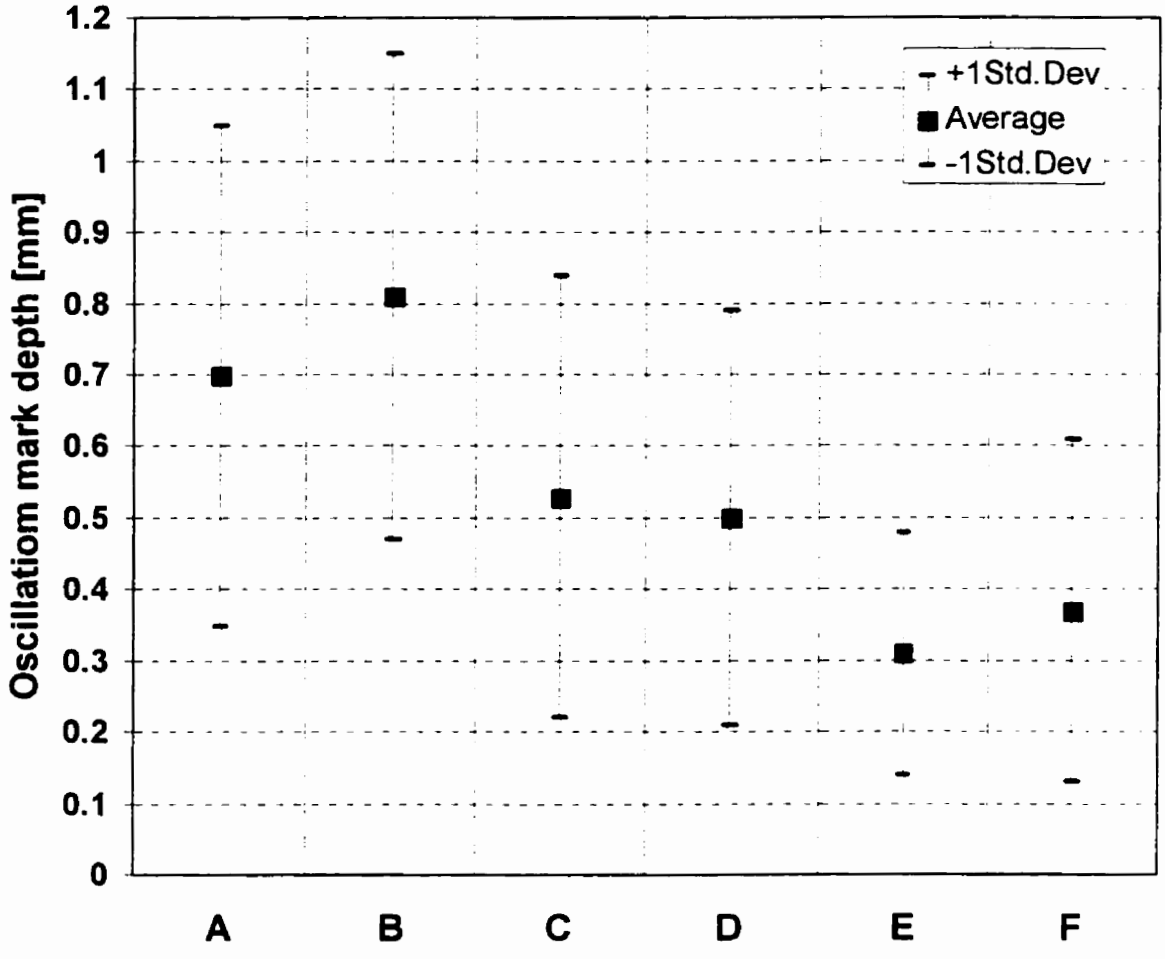

A - peritectic steel (0.11%C), powder A, f = 150 cpm
B - peritectic steel (0.12%C), powder B, f = 150 cpm
C - peritectic steel (0.14%C), powder A, f = 170 cpm
D - peritectic steel (0.13%C), powder B, f = 170 cpm
E - Boron(Ti)-alloyed steel (0.33%C), powder A, f = 137 cpm
F - Boron(Ti)-alloyed steel (0.32%C), powder B, f = 137 cpm

Figure 6.16 Oscillation mark depth: summary of measurement results

(A)

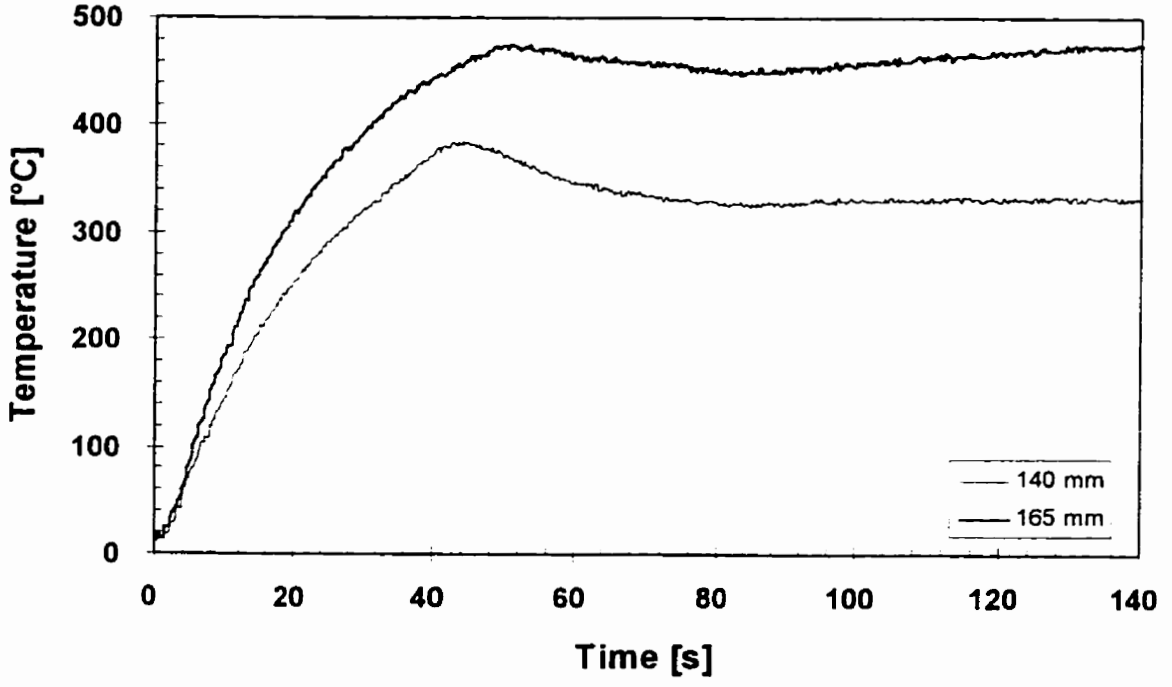

(B)

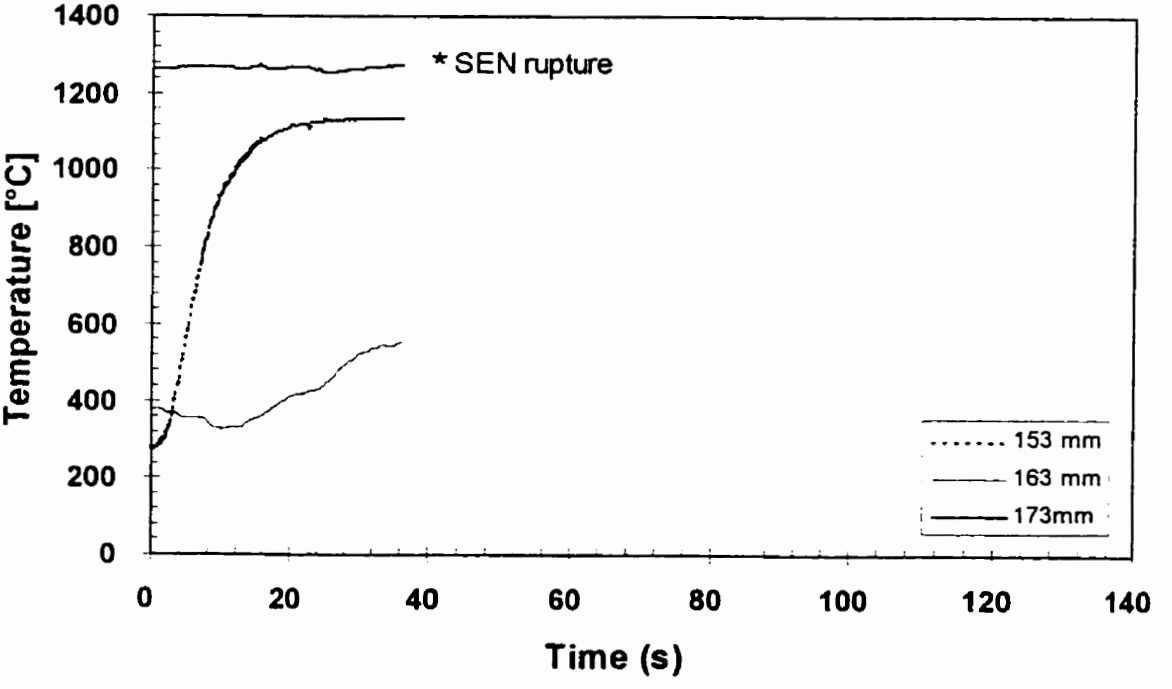

Figure 6.17 Measured mould flux temperature, the legends give thermocouple position from top of the mould; (A) Heat 313, casting speed 1.08 m/min., metal level ~190 mm; (B) Heat 316, metal level ~ 175 mm

7. RESULTS AND DISCUSSION

The main findings regarding mould heat transfer and its relationship to billet surface quality are discussed in this chapter. Detailed comparison between results obtained for heats cast with powder lubrication, the subject of this investigation, and heats cast with oil, from previous investigations, is accomplished. Explanations for similarities and differences found in the thermal behaviour and surface quality of heats cast with powder and oil are proposed. In addition, the influence of mould powder properties and casting variables on liquid flux pool depth is investigated through a sensitivity analysis of the mould powder melting model and measured values of liquid pool depth were compared to values calculated by the mathematical model using plant trial casting conditions. Simulations were also performed to verify the response of the molten flux pool depth to variations in casting speed.

7.1 Mould Heat Flux

Mould temperature data which reflected the effect of several process variables on mould heat transfer has been reported in the previous chapter. However, temperature does not provide sufficient quantitative information on heat transfer in the mould. Thus, an inverse heat conduction model of the mould, already discussed in Chapter 4, was developed to allow mould heat flux profiles to be estimated from the measured values of mould wall temperature. The heat-flux profiles in the mould have been calculated at the centreline of the East face for different casting parameters. Figures 7.1 shows an example of calculated mould heat fluxes profile together with the temperature data used for the calculation. The shape of the heat profile can be decomposed into four segments, as follow:

(1) From the top of the mould down to 145 mm the profile is characterized by very low values (<50 kW/m^2) of heat flux.

(2) From 145 to 161 mm, the meniscus region, the heat flux increases abruptly from 50 to 3200 kW/m^2. The maximum value, 3200 kW/m^2, occurs at the meniscus level which was 160 mm below the top of the mould.

(3) Below the meniscus the heat flux decreases in magnitude. Shrinkage of the solidifying shell gives rise to an increase in the gap between the shell and the mould which leads to an increase in the thermal resistance, thereby lowering the heat transfer to the mould. Since the initial shrinkage is larger due to the initial higher heat flux and in the case of peritectic steels also due to the α to γ transformation. Just below the meniscus, at 220 mm, heat flux reaches a local minimum value. Ferrostatic pressure acting on the thin shell pushes it back towards the mould wall decreasing the gap, thus increasing heat flux.

(4) From 220 mm further down the mould the progress of solidification leads to a progressive increase in the gap with a consequent decrease in heat flux. A rebound in heat flux verified at 335 mm is associated with excessive mould taper and binding, however as the shell is still very deformable the binding ceases and mould heat flux continues to decrease. Also, as the shell grows the thermal resistance of the solid shell becomes significant. At the mould exit the thermal resistance of the steel shell can represent from 20 to 40% of the total resistance, the rest is mainly constituted by the thermal resistance of the mould/strand gap. The thermal resistance of the copper wall and the cooling water are negligible.

The shape of the mould heat flux profile obtained in this study is quite similar to the findings of Mahapatra's investigations on slab casting[108]. The only noticeable difference was that Mahapatra reported all heat flux profiles with maximum value at the meniscus level, while in some cases in this study the peak heat flux occurred below the meniscus level. Figure 7.2 shows heat 262 with maximum value of heat flux at the meniscus level, while for heat 265 the meniscus level corresponded approximately to an abrupt inception of heat flux. This finding is supported by profiles reported in Chandra's investigation of billet cast with oil lubrication[109]. Although Chandra reported the peak heat flux at the meniscus as a characteristic feature of mould heat flux profile, some of his profiles showed the meniscus at the onset of an abrupt increase in heat flux. This is a very interesting observation and probably is caused by the inherently instability of the meniscus in billet casting when metal level is controlled via casting speed instead of a flow control device. Kumar[110] showed that in the mini-mill where this investigation was conducted during billet casting with oil lubrication the metal level exhibited variations between 10 and 20 mm with a frequency of approximately 0.2 Hz. Under these circumstances the metal level could not be fixed within a range narrower than the distance between two adjacent thermocouples, i.e. 15 mm, which is approximately the distance between the onset of heat flux and its maximum value.

7.1.1 Influence of process variables on mould heat flux

7.1.1.1 Mould powder

Two different types of mould powder were used in the plant trial. The two heats chosen to examine the differences in heat flux associated with the mould fluxes were cast under similar conditions, i.e., same mould oscillation frequency (150 cpm) and same mould water velocity

(7.6 m/s) while casting speed was 1.20 m/s for heat 262 and 1.17 m/s for heat 265, and the metal level was ~ 160 mm for heat 262 and ~ 175 mm for heat 265. Figure 7.2 shows that mould heat transfer is increased over the whole mould length with powder A when compared to powder B. For peritectic steels, powder A resulted in averaged heat flux ~ 20% higher than powder B, however the difference in peak heat flux at the meniscus region is only 10% higher for flux A. Similar results were found for all heats of peritectic-carbon ($0.11 \leq \%C \leq 0.14$) analyzed. However for Boron(Ti)-alloyed steels ($0.30 \leq \%C \leq 0.33$), powder A only yielded mould heat flux that was on average ~ 7% higher than powder B.

The properties of the two mould fluxes are listed in Table 5.3; both fluxes have low viscosity with flux A more viscous than flux B. However, flux A has a lower transition temperature. The literature review shows that mould heat flux increases with decreasing viscosity and transition temperature of the mould flux. The present findings confirms results of Emi et al.[40] who found that the overall heat-transfer coefficient had a stronger correlation with the transition temperature than viscosity. Although the difference in heat flux between powder A and B was not very large, it is quite significant to note that the difference in transition temperature was only ~ (-)13% while the difference in viscosity was ~ (+)42%. This suggests that not only is mould heat transfer more strongly dependent on transition temperature than viscosity, but also that in the low range of viscosity, i.e., below 2.0 poise, and at temperatures above the transition temperature, viscosity does not seem to have a strong influence on mould heat transfer. This finding is further confirmed by the fact that at the meniscus, where viscosity should be a critical factor, the difference between heat transfer for the two powders was smaller than below the meniscus.

7.1.1.2 Mould oscillation frequency

The effect of mould oscillation frequency on mould heat flux is shown in Figure 7.3. The axial heat flux profile for higher frequency is higher for most of the mould length, except at the meniscus. The displacement in the position of the peak heat flux of the two heats is because at the lower frequency (heat 260) the metal level was ~ 161 mm below the top of the mould while at the higher frequency (heat 277) the metal level was at ~ 175 mm. The average heat flux is 8% higher for an oscillation frequency of 170 cpm than for 150 cpm. As previously discussed in section 6.1.2.2 this is attributed to a decrease in oscillation mark depth (Figure 6.16), resulting from a lower negative strip-time and also to a decrease in mould flux consumption when the oscillation frequency increases. Both factors contribute to a narrower gap between the mould and strand, decreasing the thermal resistance. As pointed out before this finding is contrary to Chandra's[109] results who observed a decrease in mould heat transfer when the frequency was increased from 96 cpm to 144 cpm; he attributed the decrease in mould heat transfer to less mould shell interactions as a result of shorter negative strip-time. However, the above finding agrees with observations reported by Kumar[110] who found that mould heat transfer increased by about 15 pct. when mould oscillation frequency was increased from 100 cpm to 160 cpm. Kumar[110] attributed the enhancement in heat transfer to a decrease in the depth of oscillation marks, therefore, a narrower mould/strand gap. The studies conducted by Chandra[109] and Kumar[110] were both concerned with billet casting with oil lubrication while the present investigation is focused on powder lubrication. Kumar[110] attributed these apparently contradictory findings to the action of two opposing factors namely mould/strand interaction and depth of oscillation marks. As clearly evident in the literature and very recently quantified by Gurton[124] mould fluxes are much more

effective as casting lubricants than oil. The magnitude of mould/strand interactions are much smaller for mould flux than oil, thus mould/strand interaction should not play such important role as in the case of oil lubrication. Therefore, the increase in heat flux when the oscillation frequency was increased from 150 cpm to 170 cpm must be caused by the decrease in the depth of oscillation mark when oscillation is increased. This was confirmed by the measurement of surface profile performed in billet samples which showed that average oscillation mark depth decreased from ~0.75 mm to 0.50 mm when oscillation frequency was increased from 150 cpm to 170 cpm (Figure 6.16).

7.1.1.3 Mould water velocity

As was mentioned in the previous chapter, two different mould water velocities were employed during a given heat. Figure 7.4 shows the axial heat flux profile at two different velocities for heat 281. Significant differences in mould temperature when the water velocity was changed, as shown in Chapter 5, did not translate into significant changes in mould heat flux. Average heat flux increased only 1.4 % when water velocity decreased from 9.9 m/s to 7.6 m/s and the peak heat flux increased 10%. For peritectic steels ($0.11 \leq \%C \leq 0.14$) both the average and peak heat flux consistently increased when water velocity decreased. However, the magnitude of these increases, between 3% and 10%, were small to be considered significant. For Boron(Ti)-alloyed steels ($0.30 \leq \%C \leq 0.33$) average heat flux showed no significant difference (less than 2%) when water velocity was changed, but peak heat fluxes increased ~ 10% when water velocity was changed from 6.0 to 9.9 m/min. This latter behaviour is most likely to be related to the very low metal level position (below 190 mm) used for casting the boron steels. The metal level was lowered to avoid longitudinal depression, which had been linked to a steep taper at the top of the mould. Since the

thermocouple located at 190 mm failed during the trial, the determination of the exact position and magnitude of the peak heat-flux for the boron steels heats is not very accurate.

The findings regarding the peritectic steels offer some support to Mahapatra's observations[108] who found different heat extraction rates on the broad faces of a slab mould. He attributed lower values of heat flux on the inside radius, the side with thinner copper wall, to a thicker slag rim caused by a lower hot-face temperature of the mould in the vicinity of the meniscus. At the same time the thicker slag rim would interact more with the meniscus producing deeper oscillation marks. Therefore, based on Mahapatra's[108] results it seems reasonable to expect that a decrease in mould water velocity, which increases the mould hot-face temperature, would lead to a significant increase in mould heat flux and shallower oscillation marks. Measured values of oscillation mark depth displayed in Table E1 (Appendix E) however showed no significant effect of mould water velocity on oscillation mark depth. For heats 277 and 278 cast with mould powder A, the average oscillation mark depth decreased less than 2% (from 0.55 to 0.54 mm) when the water velocity decreased from 9.9 to 7.6 m/s. For heats 314 and 315, also cast with mould powder A, the oscillation mark decreased from 0.31 to 0.29 mm when water velocity decreased from 9.9 to 6.0 m/s. Probably one of the reasons the relative increase in heat transfer with lower velocities is small is related to the magnitude of the temperature differences necessary to affect the slag rim thickness. Mahapatra[108] reported differences over 40°C between the hot-face temperature of the inside and outside radius, while in the present study the maximum temperature variation caused by a change in mould water velocity was calculated to be 25°. Also, Mahapatra used two mould powders with very high "melting" temperatures (1125°C and 1165°C), and although he did not report values of transition temperatures, the fluxes used by Mahapatra

probably had higher transition temperatures than the mould powders used in the present investigation (1000°C and 1135°C). Since high transition temperature favors the formation of a thick slag rim, Mahapatra's results were more sensitive to the influence of the slag rim than the present investigation. Finally, as previously observed, in slab casting metal level is controlled via a liquid metal flow control system, and casting speed is completely independent from metal level. These two features maintain casting speed at a constant value and metal level within a narrow range, even if metal level control is manual as in the case of Mahapatra's[108] trials. Since the phenomenon reported by Mahapatra is localized at the meniscus an accurate positioning of the meniscus is crucial, together with constant casting speed. As previously mentioned due to the characteristics of the process studied in this investigation these two conditions could not be achieved.

7.1.1.4 Steel grade

The heat flux profiles depicted in Figure 7.5 illustrate the effect of steel grade on the mould axial heat flux profile, with an example from each of the sequences cast in the plant trial. All three profiles were obtained for heats cast with powder A and a water velocity of 9.9 m/s. Heat 262 was cast with a mould oscillation frequency of 150 cpm, heat 277 with 170 cpm and heat 311 with 137 cpm. The nominal metal level set-point for heats 262 and 277 was 127 mm and for heat 311 it was 142 mm. It is clearly seen that the actual metal level was deeper and although heats 262 and 277 had the same set-point, the actual values are different. In spite of this limitation, inherent to the process investigated, Figure 7.5 shows a remarkable result. As expected, heat 262, due to its carbon (0.11%C) content and oscillation frequency (150 cpm), has ~34% lower heat flux than heat 277. Mould heat flux as a function of the steel's carbon content has a minimum value around 0.10 and 0.11% carbon [126]. Also, heat

262 was cast with lower mould oscillation frequency than heat 277 which, according Figure 7.3, should account for a decrease of ~8% in mould heat flux.

Heat 311, a Boron(Ti)-alloyed steel (0.33% C), has averaged mould heat flux ~ 27% lower than heat 277 (0.14% C), and just 10% higher than heat 262 (011%C). Although the medium-carbon steel (heat 311) was cast with the lowest oscillation frequency (137 cpm) the difference in oscillation cannot account for the difference in heat flux. Medium-carbon steels were expected to yield much higher heat flux, since with oil lubrication mould heat fluxes for these steels have been reported to be about twice of peritectic steels with ~0.12%C [110,127].

Table 7.1 shows that the casting speed for heats 277 and 311 are very close, but even for a slightly higher casting speed, 1.3 m/min compared to 1.28 m/min for heat 277, heat 311 still had a lower peak heat flux, 2650 kW/m^2 compared to 2811 kW/m^2 for heat 277, and a much lower average heat flux, 983 kw/m^2 compared to 1349 kW/m^2 for heat 277. This is a remarkable result since previous studies on billet casting with oil lubrication showed that medium-carbon steels (C>0.20 pct) with or without Boron and Titanium give rise to much higher mould heat flux than any peritectic steel (0.09% <C<0.16%)[109-110,126-128]. It will be shown later that the behaviour of the boron steels is due to the role of the mould flux and the topology of the strand surface, i.e., smooth for boron steels and rippled for peritectic.

7.1.2 Mould hot- and cold-face temperature profiles

Figures 7.6 shows temperature profiles at the hot- and cold-face of the copper mould calculated for heat flux profiles displayed in Figure 7.5. The peak temperature at the mould cold face lies for all cases below 100°C. For all cases analyzed the maximum cold face temperature was calculated to be below 166°C (boiling temperature for the mould cooling-water under the trial conditions), which ensures no boiling takes place in the water cooling

channel. The peak temperatures at the hot-face shows that under mould flux lubrication the mould operates fairly cold. For oil lubrication the mould is considered under hot operation when the peak temperature is above 250°C[110], however this is an arbitrary temperature related to the boiling point of oil.

7.2 Billet Response

The main finding of the surface inspection was the absence of transverse depressions in Boron(Ti)-alloyed medium-carbon steels since this is the main surface problem found when this steel is cast with oil lubrication. However, the incidence of longitudinal depression was very high for both types of steel, peritectic and boron(Ti)-alloyed medium-carbon grade, which suggests that excessive mould taper was causing the mould to squeeze the shell causing resulting in inward buckling. An existing mathematical model of billet shrinkage[109], previously addressed in Chapter 4, was employed to analyze mould taper and calculate billet shell thickness.

7.2.1 Shell thickness:

A solidification model was used to calculate the thickness of the strand shell along the mould length. The heat fluxes obtained from the plant trial were used as a boundary condition for this calculations. Values of the strand shell thickness at the mould exit for different casting conditions are presented in Table 7.2

Medium-carbon steels has a lower liquidus temperature (1497°C) compared to peritectic steels (1516°C), and also a wider freezing range (liquidus minus solidus temperature) of 42°C compared to 20°C for peritectic steels. These two factors aggravated by high superheat and high casting speed can lead to very thin shell at the mould exit as in the case of heat 311 cast

with powder A. Calculations showed that an increase of 10°C in tundish superheat results in 1 mm decrease in the shell thickness at the mould exit, likewise a casting speed increase of 0.1 m/min resulted in a decrease of 0.5 mm. This two variables acting together explain the low values of shell thickness obtained for heat 311.

Metallographic examination was conducted on the cross section of all samples collected during the plant trial. In few of the macroetched samples it was possible to identify white and dark bands running roughly parallel to the billet. However in most of the sample these bands were not very distinct or did not even appear which is in agreement with Bommaraju et al.[129] who reported these bands to be not visible in low-carbon billet sections, with the exception of a few cases, because they etch more poorly than medium-carbon steels. Also, they reported that the bands were not always clear in billets having a large equiaxial structure. Titanium precipitates in the liquid steel as TiN, as will be discussed later, promotes the formation of a large equiaxial structure. Bommaraju et al.[129] reported that the outermost edge of the dark band corresponded to the shell thickness approximately at the bottom of the mould where the first sprays impinged the strand surface. They are formed because heat extraction in the sprays is greater than in the lower mould, and therefore solidification rate is accelerated significantly with consequent reduction in microsegregation and secondary-dentrite arm spacing. The low sulphur content in the steels investigated, confirmed by very light and uniform sulphur prints, also did not favored the appearance of white or dark bands since segregation was not significant.

Despite the lack of white and dark bands in most of the samples it was still possible to identify some dark bands in order to estimate the shell thickness at the mould exit and compare these values to some of the values displayed in Table 7.2. Table 7.3 shows a

comparison between the shell thickness at the mould exit calculated using the mathematical model of billet solidification and measured values taken as the outermost edge of dark bands. As the distance of the outermost edge of the dark bands from the surface of the billet varied across a given face and from face to face the values reported in Table 7.3 refer to average values measured on the East face, the same face of the heat flux profiles used for the calculations. It is clearly seen that the agreement between the measured and calculated values is quite good, which shows that the heat flux profiles used were able to accurately represent the mould heat transfer rates at the centreline of the East face.

7.2.2 Billet shrinkage calculation

Shrinkage calculations were performed using a mathematical model of billet shrinkage, developed by Chandra[109] and previously referred in Chapter 4. Billet dimension along the mould length were compared to mould dimensions to investigate mould/strand gap, mould/strand binding and mould taper. Since during casting operation the mould bulges due to thermal expansion mould distortion must be taken in account to correctly perform the above analysis. The mould distortion was assumed to be equal to values previously calculated for the same mould and peritectic steels cast with oil lubrication[121]. This is a very reasonable assumption since as shown in Chapter 6 mould temperature profiles for peritectic ($0.11 \leq \%C \leq 0.14$) and Boron(Ti)-alloyed steels ($0.30 \leq \%C \leq 0.33$; $0.0024 \leq \%B \leq 0.0028$; $0.035 \leq \%Ti \leq 0.038$), cast with powder lubrication, are within the same range as peritectic steels ($0.12 \leq \%C \leq 0.13$) cast with oil. To account for differences in metal level the calculated mould distortion was shifted so the location of the maximum distortion approximately matched the position of the maximum hot-face temperature.

Figure 7.7 shows the dimensions of the cold mould measured before the plant trial and a typical profile of the distorted or hot mould. The distorted mould profile was obtained by adding local values of mould distortion to the dimensions of the cold mould. Figures 7.8 and 7.9 present the calculated mould and billet dimensions for some of the heats investigated. It is clear that binding was occurring in all heats analyzed, which shows that the mould taper was excessive. However the degree of binding is very different when comparing peritectic steels and Boron(Ti)-alloyed medium-carbon steels. Figure 7.8 shows that for peritectic steels, heats 277 (0.14%C)and 281 (0.13%C), binding only begins at 400 mm from the top of the mould below which the billet is only slightly bigger than the mould. In contrast, Figure 7.9 shows that for boron steels, heats 311 (0.33%C) and 314 (0.31%C), binding begins just below the meniscus, at around 250 mm from the top of the mould, and from there on the billet dimension is much larger than the mould dimension. Since the billet cannot actually be larger than the mould, otherwise it would stick inside the mould, what really happens is that some binding will take place but then the billet shell is plastically deformed to the mould dimension. Table 7.4 summarizes the results of shrinkage calculations performed for the conditions presented in Figures 7.8 and 7.9 together with some other cases investigated.

The results displayed in Table 7.4 show quite clearly that the heats of Boron(Ti)-alloyed medium-carbon steels potentially bind throughout the mould length whereas the peritectic steels heats only bind slightly in the lower part of the mould. The difference in the behaviour of these two grades results from their carbon content. The boron grade is in fact a medium-carbon steel (~0.32%C), thus it has a lower liquidus temperature and wider solidification range, while the peritectic steels (~ 0.12%C) have higher liquidus temperature and narrower mushy zone. For identical casting conditions boron steels will have a thinner shell, therefore

they will shrink less resulting in a smaller strand/mould gap, or even binding, if the mould taper is too severe. As the initial taper of the mould used in the plant trial was too steep, the boron steels were binding from just below the meniscus. The peritectic steels, on the other hand, due to their δ to γ phase transformation, which takes place in the meniscus region and is accompanied by 4.7% volume shrinkage[120], evade the initial steep taper (4.9%/m) and only bind much further down in the mould (at least below 300 mm from the top of the mould).

It is important to note that if binding was really occurring in the mould, surface defects related to sticking of the shell to the mould such as laps and bleeds should appear in the billet samples of the boron grade steels. However, among 29 samples inspected only one, from a peritectic steel heat, showed signs of sticking, i.e. a small region clear of oscillation marks and surrounded by distorted oscillation marks. No similar signs of sticking was detected in the samples of Boron(Ti)-alloyed medium-carbon steels which suggests that no real binding was occurring in the mould. On the other hand all samples of Boron(Ti)-alloyed medium-carbon contained longitudinal depression, such as the one previously shown in Figure 6.14. This occurs because the mould squeezes the thin solid shell that buckles inward generating longitudinal depressions.

Longitudinal depressions were evident in all plant-trial heats, which indicates that the mould taper was too steep for casting with mould powders. This is particularly critical for Boron(Ti)-alloyed medium-carbon steel since, as will be discussed later, compared to oil lubrication, the meniscus heat flux is 30 to 50% lower when powder is used. Lower heat flux leads to smaller thermal contraction therefore requiring a shallower taper. For peritectic steels no significant difference exists in heat flux levels for oil or powder so a taper designed for oil casting can be used for casting with flux lubrication. Considering that: (i) there is no optimum

mould taper that can satisfy at the same time peritectic and medium-carbon steels, (ii) billet mould construction does not allow on-line changes in taper and (iii) most of the contraction due to solidification takes places in the upper part of the mould; to specify a taper requires to compromise. Thus, for each of the calculated billet profiles show in Figures 7.8 and 7.9, the ideal continuous taper profile was calculated. Finally, a double mould taper, which it much simpler to machine, was found to be a suitable compromise. The recommended tapers were calculated to be 1.8 pct.m^{-1} up to 450 mm from the top of the mould and 0.9 pct.m^{-1} for the rest of the mould. The above taper profile is recommended for casting speed between 1.0 and 1.3 m/min and a meniscus level of ~165 mm.

7.3 Comparison Between Powder and Oil lubrication

A major finding from the plant trial data was the absence of transverse depressions in both steel grades cast during the trial and the very low values of mould heat fluxes obtained for the Boron(Ti)-alloyed medium-carbon steels. Availability of mould temperature data for similar steels cast with oil lubrication calls for a comparison of powder and oil lubrication with respect to mould thermal response and billet surface quality.

7.3.1 Effect of lubricant on heat flux

During the plant trial three heats of low-carbon steel (0.12≤%C≤0.13) and two heats of boron steel (0.32%C) were cast using oil lubrication. These heats were cast under similar casting conditions to the other 7 heats of peritectic-carbon steel (0.11≤%C≤0.14) and 5 of Boron(Ti)-alloyed steel (0.30≤%C≤0.33) cast with powder lubrication, which made them an excellent set for comparing oil lubrication and powder lubrication in billet casting.

Temperature data for the oil heats for all four mould faces were analyzed the same way as previously described in chapter 6.1.

Figure 7.10 shows that peritectic steels (0.12~0.14%C) exhibit no major differences in the heat flux profiles of steels cast with oil or powder. The overall heat flux with oil (oscillation frequency 137 cpm) is only ~3% higher than that with powder (oscillation frequency 150 cpm). Even if the difference in oscillation frequency is accounted for, based on Figure 7.3 mould heat flux for peritectic steels cast with oil should be no higher than 10% compared to powder lubrication. For boron steels, on the other hand, the difference in heat flux arising from switching from oil to powder lubrication, is very significant. As shown in Figure 7.11, the peak heat fluxes obtained with powder lubrication, ~ 2300 kW/m^2, were about half the maximum values obtained for oil lubrication, ~ 5000 kW/m^2. The same is true for the plateau values (heat flux corresponding to 250 mm below the top of the mould), ~1000 kW/m^2 for powder compared to ~2000 kW/m^2 for oil. Overall for the case of boron grades oil lubrication resulted in heat fluxes 20 to 50% higher than powder lubrication.

The remarkable difference in mould heat-flux behaviour between boron grades and low-carbon steels (peritectic grade: 0.11~0.14%C) when oil is replaced by powder, suggests that powder strongly affects medium-carbon grades (0.30~0.33%C) but its effect is much less pronounced for peritectic steels. These results agree with findings reported by Singh and Blazek[126] and discussed by Chandra[109]. Peritectic steels, because of the δ to γ phase transformation that takes place in the meniscus region, have a larger volumetric shrinkage (4.7%)[120]. This reaction leads to the formation of a rather rippled strand surface with large gaps between the mould and the strand. For oil lubrication these large gaps would lead to low heat transfer rates. The larger mould/strand gap formed during the casting of these steels in

many instances can lack oil since most of it vaporizes and escapes within a narrow distance from the meniscus; therefore, the gap is filled mainly by nitrogen which has a lower thermal conductivity than oil or its pyrolytic products. The filling of these large gaps by the molten flux would tend to increase the thermal conductivity of the gap, thereby increasing the mould heat flux. Actually, replacing oil for molten flux can slightly increase the heat flux or decrease the meniscus heat flow depending of properties of the mould flux been used[146]. Mould taper is also a factor since it largely determines the dimensions of the mould/strand gap.

For boron grades (~0.3% C) the carbon content is outside the peritectic range therefore the billet surface is smoother and gaps are smaller. This is confirmed by Figures 6.15 and 6.16 that clearly show a significant difference in the depth of the oscillation marks of peritectic and boron steels. Average oscillation mark depth for the boron steels (oscillation frequency of 137 cpm) was below 0.4 mm, while for the peritectic steel cast with an oscillation frequency of 150 cpm average oscillation mark depth was above 0.7 mm.

Because of the smooth surface of boron steels, when oil is used as lubricant the mould heat transfer is much higher than the heat transfer of low-carbon steels. In fact the large amount of transverse depressions exhibited by boron steels cast with oil suggests that the mould/strand gap along the mould length consists of comparatively long regions free of depressions and with very narrow gaps, and shorter regions with deep gaps formed by the depressions. Kumar[110] reported values between 45 and 75 mm for the width of transverse depressions in the casting direction and values between 50 to 200 mm for the distance between consecutive depressions. In the regions of narrow gap it is thought that intermittent contact between the mould and strand can be established. When mould flux replaces oil it not only behaves as an insulator between the mould and the strand, thus decreasing heat flux, but

also suppresses intermittent contact. The suppression of contact between the strand and the mould is believed to be the major cause of the decrease in heat flux for boron grades when powder replaces oil. Molten flux acts as a better lubricant than oil, fills the gap thoroughly and exert some pressure against the strand shell forcing it away from the mould walls.

7.3.2 Transverse Depressions

Figure 7.12 shows one example of a Boron(Ti)-alloyed medium-carbon steel heat cast with oil. In this case two different heat flux profiles are presented, a lower curve corresponding to the first half of the heat and a higher curve corresponding to the second half. This more unstable thermal behaviour, different of what was observed for peritectic-carbon grade cast with oil is likely to be due to the presence of many transverse depressions in the first billets of this heat which largely contributed to decrease the heat flux. The presence of these depressions was observed in the mould temperature profiles and confirmed by billet inspection[110]. The second half of the heat resulted in a higher heat flux and a slightly higher average casting speed. The above example show how significant transverse depressions can be in Boron(Ti) medium-carbon steels cast with oil lubrication.

7.3.2.1 Influence of lubrication type and steel grade

During continuous casting with oil lubrication the magnitude of the mould heat flux for plain medium-carbon steels (0.32%C) and medium-carbon steels containing boron and titanium (0.32%C, 0.0032%B, 0.033%Ti) is quite similar. However, the billets of medium-carbon containing boron and titanium have a high incidence of transverse depressions, while billets of plain medium-carbon steel have few transverse depressions[127].

Previous work conducted by the UBC-Billet Casting Group revealed that transverse depression formation is highly dependent on steel composition. It was found that the boron and titanium containing steels are more susceptible to transverse depression followed by low-carbon steels and medium-carbon grades; high-carbon grades usually do not exhibit transverse depressions[110,127,130].

Adjei-Sarpong[127] found that transverse depressions originated about 10-15 mm below the meniscus and were preceded by a metal level rise over a period of up to 6 seconds. Other operating factors observed to influence the formation of transverse depressions were: steel composition, casting speed, lubrication oil flow rate and tundish stream quality.

Adjei-Sarpong[127] proposed that transverse depression are caused by a sudden rise in metal level which traps the lubricating oil beneath the meniscus between the solidifying shell and the mould wall. The sudden vaporization of the trapped oil generates enough pressure to push on the shell at the meniscus and force it away from the mould wall to create a depression. The gap created by the depression reduces mould heat transfer and associated shell shrinkage as the strand travels down the mould. The reduction in shrinkage can lead to binding in the lower part of the mould which can widen the depressions further.

The observed effect of steel composition on transverse depressions is thought to be via its influence on the strength of the thin shell solidifying at the meniscus. High-carbon steels (C>0.6%), which have a broader mushy zone, are unlikely to behave as a solid skin in the meniscus region; consequently any pressure build up beneath the meniscus due to oil vaporization is released by a vertical escape of the gas rather than a permanent deformation of the shell. On the other hand, low carbon steels (0.10 ~ 0.16%C) with a narrower freezing range, the skin behaves more as a solid such that a sudden generation of oil vapor pushes the

skin to form a transverse depression. It is also expected that the medium-carbon steel (~0.32%C) skin would have an intermediate behaviour.

Jenkins et al.[131] investigated transverse depression formation in 0.06 pct. carbon blooms cast with powder lubrication. Consistent with Adjei-Sarpong[127] study, it was found that formation of depression was preceded by a rise in metal level. They proposed that the depressions were formed by the shell solidifying around the mould flux rim whenever the metal level rise was too quick for the rim to melt.

Thomas and Zhu[132] modelled the thermal distortion of solidifying shell near the meniscus. They simulated a metal drop of 30 mm for 0.6 seconds, followed by a level rise of 20 mm. In both instances they obtained that the shell bent away from the mould inwards to the liquid. The bending during the metal level drop is caused by the faster cooling of the inner face of the shell after it looses contact with the molten metal. The further distortion after the level rises is caused by the expansion of the existing shell due to reheating and the contraction of the "newly solidified" shell formed on top of the existing one. The total contraction after the level rise was 1.65 mm for ultra-low carbon steel. They attributed this behaviour to a high coherency temperature, which leads to strong initial shells that can resist flattening by ferrostatic pressure. Thomas and Zhu[132] also suggest that peritectic steels (carbon content near 0.1%) should also be prone to the proposed mechanism because these steels experience the most solid state thermal and phase transformation, exhibit a high coherency temperature and also experience interdendritic weakness.

Schruff et al.[133] reported that the surface of steel billets alloyed with boron, but not titanium, was good compared to the surface of boron-titanium alloyed billets. Based on Schruff et al.[133] and Thomas and Zhu[132] results it seems reasonable to propose that the

sensitivity of Boron(Ti)-alloyed medium-carbon steels to transverse depression is related to the presence of titanium, which is added to fix nitrogen in steel as TiN and thus to avoid the formation of BN. The presence of TiN in the grain boundary strengthens the shell, i.e., increases the coherency temperature to close to the steel solidus temperature; therefore, the shell becomes stiff and prone to permanent deformation due to thermal or mechanical action. The role of TiN as a high temperature strengthened was previously proposed by Samarasekera et al.[134] and was confirmed in this study by high temperature tensile tests carried out on two samples of Boron-alloyed medium-carbon steels, one containing Titanium and the other without Titanium.

Results of the high temperature strength tests performed are shown in Figure 7.13. The tests were carried out at 1300°C in a Gleeble® machine. The results show a difference of ~ +30% in favor of the steel containing titanium, which confirmed that TiN precipitation does increase the strength of the strand shell and must be the cause of a higher susceptibility to transverse depression displayed by Boron(Ti)-alloyed medium-carbon steels.

From the above analysis and review of previous works on transverse depression it seems undeniable that peritectic steels and Boron(Ti)-alloyed medium-carbon steels are more prone to transverse depression because their high coherency temperature. Their shells, at temperature slightly below the solidus temperature, are strong enough to resist flattening by ferrostatic pressure after been bent away from the mould under the action of thermal and/or mechanical stresses. Also, it has been well established that metal level variation is the main culprit behind the formation of transverse depression. However, some questions such as what is the role of the lubricant still remain.

The results from this study showed that the samples collected from Boron(Ti)-alloyed medium-carbon steel cast with powder lubrication did not show any transverse depression and also that this steel grade cast with powder had meniscus heat fluxes 50 % lower than the same steel cast with oil lubrication(Figure 7.11). Much lower heat flux translates into a thinner, hotter, more flexible shell that can be kept flat by the action of ferrostatic pressure, which suggests that the role of the lubricant is related to the magnitude of the heat flux. However, entrapment and vaporization of oil during metal level rise, as proposed by Adjei-Sarpong[127] cannot be discarded, since the replacement of oil by powder led to a complete elimination of transverse depression in boron steels.

The quality evaluation of peritectic steel grade samples showed that heat 277 had transverse depression, as shown in the previous chapter in Figure 6.13. Mould thermal analysis showed no significant difference between oil and powder lubrication in terms of mould heat flux for this steel grade (Figure 7.10), therefore the thickness and temperature of the solidifying shell at the meniscus region is expected to be similar for both powder and oil. Although, the surface quality of the billets cast with powder were much superior, the existence of transverse depression in heat 277, even if in only one heat, shows that entrapment and vaporization of oil cannot be the only mechanism responsible for the formation of transverse depressions.

Since metal level variation is an indisputable cause of transverse depression a detailed analysis of meniscus fluctuation will be presented in Section 7.3.5. It was found that for both peritectic-carbon and Boron(Ti)-alloyed medium-carbon steel the number of meniscus fluctuations in a 10-minute period was about double for heats cast with oil, compared to heats cast with powder. Similar result was also obtained by Gurton[124]. The main reason for this

behaviour is attributed to the use of SEN during powder casting as opposed to open pouring for oil casting.. The presence of transverse depressions in heat 277 (peritectic-carbon steel cast with powder lubrication) seems to support Thomas and Zhu[132] mechanism for transverse depression. i.e., shell distortion due to purely metal level fluctuations. As will be discussed later, metal level fluctuation was a major problem during casting.

Based on the above analysis it can be concluded that during powder casting:

A) Transverse depressions are preferentially formed in high coherency-temperature steel grades (ultra-low carbon, peritectic-carbon or Boron(Ti)-alloyed medium-carbon steels) and are caused by metal level fluctuation.

B) For Boron(Ti)-alloyed medium-carbon steel cast with powder, transverse depressions were eliminated due to a substantial decrease in meniscus heat flux, thus producing a thinner, hotter, more flexible shell, and also due to a reduction in metal level fluctuations on account of pouring with SEN.

C) For peritectic-carbon grades, although transverse depressions were not completely eliminated during powder casting, a substantial reduction of these defect was obtained due to the use of SEN which reduces metal level fluctuation, and possibly also due to elimination of oil entrapment and vaporization.

7.3.2.2 Thermodynamics of nitride precipitation in Boron(Ti)-alloyed steel

In the present study, a thermodynamic evaluation of the formation of TiN and BN in low-alloy steel was conducted to elucidate the precipitation of these nitrides both in liquid steel and during initial solidification. The thermodynamic analysis performed excludes the formation of boron and titanium oxides because the boron steels investigated were aluminum-killed and

Ca-treated. The steels had enough aluminum (~70 ppm) and calcium (~20 ppm) to avoid the formation of boron and titanium oxides since their oxygen level was below 3 ppm [138].

The solubility product of TiN and BN in low-alloy steel are shown in Figure 7.14. For temperatures above the steel solidus temperature (1450 °C) equations for the solubility product of these nitrides in liquid iron were used. Below the solidus temperature equations for the solubility product of TiN and BN in γ-iron were used, which explains the sudden drop in solubility at 1450°C. The details of the thermodynamic calculation are presented in Appendix C. The solubility of TiN in liquid steel, shown in Figure 7.14, combined with the solute distribution ratio of Ti and N between liquid iron and γ-iron were used to construct Figure 7.15.

The solubility product of TiN ([%Ti][%N]) in low-alloy liquid steel is 6.15×10^{-4} at 1500°C, which is considered to be the average liquidus temperature of low-alloy steels. Additionally, the solubility curves at 1550°C (temperature of the liquid steel in the tundish) and 1450°C (solidus temperature) are shown in Figure 7.15. A typical bulk concentration of 81 ppm of nitrogen and 0.035% Ti is also shown in Figure 7.15. For these concentrations of Ti and N, very little precipitation of TiN would take place before the end of solidification since they are very close to the equilibrium line at 1450°C (solidus temperature). However, due to solute distribution during solidification the actual concentration of Ti in the interdendritic liquid is about 2.51 times the concentration in the γ-phase; the corresponding value for N is 2.23 times (Appendix C).

For a bulk concentration of 81 ppm of N and 0.035% Ti, the actual concentration in the interdendritic liquid would be 181 ppm of N and 0.088% Ti. These values as shown in Figure

7.15, are well above the equilibrium concentrations at 1550°C thereby leading to high precipitation of TiN. Figure 7.15 shows that about 44% of the N in solution precipitates before the solidus temperature is reached. This agrees well with Turkdogan's results which show that about 55% of the N is converted to TiN at the completion of 99% of local solidification[135].

The solubility product of BN ([%B][%N]) in low-alloy steel at 1500°C is 9.61×10^{-2}. Thus, for a bulk nitrogen concentration of 81 ppm, more than ~12%B is required to initiate the precipitation of BN in the liquid. The partition ratio for boron ($[B]_{liq}/[B]_{\gamma}$) is ~17 which result in a high segregation of boron in the interdendritic liquid. For a bulk concentration of 0.0024%B, the actual interdendritic concentration is 0.041% which is not sufficient for the precipitation of BN in liquid steel.

The above analysis shows that the present practice of not controlling the nitrogen content in the liquid steel will always lead to precipitation of TiN before solidification starts. To avoid the precipitation of TiN in the liquid the N content has to be kept below a maximum level, which is dictated by the following conditions:

a) To avoid precipitation of BN most of the N in solution should precipitate as TiN upon completion of solidification, thus the weight ration between Ti and N must be at least equal to the atomic weight ratio between them, i. e.,

$$\%Ti / \%N \geq 3.42$$

b) The solubility product of TiN in liquid steel at 1500°C:

$$[\%Ti][\%N] = 6.15 \times 10^{-4}$$

c) The solute distribution ratios for Ti and N in liquid steel at 1500°C:

$$[Ti]_\ell = 2.51\,[Ti]_\gamma$$

$$[N]_\ell = 2.23\,[N]_\gamma$$

To calculate the maximum content of N and Ti so that precipitation of TiN does not take place before the onset of solidification, the following system must be solved:

$$\begin{cases} \dfrac{[\%Ti]}{[\%N]} = 3.42 \\ 2.51[\%Ti] \times 2.23[\%N] = 6.5\times10^{-4} \end{cases}$$

The solution of the system gives [%N] = 0.0057 and [%Ti] = 0.0194. Therefore, to minimize the precipitation of TiN in liquid steel (interdendritic liquid), the nitrogen content of the steel must be kept below 60 ppm and the titanium content below 0.019%. These results agrees with recommendation published by Pochmarski et al.[136] for the casting of B-Ti alloyed steel billets with powder lubrication. They reported the need to keep N content below 60 ppm in order to avoid transverse corner cracks.

The thermodynamic analysis carried out shows that BN does not precipitate in liquid steel (interdendritic liquid); but more than ~40% of the N is precipitated as TiN in the interdendritic liquid before the start of solidification. TiN precipitates can act as nucleation sites for the solidification process and subsequently sit at the austenite grain boundaries. To minimize precipitation of TiN in the liquid phase the nitrogen content of the steel must be kept below 60 ppm and the titanium content below 0.019%. This is a very significant result for the improvement of oil casting practice, since the massive precipitation of TiN in the solidification front during casting of Ti-stabilized boron steels affects the mechanical behaviour of the thin shell being formed in the meniscus region. A combination of high coherency temperature and high mould heat flux, therefore thicker, colder and stiffer shell, leads to the formation of

transverse depressions during oil casting whenever the shell is bent away from the mould due to thermal and/or mechanical effects.

7.3.2.3 On-line monitoring of transverse depressions

Adjei-Sarpong[127] identified a mould temperature pattern, characterized by local drops followed by a rise, named "valleys", that travel down the mould at the velocity of the casting speed, as a manifestation of a transverse depression. Adjei-Sarpong[127] explained that under normal circumstances the gap formed between the strand and the mould, which represents about 84% of the total thermal resistance, is less than 1 mm wide. In the presence of transverse depressions large gaps can open up which can significantly reduce the heat transfer to the mould. Therefore, as a depression passes by a thermocouple the temperature signal drops then rises again.

Adjei-Sarpong[127] results were later expanded by Kumar[110] who measured the depth and width of hundreds of depressions found in billets cast with oil and open-pouring from tundish to mould. He found that about 70% of the depressions were between 0.5 and 2.0 mm deep and between 45 and 75 mm wide. By means of a mathematical model Kumar[110] simulated the effect of changes in solid shell thickness and widening of mould/strand gap on the mould temperature response. He found that at the mid-thickness location in the mould wall (at the thermocouple tip location) the changes in mould temperature due to changes in solid shell thickness were quite small and thus it would not be possible to detect these changes by the thermocouples. On the other hand, the calculated drop in heat flux caused by the widening of the gap due to transverse depressions was greater than 50%, which translated to temperature drops between 10 and 50°C at the thermocouple locations. Kumar's[110] results

confirmed that mould temperature can drastically drop in the presence of transverse depressions.

In the present investigation transverse depressions were only observed in one heat of peritectic steel, heat 277 (0.14%C). These depressions were not detected in the regular samples (2 samples per heat of ~ 400 mm long) collected during the plant trial; they were found during visual inspection of whole billets , which was performed after the completion of the trial. Although, it was not possible to exactly match the depressions with the instantaneous thermocouple data, an attempt was made to verify if the "valley"-type temperature pattern described by Adjei-Sarpong[127] and Kumar[110] could be found in the thermocouple data at approximately the time one of these depressions was traveling in the mould.

Figure 7.16 shows one of the "valley"-type pattern found. The temperature signal corresponding to the thermocouple locate at 205 mm below the top of the mould shows considerably fluctuations but it is still possible to identify three local minimums at ~ 1415, 1427 and 1447 s. The fluctuating character of the signal is related to the proximity to the meniscus and, as discussed before, to electrical noise that affected the upper thermocouples. These temperature valleys were traced down the mould and were seen at the thermocouples locations 315, 433 and 729 mm below the top of the mould; and the casting speed during the period (1400 to 1480s) was integrated to calculate the distance traveled by each one of the three temperature-valleys (pointed out by the arrows) shown in Figure 7.16. The calculated distance matched the distance between each pair of thermocouples shown in the figure. For instance, the distance traveled by the first valley between the thermocouple located at 315 and 433 mm was calculated to be 118 mm, which exactly matches the distance between the two thermocouples. The above result clearly suggests that, similar to oil lubrication, in billet

casting with mould flux, transverse depressions also can be detected by thermocouples. However, while for oil lubrication the monitoring of transverse depressions is well established[110], for powder casting further investigation involving mould temperature measurement and 100% billet inspection still needs to be carried out to establish a one-to-one correlation between defects and temperature drops.

7.3.3 Rhomboidity

Rhomboidity (or off-squareness), defined as the difference between the length of the two diagonals of a billet cross section, can be a major quality problem in billet casting. Many mini-mills consider a difference greater than 6mm unacceptable because the rhomboid billet causes difficulty in the reheat furnace and subsequent hot rolling operations. Furthermore, billets with excessively large rhomboidity can crack along the diagonal or the corners. The absolute value of the difference is a measure of the severity of the problem while the sign (positive or negative) indicates the orientation of rhomboidity.

Previous studies conducted by the UBC-Billet Casting Group have shown that in billet casting with oil, rhomboidity is associated with non-uniform cooling in the meniscus region. With respect to the severity of rhomboidity, it was shown that in addition to non-uniform cooling, the magnitude of the mould heat flux and the steel carbon content were also important. Kumar[110] showed that the impact of non-uniform cooling is the greatest for grades of steel for which the mould heat extraction is reasonably high and at the same time, the freezing range is short, such as the medium-carbon steels (0.32% C) in this study.

The difference between the two diagonals of each plant-trial sample (23 samples of peritectic steel and 10 samples of boron steel; Appendix F gives a complete report of the measurements performed) was measured and compared with values measured by Kumar[110]

from billets cast with oil lubrication (13 measurements of 0.12%C steel and 19 of boron steel). Figure 7.17 shows the frequency distribution of rhomboidity for peritectic steel ($0.11 \leq \%C \leq 0.14$) and Boron(Ti)-alloyed steels ($0.30 \leq \%C \leq 0.33$). For peritectic steel, Figure 7.17A, no apparent difference between oil and powder lubrication exists for this steel grade (~0.12%C). In both cases, the percentage of samples with rhomboidity smaller than 2mm was more than 60% and no sample had rhomboidity above 6mm.

For boron(Ti)-alloyed steels (~0.32%C) a different result was obtained. As shown in Figure 7.17B, more than 66% of the billets cast with oil lubrication had rhomboidity greater than 4mm, and 33% had it above the critical limit of 6mm. On the other hand, for powder lubrication, only 10% of the samples analyzed had rhomboidity greater than 6.0 mm, and 80% smaller than 4mm.

The results obtained are consistent with the mould thermal response of these steels. For both oil and powder lubrication, the peritectic steels have lower and more uniform heat flux, which resulted in very low values of rhomboidity. For medium-carbon steel containing boron and titanium, two features were observed: a) heats cast with oil presented a more unstable thermal behaviour, with large variations in heat flux during heats and, b) the magnitude of the mould heat transfer for heats cast with oil was 20 to 50% higher than those cast with mould powder. Since the severity of rhomboidity increases with increasing variability in cooling conditions in the meniscus region and the magnitude of mould heat flux, the results presented in Figure 7.17B are therefore consistent with the above findings.

Figure 7.18 shows measured rhomboidity plotted against the temperature difference between the hottest and the coldest mould face at ~20 mm below the meniscus, hereby called maximum temperature difference. This value was defined as the maximum temperature recorded

by one of the four mid-face thermocouples located at 205 or 220 mm below the top of mould minus the minimum temperature recorded by one of the other three thermocouples placed at the same position. For peritectic steels, Figure 7.18A shows widely scattered low values of rhomboidity with no apparent correlation between rhomboidity and maximum temperature difference. This lack of correlation must be related to the low values of rhomboidity normally found in this type of steel. On the other hand, Figure 7.18B shows that for Boron(Ti)-alloyed medium-carbon steels rhomboidity tends to increase drastically when the maximum temperature difference exceeds 40°C.

Figure 7.19 shows rhomboidity as a function of mould heat flux for Boron(Ti)-alloyed medium-carbon steel. In Figure 7.19A averaged mould heat flux was calculated using the temperature-difference measured between the water entering the water-cooling channel and the water exiting it ($Q = m\ C_p\ \Delta T$), divided by the total mould surface area. Figure 7.19B shows rhomboidity as a function of average meniscus-heat-flux. To circumvent any error associated to defining the precise location of the mould peak-heat-flux, local heat flux was integrated over a 30 mm length to obtain the average meniscus heat flux. Both curves depicted in Figure 7.19, similarly to Figure 7.18B, show an abrupt increase in rhomboidity when a critical value is exceeded. This is definitely a noteworthy result, which confirms that although the introduction of powder lubrication decreases the severity of rhomboidity, uniformity and rate of cooling, as previously found for oil lubrication, are fundamental to control rhomboidity.

The regression curves presented in Figures 7.18B and 7.19, are intended to demonstrate the possibility of building quantitative relationships for on-line control of billet quality. However, the establishment of relationships reliable enough to be used for on-line monitoring

of rhomboidity would prescribe the gathering of many more data points, mainly at more significant levels of, i.e., values of rhomboidity higher than 4 mm.

From the observations above we can conclude that,

(A) For low-carbon steel, rhomboidity is not significant for both oil and powder lubrication.

(B) For medium-carbon steel containing boron and titanium, the severity of rhomboidity is significantly lower for billets cast with mould powder.

(C) For billets cast with powder lubrication the extent of rhomboidity is dependent on both the maximum temperature difference among the mould four faces and the heat flux level.

7.3.4 Oscillation Mark

When compared to oil, mould flux lubrication resulted in deeper oscillation marks. This is clearly seem in Figure 7.20. Figure 7.20A shows a typical surface profile of a Boron(Ti)-alloyed medium-carbon billet cast with oil lubrication. Two features clearly stand out; first the presence of a transverse depression of ~ 50 mm width and ~2.2 mm depth, second very shallow oscillation marks, evenly distributed along the whole sample, of no more than 0.2 mm depth. Figure 7.20B shows an analogous example from one of the plant-trial samples, also a Boron(Ti)-alloyed but cast with powder lubrication. In this case no depression is observed however the oscillation marks are deeper, average depth equal to 0.31 mm.

The above results confirm the main role of mould flux on oscillation marks formation as predicted by Takeuchi and Brimacombe[56] by means of a mathematical model. It also shows that even for the heats cast with superheats above 30°C (Table 7.2), predicted by Saucedo et al.[137] as the value above which meniscus freezing is suppressed and therefore oscillation

marks should not be formed, oscillation marks are still formed and are deeper than the ones formed during casting with oil lubrication. This result demonstrates that when flux is used as lubricant it plays a more important role in the formation of oscillation marks than meniscus freezing.

7.3.5 Metal Level Variation

The pouring of molten steel from the tundish into the mould can be open (free jet) or through a refractory tube, the submerged entry nozzle (SEN). Mould fluxes require an SEN otherwise the flux would be carried into the steel by the tundish stream leading to contamination of the steel. On the other hand, to cast with SEN and oil is very risky since oil does not provide thermal insulation to prevent the steel from freezing between the nozzle and the mould walls, thus oil lubrication implies open stream. Open-pouring/oil-lubrication production route is cheaper than SEN/flux since oil is cheaper than flux and SEN represents an extra cost; however, higher quality is achieved with the SEN/powder-lubrication route. In slab casting the latter has established itself as the sole route but oil lubrication with open pouring is still favored by billet producers. Quality problems such as transverse depressions, which is associated with metal level fluctuations and high heat flux, has led some billet producers to switch to mould flux lubrication with SEN for casting larger billets (> 200 sqmm).

In open pouring molten steel exits the tundish as a free jet which entrains gas depending on the quality of the stream. The gas enters the liquid steel in the mould and bubbles back up creating waves on the surface. Thus a smooth stream, between tundish and mould is preferred because results in less gas entrainment. With an SEN the stream is not in contact with air hence little gas is entrained.

To compare the behaviour of the metal level during billet casting with powder lubrication and oil lubrication, the temperature of three thermocouples placed at the meniscus region- one above and two below the meniscus set-point, were plotted for periods of ten minutes. The main setback for this analysis was that the metal level signal generated by the caster radioactive sensor was not recorded correctly by the data acquisition system.

25 thermocouple were installed in the east face of the mould wall and 17 in each of the other faces; however, key thermocouples, located at the meniscus region -190, 235 and 290 mm below the top of the mould in the East-face as well as at 190 mm in the West-face of the mould wall failed. Therefore, in order to analyze meniscus level fluctuations only south and north faces thermocouples could be used. In each case only one face, i.e. south or north, the one that presented the highest temperature fluctuations was analyzed. For each heat analyzed the meniscus position was taken as the values recorded from the metal level display, located in the caster pulpit or values measured using dipsticks.

The temperature analysis showed three types of temperature changes. The first one is a very short range fluctuation with a frequency of 2.5 Hz and magnitude less than 10°C. Figure 7.21 shows an example of this fluctuation along side the mould displacement recorded by an LVDT placed on the top of the mould. For three different casting sequences analyzed (sampling rate of 10 Hz) the frequency of the noise was found constant and independent of the mould oscillation frequency recorded by the LVDT signal. Eventually this noise was identified as an electrical noise caused by a defective power supply in one of the equipment.

The second type of temperature variation is characterized by a mid-range fluctuations of magnitude greater than 10°C, i.e. bigger than the electrical noise. This type of temperature fluctuation was assumed to be caused by metal level variations due to meniscus turbulence.

Figures 7.22 and 7.23 exemplify this kind of mid-range fluctuation for heats cast with oil and powder lubrication, respectively. Figure 7.22 depicts a heat cast with oil, it shows that the thermocouple located above the meniscus (S4) at 160 mm from the top of the mould records very steady temperatures for most of the time while thermocouple S6, located just below the meniscus, exhibits 27 fluctuations ranging from 10°C to 50°C, the majority (20) below 30°. Thermocouple S8 (190 mm) shows a remarkably large number of fluctuations of the order of 50°C. Figure 7.23 shows an example of a heat cast with powder lubrication. Thermocouple N6, located just above the meniscus, shows a quite noticeable difference between what was called in this report short and mid-range temperature fluctuations. Between two mid-range fluctuations, for example from 960s to 1080s, it can be seen several local fluctuations below 10°C. Thermocouple N8 exhibits 17 mid-range fluctuations, the majority of which (12), above 30°C.

The third type of temperature variation occurs due to an intentional change in the metal level, i.e. a change in the set-point of the control system. Figure 7.24 exemplify this third type of temperature variation for a heat cast with mould flux lubrication, nevertheless similar features are found in heats cast with oil. Either for powder as well as for oil lubrication there is a well defined decrease in the temperature level of the thermocouples. In both cases, before and after the point where the metal level set-point is changed the short and mid-range temperature fluctuations are still present.

In order to compute the mid-range temperature fluctuations it was found that a 3-point moving-average was able to eliminate the short-range fluctuations. This operation was performed over the values recorded by the thermocouple located closest to the meniscus and the number of fluctuations (peaks) counted. Any temperature fluctuation above 10°C was

considered a medium-range fluctuation and therefore a reflection of the state of turbulence of the molten steel surface. Tables 7.5 and 7.6 summarize the results obtained for peritectic carbon steel (~0.12% C) and Boron(Ti)-alloyed steel (~0.33% C), respectively.

It is clear from Tables 7.5 and 7.6 that when compared to powder lubrication oil lubrication results in a more fluctuating metal level for both low-carbon and medium-carbon heats. However in most cases, as pointed out before, the magnitude of the temperature fluctuations was considerably higher for powder lubrication and in some cases presented a high degree of regularity. It seems that this unexpected behaviour is because the metal level controller was not calibrated for powder casting and also due to the adverse conditions imposed on the controller as detailed in Appendix G. It was found that the real metal level measured by dipstick was ~ 40 to 50 mm below the value recorded by the control system and the total thickness of mould powder varied between 25 to 90 mm. Thus the radioactive sensor was more likely detecting mould powder than liquid steel. The great variation in the powder thickness caused by the consumption of the powder without adequate supply of new powder was responsible for the oscillating pattern exhibited by the casting speed and temperature signals as shown in Figure 7.25. It is thought therefore that the temperature patterns, and consequently the metal level variation, resulted from the way the metal level controller was handling the casting speed. If it was not for this inadequate control, the temperature would be smoother, i.e. lower peaks.

From the above analysis it can be concluded that: (1) Three different types of temperature variation were found in the data-files collected during plant trial. The first type was identified as a short-range (2.5 Hz) variation with amplitude of ~ ± 10°C caused by electrical noise. The second type was a mid-range fluctuation (0.013-0.045 Hz) with amplitude varying from 20°C

to 50°C. The last type was a single temperature variation caused by an intentional change in the mould level set-point. (2) The frequency of mid-range temperature fluctuation for both low-carbon and boron grades were equivalent for powder casting, while for oil casting peritectic steels presented more mid-range temperature fluctuations (Tables 7.5 and 7.6); however, no clear trend emerged regarding the influence of steel grade on metal level fluctuation. (3) Oil lubrication resulted in twice more temperature fluctuations than powder lubrication. This is believed to be caused by the more turbulent meniscus due to the entrainment of gas by the open stream. On the other hand the fluctuations observed in powder lubrication had bigger amplitude, most likely due to lack of proper calibration of the mould level control system, as confirmed by the measurements shown in Chapter 6, Table 6.3. (4) To take full advantage of the benefits from casting with powder lubrication the radioactive sensor must be adjusted for it and the system should have liquid-metal flow as the control variable instead of casting speed. Having casting speed as the control variable leads to an inherently unsteady-state operation.

7.4 Simulation of mould powder melting

7.4.1 Calculation of molten flux pool for the plant trial conditions

As shown in Chapter 6, Table 6.9, the measured values of liquid flux pool, obtained using the three-wire method, resulted in extremely low values for both powders, A and B. To compare these measurements with calculated values the mathematical model was run using the same casting parameters under which the measurements were carried out. Also, two different strategies of powder addition were simulated in order to determine if the low values of liquid

pool height were caused by the powder practice or due to powder inadequacy. Table 7.7 presents the casting parameters used for the simulations.

Figures 7.26 shows that for the dark-practice the frequency of powder addition does not significantly affect the liquid pool. In Figure 7.26A the level of powder is kept constant, which simulates a perfect automatic feeding system. In this case the steady-state value for the liquid pool is 3.7 mm, the same value obtained when powder is added every time the temperature of the free surface of powder reaches 400°C, Figure 7.26B.

When the temperature for powder addition is increased to 800°C the liquid pool decreases only slightly to 3.6 mm as shown in Figure 7.26C, even when this temperature is further increased to 1000°C calculations showed that the pool height is still 3.6 mm. Of course, if the temperature of the powder free-surface increases much above 800°C (red-practice) radiation heat losses from the top surface can reach a value above which the assumed boundary condition at the steel/flux interface (constant temperature), is not valid anymore. In the latter case the high radiation loss can lead to freezing of the steel surface with serious consequences for the quality and flow of production.

Figure 7.27 is a more detailed representation of what happens to powder B when 20 mm of fresh powder is added whenever the temperature at the powder free surface exceeds 800°C. Initially, as shown in Figure 7.27B, the total amount of powder decreases from 50 mm to 10 mm depth in ~100 s, at this point the temperature at the free surface reaches 800°C and 20 mm of fresh powder is added, the whole cycle takes place again and at ~400 s the liquid pool depth reaches an average value of 3.7 mm. In Figure 7.27A a step in the temperature curve can be observed at ~450°C, this corresponds to a delay in the heating of the powder due to

the assumption that between 450°C and 500°C an endothermic reaction, decomposition of Na_2CO_3, takes place.

For powder A, a similar analysis was conducted with the objective of testing proposed values for its thermal conductivity. A conductivity of 2.0 W/mK, value previously adjusted for powder B, was compared with a value of 1.5 W/mK. Figure 7.28A shows that, as expected, the lower value of thermal conductivity (1.5 W/mK) results in a slower heating; therefore, the powder melting rate is lower, which is manifested in longer times needed to add new powder. The major difference appears in Figure 7.28B, the lower value of thermal conductivity results in a liquid pool ~2mm smaller than the higher one. The liquid pool height calculated using a thermal conductivity of 1.5 W/mK (~4mm), is closer to the measured values for powder A shown in Table 6.5 (1~3 mm).

All cases analyzed above, and presented from Figures 7.26 to 7.28, yield a striking result. It is evident from both measurements and predictions that the liquid pool depth is very small which shows that the powders used at the time of the trial were not appropriate for the casting conditions. As discussed in the literature review, values of liquid pool depth less than the mould oscillation stroke, which was 6 mm, leads to unstable casting operation with possible entrapment of solid powder by the liquid steel. Also in situations of higher powder consumption, such as a significant drop in cast speed, starvation of the liquid pool with consequent loss of lubrication can occur. Force measurements corroborate these findings[124].

During the plant trial casting forces were monitored and friction coefficients were calculated, details of this work can be found in Gurton's thesis[124]. He found a force upset during casting of heat 313, a Boron(Ti)-alloyed medium-carbon steel. When the casting speed

dropped from 18 to 13 mm/s the friction coefficient increased from 0.36 to above 1, i.e., from a non-binding to a binding situation. This loss of lubrication could only be rationalized in terms of flux starvation when an increase in flux consumption is not accompanied by an equivalent increase in molten flux supply from the pool. Equation 2.21 shows that powder consumption increases with decreasing casting speed and oscillation frequency. The casting machine had oscillation frequency synchronized with casting speed, thus a decrease in casting speed had a greater effect on powder consumption. For heat 313 the drop in cast speed doubled the estimated powder consumption. Since the liquid pool was already very small, a strong sign of melting/consumption imbalance, a further increase in consumption led to lack of liquid flux, even dragging solid material from the top flux layer, with a consequent increase in casting friction.

The low value of liquid pool depth and the lubrication upset found in heat 313 show the importance of carefully considering the melting rate of mould powders before choosing them for billet casting. The powders being used by the plant at the time of the trial were clearly not a good choice. This fact also highlight the lack of information on billet casting with powder lubrication. Both powders were originally developed for slab casting, which confirms that powders used for slab casting will not necessarily perform as well for billets. Due to the higher lateral-area/volume ratio, compared to conventional slabs, billet casting requires higher specific consumption (kg per tone of steel) than slab casting.

7.4.2 Liquid pool behaviour during casting speed variation

Simulation were conducted to test the response of the mould flux liquid pool to variations in casting speed. For these simulations the dependence of powder consumption with casting speed was based on data reported by Lee et al.[30] and partly shown in Figure 2.44.

Assuming that powder consumption would respond instantaneously to changes in casting speed, as shown in Figure 7.29A, mould-flux liquid pool would steadily increase with increasing casting speed (Figure 7.29B). Figure 7.29B shows that when the casting speed is increased from 1.0 m/min to 1.3 m/min, and at the same time powder consumption decreases from 0.8 kg/ton to 0.5 kg/ton liquid, the pool depth is perfectly bounded by the values of pool depth defined when these two pair of variables are kept constant. On the other hand, Figure 7.29B show that if the change in powder consumption lags behind the change in casting speed, the increase in casting speed initially leads to a decrease in liquid pool depth. Eventually, after powder consumption changes (decreases), the liquid pool depth begins increasing back to its initial level and further reaches its new level defined by the new set of casting speed and powder consumption values. Figure 7.29A shows the chosen profiles for changing casting speed and powder consumption. Although, a stepwise change in casting speed is an industrial standard, an abrupt change in powder consumption, as shown, is not likely to occur in practice. This type of change was chosen mainly to highlight the behaviour described above.

The above simulations agreed with the plant trial observations by Riboud and Larrecq[21] depicted in Figure 2.45. However, their explanation on how the liquid pool depth decreases after an increase in casting speed and then bounces back until it stabilizes to a new level higher than the initial level is not completely correct. They thought it to be caused by an imbalance between melting rate and consumption. Increasing casting speed would result in an increased demand for molten flux (which is valid only if the consumption does not decrease) not immediately compensated by a higher melting rate, resulting in an initial decrease in the flux pool. However, higher casting speed would lead to a greater supply of heat to the mould flux

layer resulting in a higher melting rate and therefore to a gradual increase in the pool thickness.

The weak point in Riboud and Larrecq[21] explanation is the emphasis placed solely on the role of powder melting rate without considering that powder consumption decreases with increasing casting speed. The sensitivity analysis showed that if the steel temperature is increased by 20°C the liquid pool only increases 0.3mm, while if the powder consumption is decreased from 0.8 to 0.5 kg/ton the liquid pool increases 3.4 mm. The above numbers shows that the vertical heat flux due to an increase in the flow of liquid steel bears very little influence on the liquid pool depth. On the other hand, powder consumption, which is intrinsically associated with casting speed is the major factor in determining the depth of the mould-flux pool.

As demonstrated by the simulations depicted in Figures 7.29 and 7.29 and the measurements of Lee et al.[30] the time lag between the changes in casting speed and powder consumption is by far the major contributor for the initial decrease in the molten flux pool when casting speed is increased. The subsequent increase of the liquid pool depth is caused by the combined effect of a decreased powder consumption and an increased mixing in the liquid, both associated with increases in casting speed. Increasing casting speed increases the mixing in the liquid flux, thus increasing mould powder melting rate[148], and at the same time decreases powder consumption; both effects contribute for an increased liquid flux depth. The sensitivity analysis, which does not consider the influence of mixing in the liquid flux, showed that an increase in casting speed alone would lead to a decrease in liquid pool depth, however the effect of a lower powder consumption is more than enough to compensate the former, therefore the net result of increasing casting speed is a deeper molten flux pool.

Table 7.1: Casting parameters and summary of mould thermal response for the mould heat flux profiles presented in Figure 7.5

Heat	262	277	311
Carbon content, Wt. pct.	0.11	0.14	0.33 + B, Ti
Powder (Heat)	A	A	A
Water velocity, m/s	9.9	9.9	9.9
Casting Speed, m/min.	1.21	1.28	1.30
Oscillation frequency, cpm	150	170	137
Oscillation stroke, mm	6	6	6
Heat Flux Peak, kW/m^2	2190	2811	2650
Avg. Heat Flux, kW/m^2	890	1349	983
Hot-Face Peak, °C	160	212	201
Cold-Face Peak, °C	76	96	92

Table 7.2: Calculated Shell Thickness at the exit of the mould

Heat No.	Grade	Powder	Casting Speed (m/min.)	Water Velocity (m/s)	Mould Superheat[3] (°C)	Shell Thickness at mould exit (mm)
277	0.14% C	A	1.28	7.6	32	~10.0
277	0.14% C	A	1.28	9.9	27[4]	~10.3
281	0.13% C	B	1.26	7.6	32	~7.4
281	0.13% C	B	1.31	9.9	27	~8.4
311	0.33% C(B)	A	1.39	6.0	46	~5.2
311	0.33% C(B)	A	1.29	9.9	41[4]	~6.1
314	0.31%C(B)	B	1.13	6.0	30	~7.6
314	0.31%C(B)	B	1.28	9.9	25[4]	~7.1

[3] value estimated considering a temperature drop of 10°C from tundish to mould.
[4] values estimated considering a temperature droping of 5 deg C in 30 min.

Table 7.3: Comparison between calculated (mathematical model) and measured (dark bands) values of shell thickness at the exit of the mould

Heat No.	Steel Grade	Casting Speed (m/min.)	Mould Water Velocity (m/s)	Shell Thickness calculated (mm)	Shell Thickness measured (mm)
277	0.14% C	1.28	7.6	~10.0	10~11
277	0.14% C	1.28	9.9	~10.3	~10
281	0.13% C	1.26	7.6	~7.4	7~8
281	0.13% C	1.31	9.9	~8.4	~8
311	0.33% C(B)	1.29	9.9	~6.1	6~7
314	0.31%C(B)	1.13	6.0	~7.6	~8

Table 7.4: Summary of shrinkage calculations

Heat No.	Steel Grade	Powder	Water Velocity	Potential for "Binding"
277	0.14% C	A	7.6	~500 to 790 mm
277	0.14% C	A	9.9	Below 400 mm
281	0.13% C	B	7.6	Below 450 mm
281	0.13% C	B	9.9	Below 300 mm
311	0.33% C(B,Ti)	A	6.0	Whole length
311	0.33% C(B,Ti)	A	9.9	Whole length
314	0.31% C(B,Ti)	B	6.0	Whole length
314	0.31% C(B,Ti)	B	9.9	Whole length

Table 7.5: Statistics of mid-range temperature fluctuations for peritectic carbon billets cast with powder and oil lubrication

No. Peaks	avg. number of fluctuation per 10 min	σ	n (# of samples)
Powder A	15	2	4
Powder B	16	2	4
Powder (combined)	15	2	8
Oil	27	1	4

Table 7.6: Statistics of mid-range temperature fluctuations for Boron(Ti)-alloyed medium-carbon billets cast with powder and oil lubrication

No. Peaks	avg. number of fluctuations per 10 min	σ	n (# of samples)
Powder A	8	0	2
Powder B	13	4	5
Powder (combined)	12	4	7
Oil	21	3	5

Table 7.7: Casting parameters for mould powder melting simulation

Casting Parameter	Powder A	Powder B
Casting speed [m/min]	1.22	1.24
Powder consumption [kg/ton]	1.14	1.34
Total height of powder [mm]	50	50
Powder density [kg/m^3]	700	820
Thermal conductivity [W/mK]	1.5 and 2.0	2.0
Powder addition [mm]	20	20
Temperature for addition [°C]	800	400 and 800

(A)

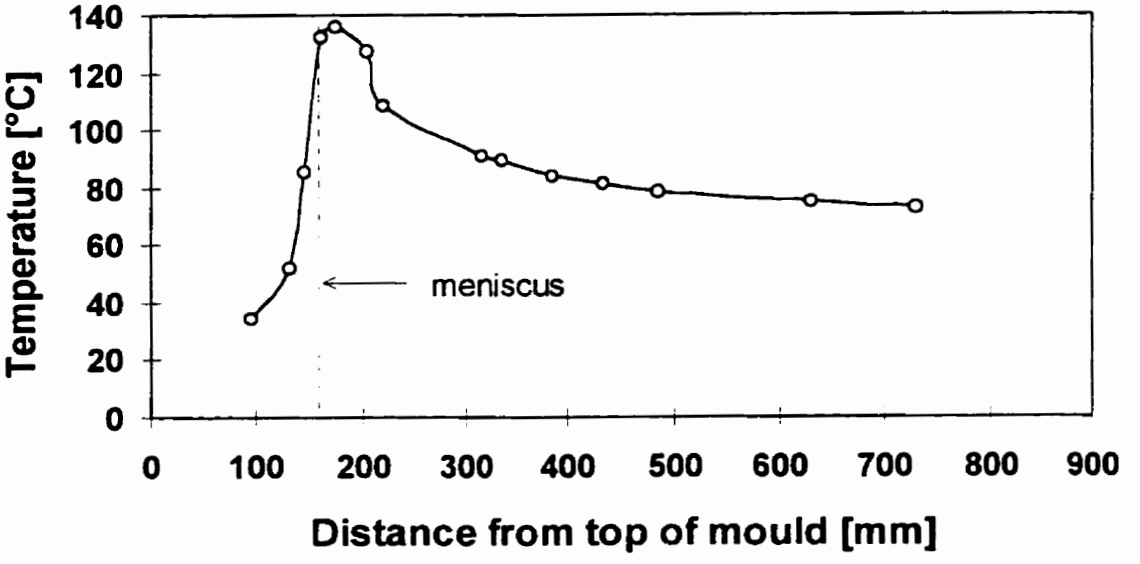

(B)

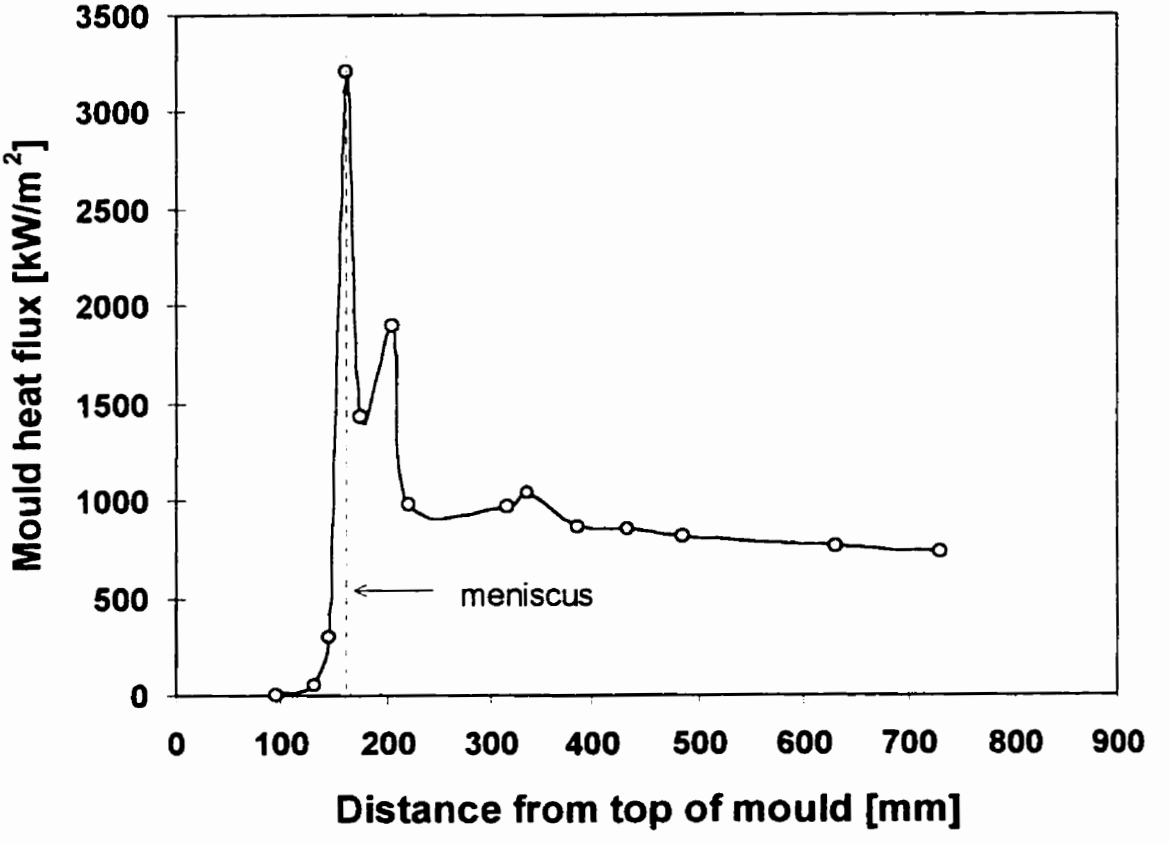

Figure 7.1 Typical mould heat flux profile - Plain carbon steel, heat 262 (0.11% C, oscillation frequency 150 cpm, water velocity 7.6 m/s, metal level ~ 160 mm); (A) temperature data, (B) calculated heat flux

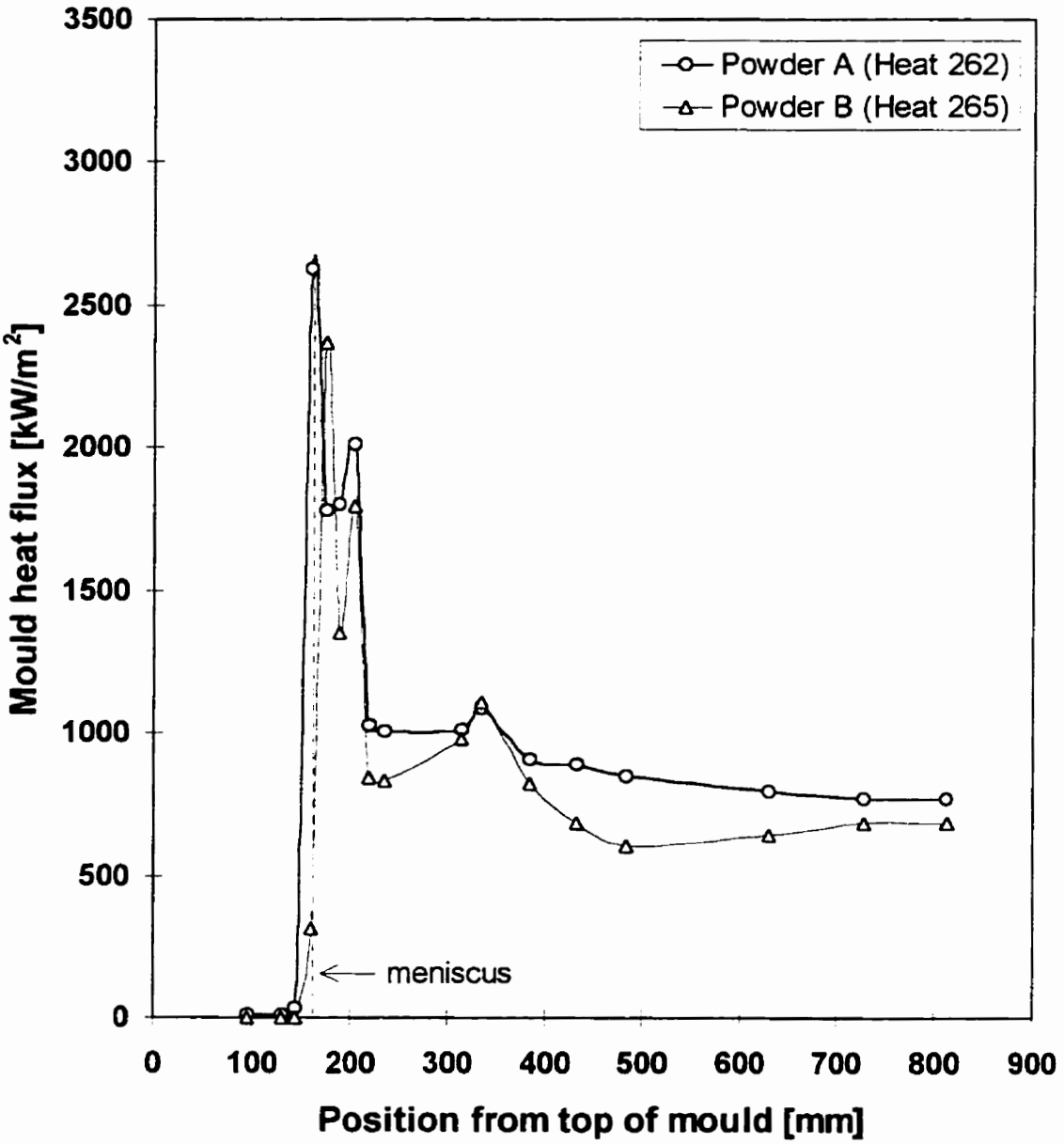

Figure 7.2 Influence of the type of mould powder on the axial heat flux profile; peritectic steel (heat 262: 0.11%C; heat 265: 0.12%C), mould oscillation frequency 150 cpm, water velocity 7.6 m/s

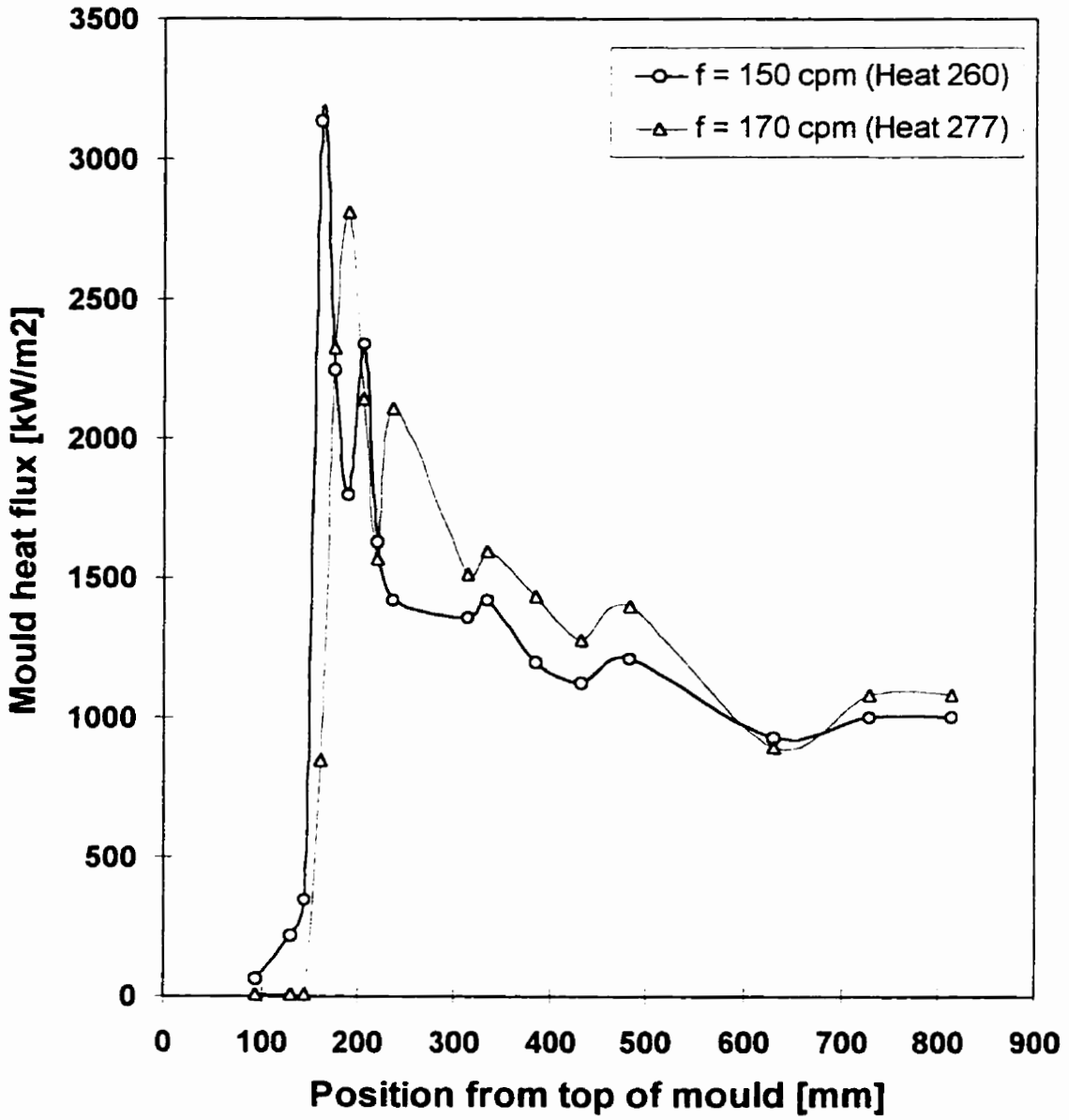

Figure 7.3 Effect of mould oscillation frequency on mould heat flux profile; peritectic steel (heat 260: 0.11%C; heat 277: 0.14%C), water velocity 9.9 m/s

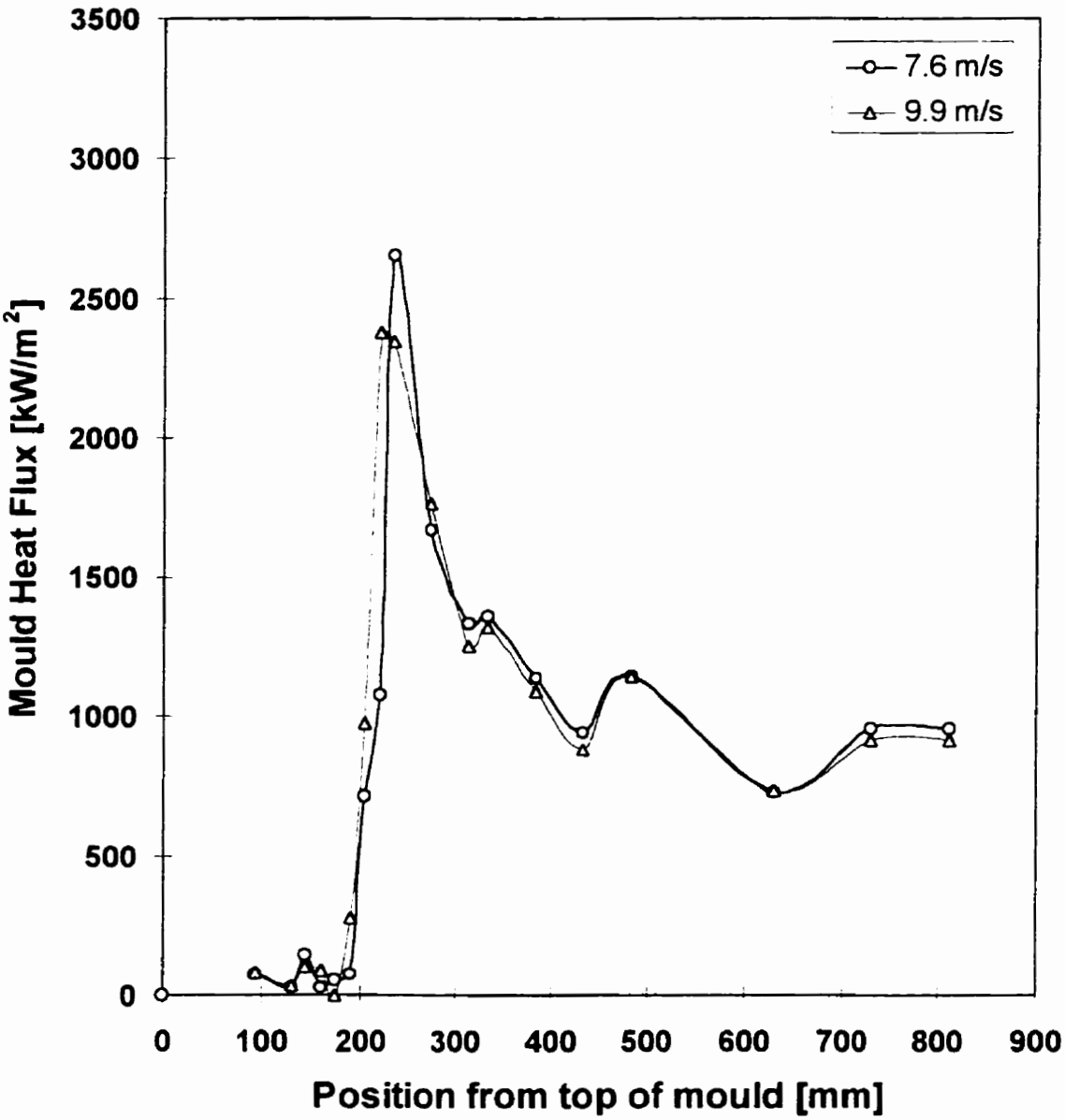

Figure 7.4 Effect of mould cooling water velocity on mould heat flux profile; peritectic steel (heat 281: 0.13%C), oscillation frequency 170 cpm, powder B

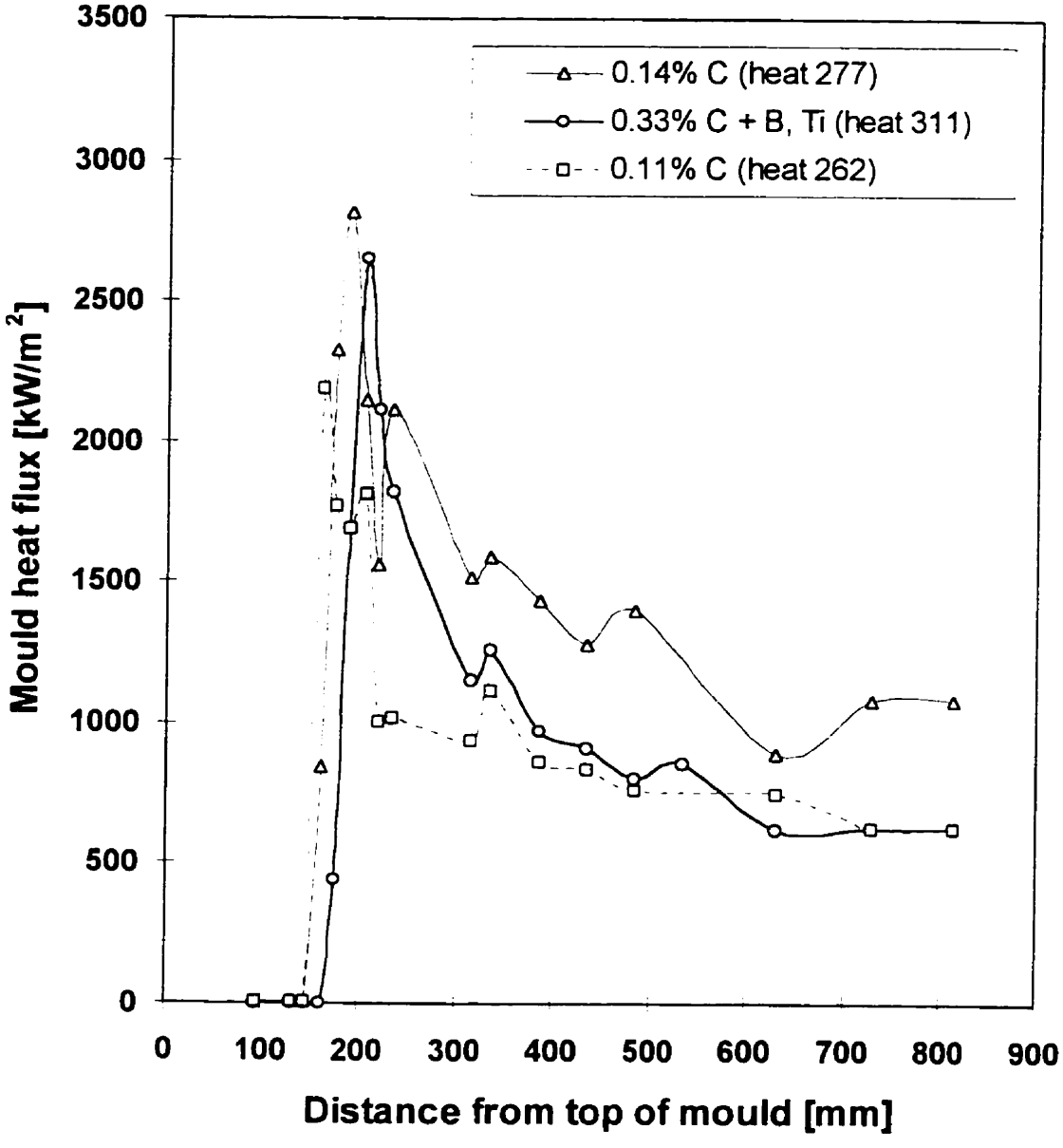

Figure 7.5 Influence of the steel grade on axial mould heat flux profile; mould water velocity 9.9 m/s, mould powder A, oscillation frequency: heat 277 f=170 cpm, heat 311 f=137 and heat 262 f=150 cpm.

(A)

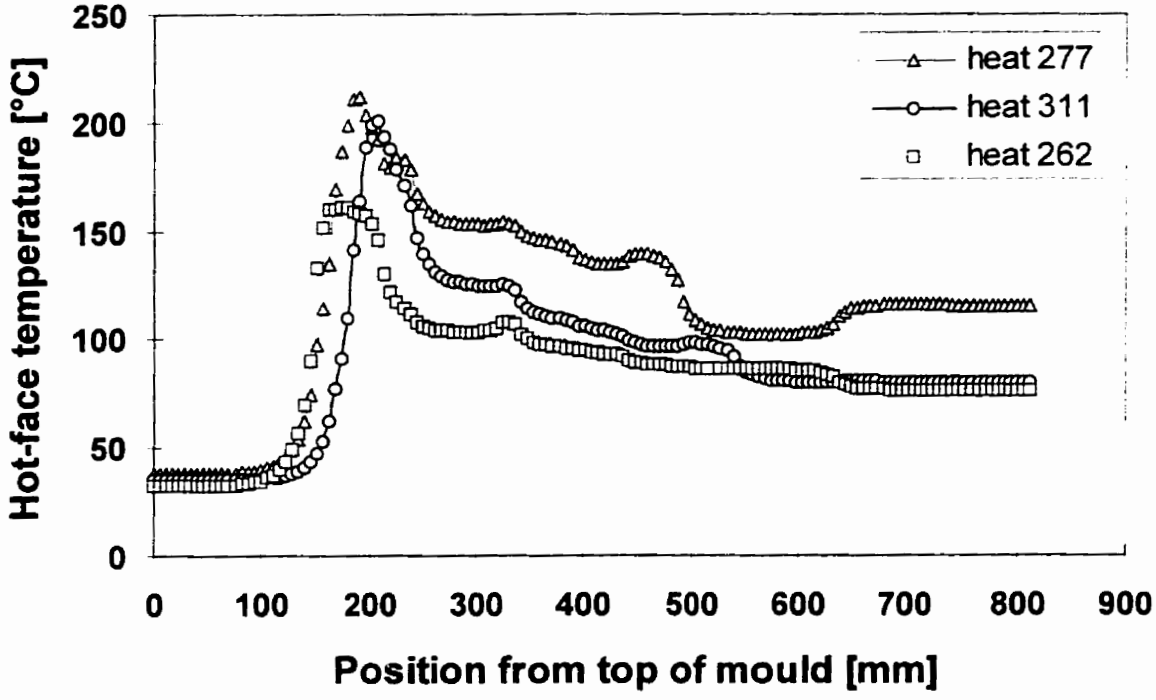

(B)

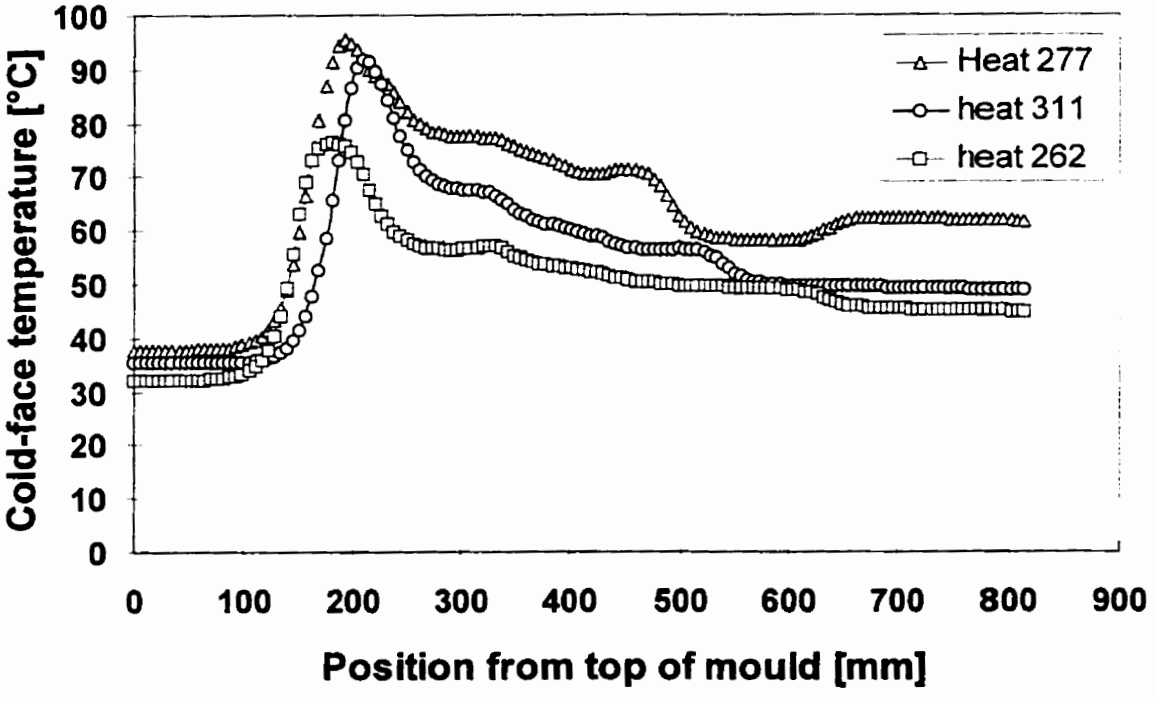

Figure 7.6 Mould wall axial temperature profiles at (A) hot-face and (B) cold-face for the heat flux profiles showed in Figure 7.5

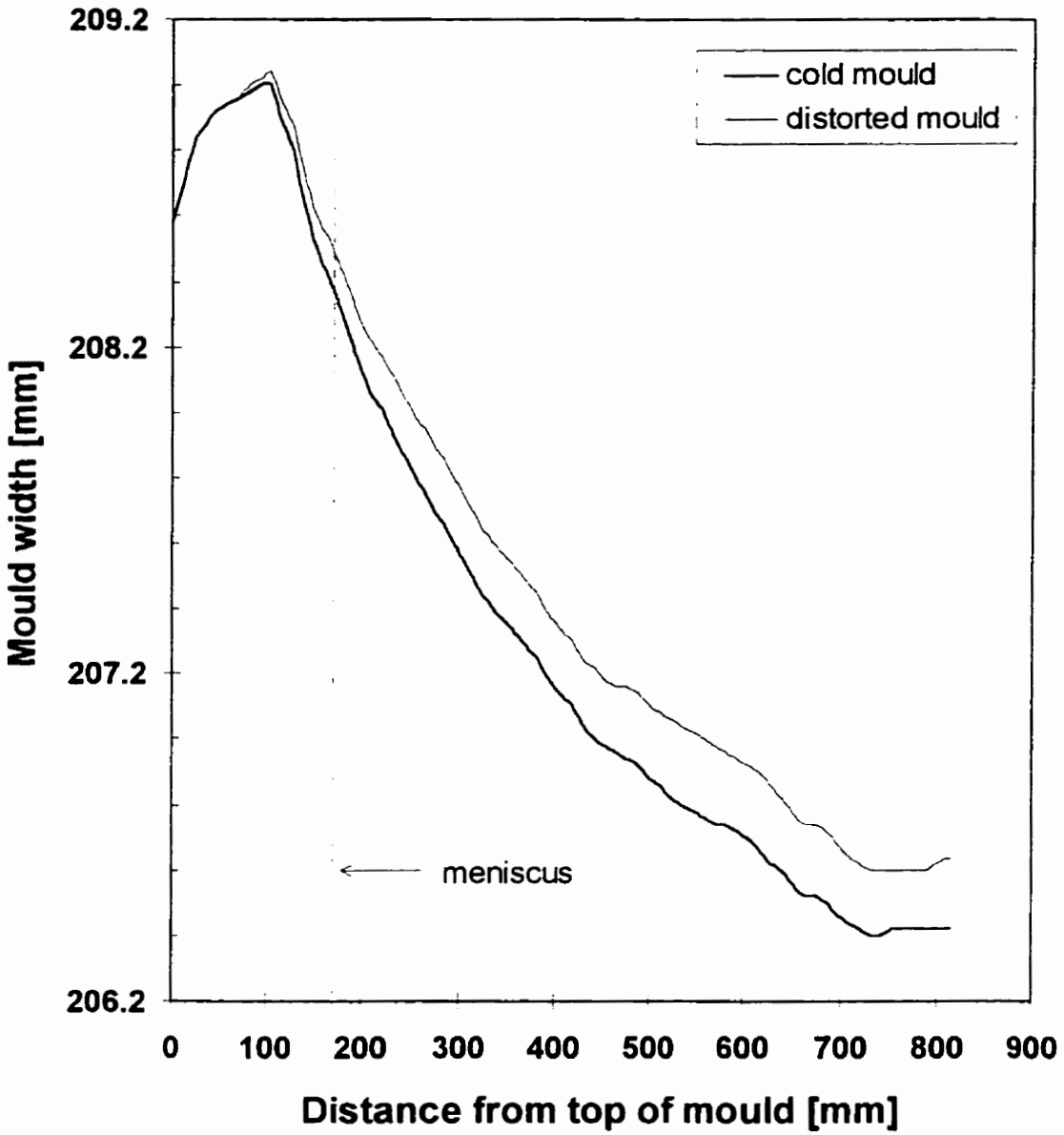

Figure 7.7 Cold mould and distorted mould width dimensions for peritectic carbon and Boron(Ti)-alloyed medium-carbon steels cast with powder lubrication and metal level at 161 mm from top of mould.

(A)

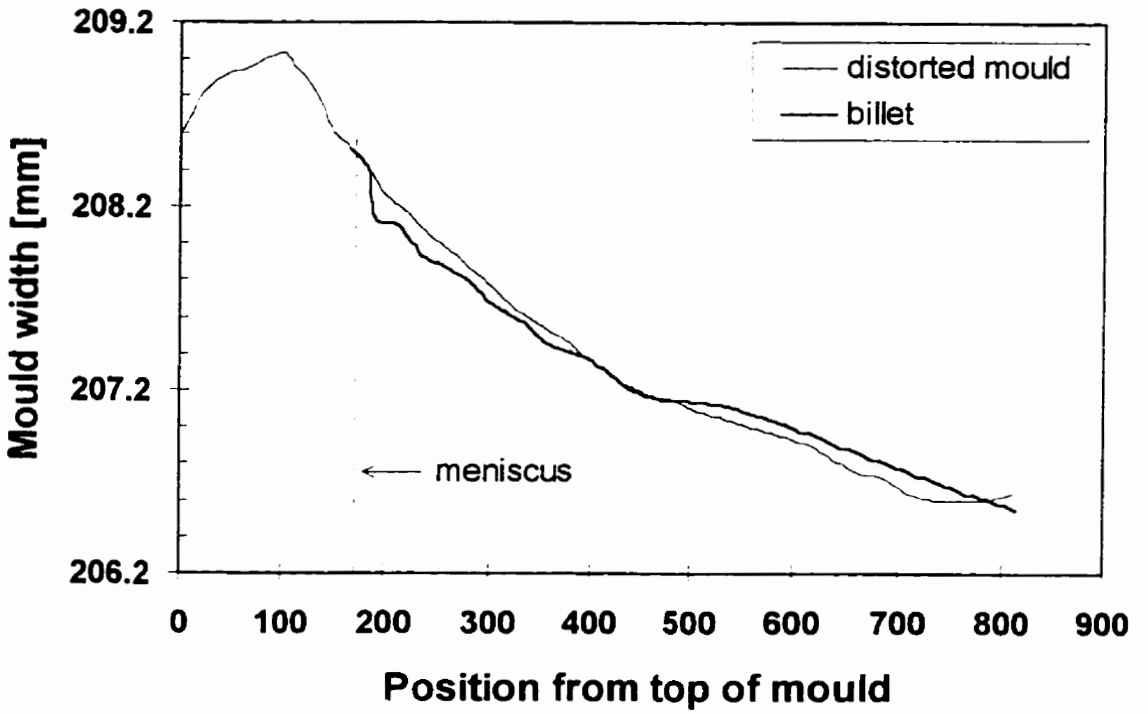

(B)

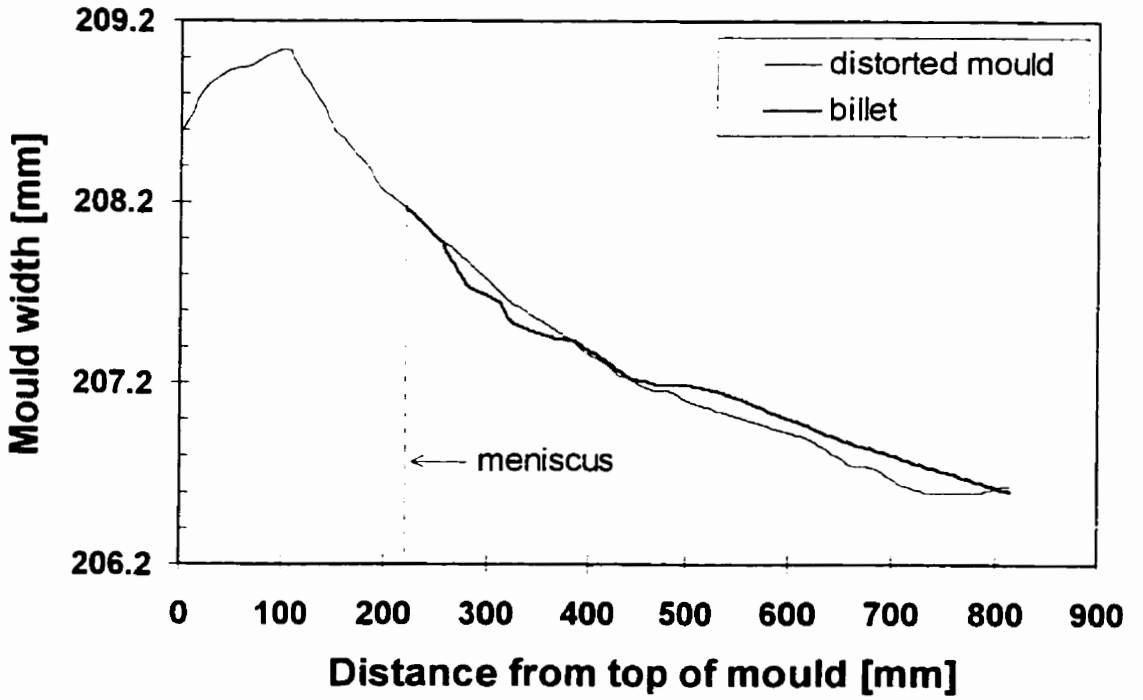

Figure 7.8 Mould and billet dimension calculated by mathematical model for peritectic carbon steel and powder lubrication; (A) Heat 277, 0.14 pct. C, powder A; (B) Heat 281, 0.13 pct. C, powder B

(A)

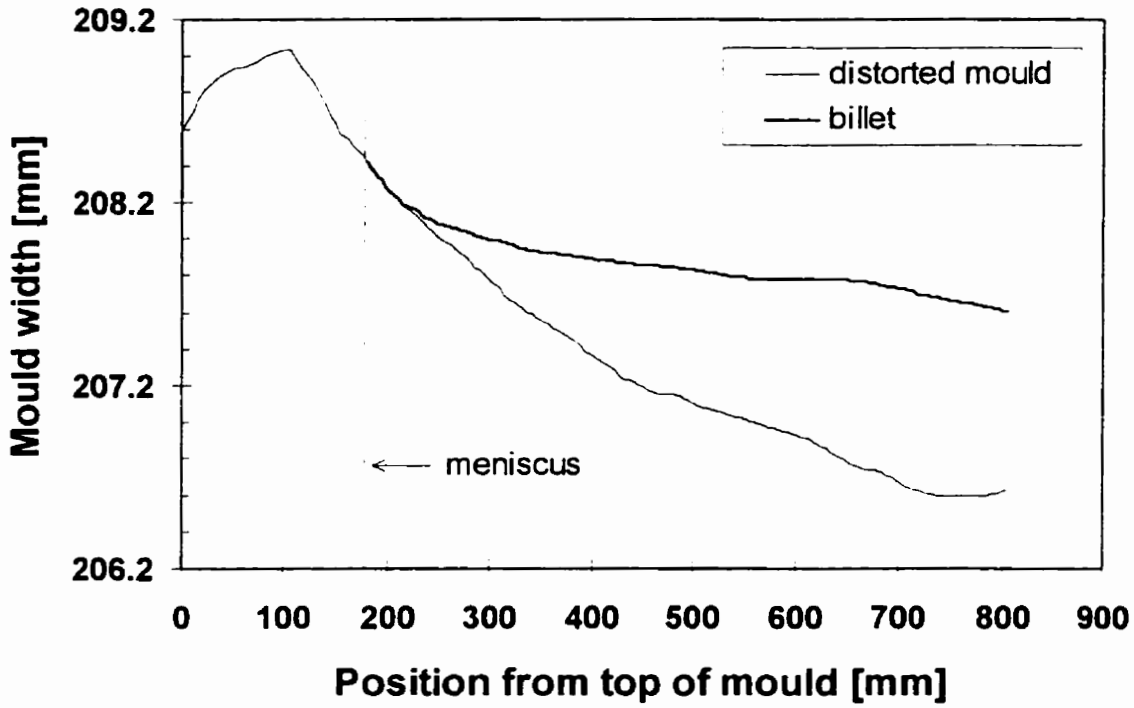

(B)

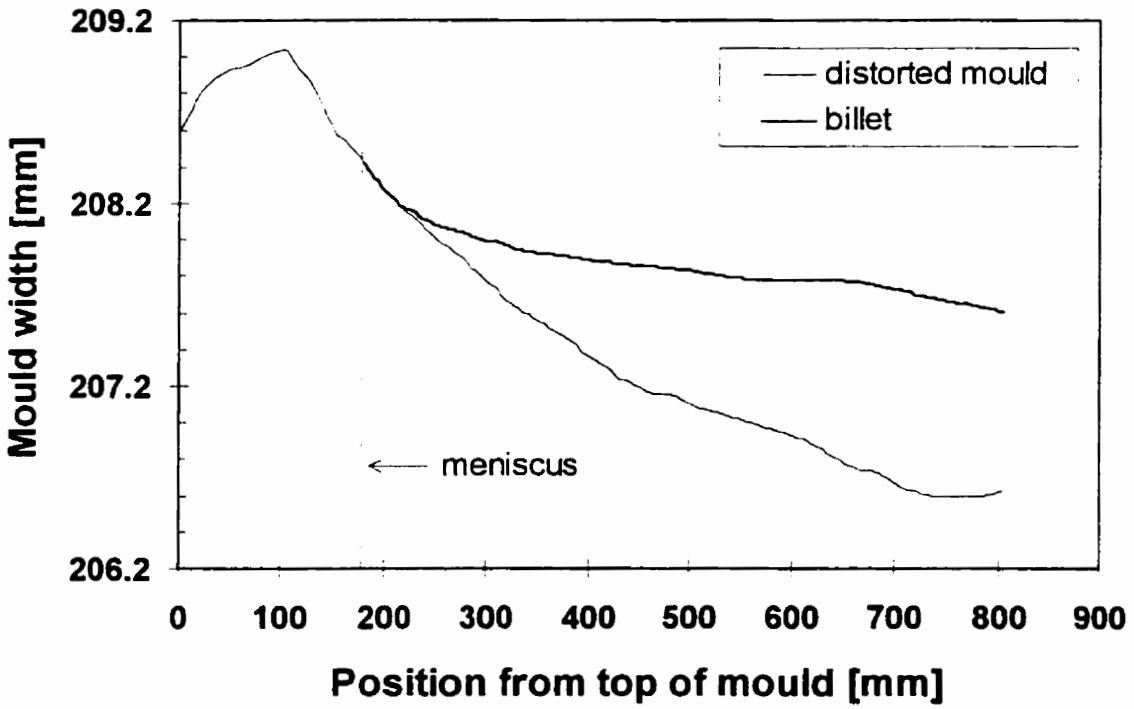

Figure 7.9 Mould and billet dimension calculated by mathematical model for Boron(Ti)-alloyed medium-carbon steel cast with powder lubrication; (A) Heat 311, 0.33 pct. C, powder A; (B) Heat 314, 0.31 pct. C, powder B

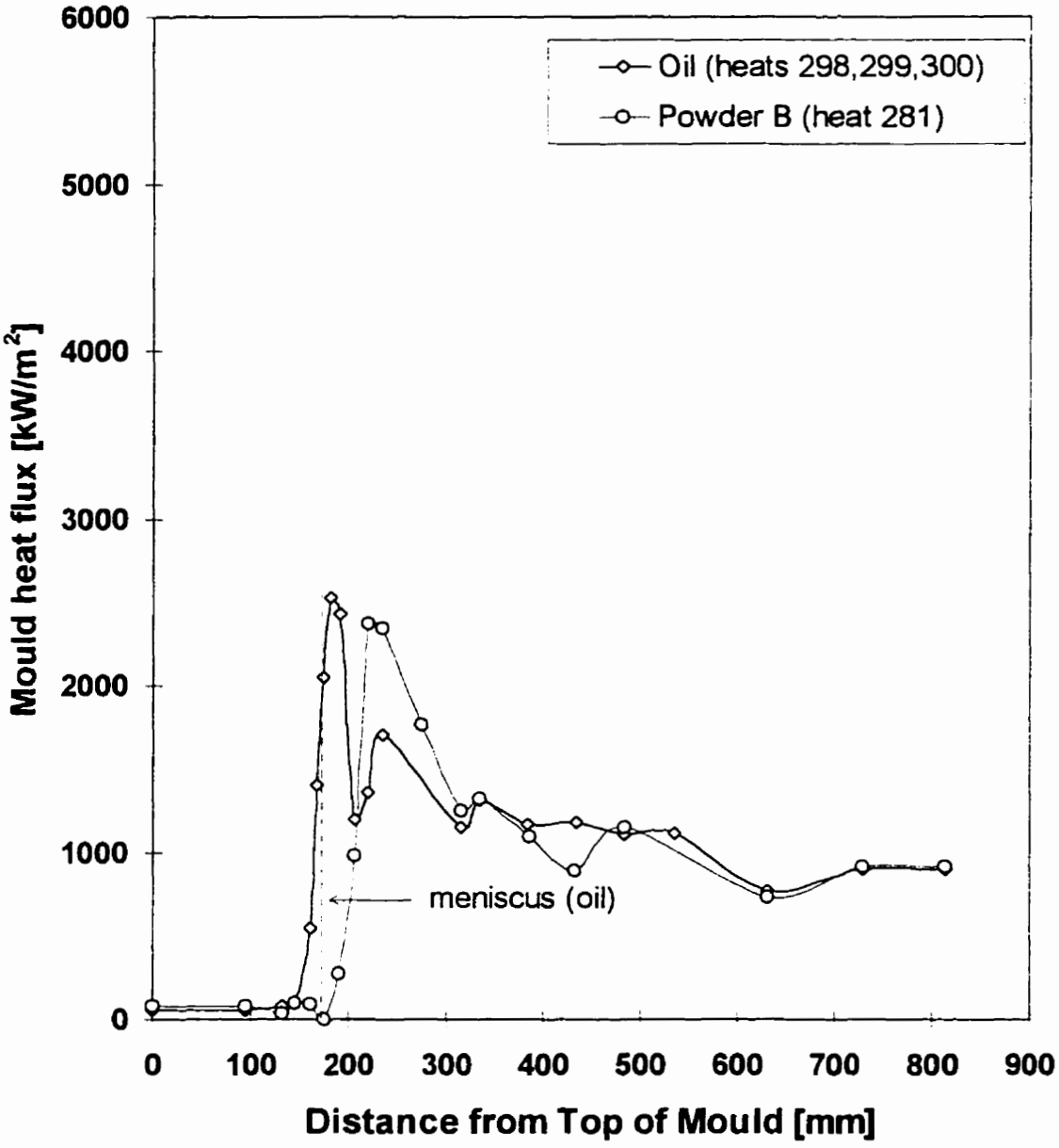

Figure 7.10 Comparison between oil and powder lubrication regarding mould heat flux for peritectic steel (0.12≤%C≤0.14) and mould cooling-water velocity 9.9 m/s; oil heats cast at 1.2 m/min and oscillation frequency 135 cpm; heat 281 cast at 1.3 m/min and oscillation frequency 150 cpm.

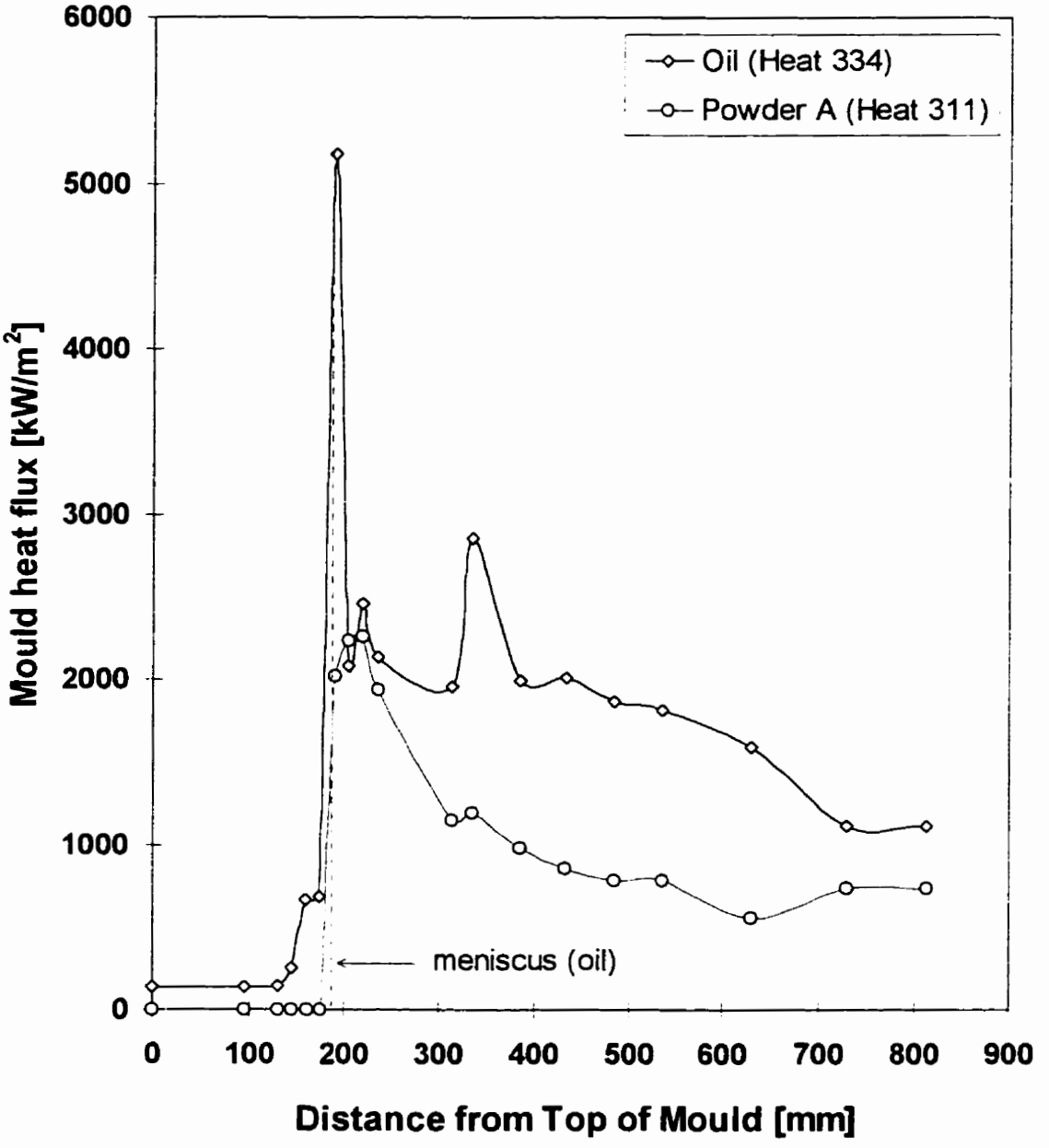

Figure 7.11 Comparison between oil and powder lubrication regarding mould heat flux for Boron(Ti)-alloyed steel (0.31≤%C≤0.33; 0.0025≤%B≤0.0028; 0.035≤%Ti≤0.038), oscillation frequency 137 cpm and mould cooling-water velocity 6.0 m/s.

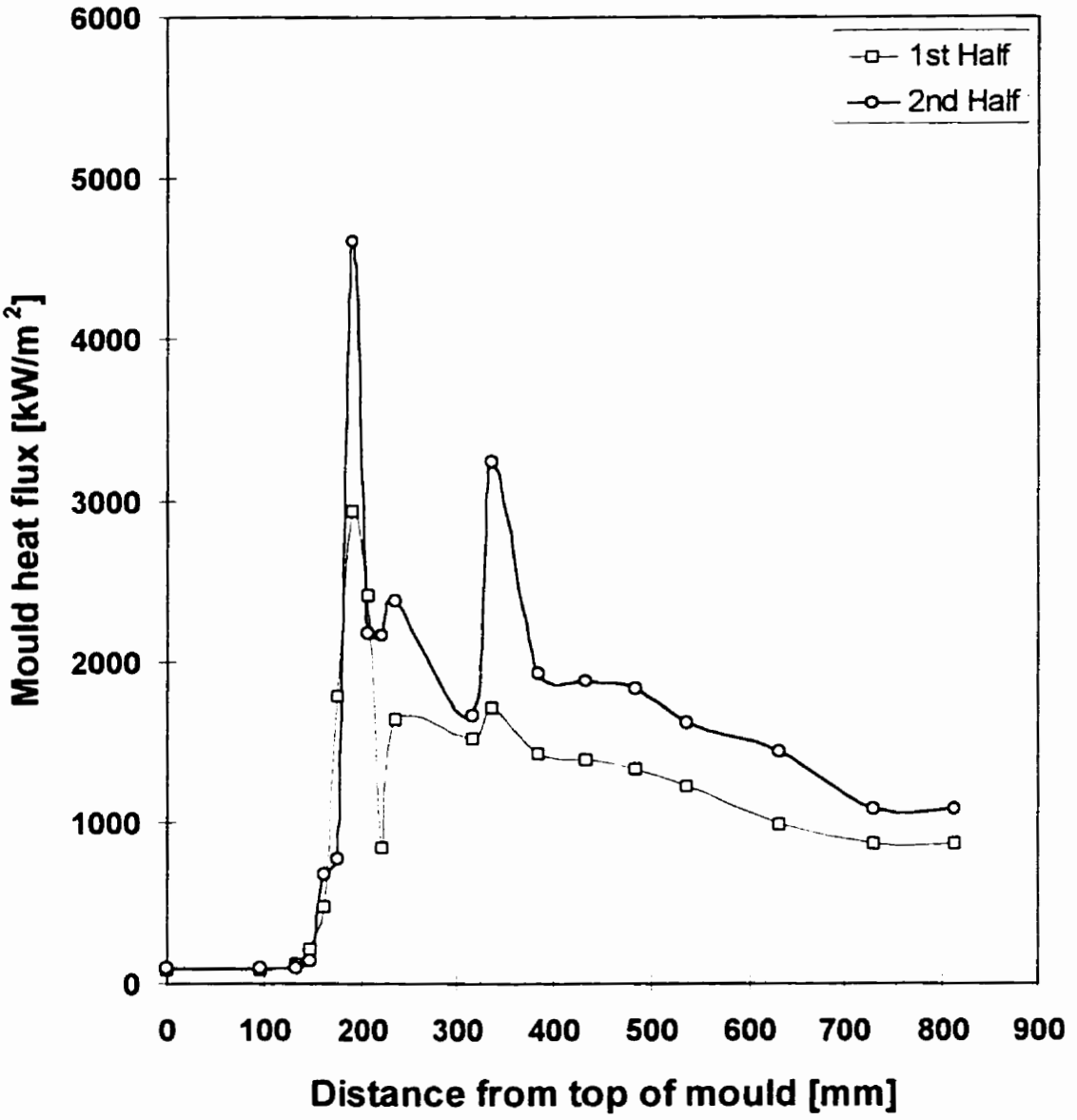

Figure 7.12 Mould heat flux for Boron(Ti)-alloyed steel cast with oil lubrication; heat 333 (0.32%C; 0.0023%B; 0.038%Ti), oscillation frequency 137 cpm and mould cooling-water velocity 6.0 m/s

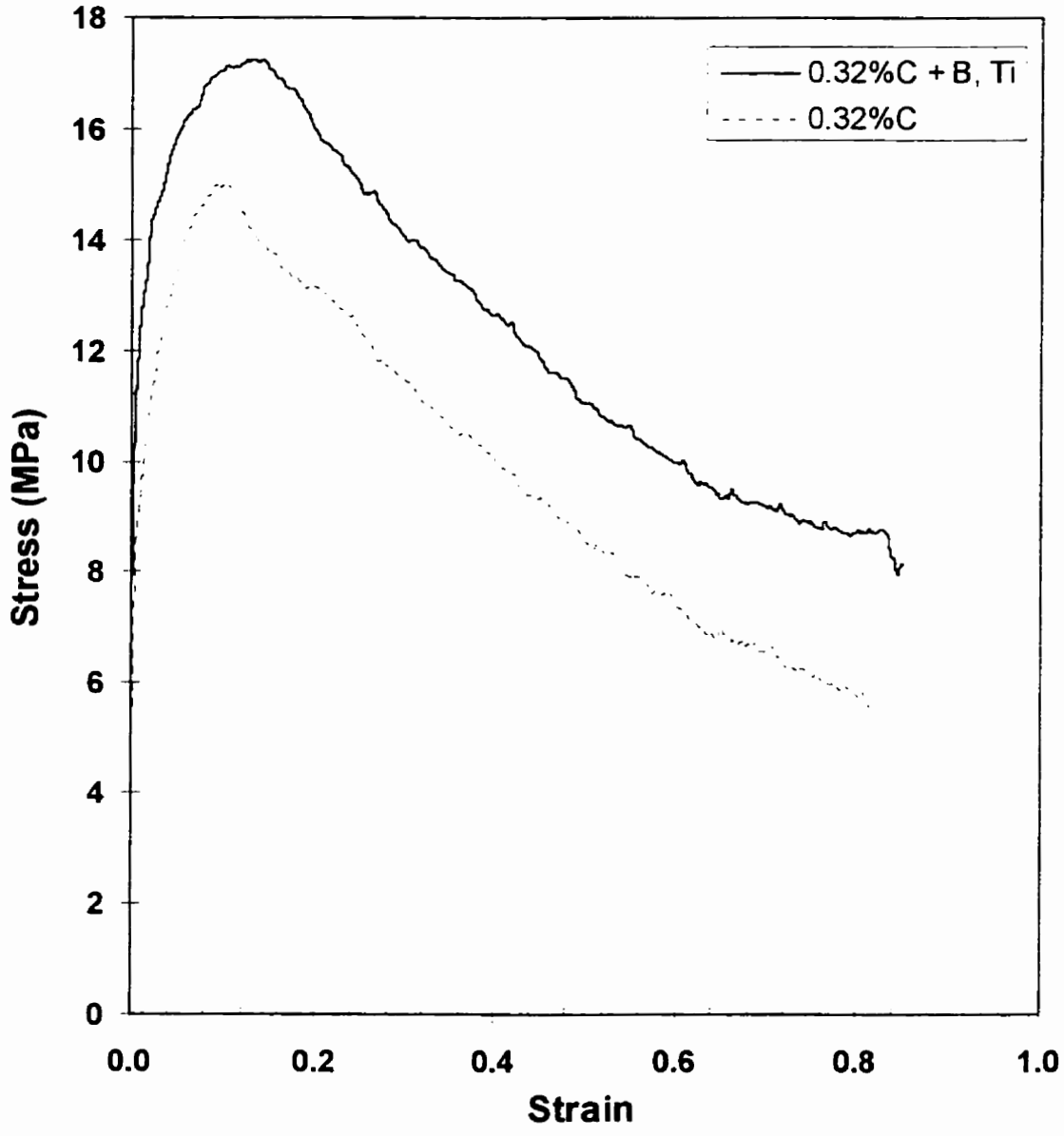

Figure 7.13 Tensile test of medium-carbon as-cast samples at a strain rate of 10^{-2} s^{-1} at 1300℃

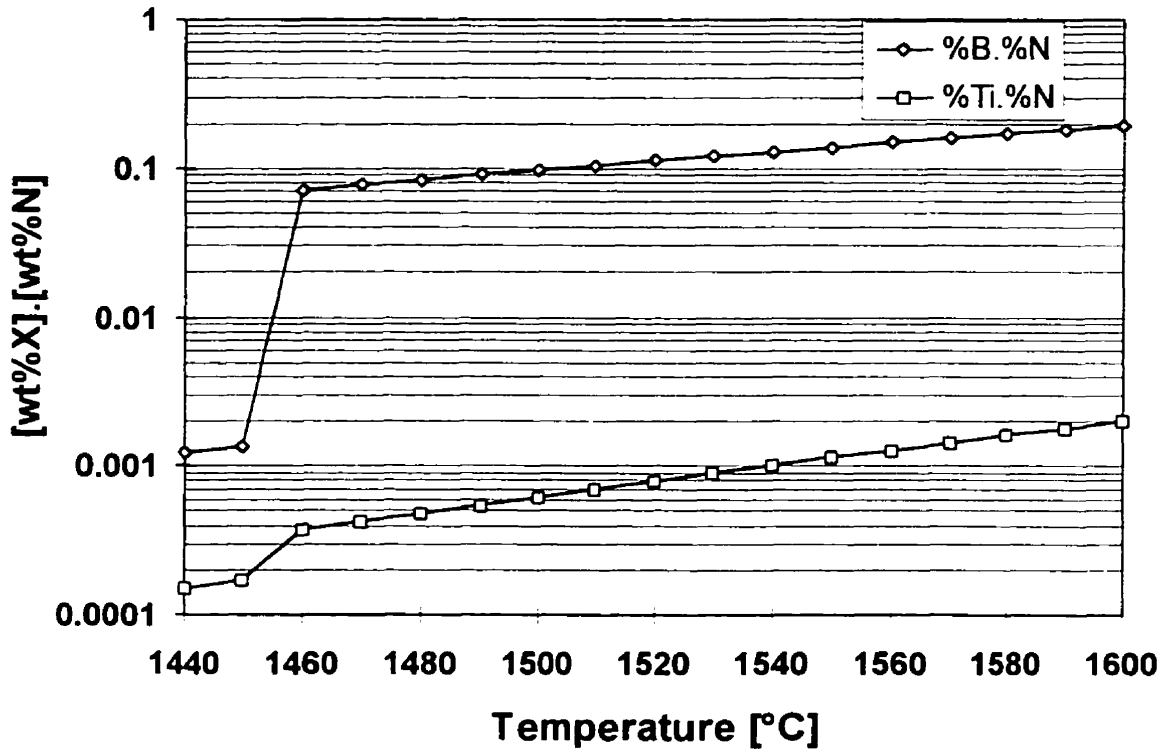

Figure 7.14 Solubility Product of [Ti] [N] and [B] [N] in low alloy steel

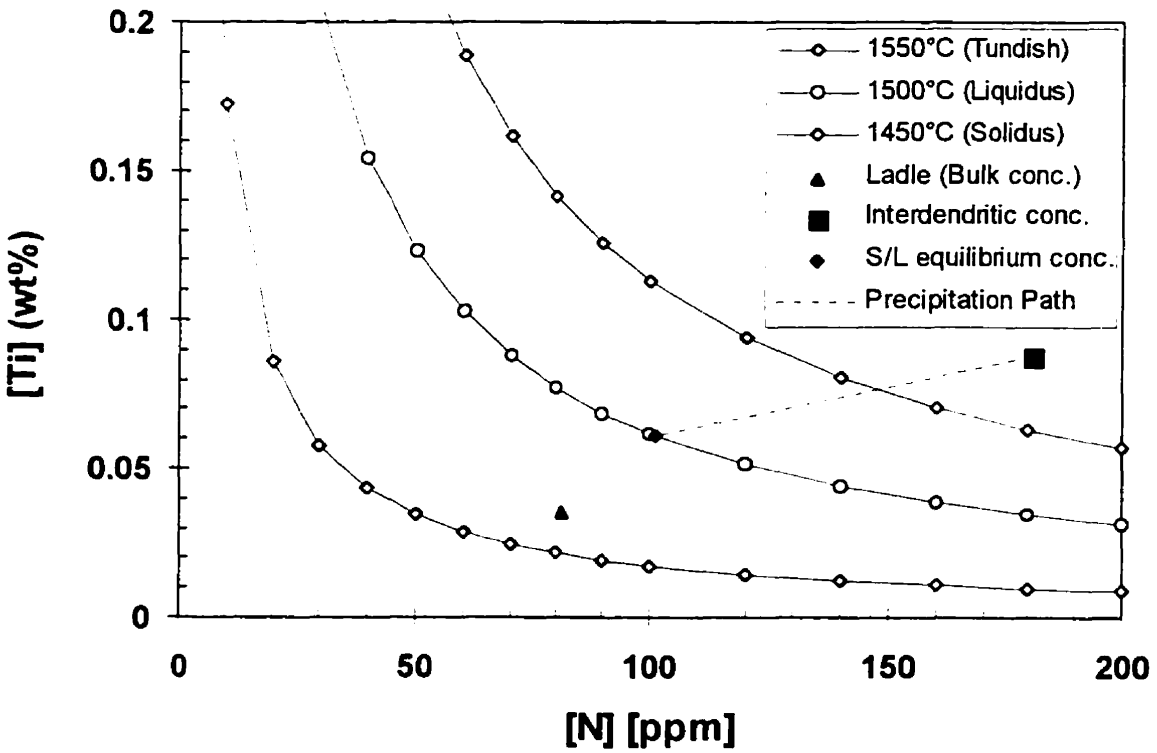

Figure 7.15 Ti-N Equilibrium in low-alloy steel

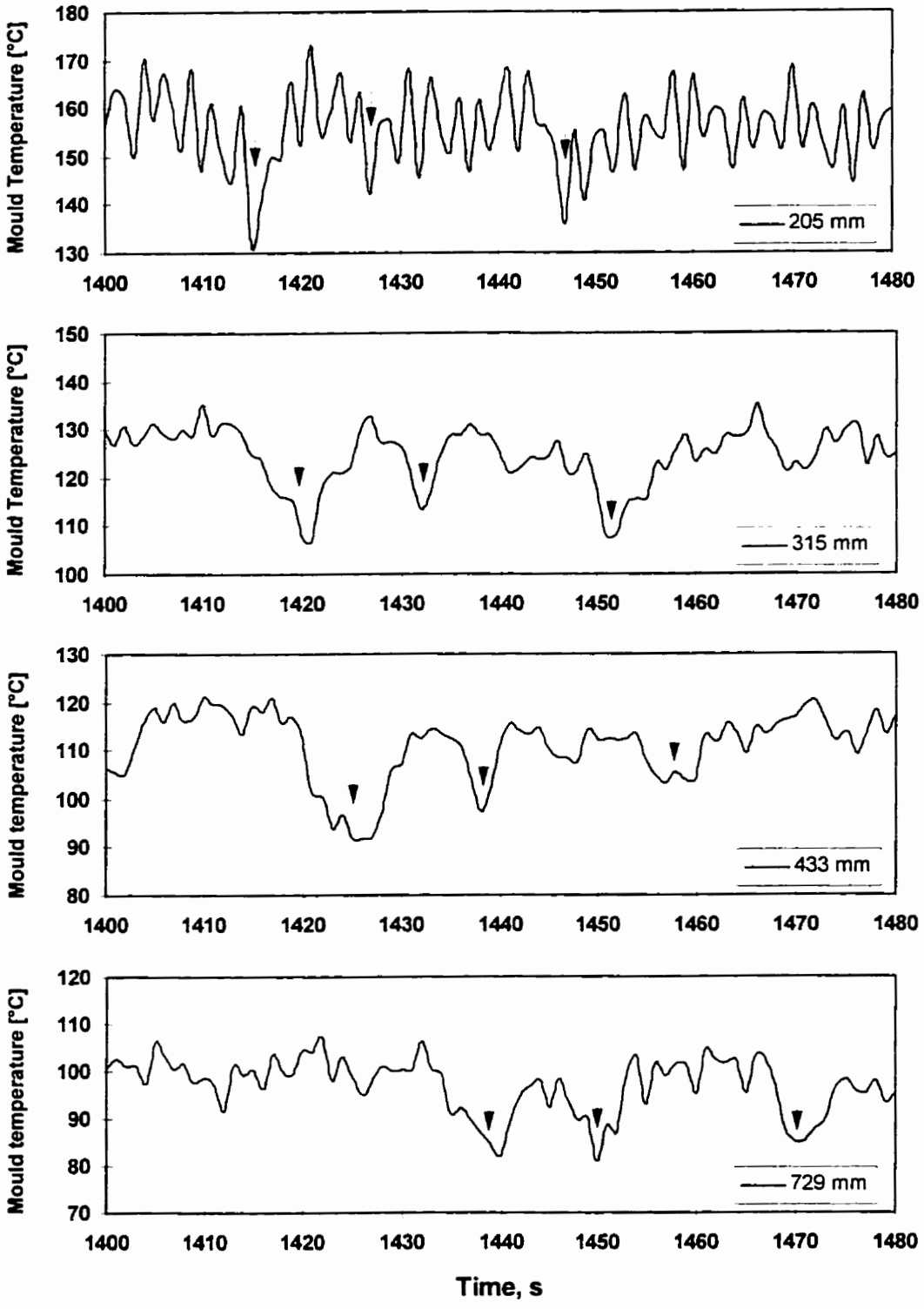

Figure 7.16 Mould temperature pattern showing transverse depression moving down the mould; heat 277, casting speed ~23.6 mm/s, oscillation frequency 170 cpm, powder A.

(A)

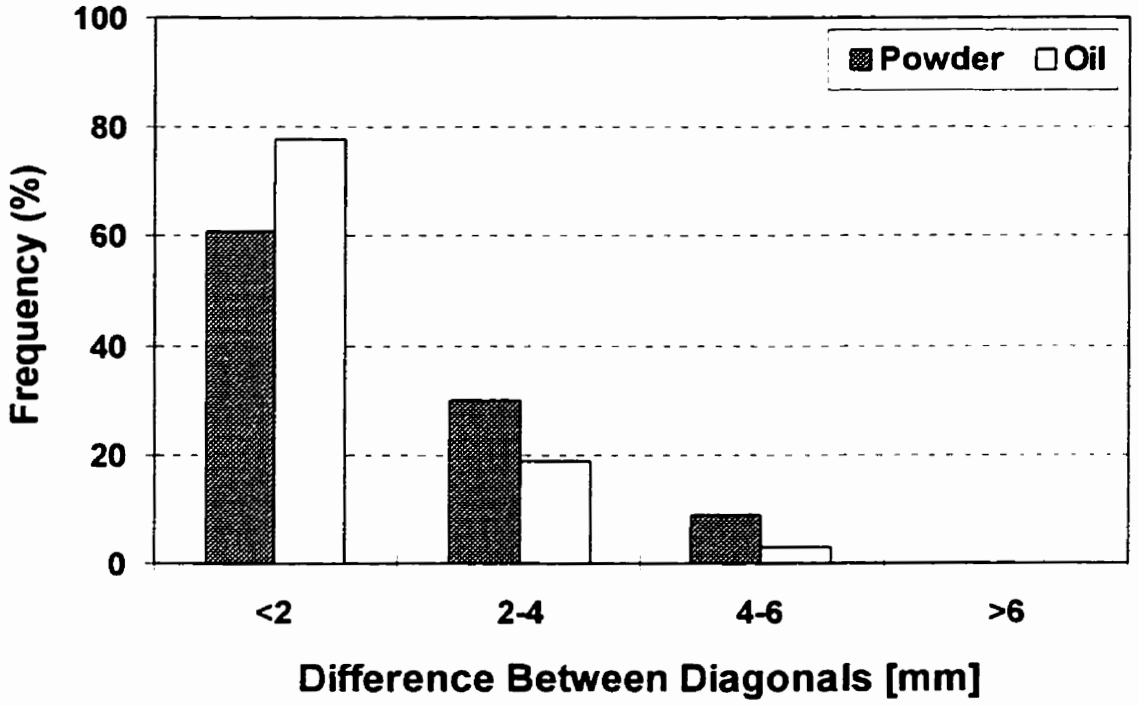

(B)

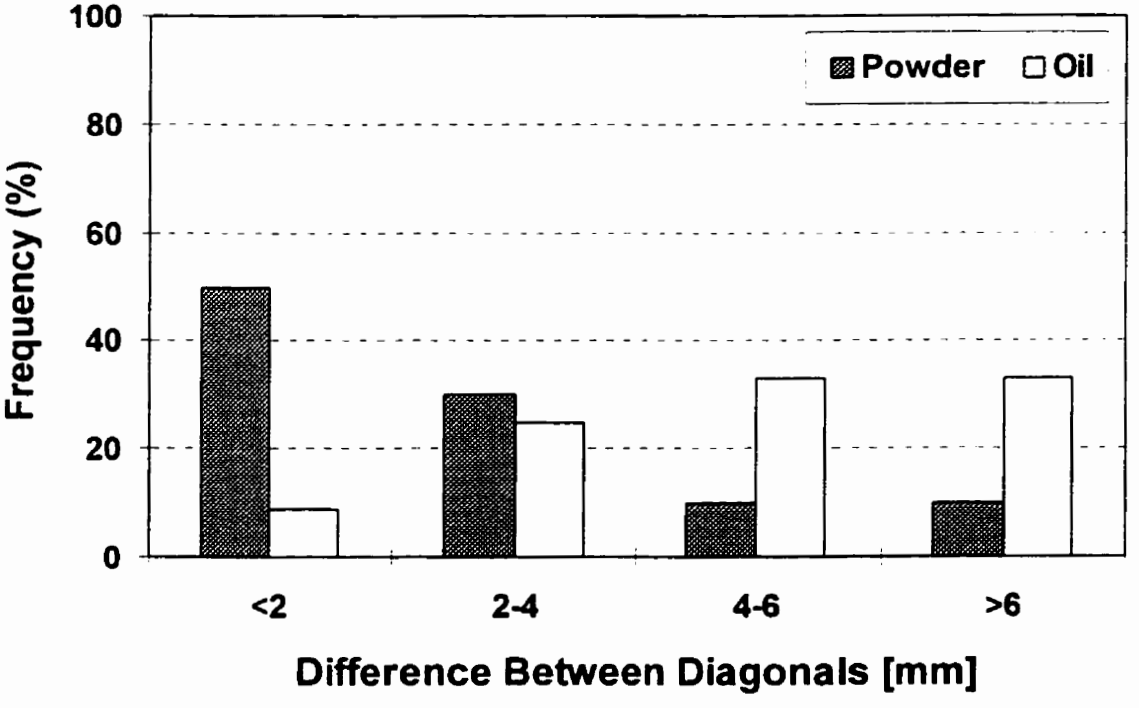

Figure 7.17 Effect of type of mould lubricant on the severity of rhomboidity; (A) peritectic steel (0.11≤%C≤0.14); (B) Boron(Ti)-alloyed medium-carbon steel (0.32 pct. C)

(A)

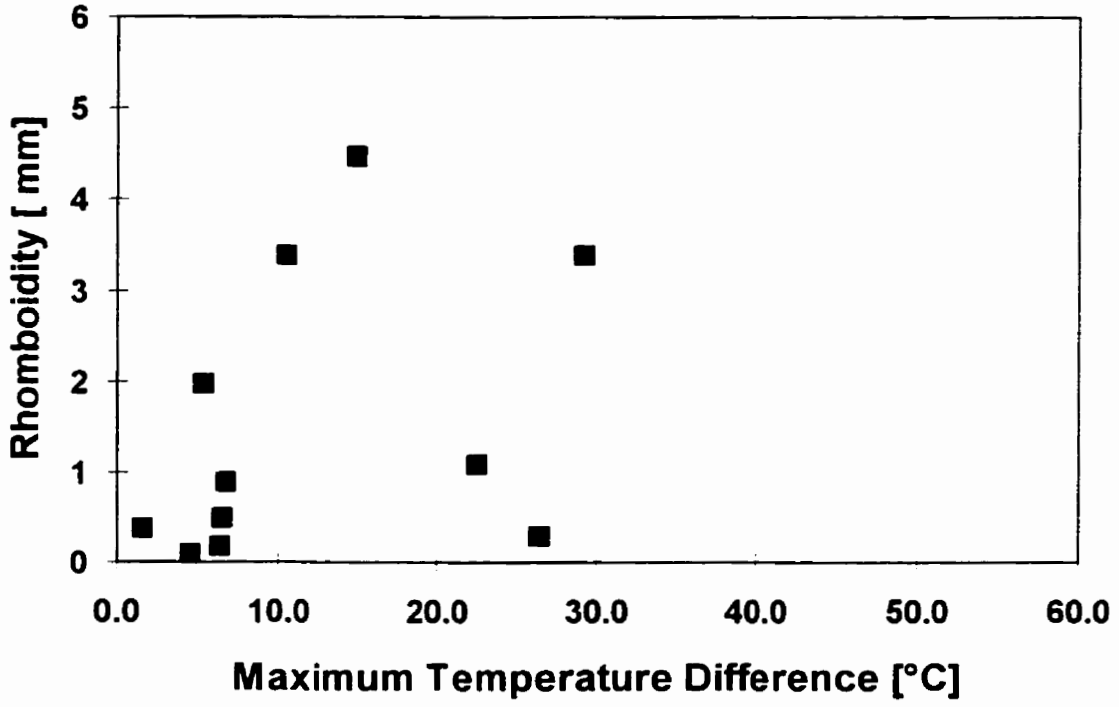

(B)

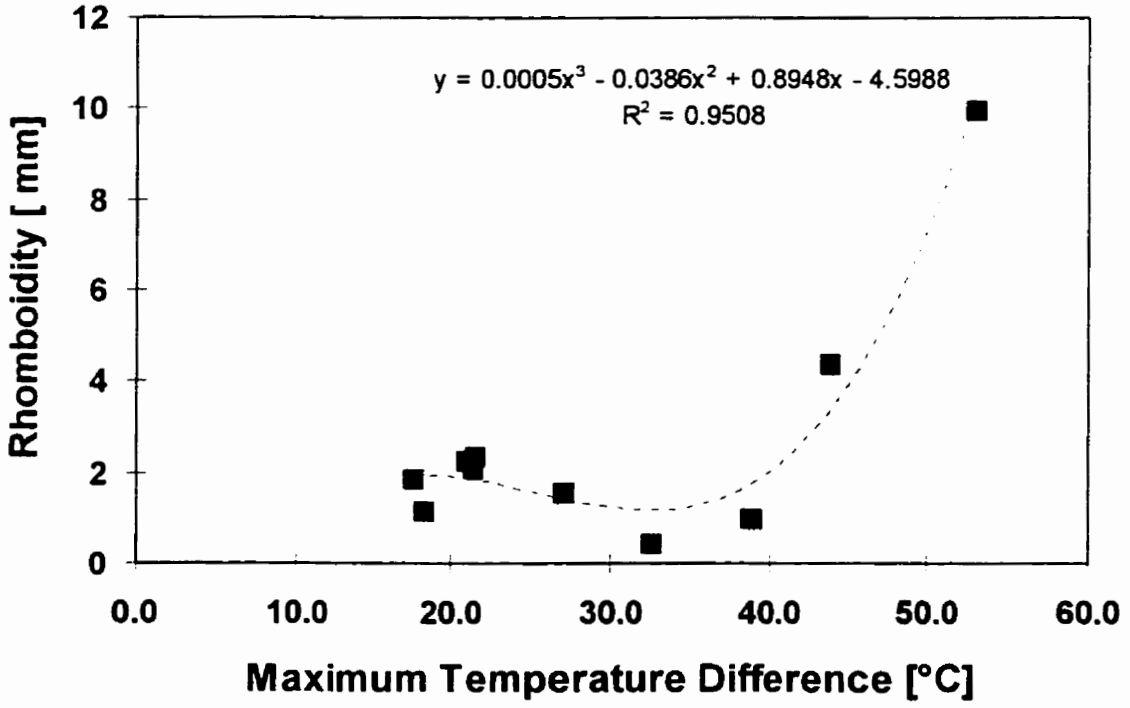

Figure 7.18 Rhomboidity as a function of maximum temperature difference; (A) Peritectic-carbon steels, 0.11~0.13 pct. C, thermocouples located 205 mm below top of mould; (B) Boron(Ti)-alloyed medium-carbon steel, ~0.32 pct. C, thermocouples located at 220 mm below top of mould

(A)

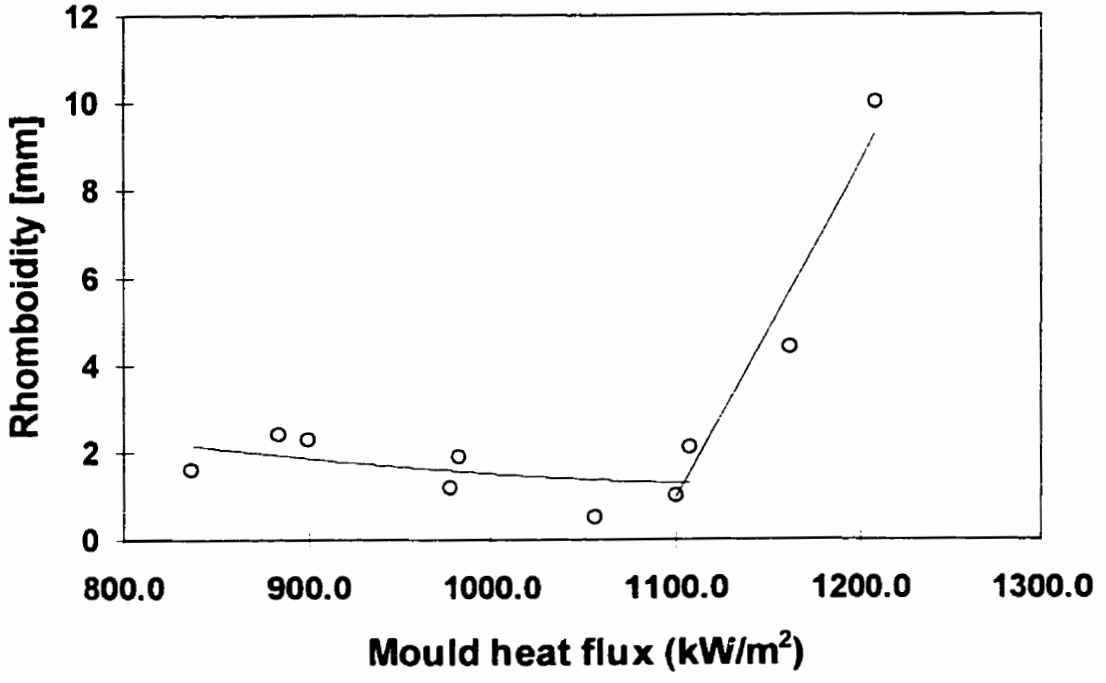

(B)

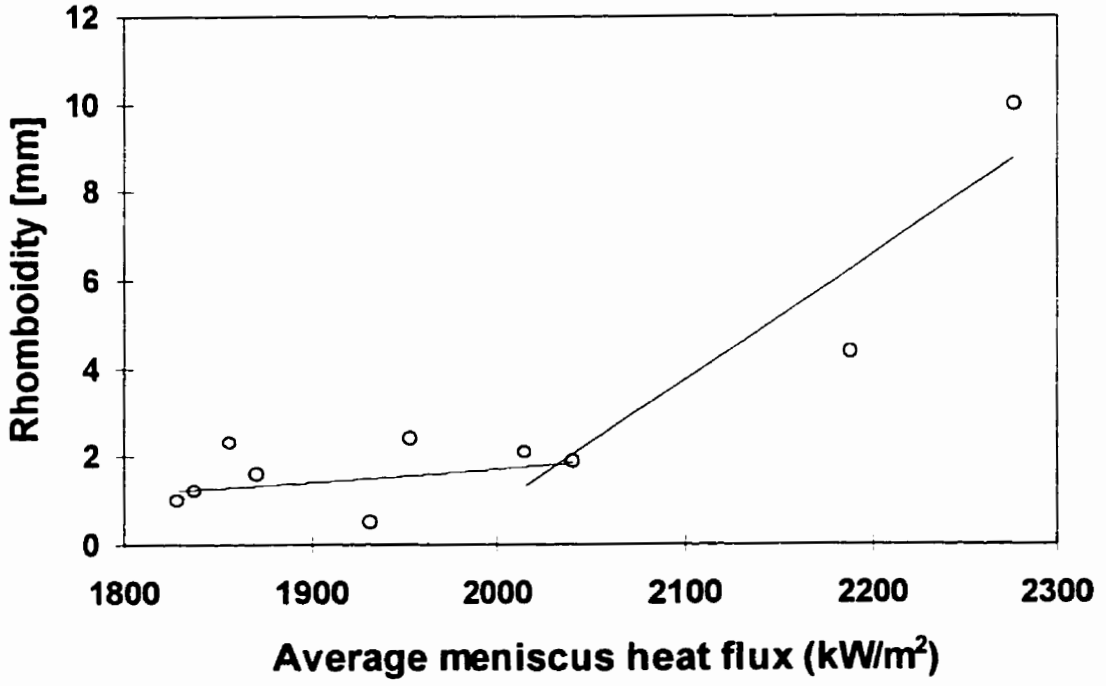

Figure 7.19 Relationship between rhomboidity and mould heat flux (Boron(Ti)-alloyed medium-carbon steel); (A) Rhomboidity as a function of average heat flux calculated from mould water temperature difference; (B) Rhomboidity as a function of peak heat flux averaged over a length of 30 mm from metal level

(A)

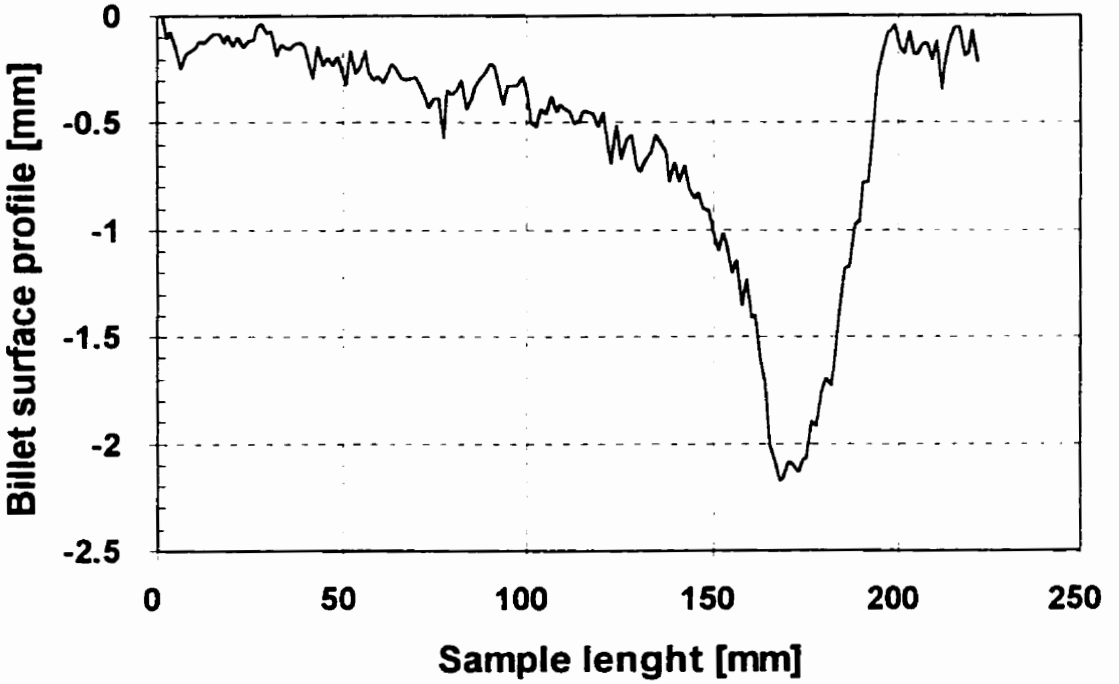

(B)

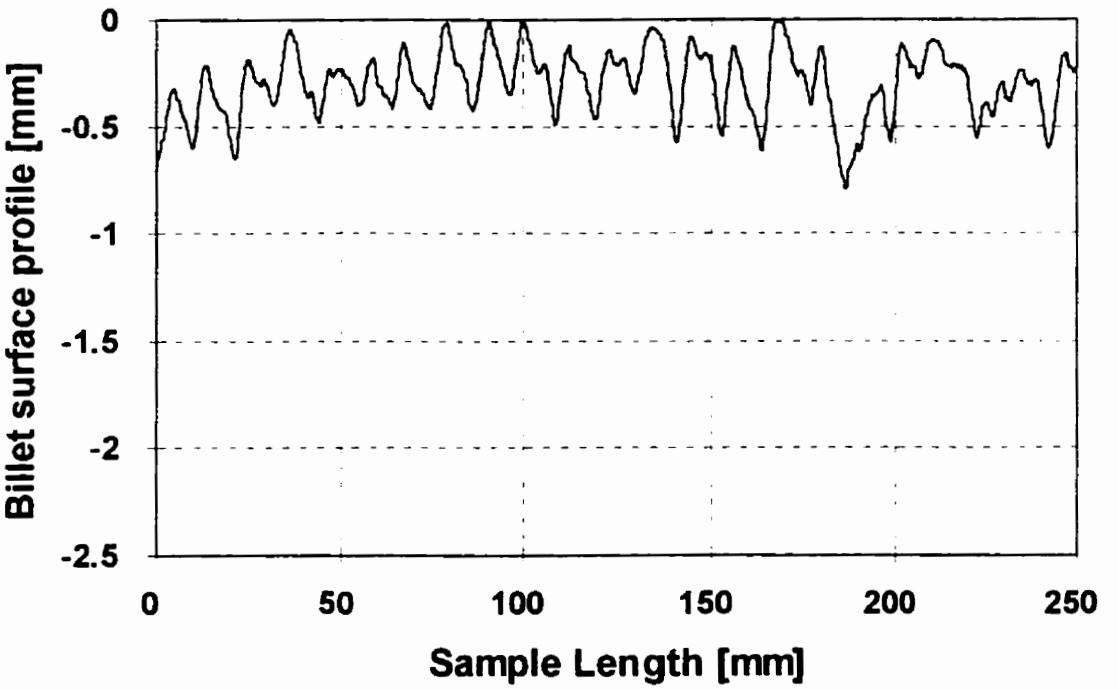

Figure 7.20 Billet sample centre-surface profile; (A) Oscillation mark and large transverse depression in a Boron(Ti)-alloyed medium-carbon steel cast with oil; (B) Same steel as (A) but cast with powder A

(A)

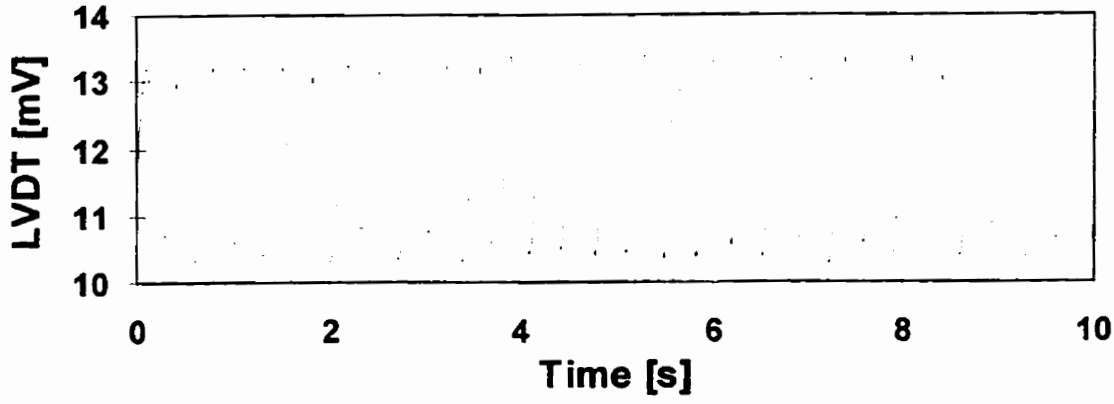

(B)

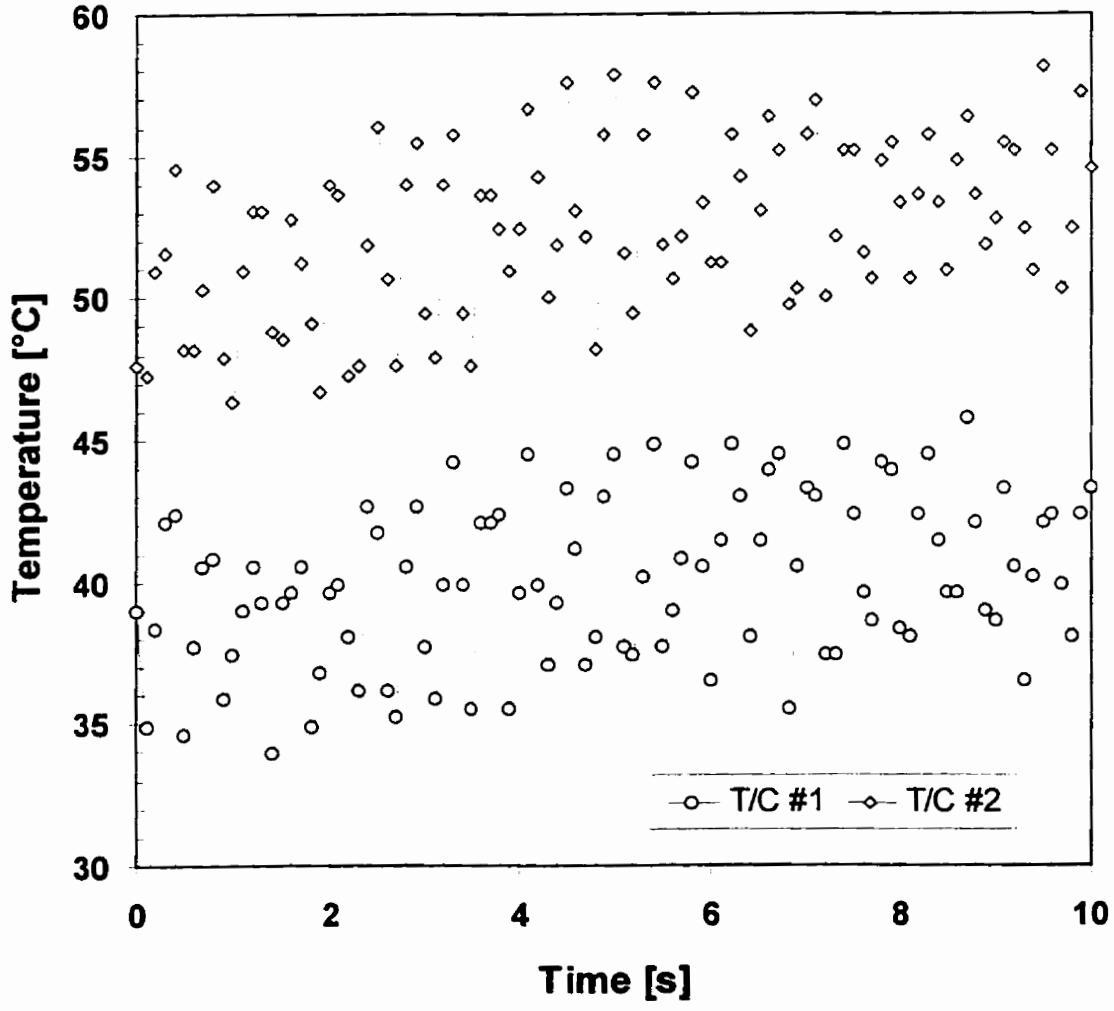

Figure 7.21 LVDT and temperature fluctuations for Heat 277, nominal oscillation frequency 170 cpm, data sampling rate 10 Hz; (A) LVDT signal; (B) temperature signals (T/C #1 and T/C #2) showing short-range fluctuations not in phase with mould oscillation (LVDT).

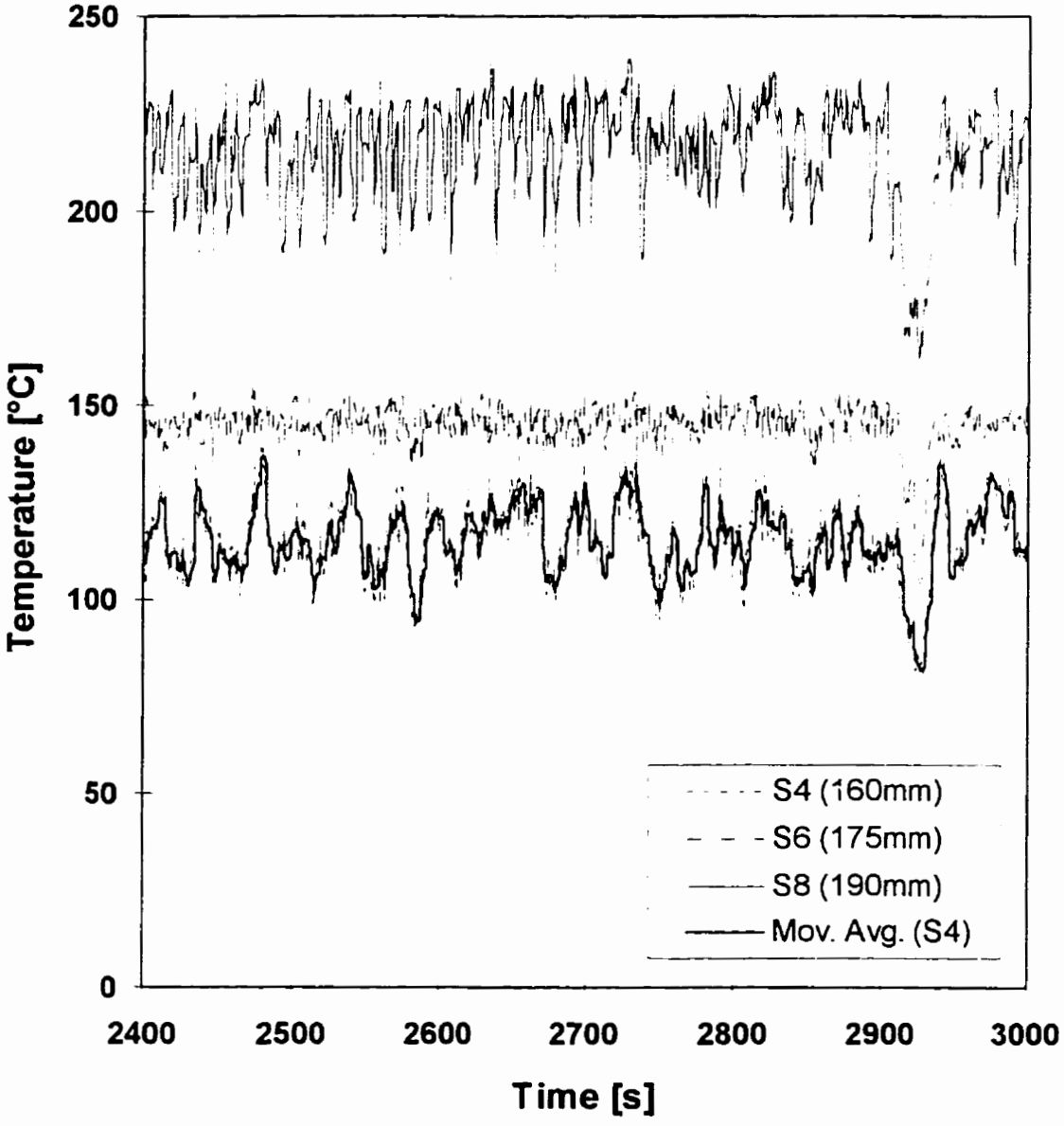

Figure 7.22 Mould temperature variation at the meniscus region for Heat 333, Boron(Ti)-alloyed medium-carbon steel, oil lubrication, metal level ~ 165 mm, south-face.

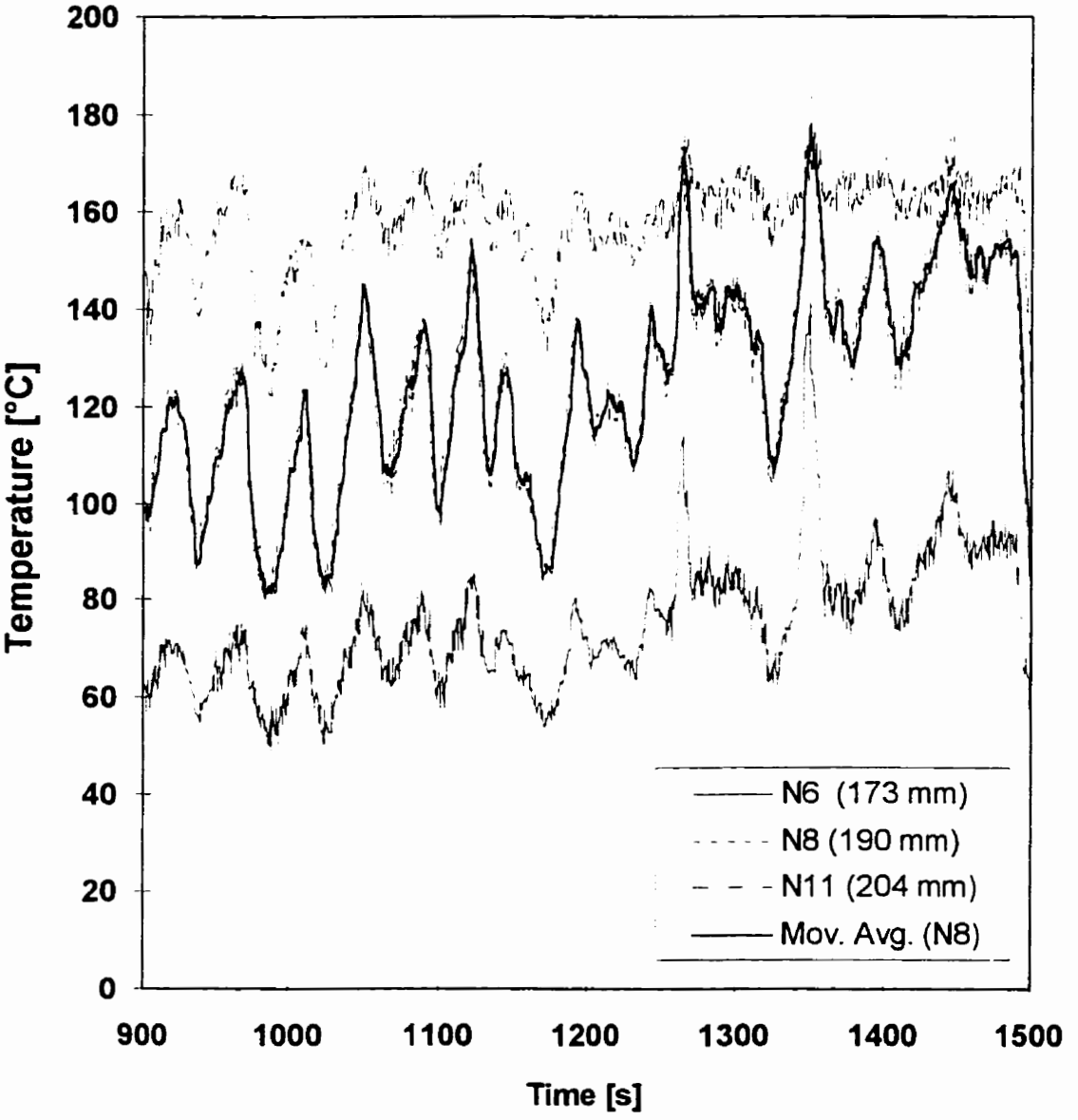

Figure 7.23 Mould temperature variation at the meniscus region for Heat 311, Boron(Ti)-alloyed medium-carbon steel, powder lubrication (powder A), metal level ~ 177 mm, north-face.

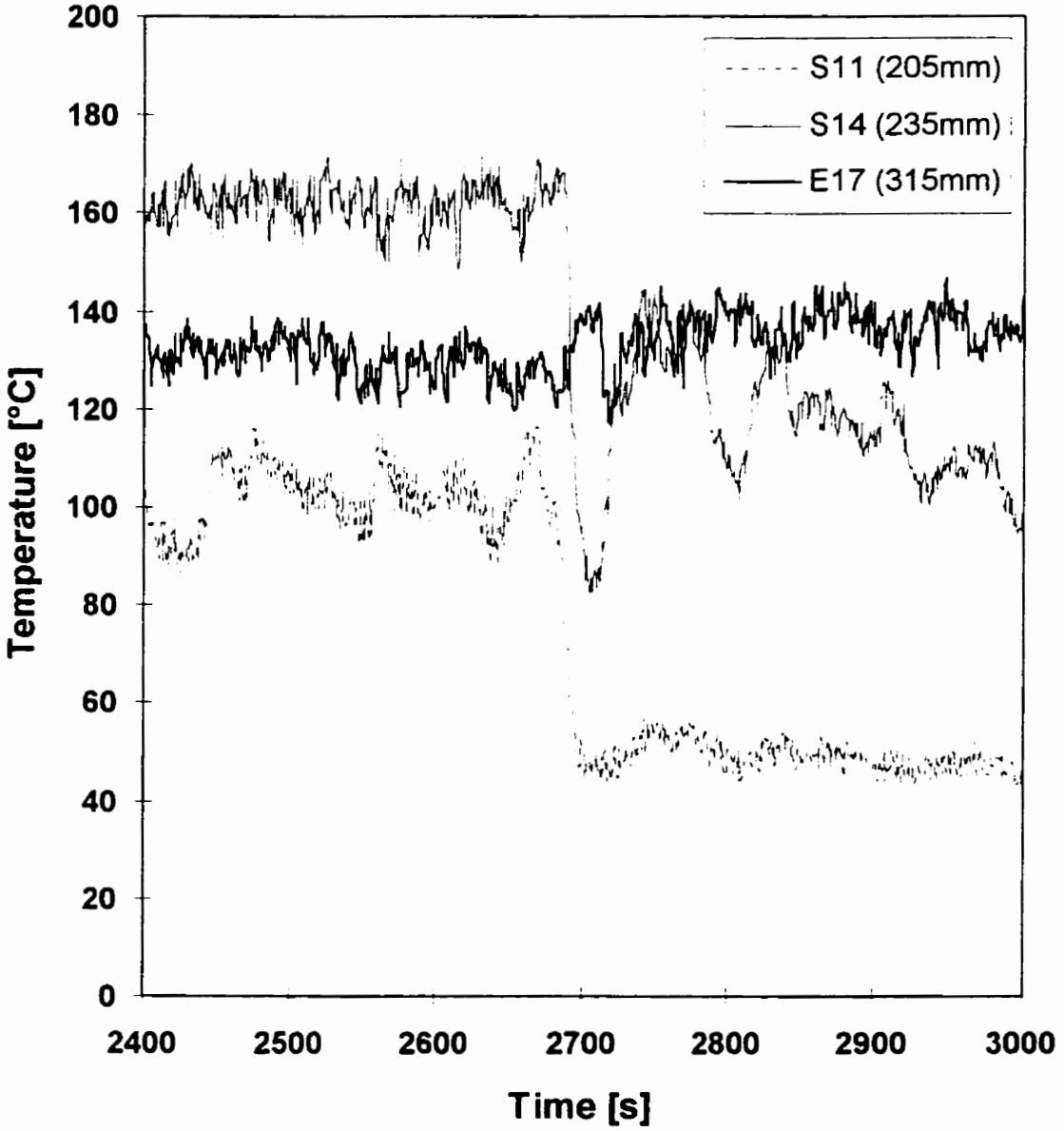

Figure 7.24 Mould temperature variation at the meniscus region due to a change in metal level set-point; Heat 278, peritectic-carbon steel, powder lubrication (powder A), mould level changed from ~205 mm to 235 mm.

(A)

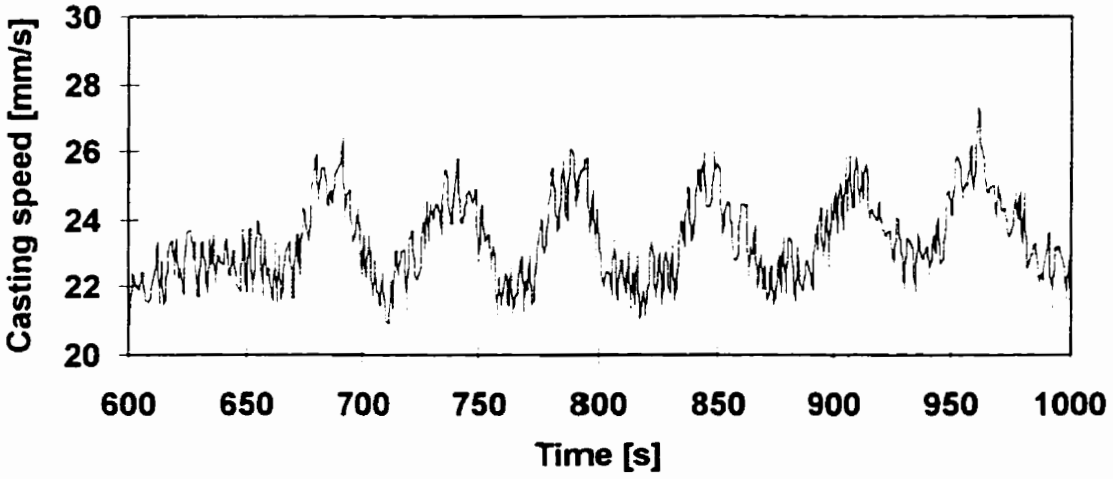

(B)

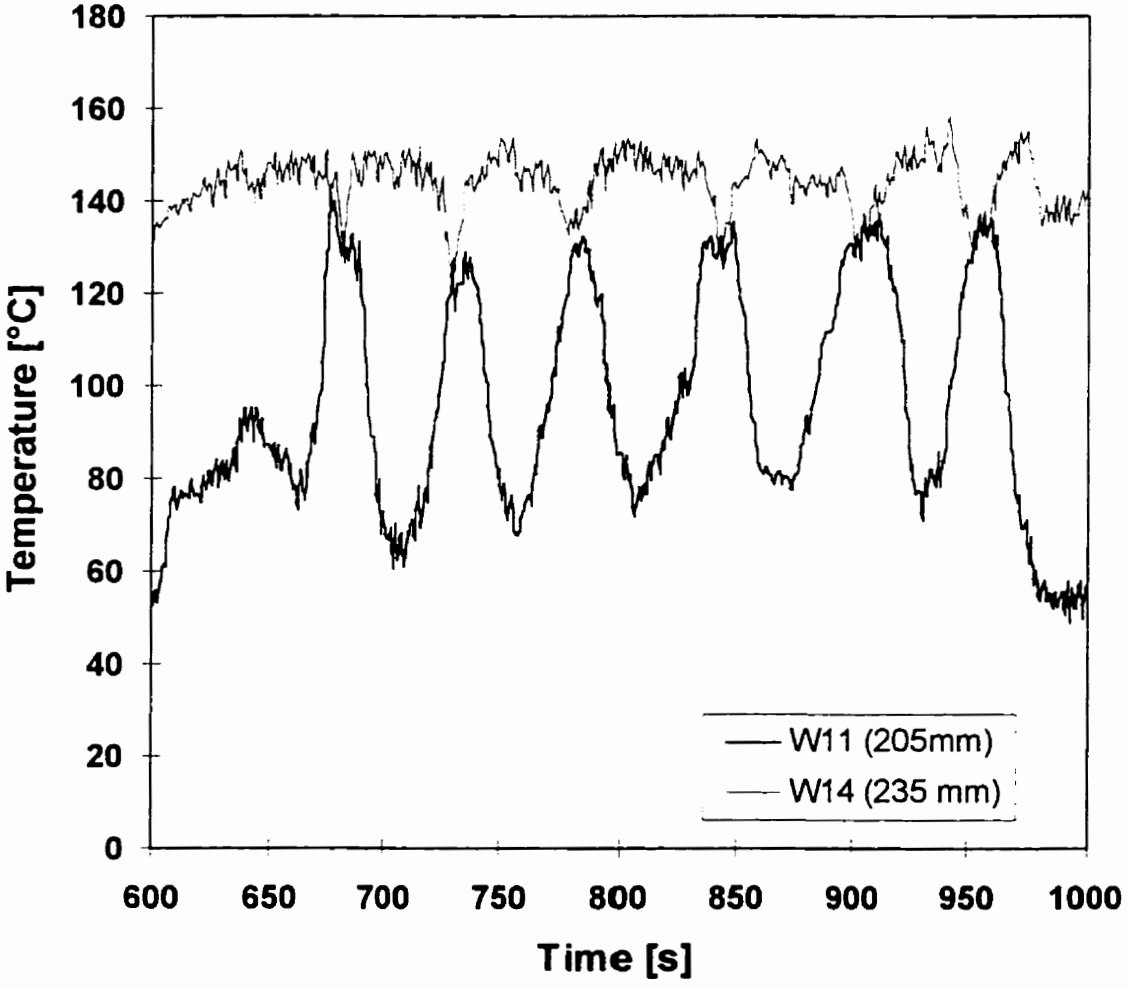

Figure 7.25 Casting speed and mould wall temperatures fluctuations that are in phase, heat 280 (peritectic steel, powder B); (A) Casting speed; (B) Temperatures, thermocouple W11 located above meniscus level and W14 located below meniscus.

(A)

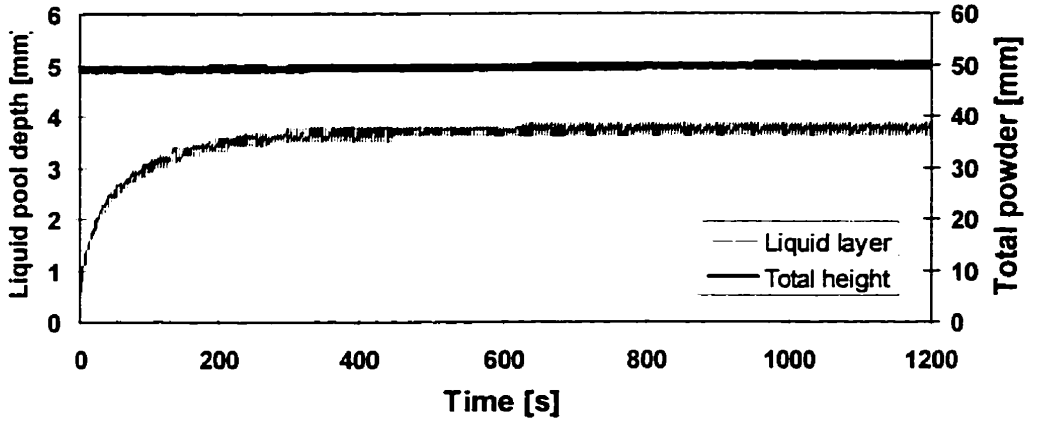

(B)

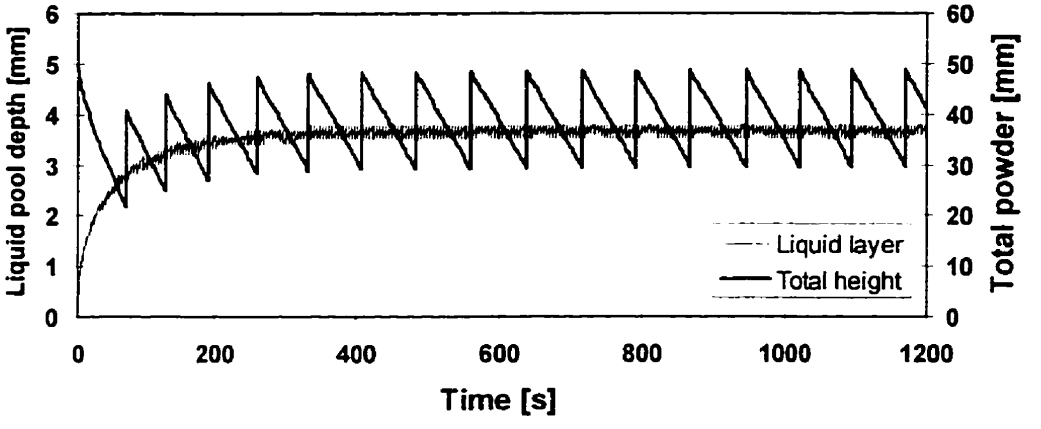

(C)

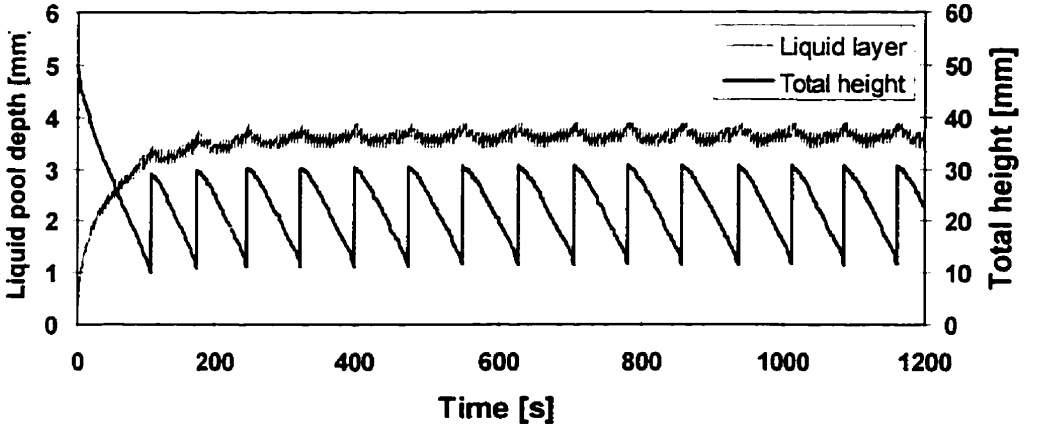

Figure 7.26 Calculated molten flux pool height for powder B (consumption: 1.34 k/ton; casting speed: 1.24 m/min); (A) constant powder level, 50 mm, (B) addition of 20 mm of fresh powder every time the temperature of the free surface reaches 400°C, (C) addition of 20 mm of fresh powder every time the temperature of the free surface reaches 800°C.

(A)

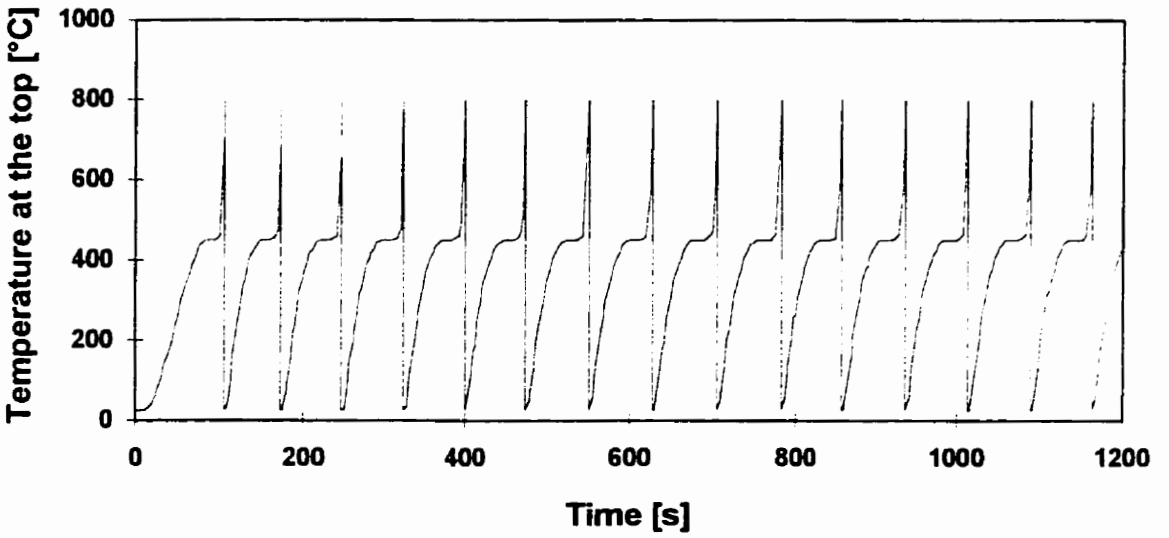

(B)

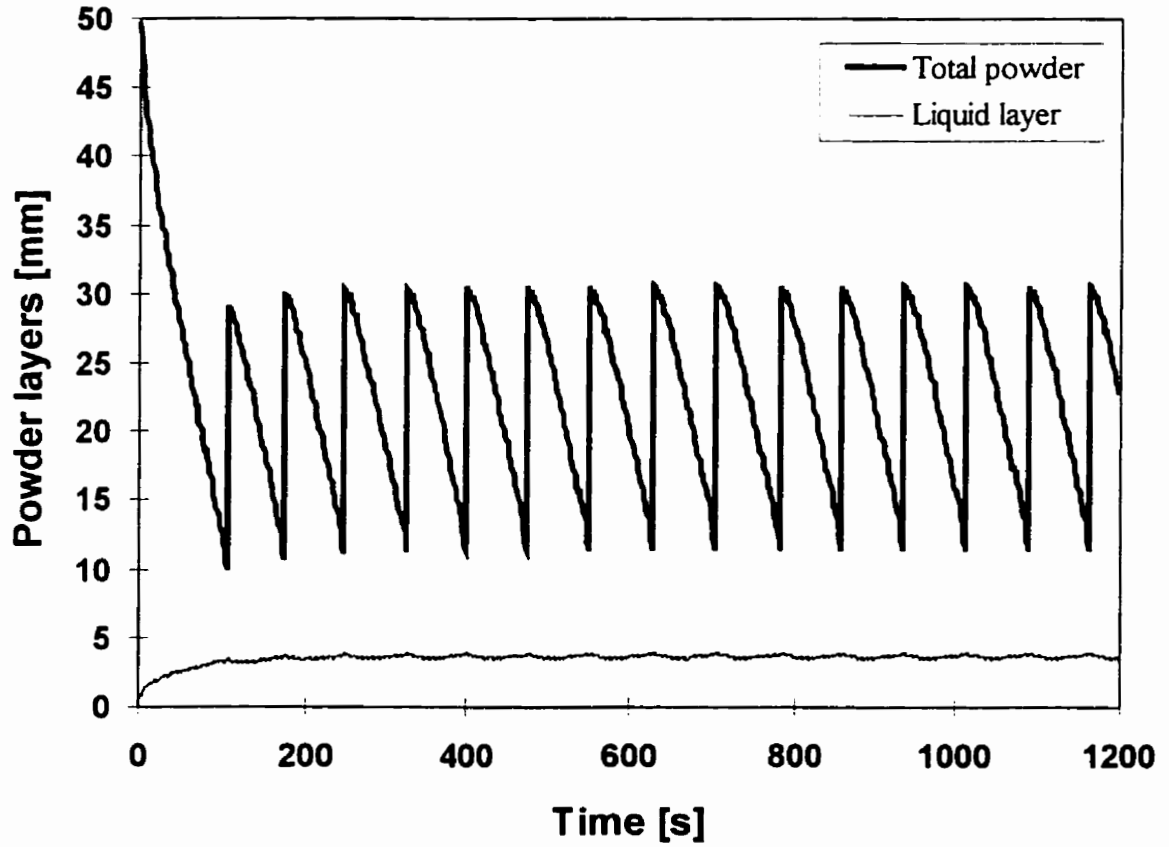

Figure 7.27 Output from the mathematical simulation of powder melting for powder B when 20 mm of fresh powder is added whenever the temperature at the top exceeds 800°C: (A)- temperature at the free surface, (B)- total height of powder (all layers) and height of the liquid pool.

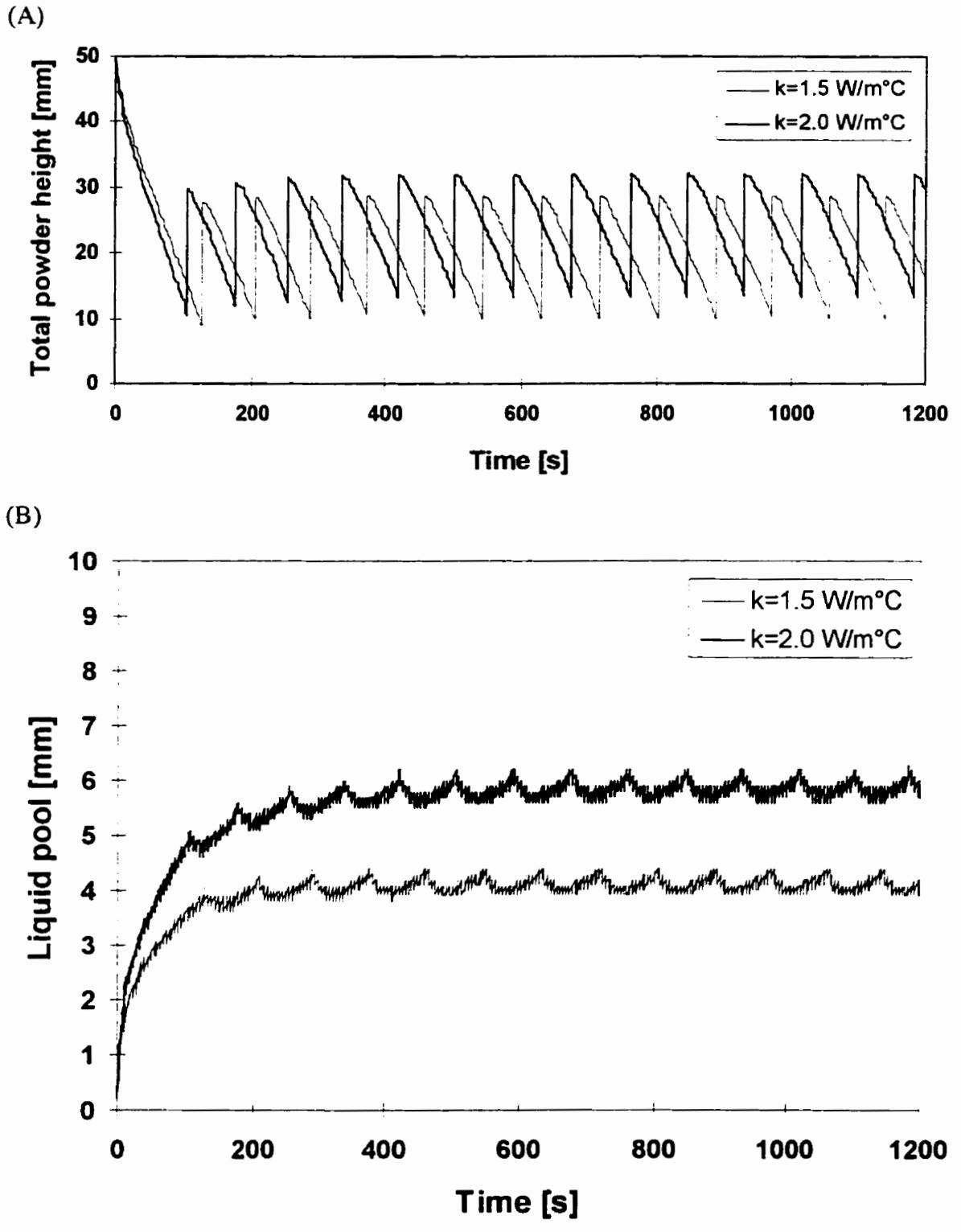

Figure 7.28 Mathematical simulation output for melting of powder A, thermal conductivity of the solidified flux taken as 1.5 and 2.0 W/m°C and addition of 20mm of fresh powder every time the free surface temperature exceeds 800°C: (A)- position of the free surface, (B)- height of the liquid pool.

(A)

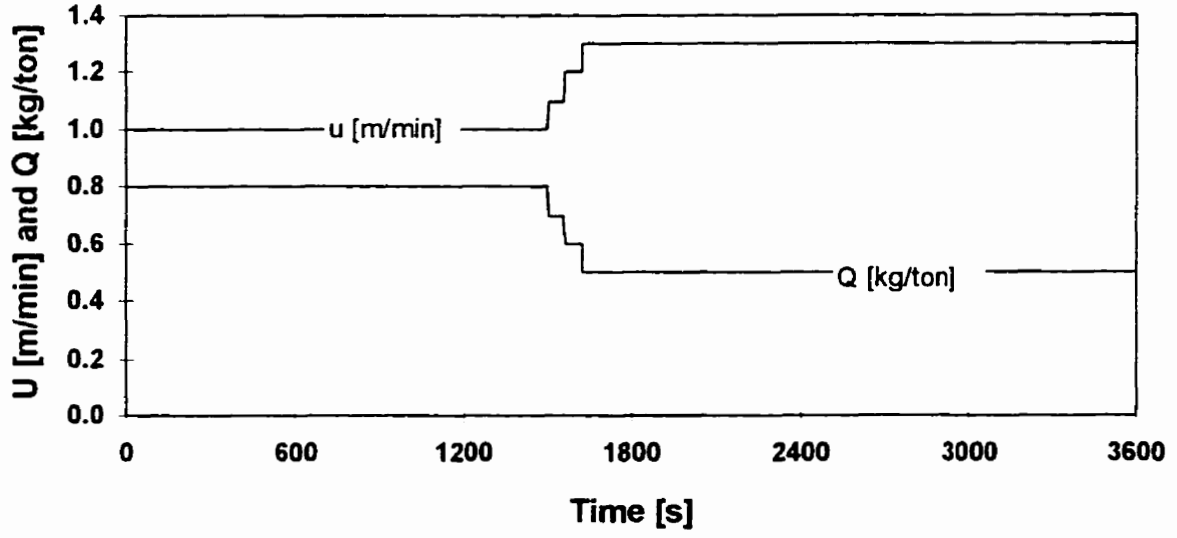

(B)

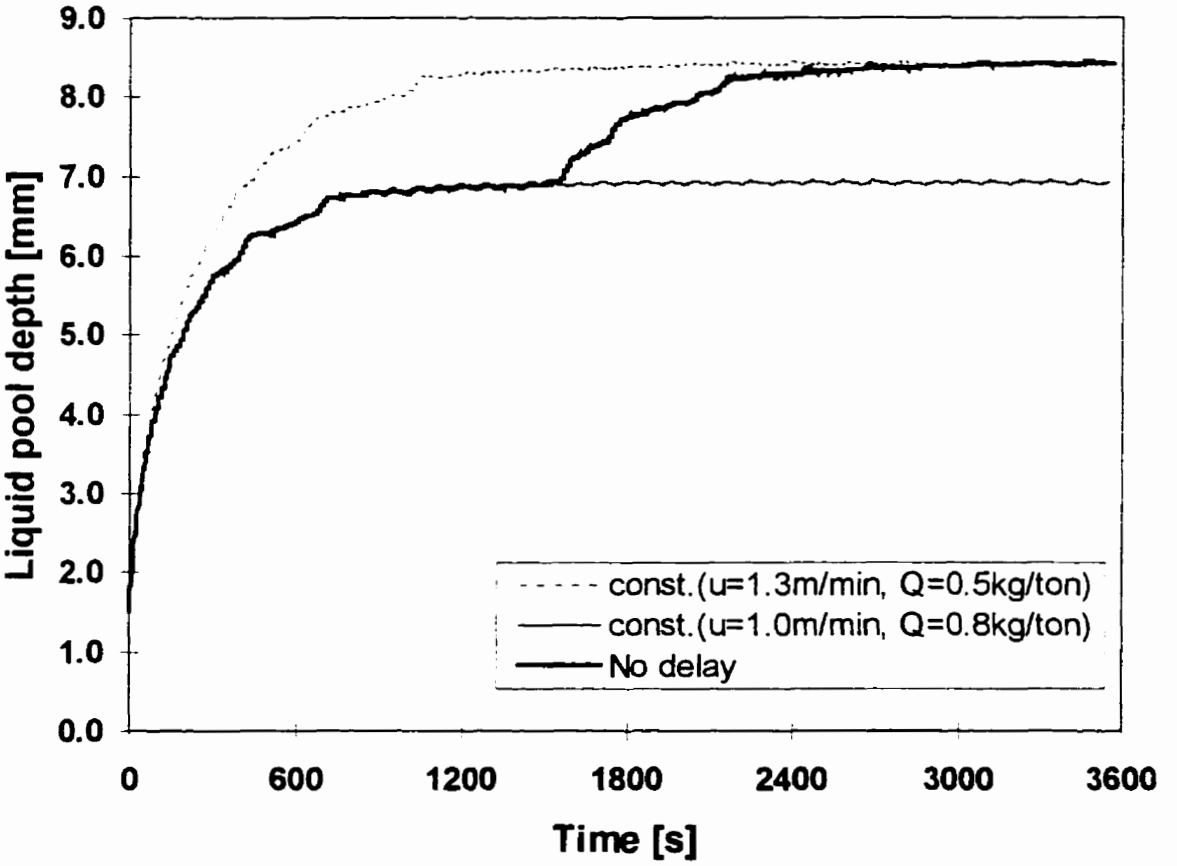

Figure 7.29 Influence of casting speed change on liquid flux pool for a simultaneous (no delay) change in casting speed (U) and mould powder consumption (Q): (A) casting speed and powder consumption changes, (B) liquid pool response to the changes shown in (A).

(A)

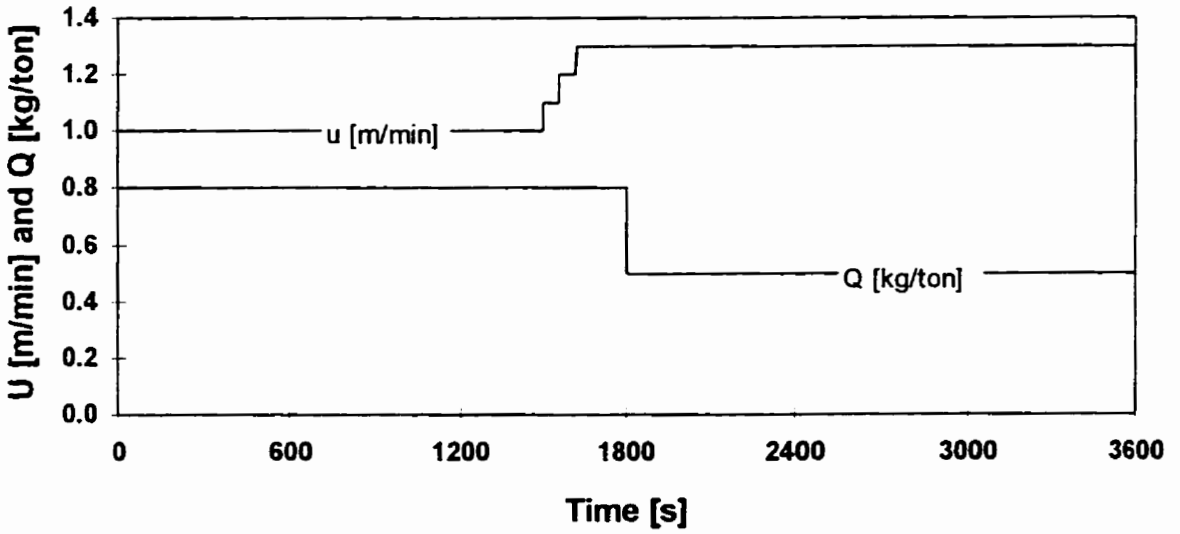

(B)

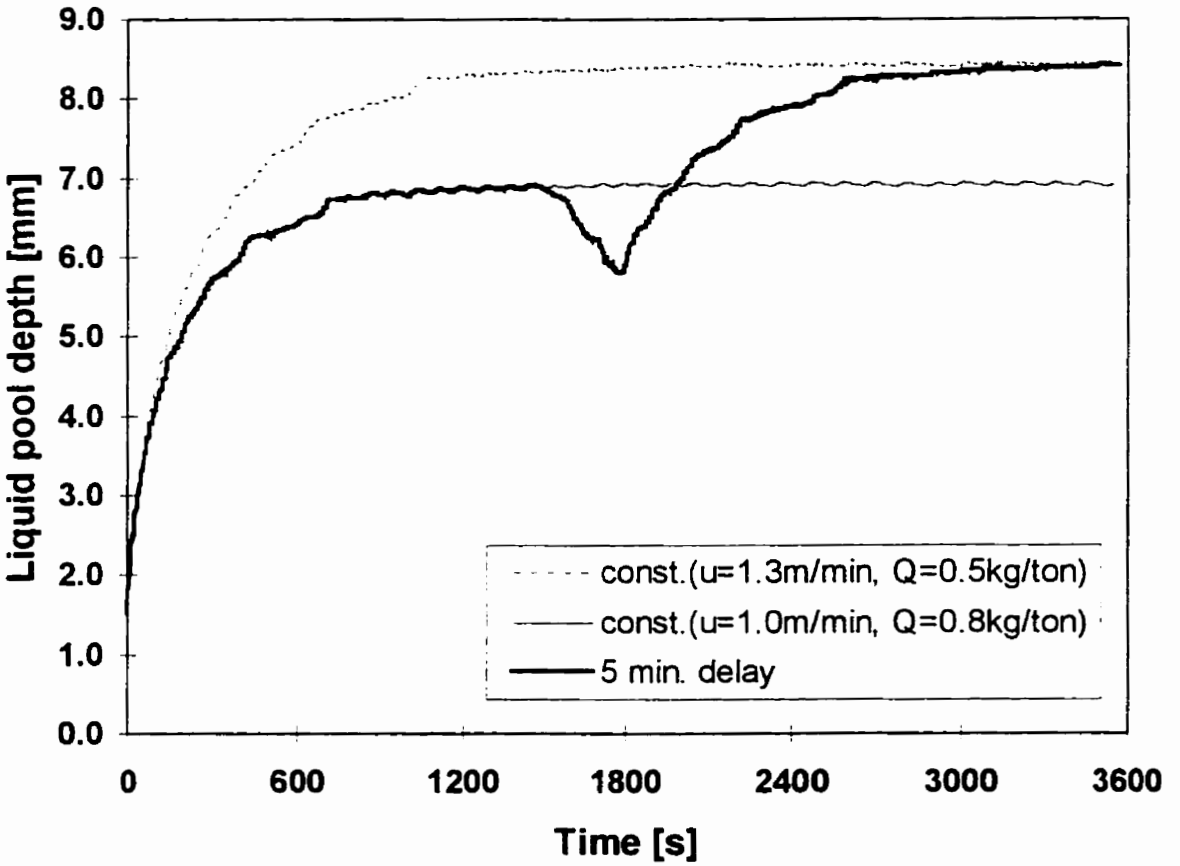

Figure 7.30 Influence of casting speed change on liquid flux pool for a 5-minute lagging between the initial change in casting speed (U) and the change in mould powder consumption (Q): (A) casting speed and powder consumption changes, (B) liquid pool response to the changes shown in (A).

8. SUMMARY AND CONCLUSIONS

A comprehensive study was undertaken to examine mould thermal response and powder behaviour during the continuous casting of peritectic ($0.11 \leq \%C \leq 0.14$) and Boron(Ti)-alloyed ($0.30 \leq \%C \leq 0.33$; $0.0023 \leq \%B \leq 0.0027$; $0.035 \leq Ti \leq 0.038$) steel billets cast with powder. Comparison between powder and oil lubrication in the context of the mould thermal response and billet surface quality allowed the elucidation of fundamental differences between these two. Previously proposed mechanisms for oscillation mark formation, transverse and longitudinal depression formation were reviewed and discussed. An inverse heat conduction code was developed to calculate mould heat flux from mould wall temperature measurements. The code proved to be a much faster tool for mould thermal analysis than the traditional trial-and error approach. Mathematical modelling of mould powder melting has led to a further understanding of the response of the molten flux pool to changes in powder properties, feeding strategies and casting speed. Finally, the understanding of mould thermal response and powder behaviour acquired allowed recommendations for further improvement in the casting process to be made.

8.1 Summary of Tasks Undertaken

1. An instrumented-mould trial was carried out to measure mould wall temperatures, mould displacement, metal level, casting speed, mould powder consumption, mould powder temperature profile and acquire billet samples. Because of electronic failure of the stepped-down voltage circuit for the metal level control signal, metal level was not properly recorded. Also, key thermocouples placed at the meniscus region and the water thermocouples failed completely. The lack of metal level and water temperature

data was partly overcome by substituting them with data collected manually from the casting machine control panel. During the trial two different mould powders, mould cooling-water velocities, oscillation frequencies and steel grades were tested.

2. An inverse heat conduction model of the mould wall was developed to determine mould heat flux from measured mould wall temperatures. The inverse code developed was used to determine steady-state mould heat flux, and mould cold- and hot-face temperatures profiles from mould wall time-average temperature. Also, a mathematical model of powder melting was developed to analyze the influence of mould powder properties and feeding strategies on its melting behaviour.
3. An existing mathematical model of billet shrinkage was utilized to investigate mould-billet binding. Strand shell thickness and billet shrinkage were calculated and optimum mould taper proposed.
4. The surface quality of billet samples was evaluated by visual inspection. The surface profile of the samples was measured using a profilometer featuring three LVDT's. Oscillation mark depth and surface defects found (transverse depression, rhomboidity and longitudinal depression) were linked to mould thermal response and mould powder properties.
5. The influence of process variables, namely type of mould powder, mould oscillation frequency, mould water velocity and steel grade, on mould wall temperature and mould heat flux was investigated.
6. Metal level was measured with a dip-stick and compared to values displayed by the metal level controller. Discrepancies between the two values were discussed and the inadequacy of the system in use to control metal level during casting with mould flux

lubrication was identified. Also, metal level fluctuations were indirectly investigated using signals from thermocouples located around the meniscus periphery. Similar analysis was performed for heats cast with oil lubrication, which showed that compared to powder, oil lubrication resulted in a more fluctuating metal level.

7. Results from the plant trial measurements, mathematical models and billet sample quality evaluation were used to compare mould powder and oil casting in terms of mould thermal response, transverse depression, rhomboidity, oscillation mark and mould level variation. Previously proposed mechanisms for oscillation marks and surface defects formation were discussed in the light of the differences in mould thermal response found between powder and oil lubrication. A major difference was found for Boron(Ti)-alloyed medium-carbon steel which was explained in terms of the role of TiN precipitates on the strength of the solidifying shell and mould powder behaviour.
8. The overall performance of the two powders used in the plant trial was evaluated in terms of mould thermal response, powder consumption and molten flux pool depth. Also, the response of the molten flux pool depth to casting speed changes was assessed.

8.2 Conclusions from Study

This work has led to a very comprehensive understanding of mould thermal response and mould-related quality problems in billet casting with powder lubrication. The following conclusions may be drawn from the mould heat transfer analysis and billet quality evaluation.

(i) The peak heat flux at the meniscus varies between 2200 and 3200 kW/m^2 (Figure 7.3) for peritectic steels (0.11≤%C≤0.14) as compared to values of 2500 kW/m^2 (Figure 7.10) for billet casting with oil lubrication; and between 2200 and 2700 kW/m^2 for Boron(Ti)-alloyed medium-carbon steels (0.30≤%C≤0.33) as compared to 4600~5200 kW/m^2 (Figures 7.11 and 7.12) for the same steel cast with oil lubrication.

(ii) Mould flux transition temperature is a more important parameter from the standpoint of controlling mould heat transfer than its viscosity. An increase of 13% in the flux transition temperature, from 1000°C (powder A) to 1135°C (powder B) was more prevalent to decrease mould heat flux than a decrease of 42% in viscosity, from 0.7 poise (powder A) to 0.4 poise (powder B), which is in accordance with the findings of Emi et al.[40]. For peritectic steels (heats 262, 265, 277 and 281) powder A resulted in average heat fluxes ~18% higher than powder B. For Boron(Ti)-alloyed steels (heats 311 and 314) powder A resulted in average heat fluxes ~7% higher than powder B.

(iii) Average mould heat flux was found to be 8% higher for a mould oscillation frequency of 170 cpm when compared to 150 cpm (Figure 7.3). The increase in heat flux with increasing frequency is caused by the consequent decrease in negative strip-time which leads to shallower oscillation marks and lower powder consumption. Both factors contribute to narrowing the gap between the mould and the strand and therefore diminishes the thermal resistance between the two.

(iv) Small increases in mould heat flux, between 3 and 10 %, were observed when mould water velocity was dropped from 9.9 to 7.6 m/s during casting of peritectic

steels ($0.11 \leq \%C \leq 0.14$), Figure 7.4. This is thought to be caused by a decrease in the slag rim (solidified mould flux) due to a hotter mould wall, therefore decreasing the thermal resistance in the mould/strand gap. For Boron(Ti)-alloyed steels ($0.30 \leq \%C \leq 0.33$) no definitive trend was observed. On the other hand, as expected, significant increase in mould temperature was observed when the mould water velocity was reduced (Figure 6.8); This is undesirable from the standpoint of mould distortion and boiling of water in the cooling channel adjacent to the cold face. However, in all cases investigated, no boiling took place due to the inherently lower values of heat flux for powders compared to oil. Therefore the mould was always working "cold", so permanent mould distortion was not an issue.

(v) Steel carbon content has a measurable influence on mould heat flux; however the influence of the carbon content is also governed by the type of lubricant. In general it was found that for a 0.11 pct. carbon steel the mould heat flux was lower than either 0.14 pct. or 0.33 pct. carbon (Figure 7.5). However, a striking result is that Boron(Ti)-alloyed medium-carbon steels exhibit lower heat flux than plain carbon steel with 0.14 pct. carbon. This result becomes still more significant when compared to[110,127] boron steels cast with oil where heat flux values are at least 50% higher than the values obtained in this investigation for powder casting.

Quality evaluation of the billets samples has shown billets with very well-defined oscillation marks, i.e. regularly spaced and straight (Figure 6.12), very little transverse depressions, very low levels of rhomboidity but a high incidence of longitudinal depressions. This is a significant improvement in quality compared to the same steel grades cast with oil which are plagued by transverse depressions. The billet shrinkage model has shown that

binding was occurring in all heats analyzed, which revealed the inadequacy of the mould taper, which had been designed for oil casting, to the new casting conditions, i.e., mould flux lubrication. The following is a summary of the main findings regarding billet quality evaluation and mould/strand interaction.

(i) The majority of the longitudinal depressions found had depths below 3 mm but some reached values of 5 mm (Figure 6.13); they were located preferably along the mid-faces of the billets or at the north corner of the billet west face

(ii) Measurement of oscillation mark depth shows that increasing oscillation frequency from 150 to 170 cpm results in shallower oscillation marks which agrees with results from Howe and Stewart[93]. Also, the measurements confirmed the influence of carbon content on oscillation mark depth; peritectic steels ($0.11 \leq \%C \leq 0.14$) exhibited deeper oscillation marks, 0.67 mm for an oscillation frequency of 150 cpm and 0.53 for 170 cpm, while medium-carbon steels had an average oscillation mark depth of only 0.34 mm (Figure 6.16).

(iii) Calculations showed that peritectic steels ($0.11 \leq \%C \leq 0.14$) were supposedly binding approximately half-way down the mould, between 300 to 500 mm from the top of the mould (Figure 7.8), while binding was beginning just below the meniscus for the Boron(Ti)-alloyed medium-carbon grade (Figure 7.9). Boron(Ti)-alloyed medium-carbon steel presents a higher degree of binding because medium-carbon ($0.30 \leq \%C \leq 0.33$) has a lower liquidus temperature and wider solidification range compared to peritectic steels; thus under the same casting conditions the shell is thinner resulting in less shrinkage. Binding results obtained through mathematical model were not corroborated by the presence of surface defects

associated with sticking of the solid shell to the mould, such as laps and bleeds. However, all samples exhibited longitudinal depressions; this indicates that the taper was excessive for these grades. The mould squeezes on the thin solid shell causing it to buckle inward which generates longitudinal depressions.

(iv) The potential for significant binding in all heats of Boron(Ti) medium-carbon steels revealed the inadequacy of using a mould taper originally designed for oil casting. It also shows the difficulty of using one optimum taper for all steel grades. Therefore, taking into account that there is no optimum mould taper that can match the shrinkage of peritectic and medium-carbon steels at the same time, a double mould taper with 1.8% m^{-1} up to 450 mm from the mould top and 0.9% m^{-1} for the rest of the mould is the best compromise.

A major finding of this investigation was the absence of transverse depression typically found on billets cast with oil and the low values of mould heat flux obtained for the Boron(Ti)-alloyed medium-carbon steels. The following conclusions may be drawn from the comparative analysis of powder and oil casting.

(i) There is no significant difference in mould heat flux for peritectic steels ($0.11 \leq \%C \leq 0.14$) if either flux or oil is used as lubrication (Figure 7.10). On the other hand, for Boron(Ti)-alloyed steels ($0.30 \leq \%C \leq 0.333$)the peak heat flux values obtained with flux lubrication, ~ 2300 kW/m^2, are about half the peak values obtained with oil, ~ 5000 kW/m^2 (Figure 7.11). Overall average mould heat fluxes obtained with oil lubrication are 20 to 50% higher than mould heat fluxes obtained with powder lubrication.

(ii) The remarkable difference in mould heat-flux between oil and powder lubrication for boron grades (medium-carbon:0.30≤%C≤0.33) contrary to a much less pronounced effect for peritectic steels (low-carbon:0.10≤%C≤0.14) agree with previous findings reported by Singh and Blazek[126] and discussed by Chandra[109]. Peritectic steels solidify with a rather rippled surface on account of the δ to γ transformation that takes place in the meniscus region. This rippled surface leads to large gaps between the mould and the strand. During oil casting of peritectic steels the larger mould/strand gap formed during the solidification process is not completely filled by oil since most of the it vaporizes and escapes within a narrow distance from the meniscus; thus the gap is filled by nitrogen which has a low thermal conductivity resulting in very low mould heat-transfer. The filling of these large gaps by molten flux alters the effective thermal conductivity of the gap. Actually, replacing oil with molten flux can slightly increase the heat flux or have no effect depending of the effective thermal conductivity of the gap compared to that of the mould flux used. Mould taper is also a factor since it largely determines the dimensions of the mould/strand gap.

(iii) Boron steels (0.30≤%C≤0.33), on the other hand have a smooth surface and the mould/strand gap is smaller. When oil is used as lubricant the mould heat transfer is much higher than low-carbon steels (0.10≤%C≤0.14). However, when mould flux replaces oil the former fills the gap thoroughly and acts as an insulator between the mould and the strand, thereby decreasing heat transfer.

(iv) Results of high temperature tests performed at 1300°C on a Gleeble® machine (Figure 7.13) showed that medium-carbon steels containing boron and titanium has

a strength ~ 30% higher than plain medium-carbon steel. This result strongly supports the belief that TiN precipitation does increase the strength of the strand shell and must be the cause of a higher susceptibility to transverse depression displayed by Boron(Ti)-alloyed medium-carbon steels. Precipitation of TiN increases the steel's coherency temperature to a temperature slightly below the solidus temperature, making the shell strong enough to resist flattening by ferrostatic pressure after it is bent away from the mould under the action of any thermal and/or mechanical stresses.

(v) Transverse depressions are formed in steel grades with high coherency temperature (ultra-low carbon, peritectic-carbon or Boron(Ti)-alloyed medium-carbon steels) due to metal level fluctuation. For Boron(Ti)-alloyed medium-carbon steel cast with powder transverse depressions were eliminated due to a substantial decrease in meniscus heat flux, thus producing a thinner, hotter, more flexible shell, and also due to lower metal level fluctuations on account of pouring with SEN. For peritectic steels, although transverse depression was not totally eliminated by replacing oil with mould powder, a drastic reduction of these defect was obtained due to the use of SEN which reduces metal level fluctuation and possibly also to elimination of oil entrapment and mould/strand binding which tend to aggravate the defect.

(vi) Thermodynamics analysis of the formation of TiN and BN in low-alloy steels elucidated the precipitation of these nitrides before and during initial solidification. The analysis showed that (a) precipitation of BN does not occur in the liquid steel; (b) for a typical boron steel, more than ~40% of the N is precipitated as TiN in the

interdendritic liquid before the start of solidification; (c) to avoid any precipitation of TiN in the liquid steel the nitrogen content of the steel must be kept below 60 ppm and the titanium content below 0.019%. The virtual elimination of transverse depression simply by replacing oil with mould powder excludes nitrogen control as imperative for powder casting; however, for oil casting practice to control nitrogen and titanium contents below the levels recommended above might be the only way of producing transverse-depression-free boron-billets.

(vii) Preliminary results showed that similar to oil casting, transverse depressions also can be monitored by thermocouples during billet casting with mould flux (Figure 7.16). However, further investigation is still needed.

Likewise for transverse depression, also a very comprehensive comparison between oil and powder casting with respect to rhomboidity, oscillation marks and metal level fluctuations was carried out. The following observations and conclusions are of importance.

(i) For peritectic steel (~0.12%C), rhomboidity is not significant for both oil and powder lubrication; all samples had rhomboidity below 6 mm (Figure 7.17). For medium-carbon steel containing boron and titanium alloyed ($0.30 \leq \%C \leq 0.33$; $0.0023 \leq \%B \leq 0.0027$; $0.035 \leq Ti \leq 0.038$), the severity of rhomboidity is significantly lower for billets cast with mould powder; for powder casting 90% of the samples had rhomboidity below 6 mm, while for oil 33% had rhomboidity above 6mm. For billets cast with powder lubrication the extent of rhomboidity is dependent on both the maximum temperature difference among the mould four faces and the heat flux level.

(ii) Compared to oil, mould-flux lubrication results in deeper oscillation marks. Billets of Boron(Ti)-alloyed medium-carbon steel (~0.32%C) cast with oil have very shallow oscillation marks, less than 0.2 mm deep; however, the presence of transverse depressions as large as 50 mm wide and 2.2 mm deep are commonly found in surface profile measurements (Figure 7.20). Comparatively, no transverse depressions were found for the boron steels cast with powder, but oscillation mark depth is deeper, with an average value of 0.31 mm. The above results substantiate the main role of mould flux on oscillation mark formation as predicted by Takeuchi and Brimacombe[56] by means of a mathematical model. Well defined and deep oscillation marks were found even in heats cast with mould superheat 16°C above the value predicted by Saucedo et al.[137] as the value above which meniscus freezing is suppressed, therefore unequivocally demonstrating that when mould flux is used it plays a more important role in oscillation mark formation than meniscus freezing.

(iii) Three different types of temperature variation were found in the data-files collected during the trial (powder lubrication). The first type was identified as a short-range variation with amplitude of ~ ± 10°C caused by electrical noise (Figure 7.21). The second type was a mid-range fluctuation with amplitude varying from 20°C to 50°C (Figures 7.22 and 7.23). The last type was a permanent temperature change caused by an intentional change in the mould level set-point (Figure 7.24). The mid-range temperature fluctuation was assumed to be caused mainly by metal level changes and it was found that for low-carbon as well as boron grades the magnitude and frequency of these fluctuations were comparable.

(iv) Oil lubrication resulted in twice as many temperature fluctuations than powder lubrication. This is believed to be caused by the more turbulent meniscus due to gas entrainment by the open-pour tundish stream entering the mould. On the other hand the fluctuations observed in powder lubrication had bigger amplitude, thought to be caused by improper calibration of the mould level control system. To fully take advantage of the benefits of casting with powder lubrication and SEN the radioactive sensor must be adjusted for the process, also the system should have liquid-metal flow as the control variable instead of casting speed. Having casting speed as the control variable leads to an inherently unsteady-state operation

Mathematical modelling of powder melting has led to further understanding of the effect of powder properties on the molten pool depth and to recommendations on choosing powder for billet casting. Also, measurement of mould powder consumption and molten flux pool depth showed the inadequacy of the mould powders used at the time of the plant trial. The following observations and conclusions are of importance.

(i) Sensitivity analysis (Figures 4.10 to 4.12) of the powder melting model showed that the depth of the mould-flux pool: (a) increases with increasing the amount of powder until the powder layer reaches 35~ 40 mm, above these values the pool depth becomes insensitive to further increases in powder height; (b) varies very little with the temperature of the steel and the enthalpy of fusion of the powder; (c) is strongly dependent on the mould-flux liquidus temperature, powder density, powder thermal conductivity and convection in the liquid pool and through the porous layers of powder; (d) decreases with the increase of powder consumption and casting speed, although for a given powder it is impossible to increase casting

speed without decreasing consumption. The above results match reasonably well with those of the models of Goldschmit et al.[55] and McDavid and Thomas[148]. All of them agree upon the strong influence of powder "melting" temperature and consumption rate on the liquid flux pool depth. Also, that as the total powder layer increases its effect on the depth of the liquid flux layer lessens.

(ii) Powder consumption, given as amount of powder consumed per lateral area of billet produced, was 0.45 kg/m^2 for powder A and 0.53 kg/m^2 for powder B. This was found to be higher than values reported for slab casting under comparable casting conditions (0.26 ~ 0.38 kg/m^2). As expected, powder B, a lower viscosity flux, resulted in higher consumption.

(iii) Measured (1~3 mm) and calculated values (~4 mm) of molten pool depth were extremely low, below the minimum recommended, i. e., below the mould oscillation stroke (6 mm). The main reason for the shallow molten flux pool is thought to be an imbalance between both powders high consumption and their melting rate, aggravated by an irregular distribution of powder in the mould. The above result showed the importance of choosing a powder with a high enough melting rate for billet casting. Powders used for slab casting, the ones used in the plant, will not necessarily perform as well for billets. Because of a much higher perimeter/area ratio, billet casting results in higher specific consumption (kg per tone of steel) than slab casting and requires powders with higher melting rates.

(iv) Simulations conducted to test the response of the mould-flux pool to casting speed changes agreed with plant trial observation by Riboud and Larrecq[21]. Contrary to what was suggested by Riboud and Larrecq[21] the time lag between changes in

casting speed and powder consumption is by far the major contributor for an initial decrease in the mould-flux pool when casting speed is increased. Subsequently the liquid pool rebounds to a level higher than the initial because powder consumption decreases.

8.3 New Knowledge and Major Contribution

The present investigation can be considered the first comprehensive study on mould thermal response and billet quality during billet casting with mould-flux lubrication. The data generated, which consists of mould wall temperature profiles, mould heat-fluxes, strand solidification, shrinkage, mould/strand gap, billet surface profiles, rhomboidity, mould-powder consumption, mould-flux pool depth and actual metal level constitute a very comprehensive body of knowledge never assembled before. Also, the explanations presented for the singular behaviour of Boron(Ti)-alloyed medium-carbon steels is a major part of the new knowledge generated from the present study.

Besides the data itself, the data analysis presented some novelty as the use of an inverse heat conduction code; it seems to be the first time that a 2-D inverse heat conduction model has been developed to estimate mould heat-flux during continuous casting of steel billets.

The most significant contributions of this work are:

1. Links between process variables such as steel grade, oscillation frequency, mould-flux type, mould temperature and mould heat-flux, and billet quality aspects such as oscillation marks, rhomboidity, transverse depression and longitudinal depression were established. Also, links between mould-flux properties and mould-flux behaviour in terms of consumption and flux pool depth were established.

2. The elimination of transverse depression in Boron(Ti)-alloyed medium carbon steel cast with mould-flux was explained in terms of mould heat-flux, metal level variation and the steel's coherency temperature.
3. The inadequacy of the mould powders used in the plant was discussed and guidelines to help choose mould-fluxes for billet casting were given. Also, The inadequacy of the mould taper was discussed and suggestion for improvement was given.

8.3.1 Recommendations for a better casting operation

A review of the casting practices in use at the mini-mill were the plant trial was carried out strongly suggests that for its improvement the following points should be considered.

1. Put an automatic liquid steel flow control system. The metal level controller should act upon a metering device (stopper rod or sliding-gate). Casting speed must be kept stable
2. Replace oil with mould-flux whenever economically and technically possible.
3. Be careful in choosing mould-fluxes, consider: viscosity (affects heat flux and powder consumption), break-point or transition temperature (affects heat-flux and friction), melting rate (a function of melting temperature and free-carbon); and powder consumption and melting rate determines the depth of the mould-flux pool.
4. Check if the radioactive-sensor/level-controller is capable to distinguish mould-flux from liquid steel.

5. If oil casting is the only option be sure to control metal level via flow control and for Boron(Ti)-alloyed medium-carbon steel to keep nitrogen content below 60 ppm and titanium below 0.019%.

8.4 Suggestions for Future Work

As a first comprehensive work on billet casting with mould-flux lubrication the present study open up several possibilities of future work. The findings of the present study clearly showed the advantages in replacing oil with mould powder, but also highlighted the inadequacy of the powders been used in the plant. It is essential to evaluate mould-flux performance in billet casting for a wider range of mould-fluxes. This only can be accomplished by industrial trials of the same nature as the one conducted in the present investigation, however it would be advised to work with mould taper appropriated for powder casting in order to avoid longitudinal depression. The recommendations outlined in the present study can be used as guidelines for a proper choice of taper.

A more extensive investigation involving mould thermal monitoring and billet surface inspection is needed to consolidate the possibility of monitoring transverse depression and rhomboidity during cast with mould-flux lubrication, also similar study should extend to the analysis of longitudinal depression.

The modelling of mould powder melting exposed the paucity of data on powder properties. This is a very broad research field that needs to be tackled; viscosity, thermal conductivity of the several mould-flux phases and transformation temperatures such as solidus, liquidus, sintering and crystallization are all needed but unfortunately not available.

The powder melting model itself can be improved by extending it to 2-D, which would include the SEN and mould wall as two new boundaries.

The inverse heat transfer code developed could be extended to include higher order regularization terms which would give more flexibility in characterizing the heat-flux profiles. Also, the inverse heat conduction model can be used to investigate optimum thermocouple layout for future plant trials.

Bibliography

[1] K.C.Mills, "A review of ECSC-funded research on mold flux", NPL Report DMM(A)10, Teddington, UK, 1990

[2] J.A.Moore, R.J.Phillips and T.R.Gibbs, "An overview for the requirements of continuous casting mold fluxes", Steelmaking Conference Proceedings, ISS-AIME, 1991, pp.615-621

[3] H.F.Schrewe, **Continuous Casting of Steel**: Fundamental Principles and Practice, Verlag Stahleisen, Germany, 1987, pp. 132-137

[4] **Continuous Casting Vol.1**: Chemical and Physical Interaction During Transfer Operations, Iron & Steel Society, Warrendale, PA, 1983, pp. 113-122

[5] J.Sadermann and H.Schrewe, "The influence of casting powder on the formation of cracks in continuous slab casting", Steelmaking Conference Proceedings, ISS-AIME, 1991, pp. 719-728

[6] T.Emi, H.Nakato, Y.Iida, K.Emoto, R.Tachibana, T.Imai and H.Bada, "Influence of physical and chemical properties of mold powders on the solidification and occurrence of surface defects of strand cast slabs", **In**: **Continuous Casting vol. 1**, ISS-AIME, 1983, pp. 135-15

[7] R.V.Branion, "Mold fluxes for continuous casting", I&SM, Sept. 1986, pp. 41-50

[8] K.C.Mills, A.Olusanya, R.Brooks, R.Morrel and S.Bagha, "Physical properties of casting powders: Part 4 physical properties relevant to fluid and thermal flow", Ironmaking and Steelmaking, n.5, 1988, pp. 257-264

[9] M.D.Lanyi and C.J.Rosa, "Casting fluxes: physical properties affecting strand lubrication", Ironmaking and Steelmaking, n.1, 1982, pp. 25-31

[10] P.V.Riboud, Y.Roux, L-D.Lucas and H.Gaye, "Improvement of continuous casting powders", Fachberichte Hütteenpraxis Metallweiterverarbeitung, n.10, 1981, pp. 859-869

[11] Y.Matoba, T.Yamamoto, M.Tokuda, T.Watanabe and H.Tomono, "Instrumentation and control technology for supporting high speed casting", 9th Conference Proceedings, ISS-AIME, 1990, pp. 101-109

[12] K.C.Mills, "An overview of ECSC-funded research on casting powders", 1st European Conference on Continuous Casting, Florence, Sept. 1991, pp. (1).59-72

[13] I.R.Lee, J.W.Kim, J.Choi, O.D.Kwon and Y.K.Shin, "Development of mold flux powder for high speed continuous casting", Conference on Continuous Casting of Steel in Developing Countries, The Chinese Society for Metals, Beijing, 1993, pp. 814-822

[14] R.Bommaraju, "Optimum selection and application of mold fluxes for carbon steel", Mold Operation for Quality and Productivity, Iron & Steel Society, Warrendale, PA, 1991, pp. 95-110

[15] H.Nakato, T.Sakuraya, T.Nozaki, T.Emi and H.Nishikawa, "Physical and chemical properties of casting powders affecting the mold lubrication during continuous casting", Mold Powders for Continuous Casting and Bottom Pour Teeming, Iron & Steel Society, Warrendale, PA, 1987, pp.23-29

[16] K.Koyama, K.Nagano, Y.Nagano and T.Nakano, "Design for chemical and physical properties of continuous casting powders", Nippon Steel Technical Report, n.34, July 1987, pp. 41-47

[17] W.L.McCauley & D.Apelian, "The role of slags in steelmaking continuous casting mold fluxes", I&SM, Dec. 1983, pp. 42-43

[18] T.Nakano, T.Kishi, K.Koyama, T.Komai and S.Naitoh, "Mold powder technology for continuous casting of aluminum-killed steel", Trans. ISIJ, vol. 24, 1981, pp. 950-956

[19] R.Scheel & W.Korte, "Effect of different flux powder composition on continuous casting slags and casting practice", MPT, n.6, 1987, pp. 22-33

[20] W.L.McCauley & D.Apelian, "Viscosity characteristics of continuous casting mold fluxes", Canadian Metallurgical Quartely, vol.20, n.2, 1981, pp. 247-262

[21] P.V.Riboud and M.Larrecq, "Fundamental study of the behaviour of casting powders", Report EUR 9560, ECSC Contract 7210 ca/131/311/810,1985, pp. D10-D22

[22] P.V.Riboud and M.Larrecq, "Lubrication and heat transfer in a continuous casting mold", The Theory and Practice of Mold Fluxes Used in Continuous Casting, Iron & Steel Society, Warrendale, PA, 1981, pp. 54-68

[23] H.Kyoden, T.Doihara, and O.Nomura, "Development of mold powders for high speed continuous casting of steel", Mold Powders for Continuous Casting and Bottom Pour Teeming, Iron & Steel Society, Warrendale, PA, 1987, pp. 45-57

[24] K.Yoshida, T.Watanabe, H.Nakajima, K.Takatani, M.Tokuda and A.Satoh, "Controlling technology for solidification of continuously cast slabs in moulds", 9th PTD Conference Proceedings, ISS-AIME, 1990, pp. 183-191

[25] K.Sorimachi, M.Kuga, M.Saigusa and T.Sakuraya, "Influence of mould powder on breakout caused by sticking", Fachberichte Hütteenpraxis Metallweiterverarbeitung, vol. 20, n.4, 1982, pp. 244-247

[26] S.H.Chang, I.J.Lee, M.R.Kim, S.M.Yang, J.Choi and J.S.Park, "Developments of new mold fluxes at Pohang Works", Conference on Continuous Casting of Steel in Developing Countries, The Chinese Society for Metals, Beijing, 1993, pp. 832-841

[27] K.Sorimachi, H.Yamanaka, M.Kuga, H.Shikata and M.Saigusa, "Crystallization of mould powder affecting quality of strand cast slabs", Modelling of Casting & Welding Process II, MS-AIME, 1983. pp. 369-375

[28] I.G.Saucedo, "Improving the casting conditions at the meniscus", Steelmaking Conference Proceedings, ISS-AIME, vol. 70, 1987, pp. 449-459

[29] T.Sakuraya, T.Emi, K.Emoto, and T.Koshikawa, "Development of mold fluxes for high speed strand casting of slabs free from surface conditioning", 2nd Process Technology Conference, ISS-AIME, 1981, pp. 141-147

[30] I.R.Lee, J.Choi, K.Shin, O.D.Kwon and D.K.Choo, "Optimization technology of mold powder according to casting conditions", Steelmaking Conference Proceedings, ISS-AIME, 1988, pp. 175-181

[31] American Iron and Steel Institute. **Survey of Ten Mold Powder Suppliers**. Metallurgical Subcommittee on Strand Casting, 1993

[32] K.C.Mills, "Physical properties of casting powders, Part 1: Scheme to represent chemical composition of powders", Ironmaking and Steelmaking, vol. 15, n.4, 1988, pp. 175-180

[33] I.Jimbo, B.Ozturk, F.Feldbauer and A.W.Cramb, "Some aspects of chemical phenomena in the mold of a continuous slab caster", Mold Operation for Quality and Productivity, Iron & Steel Society, Warrendale, PA, 1991, pp. 117-126

[34] P.V.Riboud, M.Olette, J.Leclerc and W.Pollak, "Continuous casting slags: Theoretical analysis of their behaviour and industrial performance", **In**: **The Theory and Practice of Mold Fluxes Used in Continuous Casting**, ISS-AIME, 1981, pp. 13-19

[35] T.T.Do and K.W.Lange, "Absorption of alumina by continuous casting powders" Steel Research, vol. 57, n.9, 1986, pp. 444-451

[36] M.Kaviany. **Principles of Heat Transfer in Porous Media**. Spring-Verlag, New York, USA, 1991, Ch. 3&4, pp. 115-229

[37] A.R.Balakrishnan and D.C.T.Pei, "Heat transfer in gas-solid packed bed systems, 2: The conduction mode" Ind. Eng. Chem. Process Des. Dev., vol. 18, n.1, 1979, pp. 40-46

[38] A.R.Balakrishnan and D.C.T.Pei, "Heat transfer in gas-solid packed bed systems, 3: Overall heat transfer rates in adiabatic beds" Ind. Eng. Chem. Process Des. Dev., vol. 18, n.1, 1979, pp. 47-50

[39] R.Taylor and K.C.Mills, "Physical properties of casting powders, Part 3: Thermal conductivity of casting powders", Ironmaking and Steelmaking, vol. 15, n.4, 1988, pp. 187-194

[40] M.Emi, "The mechanisms for sticking type breakout and new developments in continuous casting mold fluxes, Steelmaking Conference Proceedings, ISS-AIME, 1991, pp. 623-630

[41] H.Nakato, S.Takeuchi, T.Fujii, T.Nozaki and M.Washio, "Characteristics of new mold fluxes for strand casting of low carbon and ultra low carbon steel slabs", Steelmaking Conference Proceedings, ISS-AIME, 1991, pp. 639-646

[42] H.T.Tsai, W.J.Sammon and D.E.Hazelton, "Characterization and countermeasures for sliver defects in cold rolled products", Steelmaking Conference Proceedings, ISS-AIME, 1990, pp. 49-59

[43] H.Y.Sohn and P.C.Chaubal," Heat and mass transfer in fluid-solid reaction and reactors", In: **Advanced in Transport Process in Metallurgical Systems**, Elsevier, Amsterdam, 1992, pp. 28-32

[44] H.Lidefelt and P.Hasselström, "Characterization of the functional properties of mould powders for continuous casting of steel", Continuous Casting: 4th International Iron and Steel Congress, The Metals Society, London, 1982, pp. 10/1-10/9

[45] Y.Tsukagushi, S.Ura, A.Shiraishi, Y.Hitomi and T.Nagahata, "Development of slab casting technology for high carbon steel", Steelmaking Conference Proceedings, ISS-AIME, 1993, pp. 397-403

[46] S.Ogibayashi, T.Mukai, Y.Mimura, Y.Nagano, K.Yamaguchi, T.Takahashi, K.Koyama and T.Nakano, "Mold powder technology for continuous casting of low-carbon aluminum-killed steel", Nippon Steel Technical Report, n.34, July 1987, pp. 1-10

[47] T.Nakano, K.Nagano, N.Masuo, M.Fuji and T.Matsuyama, "Model analysis of melting process of mold powder for continuous casting of steel", Nippon Steel Technical Report, n.34, July 1987, pp. 21-30

[48] B.Xie, J.Wu and Y.Gan, "Study on amount and scheme of carbon mixed in CC mold fluxes", Steelmaking Conference Proceedings, ISS-AIME, 1991, pp. 647-651

[49] A.Delhalle, M.Larrecq, J.F.Marioton and P.V.Riboud, "Slag melting and behaviour at meniscus level in a CC mold", Mold Powders for Continuous Casting and Bottom Pour Teeming, Iron & Steel Society, Warrendale, PA, 1987, pp. 15-22

[50] C.Niggel and E.Felder, "Lubrication by slags of the continuous casting of steel", **Report EUR 9339, Contract EEC-1-117-F**, 1985

[51] M.Kawamoto, H.Nakajima, T.Kanazawa and N.Nakai, "Melting mechanism of mold powder for continuous casting", Steelmaking Conference Proceedings, ISS-AIME, 1992, pp. 389-396

[52] Y.Nakamori, O.Ichiko, Y.Mimura, K.Yamaguchi and M.Ota, "Measurement of molten powder thickness in continuous casting mold by Eddy current method", Trans. ISIJ, v.25, 1985, pp. 50-53

[53] D.J.Harris, B.A.Otterman, B.T.Sellers and J.D.Young, "Development of casting practice for defect-free steel", Steelmaking Proceedings, ISS-AIME, 1987, pp. 145-152

[54] H.T.Tsai and J.C.Mastervich, "Influence of mold powder on breakouts at Inland Steel's No.2 Slab Caster", Steelmaking Conference Proceedings, ISS-AIME, 1988, pp. 167-173

[55] M.B.Goldschmit, J.C.González and E.N.Dvorkin, "Finite element model for analyzing liquid slag development during continuous casting of round bars", Ironmaking and Steelmaking, vol. 20, n.5, 1993, pp. 379-385

[56] E.Takeuchi and J.K.Brimacombe, "The formation of oscillation marks in the continuous casting of steel slab", Metallurgical Transactions B, vol. 15B, 1984, pp. 493-509

[57] K-I.Tada, J.P.Birat, P.Riboud, M.Larrecq and H.Hacke, "Modeling of slag rim formation and pressure in molten flux near the meniscus", Trans. ISIJ, vol. 24, 1984,p. B-382

[58] E.Anzai, T.Shigezumi, T.Nakano, T.Ando and M.Ikeda, "Hydrodynamic behavior of molten powder in meniscus zone of continuous casting mold", Nippon Steel Technical Report, n.34, July 1987, pp. 31-40

[59] T.Wada, M.Suzuki and T.Mori, "High speed casting of 3.0m/min. at NKK Fukuyama No.5 slab caster", Steelmaking Conference Proceedings, ISS-AIME, 1987, pp. 197-204

[60] M.M.Wolf, "Mold oscillation guidelines", Steelmaking Conference Proceedings, ISS-AIME, 1991, pp. 51-71

[61] M.Suzuki, H.Mizukami, T.Kitagawa, K.Kawakami, S.Uchida and Y.Komatsu, "Development of a new mold oscillation for high-speed continuous casting of steel slabs", ISIJ International, vol. 31, n.3, 1991, pp. 254-261

[62] O.D.Kwon, J.Choi, I.R.Lu, J.W.Kim, K.H.Moon and Y.K.Shin, "Optimization of mold oscillation pattern for the improvement of surface quality and lubrication in slab continuous casting" Steelmaking Conference Proceedings, ISS-AIME, 1991, pp. 561-568

[63] Y.Nuri, T.Ohashi, N.Miyasaka, K.Shima and Y.Uchida, "A consumption behavior of powder during continuous casting", Trans. ISIJ, vol. 20, n.5, 1980, B170-172

[64] M.M.Wolf, "On the interaction between mold oscillation and mold lubrication", Proceedings of AIME Electric Furnace Conference, 1982, pp. 335-346 or Mold Powders for Continuous Casting and Bottom Pour Teeming, Iron & Steel Society, Warrendale, PA, 1987, pp. 33-44

[65] H.Yasunaka, T.Mori, H.Nakata, F.Kamei and S-I.Harada, "Improvement of surface quality of continuous casting steel by high cycle mold oscillation", Mold Powders for Continuous Casting and Bottom Pour Teeming, Iron & Steel Society, Warrendale, PA, 1987, pp. 61-66

[66] H.Nakato, T.Nozaki, Y.Habu, H.Oka, T.Ueda, Y.Kitano and T.Koshikawa "Improvement of surface quality of continuous casting slabs by high frequency mold oscillation", Steelmaking Proceedings, ISS-AIME, 1985, pp. 361-365

[67] S.Takeuchi, Y.Miki, S.Itoyama, K.Kobayashi, K. Sorimachi and T.Sakuraya, "Control of oscillation mark formation during continuous casting", Mold Operation for Quality and Productivity, Iron & Steel Society, Warrendale, PA, 1991, pp. 37-41

[68] H.Mizukami, T.Kitagawa, A.Ozeki, K.Kawakami and Y.Tsuchida, "Development of a new oscillation mode and a new mould powder enabling HDR at Fukuyama No.5 speed slab caster", MacMaster Symposium No. 13: Requirement for hot charging of continuously cast products, Ed. by W-K Lu, MacMaster University, Canada, 1985

[69] H.L.Gilles, M.Byrne, T.J.Russo and G.A.DeMasi, "The use of an instrumented mold in the development of high speed slab casting", 9th PTD Conference Proceedings, ISS-AIME, 1990, pp. 123-138

[70] H.Nakato, S.Omiya, Y.Habu, T.Emi, K.Hamagami and T.Koshikawa, "Optimizing mold lubrication for high-speed continuous casting of slab", Journal of Metals, march, 1984, pp. 44-50

[71] T.Darle, A.Mouchette, M.Nadif, M.Roscine and D.Salvatori, "Hydraulic oscillation of the CC mold at Sollac Florange: first industrial results, future developments", Steelmaking Conference Proceedings, ISS-AIME, 1993, pp. 209-218

[72] G.J.W.Kor, "An analysis of the fluid flow of liquid mold powder in the space between the continuous casting mold and the steel shell", 2nd Process Technology Conference, ISS-AIME, 1981, pp. 124-132

[73] R.Bommaraju and E.Saad, "Mathematical modelling of lubrication capacity of mold fluxes", Steelmaking Conference Proceedings, ISS-AIME, 1990, pp. 281-296

[74] **Continuous Casting of Steel 1985** - A Second Survey. IISI, Brussels, Belgium, 1986, pp. 2.12-2.31

[75] P.J.Zasowski and D.J.Sosinski, "Control of heat removal in the continuous casting mould", Steelmaking Conference Proceedings, ISS-AIME, 1990, pp. 253-259

[76] W.H.Emling and S.Dawson, "Mold instrumentation for breakout detection and control", Steelmaking Conference Proceedings, ISS-AIME, 1991, pp. 197-217

[77] R.B.Mahapatra, J.K.Brimacombe, I.V.Samarasekera, "Mold behavior and its influence on quality in the continuous casting of steel slabs: Part II. Mold heat transfer, mold flux behavior, formation of oscillation marks, longitudinal off-corner depressions, and subsurface cracks", Metallurgical Transactions B, vol. 22B, December, 1991, pp. 875-888

[78] K.C.Mills, P.Grieveson, A.Olusanya and B.Bagha, "Effect of casting powder on heat transfer in continuous casting", Continuous Casting'85, The Metals Society, London, 1985, paper 57, pp. 57.1-57.7

[79] R.B.Mahapatra, B.T.Sellers and J.D.Young, "Influence of slab casting practice on mould heat transfer", Steelmaking Conference Proceedings, ISS-AIME, 1988, pp. 423-431

[80] M.R.Ozgu and B.Kocatulum, "Thermal analysis of the Burns Harbor No.2 slab caster mold", Steelmaking Conference Proceedings, ISS-AIME, 1993, pp. 301-308

[81] I.V.Samarasekera, "Mould Fluxes", Course notes, UBC, Vancouver

[82] J.K.Brimacombe, and K.Sorimachi, "Crack formation in the continuous casting of steel", Metallurgical Transactions B, vol. 8B, Sept. 1977, pp. 489-505

[83] M.Vereecke, W.Vermeirsch and U.Meers, "The influence of operational parameters on the surface quality of continuously cast slabs", 4th International Conference-Continuous Casting, ICC-StahlEisen, vol. 1, 1988, pp. 128-141

[84] J.K.Brimacombe, F.Weinberg and E.B.Hawbolt, "Formation of longitudinal, midface cracks in continuously-cast slabs", Metallurgical Transactions B, vol. 10B, June 1979, pp. 279-292

[85] R.Gray and H.Marston, "The influence of mould fluxes on casting operations and quality", Proceedings of the 2nd National Open Hearth and Basic Oxygen Steel Conference, ISS-AIME, 1979, pp. 93-102

[86] T.J.H.Billany, A.S.Normanton, K.C.Mills and P.Grieveson, "Surface cracking in continuously cast products", Ironmaking and Steelmaking, vol. 18. n.6, 1991, pp. 403-410

[87] H.Nakato, M.Ozawa, K.Kinoshita, Y.Habu and T.Emi, "Factors affecting the formation of shell and longitudinal cracks in mold during high speed continuous casting of slab", Transactions of ISIJ, vol. 24, 1984, pp. 957-965

[88] K.Hamagami, K.Sorimachi, M.Kuga, T.Koshikawa and M.Saigusa, "Studies on quality improvements in strand cast slabs at Chiba Works", Steelmaking Conference Proceedings, ISS-AIME, 1982, pp. 358-364

[89] S.G.Thornton, N.Hunter and B.Patrick, "Casting powder performance assessment in continuous casting by mould instrumentation", 3rd International Conference on Molten Slags and Fluxes, The Institute of Metals, 1989, pp. 32-36

[90] Y.Sugitani, M.Nakamura, M.Okuda, M.Kawasaki and K.Nakajima, "Effects of the mould surface conditions on uneven solidification and heat removal rate through the mould", Transactions ISIJ, vol. 25, 1985, B-91

[91] K.Nakai, M.Kawasaki, K.Nakajima, T.Sakashita and Y.Sugitani, "Improvement of surface quality of continuously cast slab by reducing heat flux density in mould", Continuous Casting '85, The Institute of Metals, London, 1985, paper 71

[92] J-P.Birat, M.Larrecq, J-Y.Lamant and J.Pétégnief, "The continuous casting mold: A basic tool for surface quality and strand productivity", Steelmaking Conference Proceedings, ISS-AIME, 1991, pp. 39-50 or Mold Operation for Quality and Productivity, Iron & Steel Society, Warrendale, PA, 1991, pp. 3-14

[93] A.Howe and I.Stewart, "Reduction of reciprocation marks by high frequency vibration of the continuous casting mould", Steelmaking Conference Proceedings, ISS-AIME, 1987, pp. 417-425

[94] H.Tomono, P.Ackermann, W.Kurz and W.Heinemann, "Element of surface mark formation in the continuous casting of steel", Solidification Technology in the Foundry and Cast House, The Metals Society, London, 1980, pp. 524-531

[95] A.Delhalle, M.Larrecq, J.Petegnief and J.P.Radot, "Control of the first shell formation during continuous casting of steel", 4th International Conference-Continuous Casting, ICC-StahlEisen, vol. 1, 1988, pp. 38-48

[96] I.G.Saucedo, "Early solidification during the continuous casting of steel", Mold Operation for Quality and Productivity, Iron & Steel Society, Warrendale, PA, 1991, pp. 43-53

[97] E.Takeuchi and J.K.Brimacombe, "Effect of oscillation-mark formation on the surface quality of continuously cast steel slabs", Metallurgical Transactions B, vol. 16B, 1985, pp. 605-625

[98] A.W.Cramb and F.J.Mannion, "The measurement of meniscus marks at Bethlehem Steel's Burns Harbor caster, Mold Powders for Continuous Casting and Bottom Pour Teeming, Iron & Steel Society, Warrendale, PA, 1987, pp. 83-93

[99] K.C.Mills, "The performance of casting powders", Steel Technology International, 1994, pp. 161-166

[100] S.Terada, S.Kaneko, T.Ishikawa and Y.Yoshida, "Research of substitution for carbon- Development of mold flux for ultra-low-carbon steel", Steelmaking Conference Proceedings, ISS-AIME, 1991, pp. 635-638

[101] H.Takeuchi, H.Mori, T.Nishida, T.Yanai and K.Mukunashi, "Development of a carbon-free casting powder for continuous casting of steel", Transactions ISIJ, vol. 19, 1979, pp. 274-282

[102] K.C.Mills, T.J.H.Billany, A.S.Normanton, B.Walker and P.Grieveson, "Causes of sticker breakouts during continuous casting", Ironmaking and Steelmaking, vol. 18, n.4, 1991, pp. 253-265

[103] M.J.Lu, K.J.Lin, C.H.Kuo and W.C.Chien, "Sticker breakout theory and its prediction in slab continuous casting", Steelmaking Conference Proceedings, ISS-AIME, 1993, pp. 343-353

[104] A.Tsuneoka, W.Ohashi, S.Ishitobi, T.Kataoka and M.Tenma, "Measurement and control system of solidification in continuous casting", Mold Powders for Continuous Casting and Bottom Pour Teeming, Iron & Steel Society, Warrendale, PA, 1987, pp. 75-82

[105] Y.Mimura, "Sticking-type breakouts during the continuous casting of steel slabs", Masters Thesis, University of British Columbia, 1989

[106] I. V. Samarasekera, J. K. Brimacombe, "The thermal field in continuous-casting moulds", Canadian Metallurgical Quartelly, vol.18, 1979, pp. 251-266

[107] I. V. Samarasekera, J. K. Brimacombe, "Thermal and mechanical behaviour of continuous-casting billet moulds", Iron and Steelmaking, vol.9, n.1, 1982, pp. 1-15

[108] R. B. Mahapatra, "Mould behaviour and product quality in continuous casting of slabs", Ph.D. Thesis, UBC, 1989

[109] S. Chandra, "Heat transfer, oil lubrication and mould tapere in steel billets casting machines", Ph.D. Thesis, UBC, 1992

[110] S. Kumar, "Mould Thermal Response and Formation of Defects in the Continuous Casting of Steel Billets", Ph.D. Thesis, UBC, 1996

[111] H. W. Wong, "Heat transfer analysis of the plasma spray deposition process", Ph.D. Thesis, UBC, 1997

[112] M. N. Ozisik, "Heat Conduction", 2nd. Ed., John Wiley & Sons, New York, 1993

[113] E. Hensel, "Inverse Theory and Applications for Engineers", Prentice Hall, New Jersey, 1991

[114] J. V. Beck, B. Blackwell, C. R. St.Clair, "Inverse Heat Conduction - Ill posed problems, John Wiley & Sons, New York, 1985

[115] J. V. Beck and B. Blackwell, "Inverse Problems", In: Handbook of Numerical Heat Transfer, Editor: W. J. Minkowycz et al., Wiley-Interscience, New York, 1988, pp. 787-834

[116] R. L. Burden and J. D. Faires, "Numerical Analysis", 5th Ed., PWS Publising Company, Boston, 1993

[117] S.C. Chapra and R. P. Canale, "Numerical Methods for Engineers", McGraw-Hill Publising Company, New York, 1988, pp. 728

[118] J. Szekely and N. J. Themelis, "Rate Phenomena in Process Metallurgy", Wiely-Interscience, New York, 1971

[119] Mikrovas, A.C., S. A. Argyropoulos and I. D. Sommerville, "Measurements od the effective thermal conductivity of liquid slags", Ironmaking and Steelmaking, vol. 18, n.12, 1991, pp. 51-61

[120] Turkdogan, E. T., "Fundamentals of Steeelmaking", The Institute of Material, 1996, The University Press, Cambridge, UK, pp.170-2

[121] S. Kumar, Plant Trial Internal Report, University of British Columbia, Vancouver, Canada, June, 1995

[122] J. K. Brimacombe, I. V. Samarasekera, N. Walker, I. Bakshi, R. Bommaraju, F. Weinberg and E. B. Hawbolt, "Mould behaviour and solidification in the continuous casting of steel billets, Part I - Industrial Trials", ISS Transactions, vol.5, 1984, pp. 71-77

[123] The Temperature Handbook, vol.28, Omega Engineering Inc., Stamford, CT, USA, 1992

[124] R. M. Gurton, "Mould response and its impact on billet quality", Ph.D. Thesis, UBC, 1997

[125] K. Wilder, Convert Manual, Centre for Metallurgical Process Engineering, University of British Columbia, Vancouver, Canada, 1993

[126] S. N. Singh and K. E. Blazek, "Heat transfer profiles in continuous casting mold as a function of various casting parameters", In Open Hearth Proc. AIME, vol.59, 1976, pp. 264-283

[127] Adjei-Sarpong, Mark, "Investigation of transverse depression formation during the continuous casting of steel using real-time mould thermal data", M.A.Sc. Thesis, UBC, 1994.

[128] I. V. Samarasekera, J. K. Brimacombe and R. Bommaraju, "Mould behaviour and solidification in the continuous casting of steel billets, Part II - Mould heat extration, mould-shell interaction and oscillation-mark formation", ISS Transactions, vol.5, 1984, pp. 79-94

[129] R. Bommaraju, J. K. Brimacombe and I. V. Samarasekera, "Mould behaviour and solidification in the continuous casting of steel billets, Part III - Structure, solidification bands, crack formation and off-squareness", ISS Transactions, vol.5, 1984, pp. 95-105

[130] J. L. Brendzy, I. A. Bakshi, I. V. Samarasekera and J. K. Brimacombe, "Mould-strand interaction in the continuous casting of steel billets, Part 2: Lubrication and oscillation mark formation", Ironmaking and Steelmaking, vol. 20, No. 1, 1993, pp.63-74

[131] M. S. Jenkins, B. G. Thomas, W. C. Chen and R. B. Mahapatra, "Investigation of strand surface defects using mold instrumentation and modelling", ISS-Steelmaking Conference Proceedings, v.77, 1994, Chicago.

[132] B. G. Thomas and H. Zhu, "Thermal distortion of solidifying shell near meniscus in continuous casting of steel", JIM/TMS Solidification Science and Processing Conference, Honolulu, December 1995, pp. 197-208

[133] J. Schruff, R. Klemp and J. Sardemann, "Dry casting of boron-and-titanium-alloyed steel grades on a billet caster", McMaster Symposium on Iron and Steelmaking No.16: Eletric Steelmaking and Billet Casting of Highly Deoxidized Steels, Editor: W-K. Lu, McMaster University, Hamilton, May, 1988, Canada

[134] I. V. Samarasekera, J. K. Brimacombe, H. M. Adjei-Sarpong, P. K. Agarwal, B. N. Walker and D. P. Lorento, "Basic knowledge for the intelligent continuous casting mould", Proceedinds of 2nd Canada-Japan Symposium on Modern Steelmaking and Casting Technique, 33rd Conference of Metallurgists, Metallurgical Society of CIM. Toronto, Canada, 1994, pp.169-187

[135] Turkdogan, E. T., "Causes and effects of nitride and carbonitride precipitation in HSLA steels in relation to continuous casting", ISS-Steelmaking Conference Proceedings, v.70, 1987, pp. 399-415

[136] L. Pochmarski, W. Engleitner and H. Neubauer, 'Operational practices for casting billets of different steel grades', Proceedings of the 6th International Continuous Casting Conference - CCC'93, Voest-Alpine Ind., May 24-26, 1993, Linz, Austria

[137] I. G. Saucedo, "Heat transfer and solidification kinetics in meniscus zone during casting", Metals Technology, vol.9, 1982, pp. 282-291

[138] J. F. Elliott, Physical Chemistry of Liquid Steel, In: Electric Furnace Steelmaking, Editor: Charles R. Taylor, Iron and Steel Society, 1985, Chapter 21, pp. 291-319

[139] B. Kielhorn, Private communication, University of British Columbia, Vancouver, Canada

[140] W. E. Meyerhof, "Elements of Nuclear Physics", McGraw-Hill, New York, 1967

[141] D. R. Poirier and G. H. Geiger, "Transport Phenomena in Materials Processing", TMS-The Minerals Metals &Materials Society, Warrendale, 1994.

[142] R.B.Mahapatra, J.K.Brimacombe, I.V.Samarasekera, N.Walker, E.A.Paterson and J.D.Young, "Mold behavior and its influence on quality in the continuous casting of steel slabs: Part I. Industrial Trials, Mold Temperature Measurements, and Mathematical ", Metallurgical Transactions B, vol. 22B, December, 1991, pp. 861-874

[143] I.V. Samarasekera, R. Bommaraju and J.K. Brimacombe, "Factors Influencing the Formation of Oscillation Marks in the Continuous Casting of Steel Billets", 24th Annual Conference of Metallurgists, Proc. Intl. Symp. on Continuous Casting of Billets, CIM, Vancouver, Canada, 1985, pp.33-58

[144] F. P. Incropera and D. P. Dewitt, "Introduction to Heat Transfer", 3rd Ed., John Wiley & Sons, New York, 1996, Chapter 8.

[145] J. P. Holman, "Heat transfer", 7th Ed., McGraw-Hill, New York, 1990, Chapter 6.

[146] K.E. Blazek. I.G. Saucedo and H.T. Tsai, "An investigation on mold heat transfer during continuous casting", Steelmaking Conference Proceedings, ISS-AIME, 1988, pp.411-421

[147] J. Konishi "Modelling of the formation of longitudinal facial cracks in the continuous casting of steel slabs", M.A.Sc. Thesis, UBC, 1996.

[148] R.M. mcDavid and B.G. Thomas, "Flow and thermal behaviour of the top surface Flux/powder layers in continuous casting molds", Metallurgical and Materials Transactions B, vol. 27B, August, 1996, pp. 672-689

APPENDIX A: Details of thermocouple layout

Table A1: Depth and axial position of thermocouples used to monitor mould wall temperature.

T/C identification - Distance from top of mould (mm) - Hole depth (mm)			
Mould East Face	**Mould North Face**	**Mould South Face**	**Mould West Face**
E1 - 095 - 7.81	N1 - 130 - 7.85	S1 - 130 - 8.02	W1 - 131 - 7.94
E2 - 131 - 7.79	N2 - 145 - 7.78	S2 - 145 - 7.80	W2 - 144 - 8.05
E3 - 145 - 7.77	N3 - 161 - 8.95	S3 - 161 - 7.79	W3 - 158 - 7.64
E4 - 160 - 7.78	N4 - 160 - 7.91	S4 - 160 - 7.96	W4 - 160 - 7.95
E5 - 161 - 7.74	N5 - 162 - 7.58	S5 - 160 - 7.81	W5 - 160 - 7.82
E6 - 162 - 7.74	N6 - 175 - 7.62	S6 - 173 - 7.92	W6 - 175 - 8.19
E7 - 174 - 7.70	N7 - 189 - 8.29	S7 - 191 - 7.85	W7 - 190 - 7.73
E8 - 191 - 7.69	N8 - 190 - 7.64	S8 - 190 - 7.95	W8 - 190 - 8.38
E9 - 190 - 7.7	N9 - 190 - 7.69	S9 - 191 - 8.14	W9 - 190 - 7.84
E10 - 191 - 7.85	N10 - 205 - 8.71	S10 - 205 - 8.39	W10 - 205 - 7.88
E11 - 205 - 7.77	N11 - 205 - 7.57	S11 - 204 - 7.72	W11 - 205 - 8.02
E12 - 205 - 7.86	N12 - 206 - 7.40	S12 - 205 - 8.34	W12 - 206 - 8.01
E13 - 206 - 7.71	N13 - 220 - 7.57	S13 - 220 - 8.06	W13 - 221 - 8.29
E14 - 220 - 7.76	N14 - 234 - 7.63	S14 - 235 - 7.79	W14 - 235 - 8.43
E15 - 235 - 7.76			
E16 - 290 - 7.48			
E17 - 315 - 7.66			
E18 - 335 - 7.78			
E19 - 385 - 7.69			
E20 - 433 - 7.68			
E21 - 484 - 7.64			
E22 - 535 - 7.6			
E23 - 630 - 7.62			
E24 - 729 - 7.56	N15 - 730 - 7.63	S15 - 731 - 7.60	W15 - 729 - 7.78
E25 - 729 - 7.49	N16 - 729 - 7.33	S16 - 731 - 7.83	W16 - 730 - 8.13
	N17 - 730 - 7.48	S17 - 731 - 8.36	W17 - 730 - 8.30

APPENDIX B: Chemical composition of heats monitored at the plant trial

Table B1: Chemical composition, in weight percent, of heats monitored at the plant trial

Heat	Lub.	C	Mn	S	P	Si	Cu	Cr	Ni	Mo	Sn	Ca	Ti	B	Al	N
260	flux	.11	.85	.021	.010	.17	.32	.10	.09	.02	.013					
261	flux	.12	.85	.022	.009	.18	.31	.09	.09	.02	.014					
262	flux	.11	.85	.021	.012	.16	.39	.08	.15	.01	.019					
263	flux	.11	.80	.023	.018	.17	.35	.09	.11	.01	.018					
264	flux	.12	.88	.020	.013	.19	.35	.10	.08	.01	.018					
265	flux	.12	.85	.021	.018	.15	.38	.11	.09	.01	.016					
277	flux	.14	.84	.020	.010	.17	.28	.09	.09	.02	.014					
278	flux	.13	.82	.021	.010	.17	.30	.09	.09	.02	.015					
279	flux	.14	.85	.019	.010	.18	.27	.09	.08	.02	.015					
280	flux	.13	.89	.020	.008	.18	.29	.08	.10	.02	.017					
281	flux	.13	.86	.021	.012	.20	.26	.10	.09	.02	.015					
282	flux	.13	.88	.024	.015	.19	.30	.09	.08	.01	.014					
298	oil	.13	.82	.018	.008	.17	.33	.08	.09	.02	.014					
299	oil	.12	.84	.019	.008	.16	.35	.08	.09	.02	.017					
300	oil	.13	.88	.020	.010	.19	.33	.09	.09	.02	.016					
311	flux	.33	1.29	.007	.011	.18	.29	.24	.10	.10	.016	.002	.038	.0027	.007	.0094
312	flux	.30	1.33	.009	.010	.20	.31	.24	.09	.01	.016	.002	.038	.0027	.007	.0086
313	flux	.33	1.29	.011	.009	.18	.30	.23	.09	.02	.015	.002	.038	.0028	.006	.0086
314	flux	.31	1.26	.008	.009	.17	.30	.24	.12	.03	.014	.002	.036	.0025	.006	.0095
315	flux	.32	1.36	.006	.010	.19	.25	.25	.09	.02	.014	.002	.035	.0024	.007	.0081
333	oil	.32	1.28	.005	.007	.18	.30	.24	.09	.01	.015	.003	.038	.0023	.007	.0087
334	oil	.32	1.26	.008	.009	.19	.33	.23	.09	.01	.015	.003	.035	.0028	.006	.0081

In the above table "Lub." refers to the lubricant used. The heats cast with oil were part of a separated study been conducted by Kumar[110] and Gurton[124]. However, they were used as control heats for comparison purposes, what was done in Chapter 7.

APPENDIX C: Thermodynamics of TiN and BN formation in low-alloy steel

The temperature-dependent solubility product of Ti and B in liquid iron and γ-iron is given in Table C1,

Table C1: Solubility of TiN and BN in liquid iron and γ-iron (T in K).

Solubility Product	Liquid Iron	γ-Iron	Comments
log[%Ti][%N]	$\frac{-17040}{T} + 6.40$	$\frac{-15790}{T} + 5.40$	Data compiled by Turkdogan[135]
log[%B][%N]	$\frac{-10030}{T} + 4.64$	$\frac{-13970}{T} + 5.24$	Data compiled by Turkdogan[135]

Turkdogan[135] compiled experimental data from several independent measurements which in most cases agreed well with equations derived from compiled thermochemical data. For the solubility of Ti and B in liquid iron, the main source was Evans and Pehlke. For the solubility of BN in γ-iron, Fountain and Chipman data were used, whereas for TiN an equation was derived based on data published by Matsuda & Okumura and Kunze.

The first-order interaction coefficients, e_i^j, in liquid iron, shown in Table C2, were compiled from J. F. Elliott[138].

Table C2: B, C, N and Ti First-order interaction coefficients, e_i^j, in liquid iron[138]

i\j	Al	B	C	Cr	Cu	Mn	N	Ni	P	S	Si	Sn	Ti
B	-	0.038	0.22	-	-	-	0.074	-	-	0.048	0.078	-	-
C	0.043	0.24	0.14	-0.024	0.016	-	0.11	0.012	0.051	0.046	0.08	0.044	-
N	-0.028	0.094	0.13	-0.047	0.009	-0.02	0.0	0.01	0.045	0.007	0.047	0.007	-0.53
Ti	-	-	-	0.055	-	-	-1.8	-	-	-0.11	-	-	0.013

A typical boron steel chemical composition (wt%) is shown in Table C3

Table C3: Typical chemical composition of boron-grade steels

C	Mn	S	P	Si	Cu	Ni	Sn	Cr	Ti	B	Al	N
0.32	1.36	0.006	0.010	0.19	0.25	0.09	0.014	0.25	0.035	0.0024	0.007	0.0081

Using the first-order interaction coefficients given in Table B2 and the steel chemistry given in Table C3 the following values were obtained for the activity coefficients of B, N, and Ti, i.e., f_B, f_N, and f_{Ti}:

$f_B = 1.2195$

$f_N = 0.9927$

$f_{Ti} = 0.9976$

The solute distribution ratios for Ti, N and B between the liquid iron and γ-iron are given by the following equations[1]:

$$\log\frac{[Ti]_\gamma}{[Ti]_l} = -0.40$$

$$\log\frac{[N]_\gamma}{[N]_l} = \frac{640}{T} - 0.71$$

$$\log\frac{[B]_\gamma}{[B]_l} = \frac{-2300}{T} + 0.065$$

For calculations purposes the solute concentration in γ-phase ($[X]_\gamma$) at liquidus temperature was considered to be the same as the concentration in the bulk as given in Table C1. The solute concentration in the interdendrictic liquid ($[X]_l$) is then calculated multiplying the solute content in γ-phase by its respective solute distribution ratio.

APPENDIX D: Enthalpy method and dimensionless analysis for powder melting

Enthalpy Method for Phase Change:

The energy equation for an alloy or glassy substance undergoing solidification or melting can be expressed by:

$$\rho C_p \frac{\partial T}{\partial t} = \nabla.(k\nabla T) + \rho G \qquad (D.1)$$

where ρ is the density, C_p is the specific heat, T is the temperature, t is time, k is the thermal conductivity and G is the rate of energy generation owing to solidification or consumption during melting. Assuming that the latent heat (ΔH) is released at a rate proportional to the rate of formation of the solid fraction, f_s, hence G can be expressed by:

$$G = \Delta H \frac{\partial f_s}{\partial t} \qquad (D.2)$$

Recalling that the enthalpy of an alloy is defined by:

$$H = \int C_p dT + \Delta H(1 - f_s) \qquad (D.3)$$

therefore,

$$\frac{\partial H}{\partial T} = C_p - \Delta H \frac{\partial f_s}{\partial T} \qquad (D.4)$$

Applying the chain rule,

$$\frac{\partial H}{\partial t} = \frac{\partial H}{\partial T}\frac{\partial T}{\partial t} = \left(C_p - \Delta H \frac{\partial f_s}{\partial T}\right)\frac{\partial T}{\partial t} \qquad (D.5)$$

Combining Equations (D.1) and (D.2) we obtain:

$$\rho \frac{\partial H}{\partial t} = \nabla.(k\nabla T) \qquad (D.6)$$

For constant C_p Equation (D.3) can be written as:

$$H = \begin{cases} C_p & for\ T < T_S \quad (solid\ region) \\ C_p T + (1 - f_s)\Delta H & for\ T_S \le T \le T_L \quad (mushy\ region) \\ C_p T + \Delta H & for\ T > T_L \quad (liquid\ region) \end{cases} \qquad (D.7)$$

where T_S and T_L are the solidus and liquidus temperature, respectively. The relationships presented in Equation(D.7) are used to convert calculated enthalpies into temperatures. Thus, the evolution of the solid fraction (f_s) with temperature, within the mushy region, must be known or defined. In solidification of metals alloys a linear relationship, lever rule or Scheil equation are the most commonly used.

As shown in Equation (D.3) the advantage of this formulation (Enthalpy Method) to model solidification or melting is that the latent heat is implicit in the formulation therefore it does not require any especial method to handle latent heat.

Dimensionless analysis:

For a two-dimensional system, as shown in Figure D.1, Equation D.6 is given by:

$$\rho \frac{\partial H}{\partial t} = k_x \frac{\partial^2 T_x}{\partial X^2} + k_z \frac{\partial^2 T_z}{\partial Z^2} \qquad D.8$$

In order to non-dimensionalize Equation D.8, the following dimensionless terms were selected,

$$T_x^* = \frac{T - T_{x0}}{T_{xL} - T_{x0}}, \quad T_z^* = \frac{T - T_{zL}}{T_{z0} - T_{zL}}, \quad X^* = \frac{X}{L_x}, \quad Z^* = \frac{Z}{L_z}, \quad H^* = \frac{H}{H_M}, \quad t^* = \frac{t}{t_p}$$

where T^*, X^*, Z^*, H^* and t^* are the dimensionless temperature, axis, enthalpy and time respectively; T_{x0} is the lowest temperature in the X-direction at the mould wall side and T_{xL} is the highest temperature at the SEN side, T_{z0} is the lowest temperature at the top of the

powder layer and T_{zL} is the highest temperature at the liquid steel interface both in the Z-direction, L_x is the distance from the mould wall to the SEN (= 61.5 mm), L_z is the total height of powder (~ 50 mm), H_M is a maximum value for enthalpy and t_p is the total time of the process.

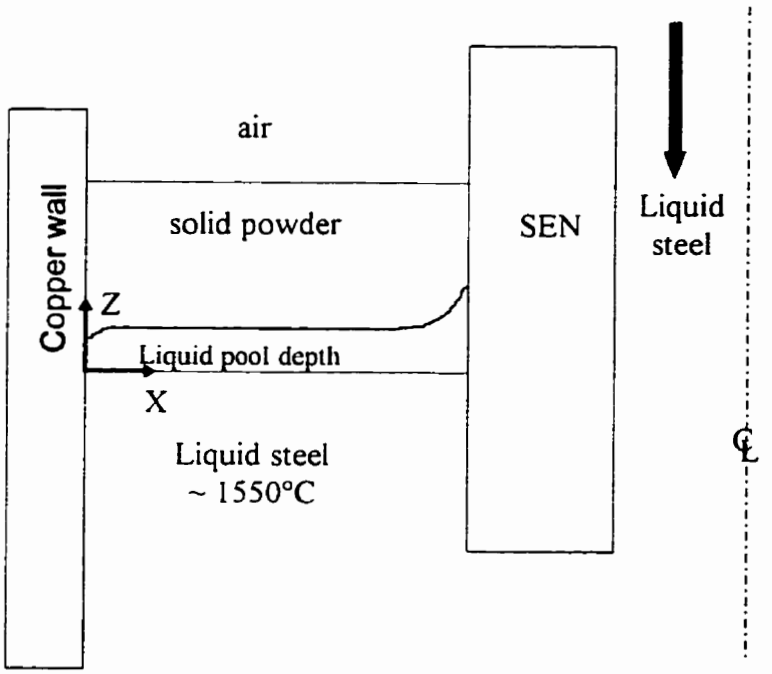

Figure D1 Physical system used for the dimensionless analysis of the powder melting model

Substituting the above dimensionless terms in Equation D.8

$$k_x\left(\frac{T_{xL}-T_{x0}}{L_x^2}\right)\frac{\partial^2 T_x^*}{\partial X^{*2}}+k_z\left(\frac{T_{z0}-T_{zL}}{L_z^2}\right)\frac{\partial^2 T_z^*}{\partial Z^{*2}}=\rho\frac{H_M}{t_p}\left(\frac{\partial H^*}{\partial t^*}\right) \qquad \text{D.9}$$

Dividing Equation D.9 by $k_z\left(\frac{T_{z0}-T_{zL}}{L_z^2}\right)$,

$$\frac{k_x}{k_z}\left(\frac{T_{xL}-T_{x0}}{T_{z0}-T_{zL}}\right)\left(\frac{L_z}{L_x}\right)^2\frac{\partial^2 T_x^*}{\partial X^{*2}}+\frac{\partial^2 T_z^*}{\partial Z^{*2}}=\rho\frac{H_M}{t_p}\left(\frac{\partial H^*}{\partial t^*}\right)\frac{L_x^2}{k_z\left(T_{z0}-T_{zL}\right)} \qquad \text{D.10}$$

To compare the magnitude of the heat fluxes in the X- and Z-directions the term multiplying $\frac{\partial^2 T_x^*}{\partial X^{*2}}$, i.e., $\frac{k_x}{k_z}\left(\frac{T_{xL}-T_{x0}}{T_{z0}-T_{zL}}\right)\left(\frac{L_z}{L_x}\right)^2 \equiv C_X$, must be evaluated; at the same time it must be realized that the equivalent term multiplying $\frac{\partial^2 T_z^*}{\partial Z^{*2}}$, C_Z, is equal to unity.

Assuming the conditions below, i.e.,

$k_z = \sim 4 \times k_x$ (the heat conductivity is enhanced in the Z-direction due to convection caused by hot gases flowing up from carbonate decomposition and combustion of carbon).

$T_{xL} = \sim 1300°C$,

$T_{x0} = 100°C$,

$T_{z0} = 1550°C$,

$T_{xL} = 200°C$,

$L_z = 50$ mm,

$L_x = 61.5$ mm.

$C_X = 0.15$, therefore for the set of conditions analyzed, the heat flux in the horizontal direction (SEN-mould wall direction) is only 15% of the heat flowing up in the Z-direction. This justifies the use of a 1-D model for the analysis of melting of mould flux in billets. Additionally, this agrees well with simulations carried out by Goldschmit et al.[55], using a 2-D model developed with the help of a general non-linear finite element code for thermal analysis called ADINAT. They found that for a 205 mm diameter round billet, and a nozzle of 78 mm diameter, the nozzle temperature had only a very localized effect on the depth of the molten flux pool.

APPENDIX E: Oscillation mark depth and pitch

Table E1: Oscillation mark depth measured on ~ 300-400 mm long samples obtained from billets cast with mould powder and different mould water velocities.

Heat #	Sample #	East Face [mm]		West Face [mm]		Water Vel.	Powder
		Avg.	Std. Dev	Avg.	Std. Dev	[m/s]	
260	60	0.58	0.23	0.66	0.43	9.9	A
261	30	0.64	0.36	0.58	0.32	9.9	A
261	60	?*	?*	0.82	0.57	7.6	A
262	30	0.44	0.23	0.77	0.38	7.6	A
262	60	0.46	0.20	0.94	0.44	9.9	A
263	30	0.83	0.41	0.94	0.33	9.9	A
263	60	0.95	0.45	0.86	0.46	9.9	B
264	30	?*	?*	?*	?*	9.9	B
264	60	0.85	0.28	0.75	0.31	7.6	B
265	30	0.97	0.29	0.77	0.33	7.6	B
265	60	0.61	0.33	0.70	0.29	9.9	B
277	30	0.74	0.34	0.57	0.31	9.9	A
277	60	0.55	0.22	0.42	0.22	7.6	A
278	30	0.51	0.33	0.51	0.30	7.6	A
278	60	0.45	0.30	0.59	0.32	9.9	A
279	30	?*	?*	?*	?*	9.9	A
279	60	0.43	0.20	0.61	0.29	9.9	B
280	30	0.49	0.27	0.57	0.32	9.9	B
280	60	0.47	0.30	0.47	0.35	7.6	B
281	30	?*	?*	?*	?*	7.6	B
281	60	0.50	0.29	0.52	0.34	9.9	B
282	30	0.52	0.25	0.42	0.28	9.9	B
282	60	0.53	0.52	0.38	0.28	9.9	A
311	30	0.31	0.14	0.31	0.13	6.0	A
311	60	0.27	0.13	0.24	0.13	9.9	A
312	30	0.30	0.21	0.28	0.13	9.9	A
312	60	0.44	0.28	0.38	0.23	6.0	A
313	30	0.24	0.14	0.31	0.21	6.0	A
313	60	0.38	0.26	0.64	0.38	6.0	B
314	30	0.29	0.22	0.47	0.31	6.0	B
314	60	0.30	0.21	0.34	0.26	9.9	B
315	30	0.28	0.20	0.40	0.26	9.9	B
315	60	0.27	0.17	0.29	0.15	6.0	B

?* billet samples with identification problems

Table E2: Oscillation mark pitch on ~ 300-400 mm long samples obtained from billets cast with mould powder

Heat #	Billet #	East Face	West Face	Mould Powder
		mm	mm	
260	60	8.51	8.51	A
261	30	8.50	8.50	A
261	60	8.60	8.60	A
262	30	8.51	8.51	A
262	60	8.94	8.94	A
263	30	8.97	8.97	A
263	60	9.04	9.04	B
264	30	8.70	?	B
264	60	8.60	8.60	B
265	30	8.45	8.45	B
265	60	8.79	8.79	B
277	30	7.33	7.33	A
277	60	7.33	7.33	A
278	30	7.44	7.44	A
278	60	7.79	7.44	A
279	30	7.69	7.41	A
279	60	7.13	7.86	B
280	30	very irreg.*	7.69	B
280	60	7.14	7.07	B
281	30	7.69	very irreg.*	B
281	60	7.69	7.69	B
282	30	very irreg.*	very irreg.*	B
282	60	very irreg.*	very irreg.*	A
311	30	9.38	9.17	A
311	60	9.26	9.26	A
312	30	9.29	9.29	A
312	60	9.56	9.56	A
313	30	?**	?**	A
313	60	9.68	9.38	B
314	30	9.56	9.85	B
314	60	9.17	9.43	B
315	30	9.69	9.55	B
315	60	9.44	9.44	B

* very irregular oscillation marks made it difficult to count them

?** sample identified incorrectly

APPENDIX F: Rhomboidity Measurement

Table F1: Rhomboidity measurement on ~300-400 mm long samples obtained from billets cast with mould powder

Heat #	Billet #	Diagonal a (mm)	Diagonal b (mm)	Difference (mm)	Powder
260	60	280	282.6	-2.6	A
261	30	280	283.5	-3.5	A
261	60	281.6	281	0.6	A
262	30	282.1	280.5	1.6	A
262	60	280.9	280.1	0.8	A
263	30	279.5	281.7	-2.2	A
263	60	280.7	279.8	0.9	B
264	30	280.9	281.2	-0.3	B
264	60	280.7	280.8	-0.1	B
265	30	279.9	282.3	-2.4	B
265	60	280.4	280.2	0.2	B
277	30	283	278.5	4.5	A
277	30	279.6	280	-0.4	A
277	60	279.4	282.8	-3.4	A
278	30	278	282.5	-4.5	A
278	60	280	279.9	0.1	A
279	30	???	???*	???*	A
279	60	280.9	280.4	0.5	B
280	30	280.3	281.2	-0.9	B
280	60	281.6	279.6	2.0	B
281	30	???	???*	???*	B
281	60	281	281.2	-0.2	B
282	30	280.4	281.5	-1.1	B
282	30	280.4	280.7	-0.3	B
282	60	278.8	282.2	-3.4	A
311	30	284.1	279.7	4.4	A
311	60	286.5	276.5	10.0	A
312	30	281.6	281.1	0.5	A
312	60	282.1	281.1	1.0	A
313	30	281.2	279.6	1.6	A
313	60	281.7	279.4	2.3	B
314	30	282.6	281.4	1.2	B
314	60	283.4	281.3	2.1	B
315	30	282.8	280.9	1.9	B
315	60	282.5	280.1	2.4	B

*??? samples with identification problems

APPENDIX G: Metal level detection

The radioactive source of the metal level control system consists of Ce^{137} pellets with 500 millicuries (19 gigabecquerels) activity, mounted in a proprietary holder type SA-1. The beam is not significantly collimated and emerges in a conical fashion with a angle of 45° centrered on the pellet location in the source holder[139].

In order to estimate the effect of mould-flux on the metal level controller the intensity of radiation reaching the detector was calculated using the following equation,

$$I = I_0 \exp(-\mu \times X)$$

where I_0 is a system-dependent constant, μ is the attenuation coefficient for gamma rays generated by Ce^{137} in cm^2/g, and X is the distance traveled by the gamma rays. For Ce^{137} the mass attenuation coefficient, given by μ/ρ, is equal to 0.075 where ρ is the density of the medium being penetrated, in g/cm^3[140].

To simplify the calculations the beam was considered constant with a diameter of 100 mm and all gamma absorption occurring outside the mould cavity is assumed to be included in I_0. The internal dimension of the mould (X) is 20.3 cm. The densities of the gamma-absorbing medium, air, solid powder, liquid mould-flux and steel were taken as:

$\rho_{air} = 1.16\ g/cm^3$

$\rho_{powder} = 1.0\ g/cm^3$

$\rho_{flux} = 3.0\ g/cm^3$

$\rho_{steel} = 7.2\ g/cm^3$

Figures G1 and G2 show the results obtained. In Figure G1 the intensity of radiation detected by the sensor for oil casting is compared with mould-flux casting for three different levels of total amount of powder above the liquid metal.

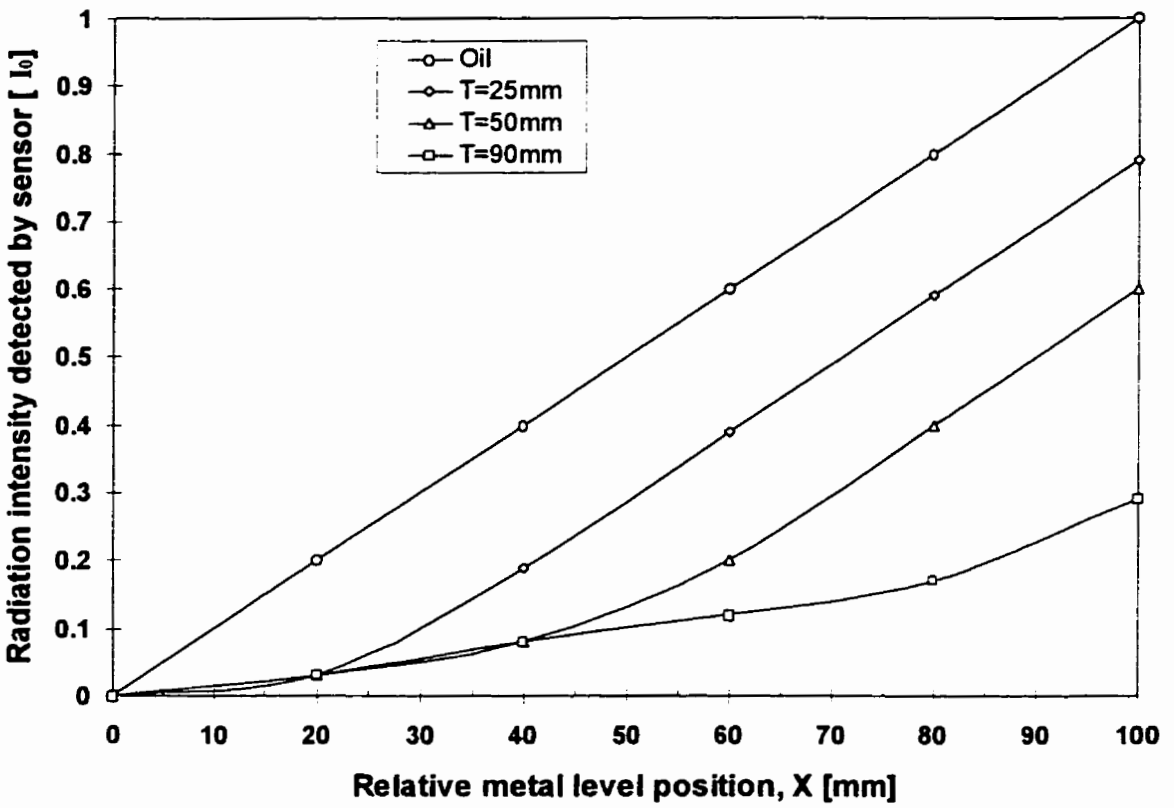

Figure G1 Influence of lubrication type and total amount of mould powder on the radiation intensity reaching the metal level sensor; T is the total amount of powder, X=0 is the top of the gamma-beam and X=100 is the bottom.

Figure G1 shows that for oil the radiation intensity is a linear function of the metal level position throughout the whole control range. For mould-powder the following features can be pointed out: (i) radiation intensity is lower than oil, which is heightened by increasing the total amount of powder, (ii) radiation intensity looses linearity towards the top of the beam, which is also intensified as the total amount of powder increases and (iii) the slope of the curves decrease substantially as the total amount of powder increases. The high dependency of the intensity of radiation on the total amount of powder and small values of slope are both detrimental for having a reliable metal level control when mould-powder replaces oil. Based on the above observations it can be concluded that a radioactive-based system requires that a

constant and small amount of powder be kept on the top of the liquid steel. Under the conditions of the plant trial the metal-level controller could not respond well to metal level variations since the total amount of powder was high and variable, between 50 and 90 mm.

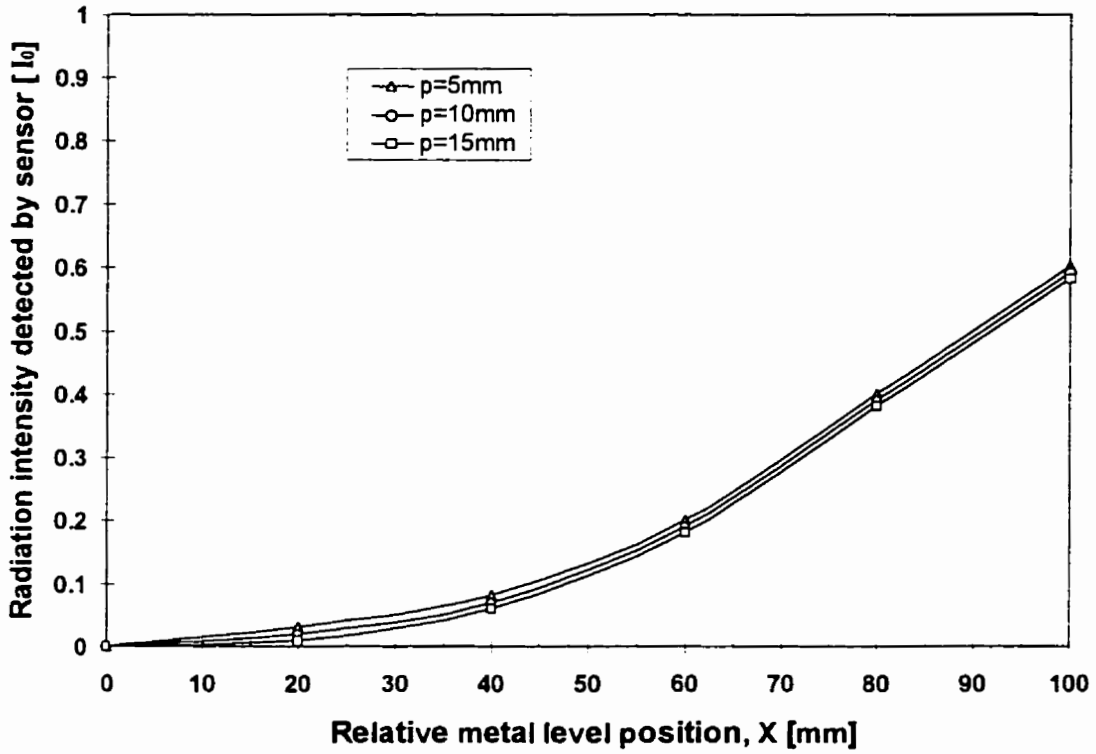

Figure G2 Influence of molten-flux pool depth on the radiation intensity reaching the metal level sensor; p is the pool depth, X=0 is the top of the gamma-beam and X=100 is the bottom.

Figure G2 shows the effect of the molten-flux pool depth on the intensity of gamma rays reaching the radiation sensor. It is clear that there is no substantial difference in the radiation intensity when the pool depth increases from 5 to 15 mm. The results presented in Figures F1 and F2 show that the effect of the total amount of mould-powder on the radiation absorption is much greater than the effect of the depth of the molten-flux pool, the reason being simply that the difference in the length of layers prevails over the difference in their density, since the height of the powder is several times larger than the pool depth.

IMAGE EVALUATION TEST TARGET (QA-3)

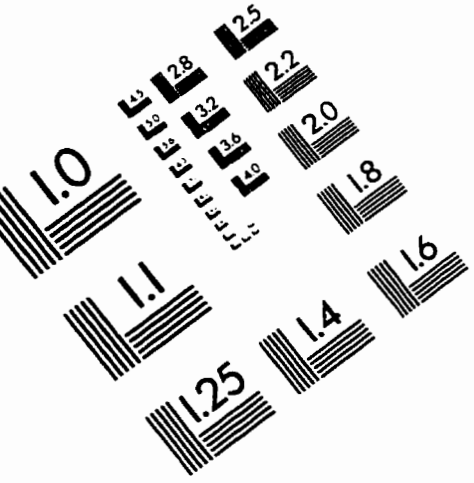

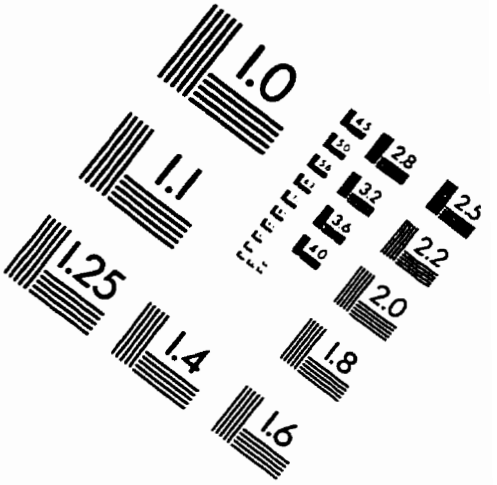

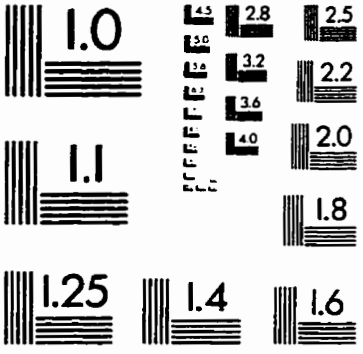

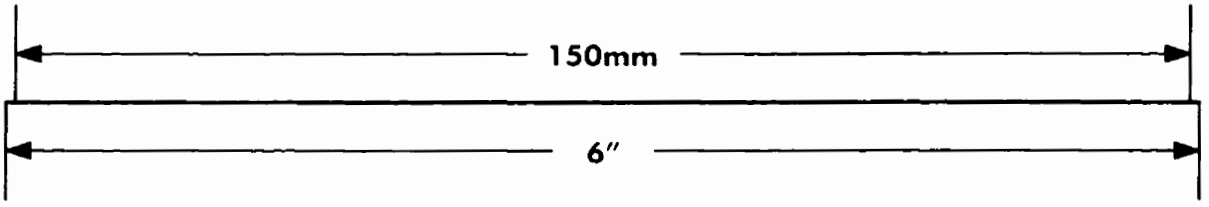

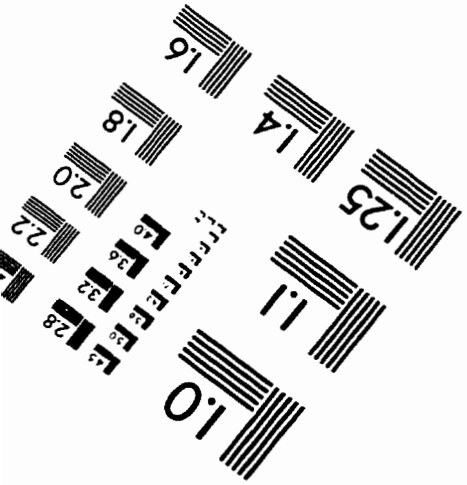

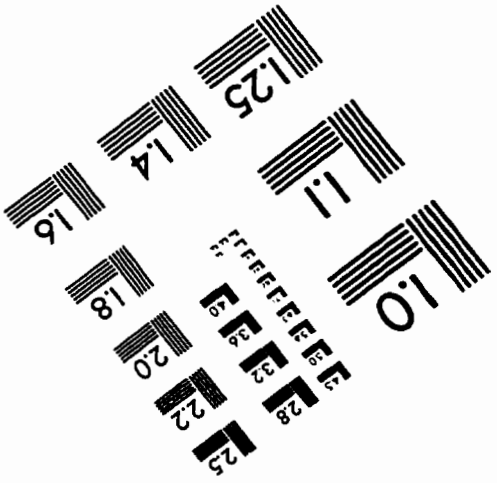

APPLIED IMAGE, Inc
1653 East Main Street
Rochester, NY 14609 USA
Phone: 716/482-0300
Fax: 716/288-5989